Quaternary Tephrochronology of the Scotia Sea and Bellingshausen Sea, Antarctica.

Steven Grahame Moreton

A thesis submitted to Cheltenham and Gloucester College of Higher Education in accordance with the requirements of the degree of Doctor of Philosophy in the Faculty of Environment and Leisure.

British Antarctic Survey.

September 1999.

Abstract

The Southern Ocean is a region of the world's ocean which is fundamental to the generation of cold deep ocean water which drives the global thermo-haline circulation. Previous investigations of deep-sea sediments south of the Polar Front have been significantly constrained by the lack of a suitable correlation and dating technique.

In this study, deep-sea sediment cores from the Bellingshausen, Scotia and Weddell seas have been investigated for the presence of tephra layers. The major oxide and trace element composition of glass shards have been used to correlate tephra isochrons over distances in excess of 600 km. The source volcanoes for individual tephra layers have been identified. Atmospheric transport distances greater than 1500 km for >32 μm shards are reported.

One megascopic tephra is identified and correlated across 7 sediment drifts on the continental rise in the Bellingshausen Sea. Its occurrence in a sedimentary unit that has been biostratigraphically dated to $\delta^{18}O$ substage 5e identifies it as a key regional marker horizon for that stage.

An unusual bimodal megascopic ash layer erupted from Deception Island, South Shetland Islands, has been correlated between 6 sediment cores which form a 600 km NE-SW transect from the central Scotia Sea to Jane Basin. This megascopic ash layer has been ^{14}C dated at c.10,670 years BP. It represents the last significant input of tephra into the Scotia Sea or Jane Basin from that volcano and forms an important early Holocene marker horizon for the region.

Five disseminated tephras can be correlated to varying extents across the central Scotia Sea cores. Together with the megascopic tephra they form a tephrostratigraphic framework that will greatly aid palaeoclimatic, palaeoenvironmental and palaeoceanographic investigations in the region.

Declaration

I hereby declare that the ideas and results contained in this thesis are my own excepted where acknowledged otherwise.

I further declare that no part of this thesis has been submitted for any other degree at any other academic institution.

Steven G. Moreton

Acknowledgements.

So many people have played a part in helping me make it through to the completion of this thesis that, unfortunately, it would not be possible to mention them all individually. However, I would particularly like to thank the following people.

My Mother and Father, Marjorie and Jack Moreton, the financiers at Parental Banking who so readily agree to my frequent loan requests, and for their love and support.

John Hunt, for thinking of such a good project and then getting it funded.

Carol Pudsey and John Smellie, for their excellent supervision, without them I never would have made it this far.

Bridget Wade, for love, friendship and support.
Helen Medley, ditto, and for keeping me sane, then driving me mad, then keeping me sane, then driving me mad….

Pete Hill, for friendship, advice and for assistance with the EPMA which is at the heart of this thesis.
Richard Hinton and John Craven, for their assistance with the ion-microprobe analysis.
Ken Robinson, for assistance with scanning electron microscopy and EDS analysis.
Sidney Hemming, for her willing collaboration in trying to date the northern Bellingshausen Sea tephra by ^{40}Ar-^{39}Ar dating.

Moya and Hugh Flockhart, for making their home my home.

Thanks also to 'Clur', Morag, Nicky, John, Laura and Shelley, Andy and Julie, Dan and Jo, Phil, Clare, Amy and Charlotte, and to all the Exe-pats for all the booze and for listening to my constant gripes.

Thanks to everyone who has played 5-a-side football either for or against BAS in the last few years.

Love and best wishes also to Lesley, Meredith, Vicky, Emily, Tracy, Lisa, Ange, Juliet and Andrea.

List of contents

List of Figures

List of Tables

1 Introduction

1.1 Antarctica and Global Climate

The cryospheric, palaeoceanographic and palaeoclimatic development of Antarctica are basic components of an understanding of the important role of this continent in the functioning of the world's climate system. Despite increased interest and strenuous efforts, however, our present knowledge of Antarctica's glacial history still suffers from severe inconsistencies (De Batist *et al.* 1997).

The Antarctic is fundamental in driving the global atmospheric regime owing to its strong negative radiation budget (Drewry *et al.* 1993). The Southern Ocean, which provides the only deep-water linkage between the Atlantic, Indian and Pacific oceans, allows the transport of heat, salt and nutrients around the globe. It also plays an influential, but poorly understood role as a major sink for atmospheric carbon dioxide (Nowlin and Klinck 1986, Drewry *et al.* 1993, Whitworth *et al.* 1998).

The seas of the Southern Ocean play a major rôle in the production of the cold, dense bottom water which is largely responsible for driving the global thermohaline circulation system. The global thermohaline circulation system is now thought to be a major factor in driving general ocean circulation and its activity is implicated in the fluctuations of climate that characterize the Quaternary (Broecker *et al.* 1985, Harland *et al.* 1998). Most of the world's bottom water is formed in the large embayments of Antarctica, namely the Weddell and Ross seas, with only a minor secondary component from the Nordic seas of the northern hemisphere (Harland *et al.* 1998). The well-oxygenated cold dense water flows toward the equator and ventilates the deep oceans (Broecker and Peng 1982, Nicholls *et al.* 1991).

As global climatic and oceanic circulation patterns change they leave an imprint in the sedimentary record. Past climatic and palaeoceanographic regimes can therefore be reconstructed from evidence in sediment cores. However, such reconstructions for the Southern Ocean have been significantly constrained by the lack of suitable correlation and dating techniques.

1.2 Aims of the Project.

The over riding objective of the thesis is to demonstrate the utility of tephra isochrons as stratigraphic marker horizons in the Antarctic deep-marine sedimentary environment. By correlating individual tephra layers across each study area and attempting to correlate tephra layers between two study areas, it was hoped that a tephra-based stratigraphy (tephrostratigraphy) could be developed that could be applied to other palaeoenvironmental investigations in the Antarctic Peninsula region. In order to accomplish this objective the first systematic search for disseminated as well as megascopic ash layers had to be undertaken. In this thesis, tephra layers have been identified and successfully correlated, even in sediments containing only four per cent vitric shards in the >32 μm sediment fraction.

Through comparisons with published and unpublished geochemical data, it was initially hoped that individual tephra layers might be correlated between different environmental settings - marine, lacustrine, peat bog, ice core and volcanic edifice - enabling different lines of evidence for the timing and extent of recent climatic fluctuations to be brought together. This is the ultimate goal for tephrochronological studies and has already been achieved to some degree in the North Atlantic and NW European region amongst others (e.g. Mangerud *et al.* 1984, Grönvold *et al* 1995).

Where possible, individual source volcanoes or at least the source volcanic province were identified for each tephra layer. In such a little-explored region where few volcanoes are well exposed, distal proxy records are invaluable in adding to the knowledge of the volcanic history. One particular aim was to investigate whether there was any significant difference in volcanic activity between the Late Pleistocene and the Holocene. Cores extending back to Oxygen Isotope Substage 5e were examined to determine whether there was any significant variation in the frequency of volcanic activity over glacial – interglacial cycles. Any difference could be attributable to loading or unloading of the crust due to ice sheet growth or decay (Sigvaldason *et al.* 1992, Zielinski *et al.* 1996, McGuire *et al.* 1997).

A database of major oxide geochemical analyses was constructed for each ash layer. Where possible the source volcano or source volcanic province were determined for each ash layer.

Dating of the tephras was by ^{14}C, where sufficient organic carbon occurred in the sediments, and comparison with the sub-Antarctic ^{18}O curve for tephras found sufficiently far north or in water shallow enough to retain biogenic carbonate. Tephras were also stratigraphically dated by comparison with published and unpublished proxy records (e.g. biostratigraphy and Ba/Al ratios). Experimental direct dating of tephra by ^{40}Ar-^{39}Ar was also attempted for tephras thought to be of sufficient age (>100ka) with sufficiently high K_2O contents (>4.5 wt.%).

1.3 Previous Antarctic Tephrochronology

In geological terms, the deposition of volcanic ash from widely dispersed eruption plumes is a virtually instantaneous event. Tephra fall layers thus form ideal chronostratigraphic markers which can be used to correlate between different sedimentary environments and establish well-constrained chronologies (Sparks *et al.* 1997). The utility of tephra layers lies in their wide geographical dispersal, amenability to dating and distinct lithology. Tephra from individual volcanic eruptions can be identified, distinguished and correlated using layer thickness, particle size and shape, colour, stratigraphic relationships, mineral assemblages and glass chemistry (Hunt *et al.* 1995). Geochemical analysis is a vital tool for demonstrating or refining tephra correlations. This is most frequently achieved using electron-probe microanalysis (EPMA) of individual glass shards. Although the composition of some tephras are known to vary during the course of the eruption (J.L.Smellie pers.comm), unless there is prior knowledge to the contrary, it is assumed that tephras derived from single eruptions are homogenous and represent the composition of the source magma (Smith and Westgate 1969, Hunt and Hill 1993).

Results of previous tephrochronological studies in the northern Antarctic Peninsula region were reviewed by Smellie (in press). The studies concentrated on shallow marine or terrestrial environments, including, moss banks limnic sediments and glacial
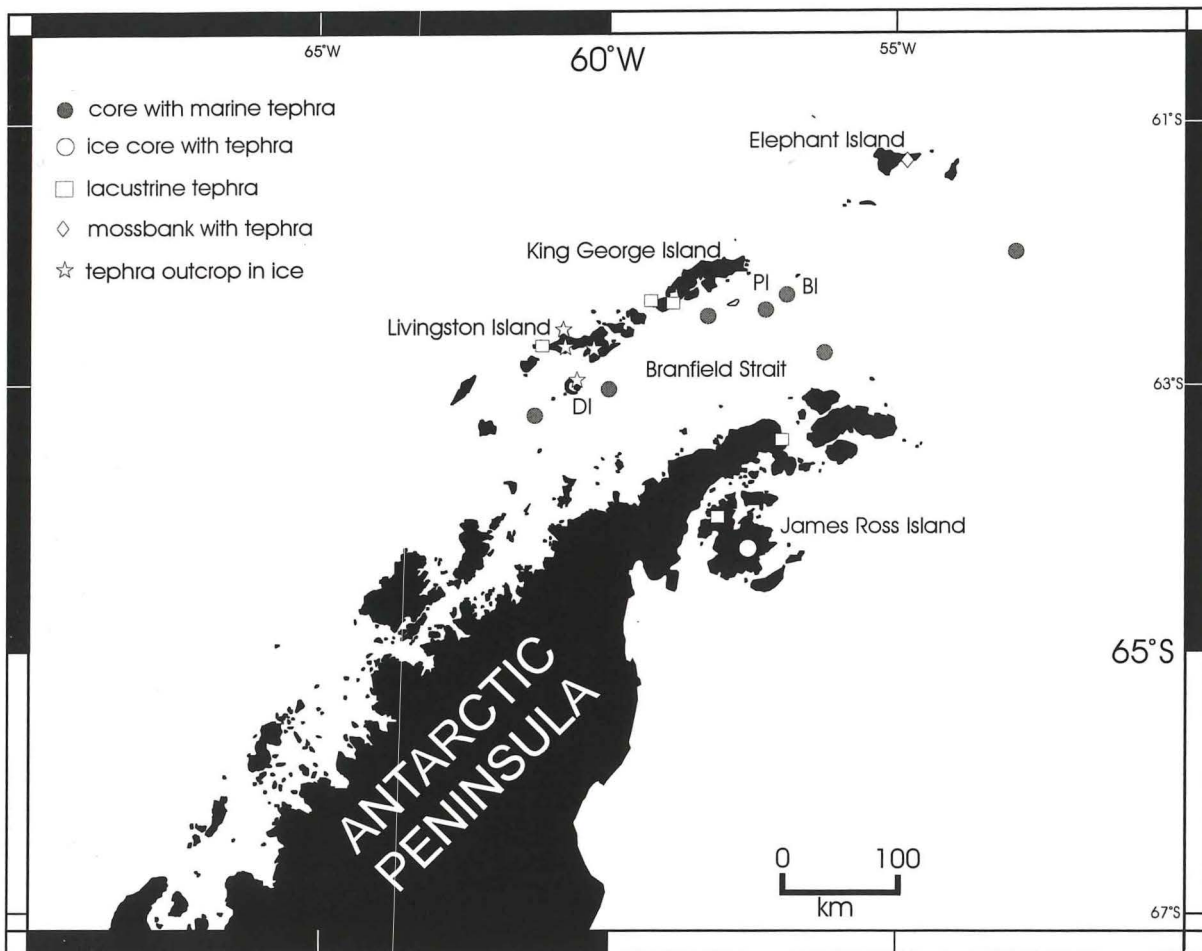
Figure 1.1 Map of the northern Antarctic Peninsula (Graham Land) region showing locations of samples analysed in previous tephrochronological investigations (after Smellie in press).DI = Deception Island, PI = Penguin Island, BI = Bridgeman Island.

ice (Orheim 1972; Matthies *et al.* 1988, 1990; Björck *et al.* 1991a,b,c; Tatur *et al.* 1991; Calvet *et al.* 1997; Hodgson *et al.* 1998) (Figure 1.1). All of these ash layers have been dated to the Holocene. With the exception of two ash layers from Bransfield Strait and King George Island, which have been attributed to eruptions on Bridgeman and Penguin islands, all tephra layers documented have been identified as originating from Deception Island, suggesting that it has been the most active of the Quaternary volcanoes in the region. However, none of the ashes is well characterised, and few analyses have been published (e.g. Moreton and Smellie 1998).

Most terrestrial depositional environments in the region have only been ice-free since the Last Glacial Maximum at the earliest. Recent re-evaluation of the timing of deglaciation in the northern Antarctic Peninsula suggests that the onset of retreat of land-based glaciers occurred later than in the northern hemisphere, beginning around 9000 ^{14}C years BP and progressing only slowly for the first half of the Holocene, 9000–5000 ^{14}C years BP (Hjort *et al.* 1998). Therefore, only ice-cores and marine sediments offer the potential for constructing a regional tephrochronology spanning a complete glacial–interglacial cycle, and marine sediments alone can extend the tephrochronological record back to pre-Quaternary times.

Few ice cores have been drilled on the Peninsula itself as most drilling has been concentrated on the major ice sheets where a more complete and longer ice record is preserved. However, drilling is currently in progress on the James Ross Island ice-cap where ice accumulation may be sufficient to preserve a >10,000 yr B.P. ice record (R. Mulvaney pers. comm.). James Ross Island is c. 200 km from Deception Island and it has the potential to record even small scale eruptions on that island. None of the Peninsula ice-cores have been subject to a detailed study to identify and locate tephra layers, although there are known to be increases in particulate material incorporated in the ice from years of known volcanic activity in the region (R. Mulvaney pers. comm.).

Ice cores extending back to >100 ka B.P. have been obtained from four widely spaced localities on the West and East Antarctic ice sheets (Figure 1.2; Smellie in press). The Byrd Station Ice Core (BSIC) is the most extensively studied (Kyle and Jezek 1978,
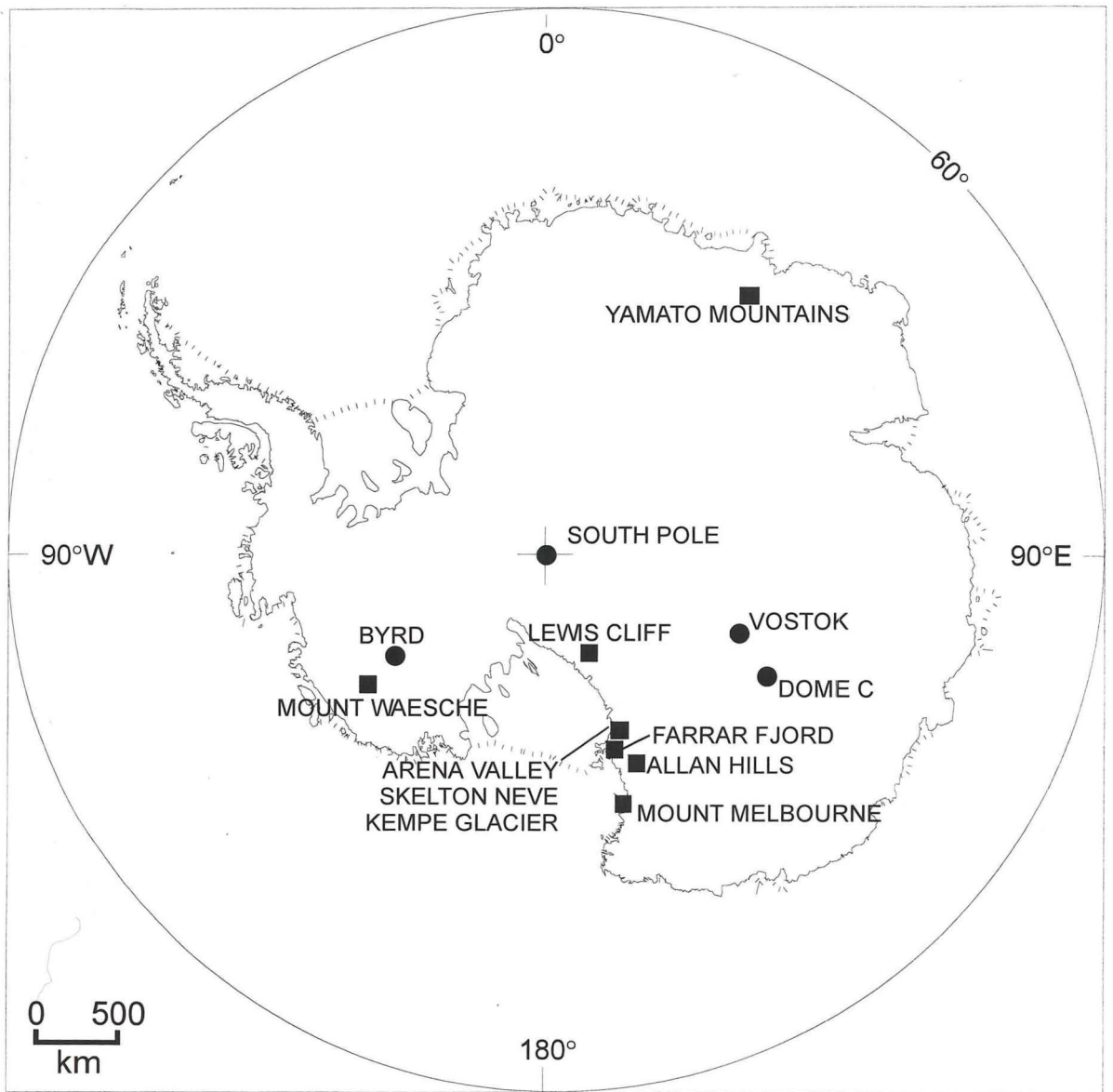
Figure 1.2 Map showing locations of previous tephrochronological investigations from continental Antarctica (after Smellie in press). Circles = ice core with tephra, squares = other tephra localities.

Kyle *et al.* 1981, Kyle *et al.* 1982, Palais and Kyle 1988, Palais *et al.* 1988). BSIC contains >2000 dust bands in which tephras are common, in addition to 25 distinct tephra layers. One BSIC tephra has been correlated with tephra found in glacial ice on the slopes of Mt. Waesche. Mt. Berlin, Marie Byrd Land (MBL) is identified as the source whereas Mt. Takahe (MBL) is identified as the source of the remaining BSIC tephras (Wilch and McIntosh in prep.). Marie Byrd Land is therefore identified as the source region of all the BSIC tephras. The tephras range in age from 7.5 ka to 40 ka with the peaks of volcanic activity occurring 16–30 ka BP (Kyle and Jezek 1978), 14–20 ka BP (Palais *et al.* 1988) and 30–40 ka BP (Wilch and McIntosh in press).

Ice cores from the other three localities contain fewer tephra and dust bands but show a greater range of contributing source regions, namely southern Victoria Land and South Sandwich Islands (Vostok Ice Core), South Shetland Islands and South America (South Pole Ice Core), and MBL (Dome C) (Gow *et al.* 1968, Gow and Williamson 1971, Kyle and Jezek 1978, Kyle *et al.* 1982, Palais *et al.* 1987). Atmospheric transport distances in excess of 3500 km (South America to SPIC) and >4000 km (South Sandwich Islands to VIC) highlight the potential for an ice-core tephrochronology based on volcanic dust, although such small particles (<16μm) are too small for conventional dating methods (Wilch and McIntosh in press) and cannot be reliably analysed by grain discrete EPMA (unpublished observations of S. Moreton).

Tephra layers in blue ice exposures have been reported in the Transantarctic Mountains, Victoria Land, Marie Byrd Land and the Yamato Mountains (Figure 1.2). These tephras are mainly proximal deposits and have been correlated with volcanoes in northern Victoria Land (Mt. Melbourne and The Pleiades), southern Victoria Land (Mt. Erebus) and MBL (Mt. Waesche). However, some long distance transport is evident by the correlation of ash from the Yamato Mountains with a source in the South Sandwich Islands, 3000km distant (Dunbar *et al.* 1995, Smellie in press).

Layers and lenses of tephra found in the Dry Valleys have been dated to 4.3 Ma and attributed to an eruption of Mount Discovery (Erebus Volcanic Province) (Marchant *et al.* 1993, Marchant *et al.* 1996). Its presence was used by Marchant *et al.* (1993) as

evidence to support the theory of a stable cold-desert climate and hence a stable East Antarctic Ice Sheet. Conversely, Barrett *et al.* (1992) described ash interbedded within marine diamictite in a core from the CIROS-2 drill-hole in the Ferrar Fjord (Victoria Land), which they interpreted as evidence for a fluctuating East Antarctic ice sheet.

Marine tephra studies in the Southern Ocean have, to date, been largely restricted to three regions, the South Pacific, the South Atlantic (east of the South Sandwich islands) and the Scotia Sea. Late Pliocene and Pleistocene tephras have been identified in marine cores from the South Pacific sector (Watkins and Kennett 1972, Huang *et al.* 1973, Huang and Watkins 1982, Froggatt *et al.* 1986, Shane and Froggatt 1992) (Figure 1.3). The South Pacific tephras were originally ascribed a New Zealand source (e.g. Kyle and Seward 1984, Froggatt *et al.* 1986). However, recent publications (e.g. Shane and Froggatt 1992), based on a larger data set of geochemical analyses, have identified the Balleny Islands and Marie Byrd Land as more likely sources.

Numerous ash layers were encountered in 12 piston cores obtained during cruises of the R/V *Vema* and USNS *Eltanin* to the southern South Atlantic east of the South Sandwich Islands (Ninkovitch *et al.* 1964, Echols 1971, Federman *et al.* 1982) (Figure 1.4). Federman *et al.* (1982) found that pumice fragments were dispersed throughout the core and did not form visible layers. The South Sandwich Islands have been identified as the source of all of the glass and pumice found, based on refractive indices (Ninkovich *et al.* 1964) and chemical compositions (Federman *et al.* 1982). Nine samples of lower Miocene to Pleistocene ash obtained during ODP leg 114 were analysed by Hubberten *et al.* (1991). The highly variable K_2O content of the glass enabled Hubberten *et al.* (1991) to group the tephras into three separate magmatic series. The Miocene tephras were ascribed a South Shetland or possibly Discovery Arc or Jane Bank source. The Pliocene ashes were identified as probably South Shetland Islands in origin, whereas the Quaternary tephras were probably derived from the South Sandwich Islands. More recently, late Quaternary (<300 ka) tephra layers in sediment cores collected from the South Atlantic have been analysed by electron microprobe and ICP-MS (Figure 1.4). The South Sandwich Islands have unequivocally been identified as the source of all the tephras analysed, although none of the tephras could be
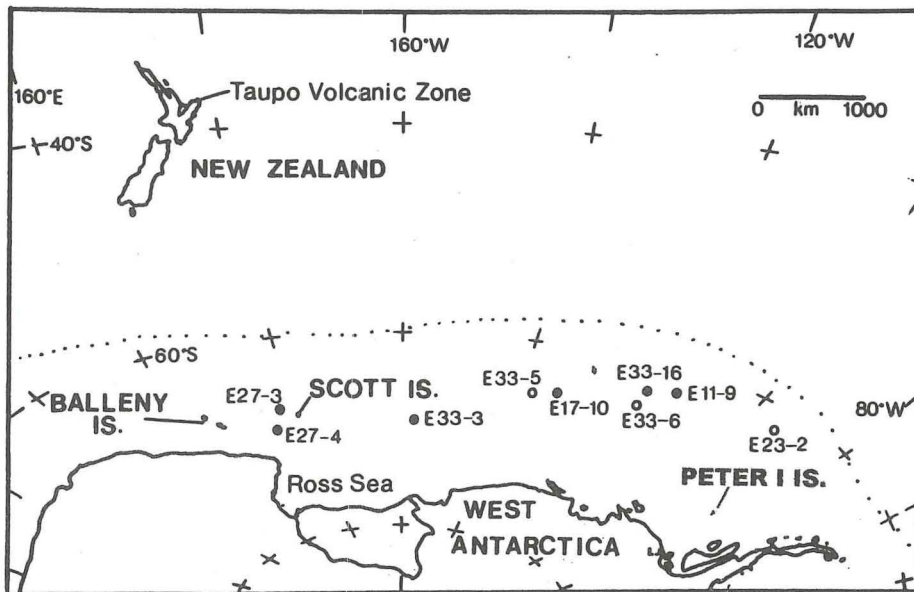
Figure 1.3 Location of USNS *Eltanin* cores from the South Pacific containing tephra layers (after Shane and Froggatt 1992)
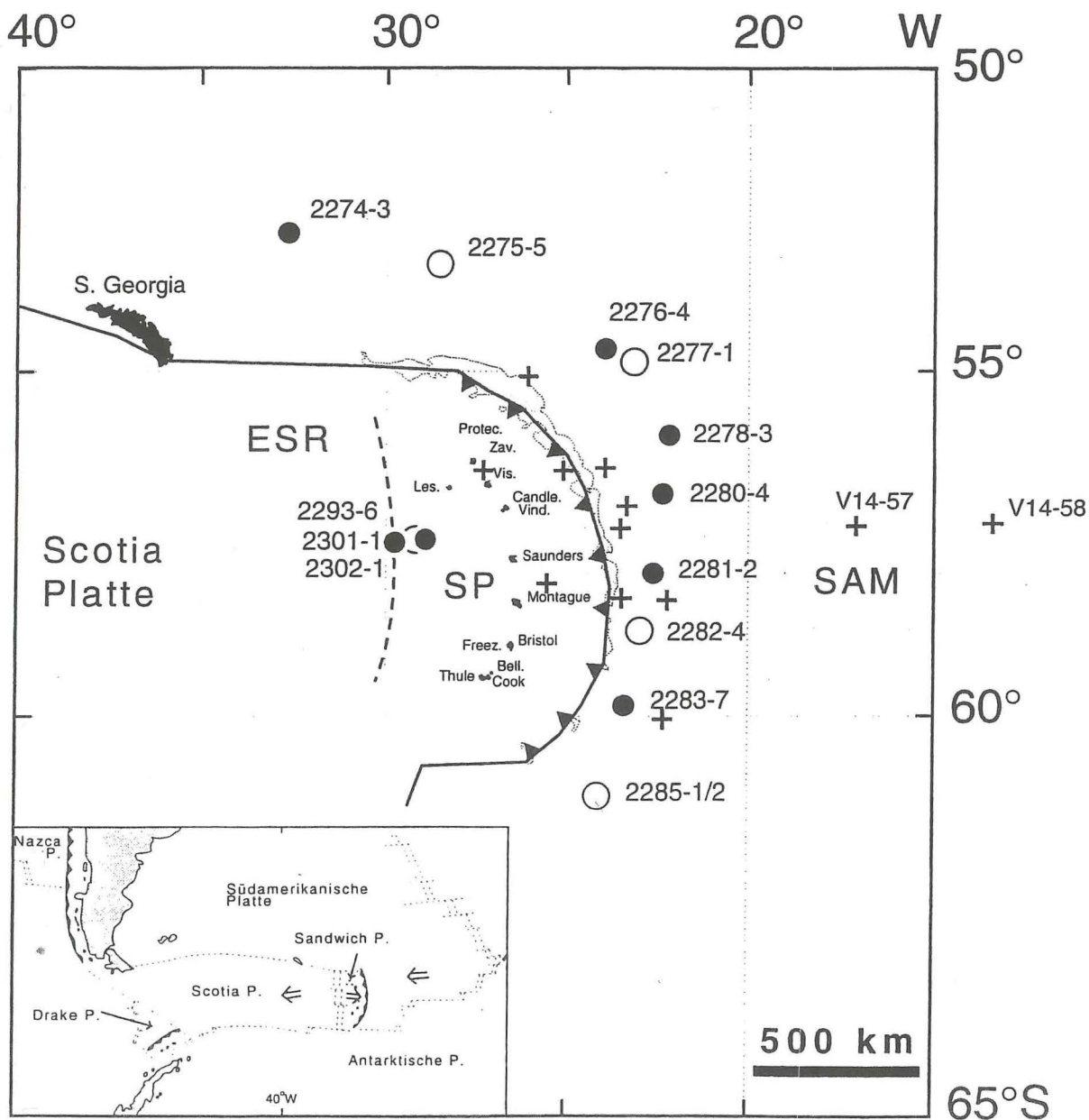
Figure 1.4 Location of containing South Sandwich Island tephra. Circles mark the location of RV *Polarstern* cores examined by Straub et al. 1996, crosses indicate location of USNS *Eltanin* cores examined by Federman *et al*. 1982 (after Straub *et al*. 1996).

correlated and individual source volcanoes could not be identified (Straub *et al.* 1996). Straub *et al.* (1996) postulated that tephra layers in two of the cores may have been ice-rafted.

Despite a large number of marine geological publications identifying the presence of pristine and altered ash layers in sediment cores from the Scotia Sea and northern Weddell Sea (e.g. Pudsey *et al.* 1988, Jordan *et al.* 1991, Pudsey 1992, Jordan and Pudsey 1992, Gilbert *et al.* 1998, Pudsey and Howe 1998), only three publications have so far produced geochemical compositions for the glass fractions (Hubberten *et al.* 1991, Straub *et al.* 1996, Moreton and Smellie 1998). Hubberten *et al.* (1991) examined 22 samples of ash from ODP Leg 113 in the northern Weddell Sea. However, glass shards were abundant in only a few samples. All of the Leg 113 ash is Pliocene in age. Two of the tephras have bimodal compositions with basaltic–andesite and rhyodacite components. Comparison between the Leg 113 tephra and analyses of Pliocene lavas from the South Shetland Islands and Antarctic Peninsula (Saunders *et al.* 1982, Smellie *et al.* 1984) show the Leg 113 tephra to have a greater affinity to Antarctic Peninsula lavas. Straub *et al.* (1996) investigated Quaternary ash turbidites from two cores collected from the eastern Scotia Sea (Figure 1.4). The tephra show variable compositions ranging from basalts to highly evolved rhyolites. The South Sandwich Islands are identified as the source of the tephra.

To date only one study (Moreton and Smellie 1998) has published geochemical analyses and proposed correlations for Quaternary ash layers from the central Scotia Sea. Moreton and Smellie (1998) showed that one visible, early Holocene tephra can be correlated over a horizontal distance >400km. Deception Island was identified as the source of that tephra. The publication by Moreton and Smellie (1998) stems directly from the work conducted as part of this project [see chapters 4 and 5].

Based on the paucity of publications for such a large region, there is clearly a need for a detailed study of the Quaternary tephras deposited in the Scotia Sea. This region of the Southern Ocean has the potential to receive distal tephra from a number of volcanic provinces that are known to have been recently active, namely; the South Shetland

Islands–Bransfield Strait; the Antarctic Peninsula; South America and possibly the South Sandwich Islands and Marie Byrd Land, each of which has a distinctive geochemistry.

1.4 The Southern Ocean

Circum-Antarctic marine sediments contain a record of past climate and Southern Ocean circulation that both complements and considerably extends the record in the continental ice. Climatically-induced variations in primary biological production and the supply and deposition of terrigenous material from the Antarctic continent, reflect changes in sea-ice cover, sea surface temperature, bottom current strength and the size of the grounded continental ice sheet. All of these variables contribute to changes in sediment characteristics, in a record extending back many million years (Barker 1992, Kennett and Warnke 1992).

1.4.1 Southern Ocean Circulation

Southern Ocean circulation is dominated by the Antarctic Circumpolar Current (ACC). The ACC is driven by a broad zone of near-continuous westerly winds (the West Wind Drift) which blow unobstructed around the Antarctic Continent (Figure 1.5). Although wind driven, the ACC reaches the sea bed in many areas (Maksimov and Vorob'ev 1964, Orsi *et al.* 1995, Harland *et al.* 1998) Between the broad zone of the West Wind Drift and the Antarctic continent high-pressure area lies a low-pressure zone centred on about latitude 65° S; winds within this zone (the East Wind Drift) drive a thin, discontinuous, westward surface current around the Antarctic coast and more vigorous, more stable cyclonic gyres in the Ross and Weddell Sea embayments (Deacon 1963, Orsi *et al.* 1992) (Figure 1.5). South of 65° S winds become variable again coinciding with the west – east passage of centres of low pressure, often with a southward component as well (Mullan and Hickman 1990). At a pressure altitude of 500 hPa (approximately 5 km above sea level) the circulation is dominated by a circumpolar westerly airflow throughout the year (Mullan and Hickman 1990).
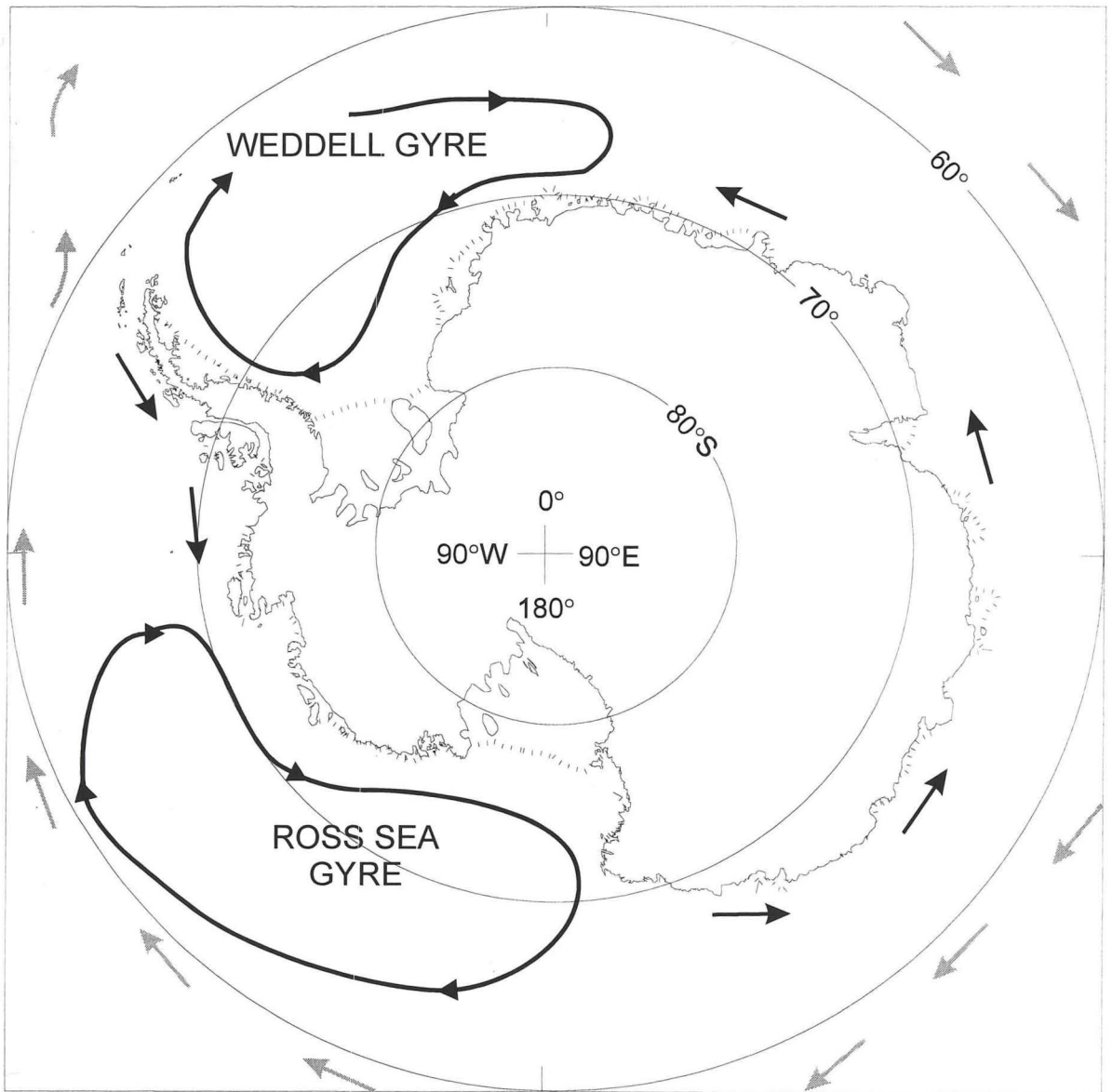
Figure 1.5 Generalised oceanic circulation patterns around the Antarctic. The grey arrows indicate the path of the Antarctic Circumpolar Current driven by the prevailing westerly winds. Black arrows show coastal counter current flow driven by the east wind drift (after Sugden 1982).

13

The world oceans' densest waters are created in the Weddell Sea and, progressively modified by mixing, form the basal layer over much of the deep-sea floor (Mantyla and Reid 1983). Weddell Sea Bottom Water (WSBW) is produced in the southern and western Weddell Sea by modification of the ambient Warm Deep Water by a combination of surface cooling, increased salinity from extraction of fresh sea-ice and 'supercooling' on the continental shelf beneath a floating ice shelf (Foldvik and Gammelsrod 1988, Nichols *et al.* 1991). Newly-formed WSBW becomes a dense basal addition to the clockwise Weddell Gyre, mixing with and renewing the overlying Antarctic Bottom Water (AABW). AABW exits the Weddell basin along deep pathways into the South Atlantic, Indian and South-east Pacific oceans, beneath the Circumpolar Deep Water of the ACC. Oxygen dissolved in the surface component of the WSBW and North Atlantic Deep Water serves to ventilate the deep ocean (Broecker and Peng 1982, Nichols *et al.* 1991).

Weddell Sea circulation is dominated by the clockwise flow of the Weddell Gyre which is driven by high latitude easterly winds (the East Wind Drift) and constrained by the physical barriers of the Antarctic Peninsula and the South Scotia Ridge (Deacon and Moorey 1975, Deacon and Foster 1977, Jordan and Pudsey 1992). The gyre is fed by water branching off from the ACC and entering the Weddell Sea from the east. Two pathways, Jane Basin and the South Sandwich trench, allow outflow of WSBW into the Scotia Sea and south-eastern South Atlantic. Some WSBW flows westward into Protector Basin and then into the Pacific Ocean (Nowlin and Zenk 1988).

The eastward flow of the ACC dominates circulation in the Scotia Sea. The constricted flow through Drake Passage means that increases in flow volume of the ACC can only be accommodated by increased velocity. Drake Passage also limits the latitudinal migration of the Polar Front during glacial and interglacial cycles. At depth, water flowing through Jane Basin into the Scotia Sea is partly responsible for deflecting the ACC northward through a gap in the North Scotia Ridge at 48° W.

To date, the Antarctic coastal circulation between 120° W and 70° W is poorly investigated. The ACC is the most prominent feature of the South Pacific sector of the

Southern Ocean. Unlike the Scotia and Weddell seas, there are no topographic controls to flow and the ACC increases to a width of approximately 2500 km (Grotov *et al.* 1998). Along the western side of the Antarctic Peninsula, coastal circulation is characterised by a westward flowing current which is assumed to be a continuation of the Antarctic Polar Slope Current emerging from the Weddell Sea (Nowlin and Zenk 1988, Camerlenghi *et al.* 1997, Grotov *et al.* 1998).

1.4.2 Controls on Biogenic Productivity

The position and migration of the Polar Front, sea surface temperature, nutrient supply and the maximum extent of spring sea-ice cover are important controls on biogenic productivity in the Southern Ocean (Brasier 1995, Murray 1995). These factors are, in turn, climatically controlled such that microfossil species assemblages in marine sediments can be used as palaeoclimate proxies (e.g. Hays *et al.* 1976, Denton *et al.* 1989, Bard *et al.* 1990a, Grobe *et al.* 1990, Zielinski and Gersonde 1997, Burckle and Mortlock 1998). Pudsey and Howe (1998) observed that biogenic silica dominates the Holocene surface sediments in the Scotia Sea but accounts for only 20–25% of Last Glacial Maximum age sediments.

1.4.3 Controls on Sedimentation

Whereas climate is one of the major influences on biogenic productivity, primary biological productivity is one of the major influences on sedimentation in the Southern Ocean. Other significant factors are test dissolution (Anderson 1975), bottom current strength, the availability of terrigenous debris and ice rafting (Harland *et al.* 1998).

Bottom water flow controls sedimentation in the western Weddell Sea and Jane Basin. Except around topographic obstacles, flow is relatively slow and sedimentation is continuous (Pudsey *et al.* 1998).Towards the axis of the ACC, however, in the northern Scotia Sea, bottom water flow is considerably faster, and hiatuses in sedimentation are common (Ledbetter and Ciesielski 1986, Jordan and Pudsey 1992). Production of Weddell Sea Bottom Water probably lessened during times of greater sea-ice cover (Pudsey 1992, Gilbert *et al.* 1998). Such changes in the volume and velocity of the

Southern Ocean Bottom waters are reflected in the grain size distribution in the sedimentary record.

Sea floor sediments south of the Polar Front ranges from siliceous ooze, through biosiliceous muds, to terrigenous turbidites and barren tills (Goodell *et al.* 1973). The distribution of these sedimentary facies, therefore, indicates the past extent of sea-ice and the ice sheet, and the former position of the Polar Front (Barker 1992). Most Southern Ocean waters are undersaturated with respect to calcite and, to a lesser extent, silica, so that calcareous skeletal debris is rarely preserved below 500m (Echols and Kennett 1973). Biogenic $CaCO_3$ which is used elsewhere to date sediments through comparison with the ^{18}O isotope curve, is largely absent and cannot be used here. This restriction has led to the development of other methods of dating the sediments, for example, magnetostratigraphy (Pudsey *et al.* 1988), siliceous biostratigraphy (Jordan and Pudsey 1992, Paramor 1999? unpublished), thorium dating (Shimmield *et al.* 1994), Ba/Al ratios (Dymond 1992, Shimmield 1992, Shimmield *et al.* 1993, Pudsey and Howe 1998), AMS ^{14}C dating of organic carbon (Pudsey and King 1997) and tephrochronology (this study and Moreton and Smellie 1998).

Terrigenous sediment supply is largely excluded from the Scotia Sea with fluvial inputs from the southern tip of South America and ice-rafting being the only significant sources. However, terrigenous supply from land-based glaciers and turbidity currents is of greater significance in the Weddell Sea (Gilbert *et al.* 1998) and is the dominant source of sediment in the Bellingshausen Sea (Larter and Barker 1991, Larter and Cunningham 1993, Pudsey and Camerlenghi 1998).

The US National Ice Center tracks the paths of large icebergs leaving the Weddell Sea (Figure 1.6). The main axis of migration for the icebergs runs from Powell Basin to South Georgia. Ice-rafted debris (identified as sediment grains >500μm) is a minor component, constituting less than 1% of the Scotia Sea and Jane Basin sediments; (Pudsey and Howe 1998). However, it should be noted that ice rafting will transport all grains of all sizes, and ice rafting has been implicated in the transportation and re-

Figure1.6 Map of the Scotia Sea and surrounding region. Sediment cores used in this study are shown as red filled circles. The 2000 metre bathymetric contour is shown by a thin pecked line. The generalised route of icebergs leaving the Weddell Sea is mark by a solid black line, with the zone of densest concentration shaded (after US National Ice Centre data). Blue arrows = path of the ACC (after Orsi *et al*. 1995). DI = Deception Island, PI = Penguin Island, BI = Bridgeman Island.

deposition of tephra in both the North and South Atlantic (Hunt unpublished Ph.D. thesis, Hunt *et al.* 1995, Straub *et al.* 1996).

1.4.4. Effects of Bioturbation

The theoretical models of mixing of marine sediments, proposed by Berger and Heath (1968) and Guinasso and Schink (1975) have been applied to tephra bearing sediments from the North Atlantic (Ruddiman and Glover 1972, 1982). Ruddiman and Glover (1982) identified four basic shape parameters that accounted for the observed patterns of tephra distribution. These parameters allowed interpretation of the rate and depth of the active mixing layer. The intensity and depth of active mixing was found to vary both temporally and spatially. It was also found that reconstructed ash layer thicknesses of between 0.005 cm and 0.7 cm did not noticeably inhibit bioturbation.

Bioturbation is an active agent of sediment reworking in the Antarctic Peninsula region. Structureless and /or mottled sediments are common (Pudsey *et al.* 1988, Pudsey 1990, Pudsey 1992, Pudsey *et al.* 1994, Pudsey and Camerlenghi 1998,). Ash laminae have previously been observed to be dispersed over a 10 cm vertical distance in Weddell Sea cores (Pudsey *et al.* 1988). It is therefore likely that tephras of small volume will be thoroughly diffused throughout the cores and may not be recognised. As this study is the first systematic study of disseminated distal tephras in the region only those tephras with volumes above an arbitrary threshold were investigated (see Chapter 2).

1.5 The Study Areas

1.5.1 The Scotia Sea

The Scotia Sea is a small deep water basin that extends from Drake Passage in the west to the South Sandwich Islands in the east (Figure 1.6). It is bounded elsewhere by the North and South Scotia ridges. Much of the Scotia Sea lies at depths of 3000-4500 m and the troughs and surrounding ridges, which rise to depths of less than 1000 m along much of their length, largely isolate the basin from major continental margin sources of sediment (Pudsey and Howe 1998). The high-energy bottom currents associated with the ACC prevent deposition along the central axis of the current and at major

constrictions such as Drake Passage. However, the sea-floor topography of the Scotia Sea allows localised sediment accumulation. Terrigenous silt and clay-sized sediments and biogenic material dominate the Scotia Sea floor, together with a lesser amount of ice-rafted debris. Sediments gradually coarsen northward and Holocene sediments are coarser than those of the Upper Pleistocene (Pudsey and Howe 1998). Sedimentation rate estimates range from 5 – 13cm/ka (Jordan and Pudsey 1992) to 3 – 17 cm/ka (Pudsey and Howe 1998). Most Quaternary sediments within the Scotia Sea lie below the carbonate compensation depth as this gradually rises south of the Polar Front to a minimum depth of 500 m in the vicinity of the South Orkney Islands (Echols 1971).

Hemipelagic sediments from the northern Weddell Sea (Jane Basin) and southern Scotia Sea have previously been described by Pudsey and others (Pudsey 1990; 1992, Pudsey *et al.* 1988, Jones and Pudsey 1994, Jordan *et al.* 1991, Jordan and Pudsey 1992, Gilbert *et al.* 1998, Howe *et al.* 1997). Pudsey and Howe (1998) subdivided the late Pleistocene and Holocene sediments into three broad units distinguished as a terrigenous unit sandwiched by upper and lower biogenic units (named units T, U and L respectively) based on the relative proportions of biogenically produced silica and terrestrially derived minerals. However, the interpretations of palaeo-climate and palaeo-oceanography that can be derived from the sediments are constrained by the relatively imprecise dating of the sediments (Jordan and Pudsey 1992).

Using Ba/Al ratios as a measure of organic palaeo-productivity, Pudsey and Howe (1998) have identified the base of the Holocene ($\delta\ ^{18}O$ Stage 1) in several cores used in this thesis. They also identified the most recent peak abundance of the radiolarian *Cycladophora davisiana*, which Hays *et al.* (1976) recognised as indicative of the Last Glacial Maximum and dated as 18,000 BP through correlation with oxygen isotope curves from carbonate-bearing sub-Antarctic cores. The positions of these time planes represent the only previously datable surfaces currently available for the cores used in this thesis.

A concurrent studentship held by Tracey Paramor at University College London is aimed at reconstructing Late Quaternary radiolarian communities in the region and

reappraising the position of the *C. davisiana* peak abundance by improving upon the initial 10-20 cm sampling resolution of Pudsey and Howe (1998).

1.5.2 The Weddell Sea

The Weddell Sea is a deep embayment extending eastward from the Antarctic Peninsula to Coats Land and Kronprinsesse Märtha Kyst. To the south it extends to the edge of the Filchner-Ronne ice shelf. Its northern limit is marked by the South Scotia Ridge (Figure 1.7).

Virtually the whole of the Weddell Sea is covered by sea ice throughout the year (Figure 1.7). The extensive ice cover limits the growth of planktonic organisms to the extent that biogenic sediments are subordinate to terrigenous material throughout glacial-interglacial cycles. Being largely constrained on three sides, the circulation of the Weddell Sea is dominated by a clockwise gyre extending to all depths. The coriolis effect deflects water in the gyre to the left. Some relatively shallow water flows around the South Shetland Islands to form the anti-clockwise counter current flowing along the continental slope of the Western Peninsula margin. Another substantial volume of water flows northward through Jane Basin. This northward flow of water controls the sedimentation in Jane Basin.

Sediments in the western Weddell Sea are not well known due to extensive pack-ice cover even during the height of the austral summer. However, sediments of the continental slope and rise did not experience grounded ice during glacial maxima, so that sedimentation processes are dominated by current transport and deposition. Sediment supply is predominately from ice-rafting, turbidity currents and resuspended sediment transported in the nepheloid layer. Petrological analysis of the sediments indicates a consistent Antarctic Peninsula source (Gilbert *et al.* 1998).

Jane Basin, located south-east of the South Orkney Islands, extends to depths in excess of 3500 m and is the major spillway for deep water flowing out from the Weddell Sea
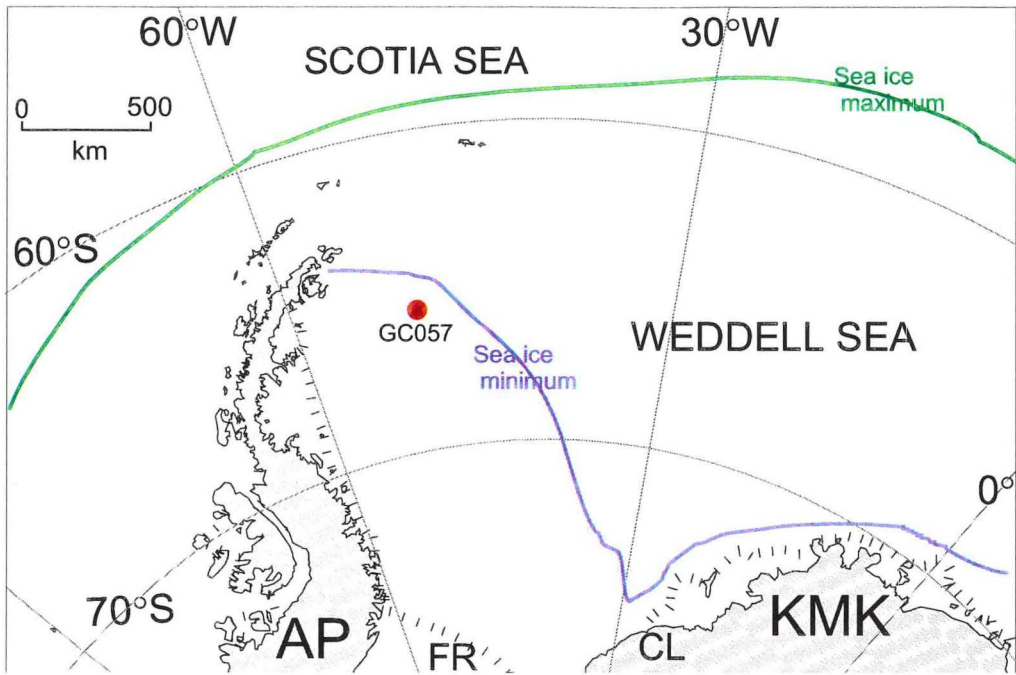
Figure 1.7 Average winter maximum and summer minimum sea ice cover in the Weddell Sea (After Pudsey and King 1997). AP = Antarctic Peninsula, KMK = Kronprinsesse Martha Kyst, FR = Filchner-Ronne ice shelf, CL = Coats Land.

into the Scotia Sea. Sediments in Jane Basin consist mainly of fine-grained terrigenous mud deposited from suspension in the nepheloid layer, with minor amounts of ice-rafted debris and volcanic ash. Turbidites and lag deposits are absent (Jordan *et al.* 1991, Pudsey 1992).

1.5.3 The Bellingshausen Sea

The Bellingshausen Sea is located to the west of the Antarctic Peninsula and extends from the Peninsula margin to the South Pacific. No physical barriers separate it from the neighbouring Amundsen Sea, Drake Passage and southern South Pacific. The predominant eastward flow of the ACC is modified locally over much of the continental shelf and slope by a westward flowing counter current driven by the East wind drift (Figure 1.5) and fed by water flowing out of the Weddell Sea through the Protector Basin.

Investigations of the sediments of the continental slope reveal the presence of at least 9 sediment drifts between 63°S and 69°S (Rebesco *et al.* 1994, McGinnis and Hayes 1994, 1995, Camerlenghi *et al.* 1997, Pudsey and Camerlenghi 1998). The drifts occur in water depths of 2900-4000 metres and are oriented perpendicular to the shelf edge Figure 1.8 (Pudsey and Camerlenghi 1998). They are separated from the shelf and slope by a zone of non-deposition at the base on the slope, and from each other by large turbidity-current channels. The role of the westward flowing bottom current in the formation of the drifts is currently debated with Rebesco *et al.* (1996, 1997), Camerlenghi *et al.* (1997) and Pudsey and Camerlenghi (1998) implicating the bottom current in transporting fine sediments as a nepheloid layer whereas McGinnis and Hayes (1995) and McGinnis *et al.* (1997) view the sediment mounds as the result of turbidity currents alone. Two visible ash layers are present in the drift sediments (Camerlenghi *et al.* 1997, Pudsey and Camerlenghi 1998). These drifts are currently a focus of international collaboration between the British Antarctic Survey, the Italian Osservatorio Geofisca Sperimentale (OGS) and most recently the Ocean Drilling Program (ODP) (Leg 178).
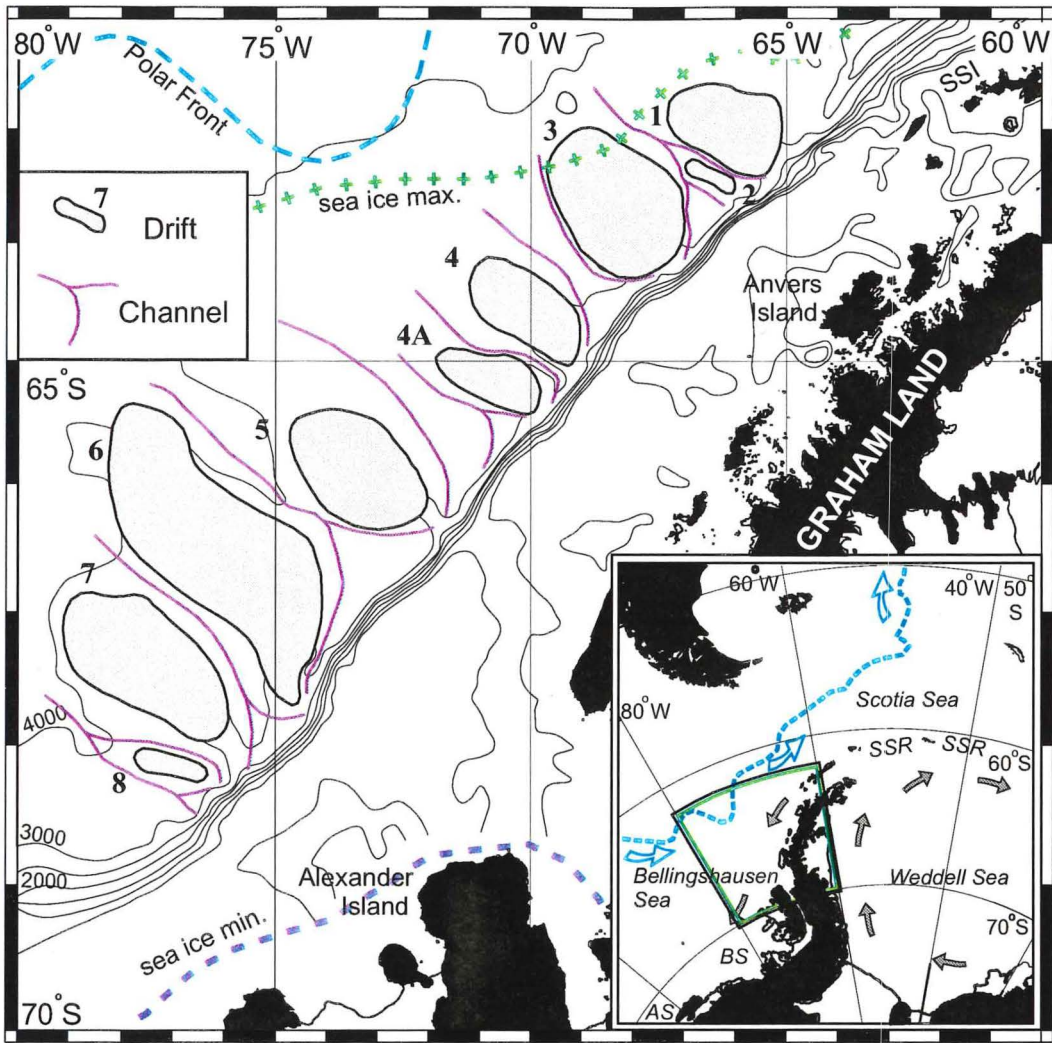
Figure 1.8 Map showing the location of the northern Bellingshausen Sea sediment drifts and separating channels, in relation to the Antarctic Peninsula coast. Potential sources of tephra, Graham Land and the South Shetland Islands (SSI), are also shown. (After Pudsey and Camerlenghi 1998). Inset the path of the ACC, Weddell Gyre and easterly coastal current are shown.

The BAS Marine Geoscience cruise JR19 in 1997 collected 3.5 kHz profiles and a total of 13 piston cores from the drifts. The study of the formation and history of these drifts will be greatly assisted if a high precision stratigraphical/chronological framework, independent of the uncertainties of biostratigraphy, can be developed.

1.6 Recent Antarctic Volcanism

1.6.1 Potential sources contributing tephra to the Scotia Sea and Weddell Sea

1.6.1.1 The South Shetland Islands and Bransfield Strait.

Since early Tertiary times the oceanic Drake Plate (elsewhere called the Phoenix Plate or Aluk Plate) has been subducted beneath the Antarctic Plate at the South Shetland trench leading to the formation of the South Shetland Islands volcanic arc (Saunders *et al.* 1982, Smellie *et al.* 1984, Smellie 1990). This phase of subduction was the final part in a sequence of subduction that had progressed northward along the Antarctic Peninsula since the Jurassic (Barker 1982, Barker and Burrell 1982, Barker and Dalziel 1983). The associated arc magmatism has ceased progressively south to north as offset sections of the spreading centre collided with the trench west of the peninsula and the Pacific and Antarctic plates became coupled. The final remnant of the spreading centre, in Drake Passage, finally became inactive about 4 Ma (Barker 1976, 1982, Smellie 1990).

After the cessation of spreading the subducted plate continued to cool and sink under its own weight causing the northwest-ward migration, 'trench roll-back', of the South Shetland Trench (Jeffers *et al.* 1991). Incipient rifting initiated by the trench migration led to the formation of the Bransfield Basin, a narrow elongate, marginal basin, about 100 km wide and 450 km long and floored by quasi-oceanic crust (Tarney *et al.* 1977, Weaver *et al.* 1979, Keller and Fisk 1992). The basin separates the South Shetland Islands from northern Graham Land and is one of the few modern examples of a marginal active rift-basin within an ensialic arc (Saunders and Tarney 1982, Keller *et al.* 1991).
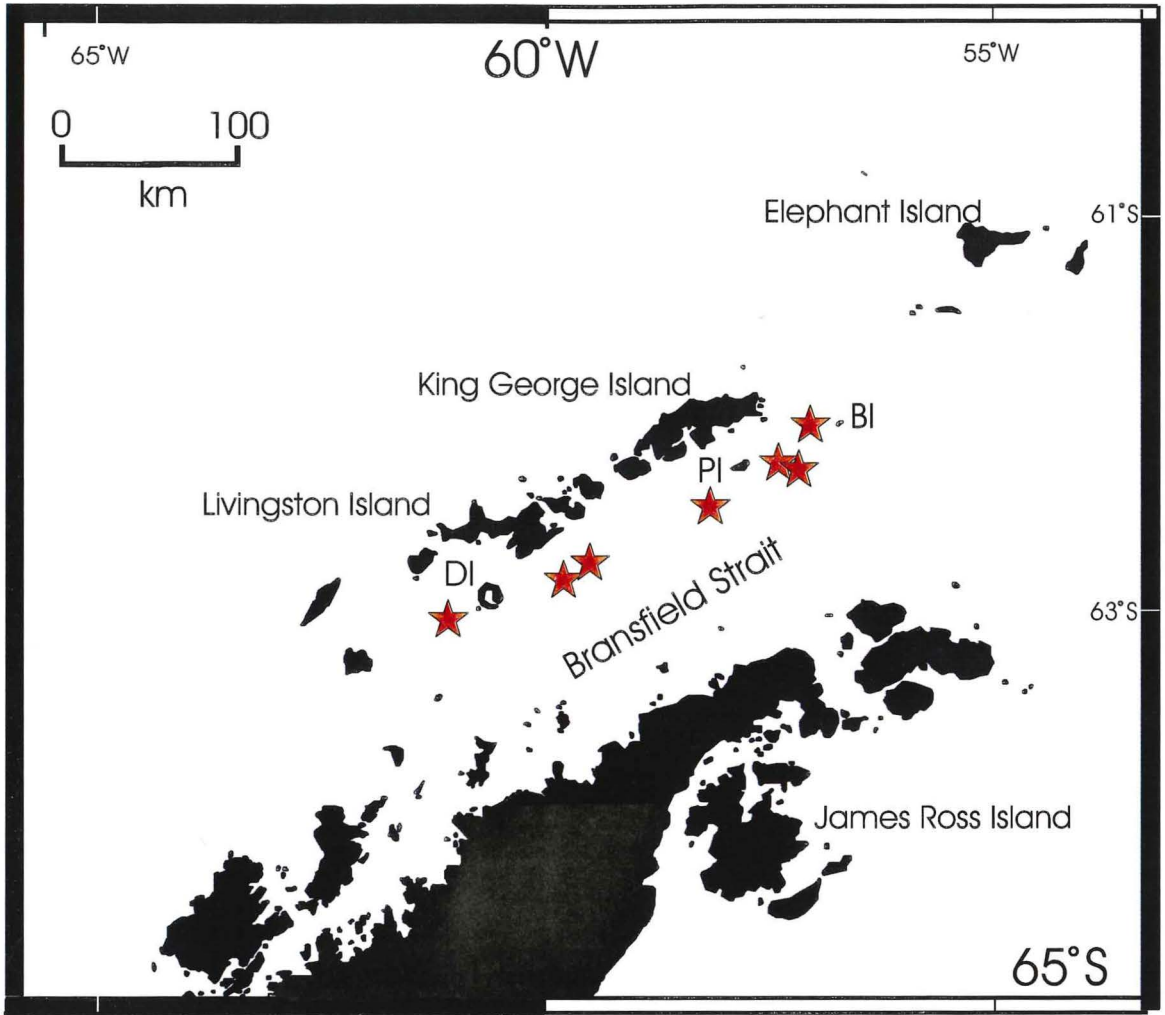
Figure 1.9 Pleistocene-Recent volcanoes and seamounts in Bransfield Strait. Subaerial volcanoes Deception Island, Penguin Island and Bridgeman Island are marked DI, PI and BI respectively. The location of seamounts are indicated by red star symbols.

The Bransfield basin is asymmetrical with a deep axial zone juxtaposed to the South Shetland Islands (Jeffers *et al.* 1991). The basin is divided into three sub-basins by the ridges associated with two volcanic islands, Deception Island and Bridgeman Island. A third subaerial volcanic island, Penguin Island, is located on the western flank of the spreading axis (Figure 1.9). At least 7 seamounts and several smaller submerged volcanic centres have been mapped along the rift and on its north-western flank (González-Ferrán 1991, Canals *et al.* 1997). Quaternary volcanism is known from several seamounts, on the three volcanic islands and on Sail Rock, Livingston Island, Greenwich Island and King George Island (Smellie *et al.* 1984, Keller *et al.* 1991).

However none of the seamounts would have been subaerially exposed during the last glacial maximum (currently the summit of the shallowest seamount is at a depth of 200 m (González-Ferrán 1991)) and although explosive submarine eruptions have been known to throw ash-laden steam into the air, it is unlikely that the eruption columns would have risen sufficiently high within the troposphere to enable long-distance transport of the tephra. Furthermore, observations and modeling of submarine eruptions indicates that tephra and pumice from submarine eruptions draws in water as it cools, making it more prone to rapid sinking (Williams and McBirney 1979, Whitham and Sparks 1986).

The recent eruptions of Deception Island in 1967, 1969 and 1970, continuing earthquake activity on and around the island and hydrothermal activity in Bransfield Strait (Baker *et al.* 1975, González-Ferrán 1991, Rey *et al.* 1995, De Baptist *et al.* 1997) suggest that volcanism related to spreading is still taking place. Rey *et al.* (1995) however, disputed that ongoing volcanic and hydrothermal activity can be explained by a simple model of arc magmatism.

The most active volcano in the South Shetland Islands – Bransfield Strait system is Deception Island, a ring-shaped volcanic island with a flooded caldera (Figure 1.10). The crater wall is breached at Neptune's Bellows allowing passage to the safe anchorage in the caldera called Port Foster. This safe haven and ready access to the interior means that Deception Island is the most extensively studied of the Bransfield

Figure 1.10 Aerial view of Deception Island looking northwest. The diameter of the island isabout 13km (photograph courtesy of J.L. Smellie)

Strait volcanoes and it was inhabited by several nations at the time of the recent historical eruptions.

Previous investigations (Holtedahl 1929; Hawkes 1961; Baker *et al.* 1975; Birkenmajer 1995), subdivided the lava, tephra and tuff layers on the island into broadly pre-, syn- and post-caldera units, although there is still considerable debate over the correlation of the various named formations and assignment to their respective chronological units. There is also debate as to the number of active centres responsible for the pre-caldera edifice (c.f. Hawkes 1961; Baker *et al.* 1969).

The oldest lavas on the island have been dated by K-Ar as $150,000 \pm 46,000$ years B.P. (Keller *et al.* 1992). Birkenmajer (1995) assigned a late Pleistocene or possibly early Holocene age for the caldera collapse (although no dating evidence was offered to support this theory). However, based on the rate of sedimentation in the caldera (Cooper *et al.* 1998, Smellie in prep.) Smellie (in prep.) has argued for a young (i.e. Holocene) age for caldera formation. Furthermore although it has traditionally been accepted that caldera collapse occurred through a series of radial and ring faults formed over an evacuated magma chamber (possibly following a cataclysmic eruption (Holtedahl 1929; Hawkes 1961; Baker *et al.* 1975; Smellie 1988, 1989; Birkenmajer 1992, 1995, Smellie *et al.* 1998)), it has recently been suggested that caldera collapse occurred purely as a result of regional extensional tectonics (Marti *et al.* 1996).

Mass balance calculations suggest that any large, cataclysmic eruption directly related to and preceding caldera formation, may have expelled about 30 ± 10 km^3 of tephra (Smellie *et al.* 1997). Such a large eruption during the last 150,000 years would be an obvious target for a tephrochronological investigation of late Quaternary marine sediments downwind of Deception Island.

1.6.1.2 South America.

Several active and dormant volcanoes are found in the Southern Andean Volcanic Zone (Simpkin and Siebert 1994). In general, atmospheric circulation will tend to keep eruption plumes away from the Scotia Sea for all but the most southerly volcanoes.

However the plume from an eruption of Mount Hudson, Chile on 12–15 August 1991, was transported east-southeast directly over the Falkland Islands and Bird Island (near South Georgia) and then eastward around Antarctica (Scasso *et al.* 1994, Sparks *et al.* 1997 plate III figure 11.24, Smellie in press). Ash from that plume was deposited on the Falkland Islands and Bird Island (Smellie in press). Under similar atmospheric conditions, similar sized and larger plumes could reach as far as the Scotia Sea. However, circulation models suggest that plumes ejected to low stratospheric altitudes would only cross the polar vortex with great difficulty (Pierce and Fairlie 1993).

1.6.1.3 South Sandwich Islands.

The South Sandwich Islands are built on oceanic crust created at the back-arc spreading centre formed by the Scotia Sea Rise over the last 8 m.y. (Baker 1990). There are 11 main islands in the group. Ten of the islands lie on a single arcuate axis which is parallel to the axis of the South Sandwich Trench situated 100 km to the east.

Basalt is the dominant rock type of the South Sandwich Islands, accounting for 70% of the total volume. The remaining volume of rock is dacitic or andesitic with the 1962 submarine eruption of the Protector Shoal producing the only example of rhyolitic rock in the island chain (Baker 1990). On average 60% of the total volume is made up of lava and 40% by tephra.

Potassium-argon dating of samples from different islands give age ranges for the whole arc between 3.1 ± 0.1 Ma and 0.3 ± 0.1 Ma (Baker 1990) and the whole arc is probably younger than 5 Ma. Although the islands are uninhabited and rarely visited, eruptive or fumarolic activity has been observed on 8 of the 11 islands, suggesting that volcanic centres in the island arc are highly active.

In general, alkali metal concentrations are low in the South Sandwich Islands lavas in comparison with other island arcs. However, the range of total alkalis and their abundance relative to silica varies considerably between islands (Pearce *et al.* 1995).

1.6.1.4 Graham Land

Several volcanic centres are located along the north-western tip of Graham Land (Smellie 1990). Potassium–argon dating has established that several of these volcanoes were active during the Late Pleistocene, with dates as young as < 0.2 Ma (del Valle *et al.* 1983). Larsen (1894) described Christensen Nunatak, at Seal Nunataks on the east flank of Graham Land, as being 'in full activity' and abundant black and red tephra were seen covering the ice around Murdoch Nunatak; also at Seal Nunataks (Gonzáles-Ferrán 1983). These observations have since been disputed on the grounds that the tephra was windblown and there are no primary landforms preserved (Smellie 1990, Smellie and Hole 1997).

Due to the small sizes of the volcanoes and high sedimentation rates in the Scotia Sea it is unlikely that the Northern Graham Land volcanoes will have contributed any significant thickness of tephra to the short cores being examined in this thesis.

1.6.2 Potential Sources contributing tephra to the Bellingshausen Sea

1.6.2.1 South Shetland Islands and Graham Land

As well as being potential tephra sources for the Scotia Sea cores, the Quaternary volcanoes of the Northern Antarctic Peninsula and the South Shetland Islands are the closest volcanoes to the northern Bellingshausen Sea sediment drifts. The westernmost of the sediment drift cores investigated is located <1000km from Deception Island. The presence and influence of the East Wind Drift driving coastal currents and drifting pack-ice (Figure 1.8) suggests that tephra from even relatively small-scale eruptions have the potential to be transported as far as the sediment drifts.

1.6.2.2. Marie Byrd Land

The volcanoes of Marie Byrd Land form a coherent province with distinctive petrological characteristics and spatial and chronological patterns of volcanic evolution. The province has a bimodal, sodic alkaline lineage dominated by basaltic rocks and felsic differentiates (LeMasurier 1990). The province contains 18 large central volcanoes and 30 small satellitic volcanic centres (Figure 1.11). At least three
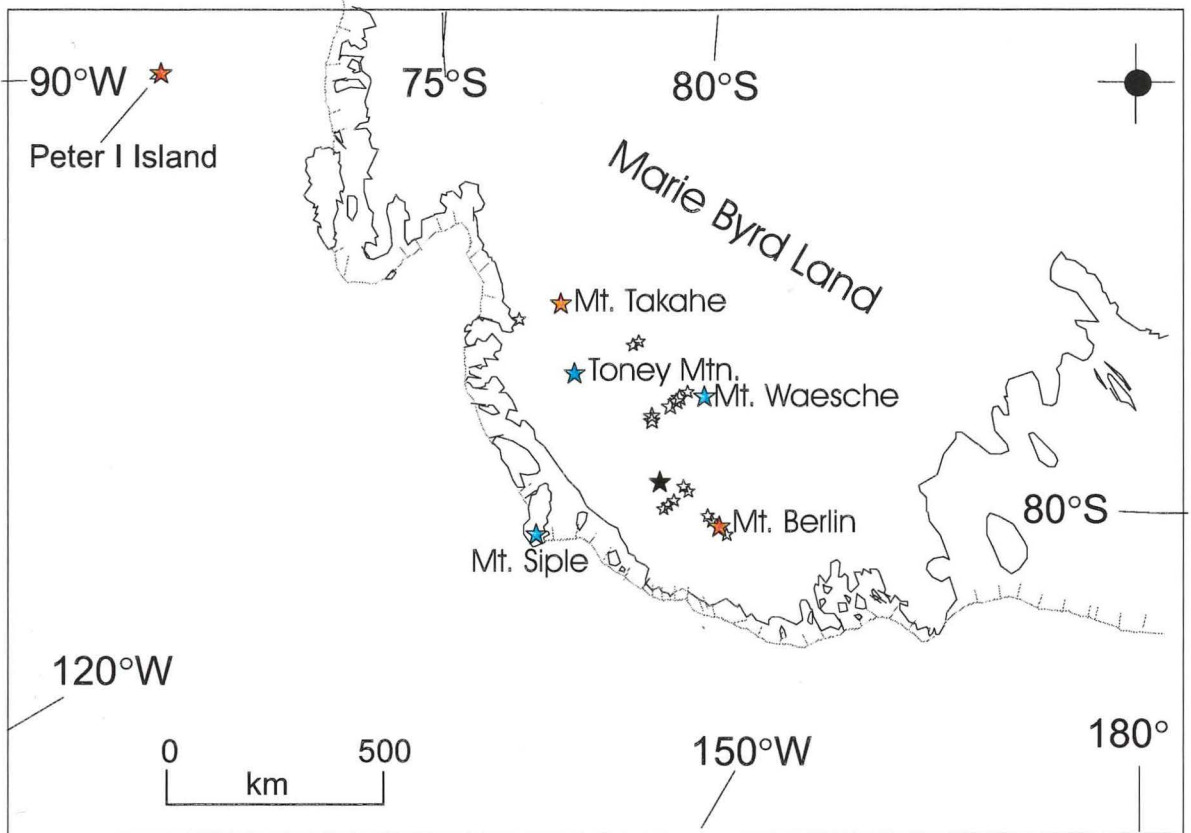
Figure 1.11 Map showing location of volcanoes in the Marie Byrd Land
Volcanic Province. Red symbols indicate active volcanoes, blue symbols
indicate volcanoes that are possibly active. Dormant (white) and extinct
(black) volcaoes are not individually named. Satellitic cones are not shown.
The oceanic island Peter I Island is also shown.

of the volcanoes (Mt. Berlin, Mt. Waesche and Mt. Takahe) are probably active. All three have been identified as sources of tephra found in ice cores and blue ice (see above) although no eruption has been observed. Two more centres are thought to have been active during the Quaternary (Toney Mtn. and Mt. Siple) (LeMasurier 1990).

Complex relationships exist between the felsic and mafic volcanoes, with felsic activity migrating along linear paths whereas the basaltic rocks show no migration pattern (LeMasurier and Rex 1989). The felsic lavas range compositionally from highly unsaturated (phonolites) to highly oversaturated (trachytes and rhyolites). Intermediate rocks appear to be uncommon except at Mt. Takahe and Mt. Waesche and are most common in the youngest volcanoes (LeMasurier and Wade 1976).

Volcanic activity in the province began at about 28–30 Ma and has become increasingly frequent toward the present with peaks in activity at 8–12 Ma and <1 Ma (LeMasurier 1990). Hyaloclastites are common at the base of the volcanic sequence throughout the region and provide evidence for the existence of a West Antarctic Ice Sheet about 30 Ma. The presence of the alkaline suite suggests that an extensional tectonic environment has affected continental West Antarctica for a large part of the Cenozoic.

1.6.2.3 Oceanic Islands: Peter I Island and the Balleny Islands

The Balleny Islands are frequently surrounded by pack-ice and have not been subject to a systematic geological survey. None of the lavas has been dated but eruption columns were reported in 1839 and 1899 suggesting that the islands are still active (Quatermain 1964). Petrologically the islands consist of basalt, trachybasalt, basanite and hawaiite. The Balleny Islands are located c.5000 km upwind of the nearest study area in this investigation. The inferred low explosivity of the lava types found on the islands suggests that tephra from the Balleny Islands volcanoes would have difficulty reaching the Bellingshausen Sea core sites, although rafting on pack-ice is a possibility.

K-Ar dating of rocks from Peter I Island (0.1 to 0.35 Ma) shows that volcanism responsible for forming the island occurred at the same time as post-subduction, rift

related volcanism in nearby Marie Byrd Land (Prestvik *et al.* 1990). Peter I Island lavas range from alkali basalts and hawaiite to benmoreites and trachytes but the characteristic eruptive style (effusive/pyroclastic) is unknown. The rocks are compositionally distinctive and contain relatively high MgO (7.8–10.2 wt.%) and TiO_2 (3.1–3.7 wt.%) compared to other volcanoes in the region.

1.6.2.4 New Zealand

Investigations of ash layers from South Pacific sediments east and south-east of New Zealand (as far east as 120° W) suggest that New Zealand volcanoes are potential sources of Southern Ocean tephra (see above). Although New Zealand has been ruled out as a source for the Southern Ocean tephra described by many authors (Huang *et al.* 1973, Huang and Watkins 1982, Watkins and Kennett 1972, Froggatt *et al.* 1986, Shane and Froggatt 1992), New Zealand is home to many active explosive calc-alkaline volcanoes which have the potential to inject tephra into the stratosphere. Theoretically (Shaw *et al.* 1974), tephra >32 µm injected into the stratosphere should be able to travel the c.5000 km distance from New Zealand to the most westerly study area examined in this project. However, as noted for the Mt. Hudson eruption, volcanic particles entrained in the upper atmosphere can cross the polar vortex only with great difficulty (Pierce and Fairlie 1993). Evolved calc-alkaline New Zealand volcanoes are therefore possible but unlikely sources for the Bellingshausen Sea tephra layers.

1.7 The samples

Table 1.1 Location of the Scotia Sea and Weddell Sea cores examined.

Core	Latitude	Longitude	Water Depth (m)	Core Length (m)
GC027	61° 47.3' S	40° 08.3' W	3470	4.7
PC029	56° 25.3' S	41° 09.9' W	3369	4.4
GC037	61° 06.3' S	39° 10.7' W	4025	4.1
GC057	65° 57.3' S	49° 23.6' W	3592	1.5
PC063	53° 56.0' S	48° 02.6' W	3956	7.0
PC078	55° 33.0' S	45° 00.9' W	3840	4.2
PC079	56° 45.0' S	43° 16.9' W	3733	8.0
KC081	56° 44.3' S	42° 58.1' W	3662	3.2

Seven cores (GC027, PC029, GC037, PC063, PC078, PC079 and KC081) recovered by BAS during cruises aboard RRS *Discovery* in 1984-1985 and 1987-1988, and RRS *James Clark Ross* in 1992-1993, were chosen to form a 400 km NW–SE transect across the Scotia Sea from the North Scotia Ridge to Jane Basin. Jane Basin breaches the South Scotia Ridge and connects the Weddell Sea with the Scotia Sea (Figure 1.6 and Table 1.1). The selected cores were recovered from depths of 3370 – 4025 m and were all taken from sediment mounds. The mounds are sites of rapid sediment accumulation form suspension and are not subject to turbidity currents (Pudsey 1992, Pudsey and Howe 1998, Howe and Pudsey 1999). The initial core descriptions indicated that each core contained substantial quantities of silt - fine sand material in the approximate size range of the tephra that was being targeted (i.e. >32 µm). Recent publications (Jordan and Pudsey 1992, Jordan *et al.* 1991, Gilbert *et al.* 1998, Pudsey 1992, Pudsey *et al.* 1988) also suggested the presence of numerous ash layers, although no investigation of any of those ashes has previously been undertaken. The core locations lie down-wind and down-current of three potential volcanic source regions: South America, the South Shetland Islands and Bransfield Strait, and northern Antarctic Peninsula (Graham Land). A fourth potential source area, the South Sandwich Islands, lies upwind of the core stations but cyclonic storm tracks passing to the north of the islands could disperse volcanic plumes southward and westward over the Scotia Sea (Mullan and Hickman 1990).

One core station (GC057), from the north-western Weddell Sea is located 400 km east of the Antarctic Peninsula, 400 km east-south-east of a reportedly active volcano at Seal Nunataks (see above), and 620 km south-east of Deception Island. The core was selected as a potential site for the deposition of air-fall tephra and for ice-rafted tephra deposited from melting pack-ice which drifts northward with the Weddell gyre.

Thirteen cores were collected during British Antarctic Survey geological sciences cruise JR19 (March - April 1997) from the sediment drifts in the northern Bellingshausen Sea (Table 1.2). The presence of tephra in drift sediments had previously been established in cores recovered by Osservatorio Geofisca Sperimentale

(OGS) from Drift 7 (January - February 1995, Camerlenghi *et al.* 1997). Four samples of ash from three OGS cores (SED04, SED06 and SED07) were also made available for analysis (courtesy of A. Camerlenghi) (Figure 1.12). A further core (GC114) was also taken to the east of Smith Island (62° 56' S, 62° 07' W). That core station is only 80 km from Deception Island (Figure 1.6).

Five samples of ash were obtained (by C.J.Pudsey) from the Antarctic Research Facility, Florida State University core repository in Tallahassee. One sample (E5-24) was recovered from the distal slope of drift 4 during USNS *Eltanin* cruise 5 (Goodell 1964). Another four ash samples were obtained from cores recovered in the vicinity of Peter I Island in the southern Bellingshausen Sea (Figure 1.12) (USNS Eltanin cruises 11 and 42 (Goodell 1965, Frakes 1971)).

One sample of the Mt. Hudson tephra that fell on the Falkland Islands following the 1991 eruption was provided by J.L. Smellie. The sample was collected for Dr. Smellie by M Booth on 5-6 September 1991, at Fox Bay, West Falkland, Falkland Islands (Figure 1.6). The Mount Hudson ash is the only contemporary air-fall tephra examined in this thesis. As such it serves, not only as an indication of the morphology and chemical composition of recent southern Andean tephras, but also as an indicator of the degree of homogeneity that might be expected from tephra dispersed from a single eruption prior to any post-depositional reworking. However, as this sample represents one point sample from a single eruption, significant meaning cannot be attributed to similarities or differences between this sample and others in this study.
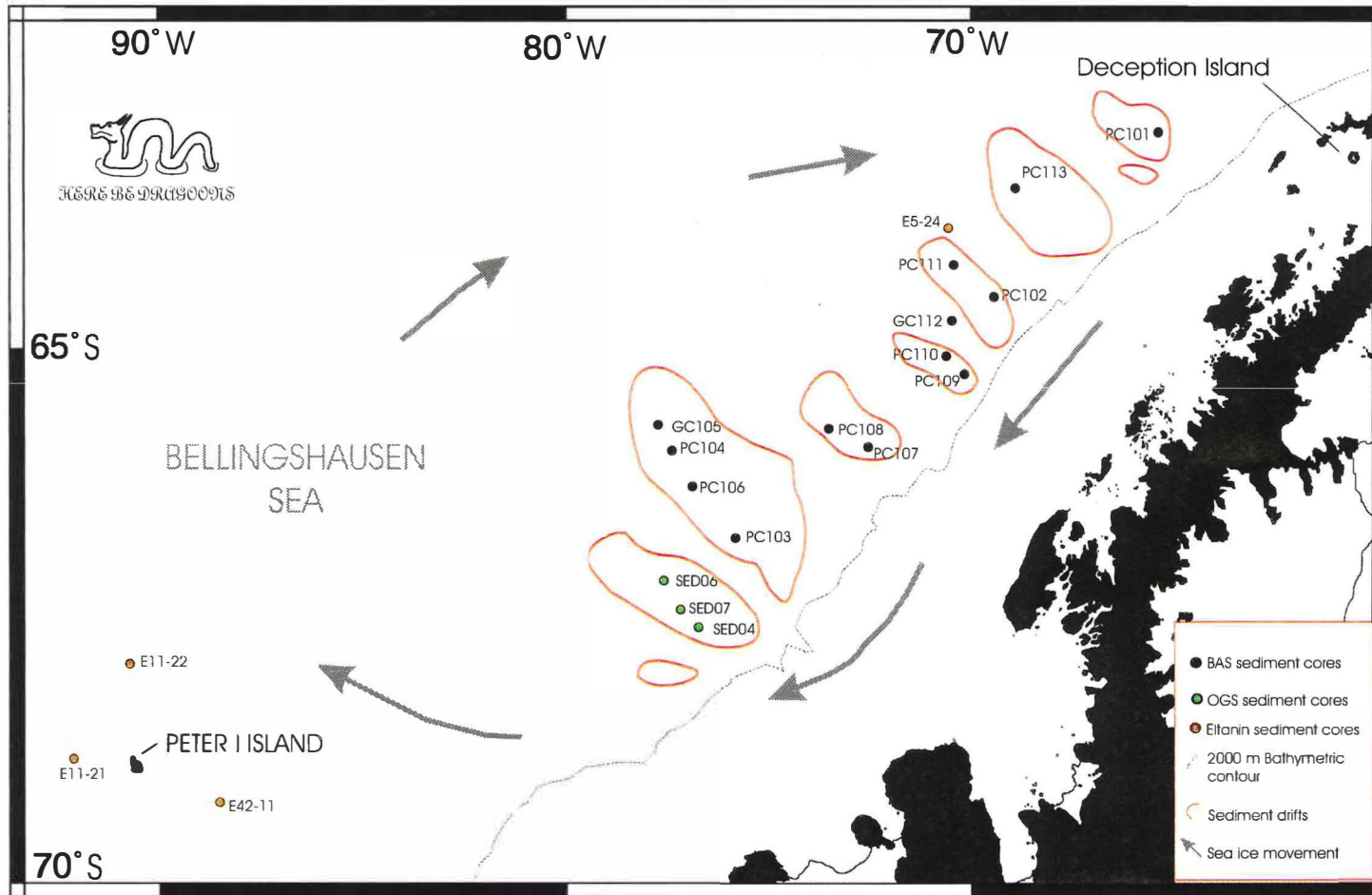
Figure 1.12 Map showing the location of all of the Bellingshausen Sea cores and tephra samples used in this study. Sea lice movement from Keys (1990) (after Pudsey and Camerlenghi (1998), Goodell (1964, 1965), Frakes (1971), BAS unpublished cruise report (JR19). Other observations courtesy of Hobgoblin.

Table 1.2 Locations for the Bellingshausen Sea cores and tephra samples available during the course of this project. Core lengths have been corrected to take into account the splicing of the trigger cores onto the piston or gravity cores.

Core	Latitude	Longitude	Water Depth (m)	Core Length (m)
SED04	67° 37.0' S	76° 58.1' W	3066	5.5
SED06	67° 16.6' S	77° 45.2' W	3606	5.9
SED07	67° 29.3' S	77° 21.1' W	3266	5.8
E5-24	63° 58.0' S	71° 07.0' W	1058	11.6
PC101	63° 05.7' S	65° 30.8' W	2930	6.6
PC102	64° 35.2' S	69° 24.8' W	2787	9.4
PC103	66° 48.4' S	75° 56.8' W	2941	9.4
PC104	65° 55.0' S	77° 13.6' W	3832	5.6
GC105	65° 42.5' S	77° 31.5' W	3986	4.9
PC106	66° 18.8' S	76° 58.7' W	3662	9.3
PC107	65° 54.0' S	72° 39.9' W	3080	8.4
PC108	65° 42.0' S	73° 38.1' W	3601	9.2
PC109	65° 14.5' S	70° 20.0' W	2729	11.0
PC110	65° 08.8' S	70° 35.3' W	3025	7.7
PC111	64° 19.0' S	70° 26.2' W	3357	11.1
GC112	64° 41.0' S	70° 32.5' W	3337	5.4
PC113	63° 27.3' S	68° 58.0' W	3552	10.8
GC114	62° 56.0' S	62° 07.0'W	772	3.4
E11-21	68° 44.8' S	91° 53.0' W	2240	2.5
E11-22	67° 56.4' S	90° 49.9' W	2264	12.8
E42-11	69° 13.1' S	88° 24.4' W	1850	5.0

2 Sample Preparation and Analytical Methods

2.1 Tephra identification and enumeration

Two approaches to locating and quantifying the abundance of tephra in sediment cores were used - a rapid search to identify megascopic ash layers and a systematic, high resolution sampling strategy to locate concentrations of glass defining disseminated tephras.

2.1.1 Rapid Search Technique

Optical examination of the cores for obvious colour and/or textural variations was used to identify megascopic ash layers that could be sampled directly.

It was initially thought that a rapid search technique based on the magnetic susceptibility profile of the sediments could be used to identify concentrations of tephra from disseminated tephra layers. To this end, peaks in the magnetic susceptibility profile were targeted as potential indicators of the presence of significant quantities of volcanic material due their presumed high iron content relative to quartz and biogenic silica rich sediment. However, the volume magnetic susceptibility of the sediment is dependent on the grain size as well as the overall concentration of ferromagnetic minerals, and it was quickly realised that increases in the magnetic susceptibility rarely indicated the presence of tephra. Such increases in the intensity of the signal more commonly indicate the presence of micro-manganese nodule concentrations, ice-rafted debris and aeolian dust (Robinson 1990; Hofmann *et al*. Unpublished; C. J. Pudsey pers comm). It also became apparent that the greatest influence on the magnetic susceptibility of the sediment was the down-core variation in the quantity of non-magnetic biogenic silica.

Although magnetic susceptibility could not be utilised to pinpoint individual disseminated tephra layers, there is a broad correlation in the down-core magnetic susceptibility curves between cores (Figure 2.1 and Pudsey and Howe 1998 figure 7). This approach facilitated the stratigraphical comparison of cores, enabling selected
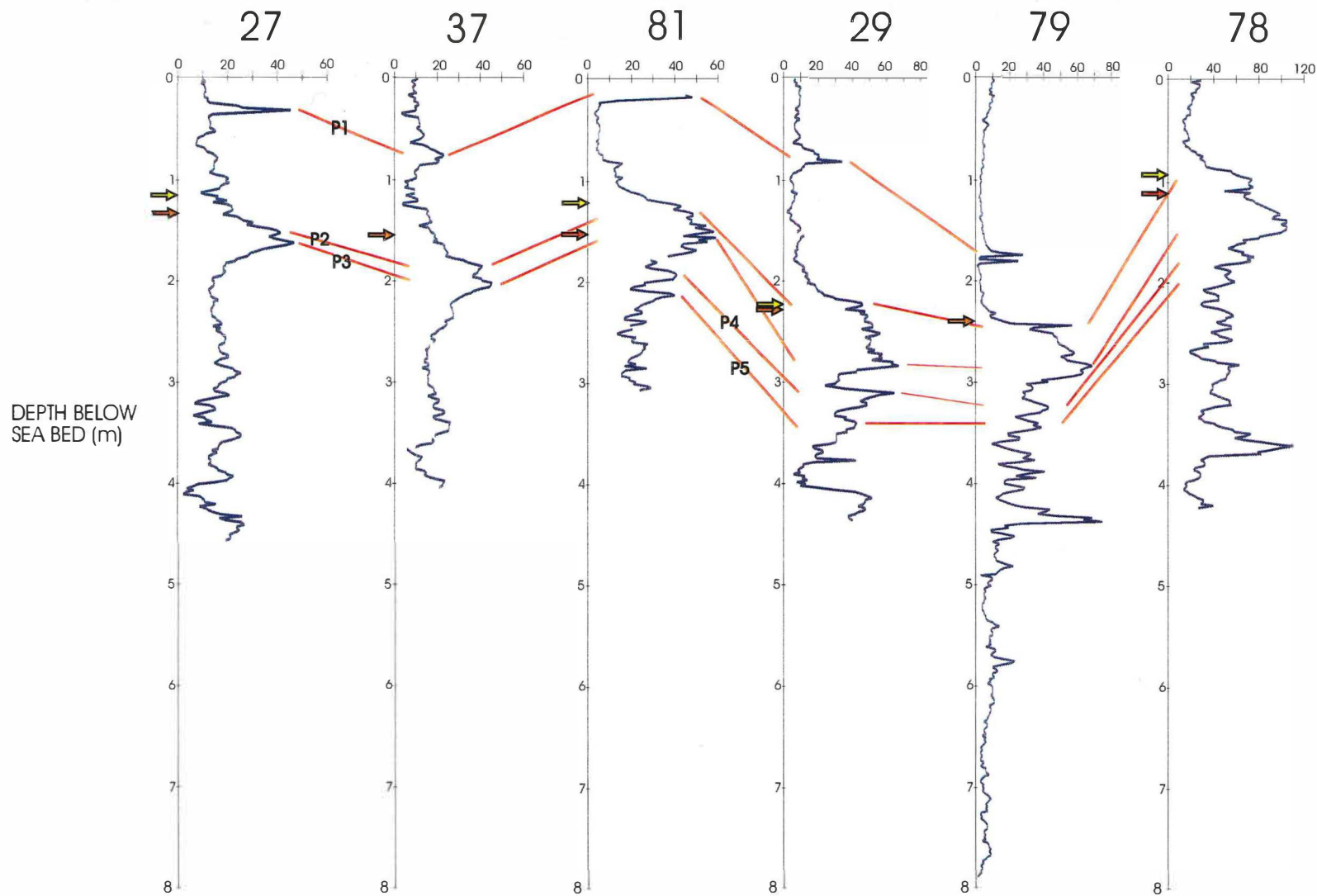
Figure 2.1 Correlatable peaks (P1-P5) in the magnetic susceptibility curves for the central Scotia Sea and Jane Basin cores. Yellow arrow = onset of the Holocene calculated form Ba/Al ratios. Red arrow = Last Glacial Maximum calculated from peak abundance of *Cycladophora divisiana* (after Pudsey and Howe 1998). The megascopic tephra layer corresponds to magnetic susceptibility peak P1.
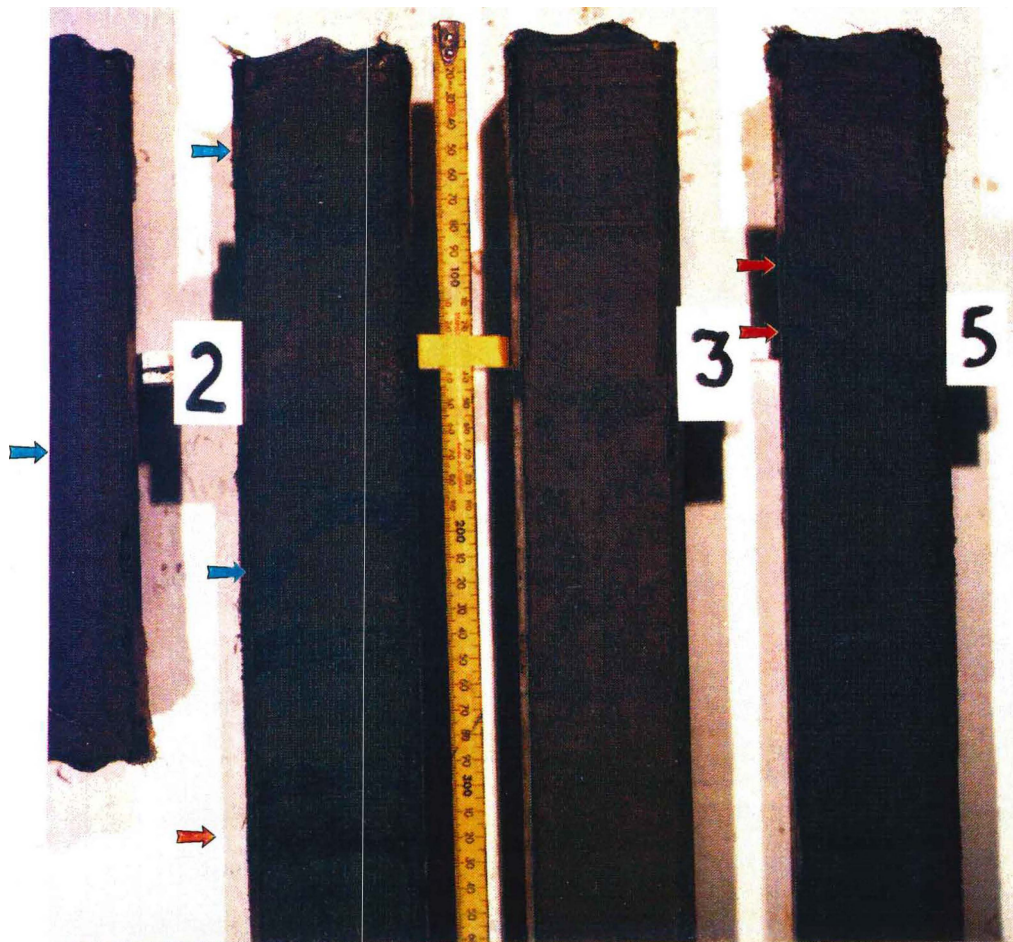
Figure 2.2 Photograph of the upper parts of sections 1,2, 3 and 5 of core GC027. Tephra layers are indicated by blue arrows, not all of which correspond with dark layers. The dark bands indicated by the red arrows are concentrations of micromanganese nodules. Photograph courtesy of C.J. Pudsey.

parts of the cores to be targeted for high resolution sampling to locate positions of peak tephra abundance.

It was also discovered that several of the colour changes observed in the core were the result of increases in the amount of micromanganese nodules in the sediment, rather than volcanigenic material (Figure 2.2). Similarly, several ash layers that had been identified in the original sediment core logs and in the literature (e.g. Jordan *et al.* 1991, Jordan and Pudsey 1992) were not confirmed. One reason for this is that only unaltered glass shards were used to identify tephra layers. Any altered ash layers (e.g. devitrified) were not identified in this study.

In view of the limitations of using down-core magnetic susceptibility measurements and textural and colour changes to identify tephra it was decided to switch to a catch-all high resolution systematic sampling method.

2.1.2 High Resolution Sampling

The second approach involved systematically sampling the sediment and noting the presence or absence of tephra on smear slides using a light microscope. A set-interval high resolution sampling strategy was adopted. As cyclical events were not being sought, it was not necessary to use a time-dependent sampling strategy which would take into account variations in sedimentation rate (c.f. Ledbetter and Ellwood 1976).

For this study 1cm^3 of sediment was sampled every 4 cm. This sampling interval gives a much higher resolution than the 10 cm or 20 cm intervals previously used on these cores. More intensive sampling was also undertaken in order to fix the position of tephra peak abundances. The presence of glass shards was used to identify tephra layers.

Sedimentation rates of 3–17cm - 1000yr^{-1} were calculated by the depth to the Last Glacial Maximum (LGM) and the base of the Holocene (Shimmield *et al* 1993, Pudsey and Howe 1998). Bioturbation is active in the region causing the redistribution of

tephra layers within the core. Pudsey *et al.* (1988) report individual ash laminae disseminated over a vertical distance of 10cm.

2.1.3 Sample treatment

The core locations deliberately targeted deep sea sediment mounds and drifts away from the axes of strong bottom currents and turbidity currents. Fine silt and clay dominate many of the sample sites together with biogenic silica comprising radiolarian tests, diatoms, sponge spicules and echinoid spines in various states of fragmentation. Because biogenic silica and glass have the same optical properties, the shards are very difficult to distinguish without recourse to refractive indices or analytical methods.

As much of the fine silt and clay-grade sediment as possible was removed by wet sieving using a 32 µm sieve. By removing shards less than 32 µm this also largely excludes redeposited glass brought in by aeolian remobilisation. Aeolian material that is greater than 32 µm rarely travels more than a few kilometres from its source (Jackson *et al.* 1971; Middleton 1989). All of the core stations were located in excess of 250 km from the nearest land mass that would have been exposed by lower sea levels at the last glacial maximum and which could have acted as a source of wind transportable sediment. Additionally there would have been very little ice-free land exposed in the northern Antarctic Peninsula region at that time, thus reducing the likelihood of aeolian remobilisation of very fine grained tephra.

Although discarding sediment <32 µm in diameter will also remove very fine tephra particles, they are generally too small for reliable electron-probe microanalysis. For example a 1 µm focused beam will evolve X-rays from a tear-drop shaped area of the sample with an diameter of approximately 5 microns (P.G.Hill pers. comm., J.B. Hunt pers. comm., Reed 1993, 1996). Therefore, when glass shards have been mounted and polished for microprobe analysis they need to be large enough to contain vesicle-free and contaminant-free areas at least 5 microns in diameter beneath a scratch and pit-free surface.

2.1.4 Point Counting

Sieved samples were thoroughly mixed and a small amount was mounted on a microscope slide using Norland Optical Adhesive 61, a colourless, liquid adhesive that cures under ultra-violet light. A cover slip was added before the adhesive was cured.

To identify the ash layers, between 500 and 1000 particles were counted to determine the relative proportions of glass, lithics, biogenic material and opaque minerals in the sieved sample. Similar techniques have also been adopted in other investigations of microtephra (e.g. Fretzdorff 1997).

The lithic and mineral phases were not investigated in this thesis, although important information about the direction and velocity of bottom currents and the provenance of the ice-bergs and hence ice-berg migration routes could be obtained from such a study.

Initially four counts of 250 particles were undertaken on each sample rather than a single count of 300 more commonly used in micropalaeontological and microtephra investigations. A technique that produced constant reproducible results gave greater confidence in the identified peaks of tephra abundance. Later, only two counts of 250 with consistent results were made to halve the counting time without any significant loss in confidence in the data.

The results of the point counting are reported as a percentage abundance of glass, and as a ratio of glass shards to lithics. The latter approach removes the effect of dilution by biogenic silica in the sediment and should distinguish between air-fall tephra layers and concentrations of glass produced by post-depositional processes (e.g. increased sedimentation by ice-berg rafting, reworking and redeposition from the nepheloid layer, or the winnowing of finer material leaving a lag deposit).

In this thesis no attempt was made to identify lithic and mineral grains that may have been deposited directly from the same volcanic plume as the glass. This was due to the small size of most of the lithic fragments and the lack of features diagnostic of origin (e.g. adhering glass, weathered surfaces). Additionally, glacial plucking tends to erode

fragments from the rock surface before any significant chemical weathering can affect the minerals making it difficult to distinguish volcanic ejecta from ice transported and deposited material.

2.2 Methods of Tephra Concentration

Microtephra particles can easily be concentrated from organic-rich sediments by ashing or acid digestion of the organic component (Pilcher and Hall 1992), but they are notoriously difficult to remove from minerogenic sediments (Lowe and Turney 1997). Besides the removal of fragmentary biogenic silica, fine silt and clay by wet sieving, several standard mineral separation techniques were experimented with as a means to concentrate the tephra. In most instances the results were poor and a combination of several complementary techniques was necessary to obtain satisfactory results. In this study the extra time and resources required for the implementation of these techniques could not be justified.

2.2.1 Heavy Liquid Density Separation

Solutions of Di-iodomethane diluted with Dimethylformaldamide were made with densities ranging from 2.2 to 2.7 g cm^{-3}. The specific gravity of volcanic glass is variable and depends on the composition and degree of vesicularity of the shards; it was assumed that basaltic glass has a density close to 2.6 g cm^{-3}, whereas the rhyolitic shards would have a specific gravity in the range 2.4 - 2.5 g cm^{-3} (Lowe and Turney 1997). Unfortunately, these values lie close to those of quartz (2.65 g cm^{-3}) and biogenic opaline silica (1.8 - 2.4 g cm^{-3}) which dominate the sieved sediment. Further complications caused by the buoyancy of the glass due to enclosed vesicles could only be overcome by increasing the length of time the samples were immersed in the solutions. Similar problems to those described above were also reported by Lowe and Turney (1997).

Given the need to have some knowledge of the chemistry of the glass prior to the heavy liquid separation, and the great care needed throughout the process to ensure that all of the glass sub-populations were retained, it was decided that there was little to be gained

from this approach as EPMA is capable of selectively analysing individual glass shards irrespective of their abundance.

2.2.2 Hand Picking and Magnetic Separation

The fine grain size of the sediments and microtephra used in this thesis (typically 32 – 63 µm) proved too small for hand picking, or magnetic separation. Magnetic separation (using a Frantz Isodynamic Magnetic Separator Model L-1) is best suited to grain sizes in the range 125 – 500 µm. Some electrostatic charging of the sample is unavoidable with this technique. When grain sizes are less than 125 µm the small mass of the individual grains cannot overcome the electrostatic charge that they gain, causing the particles to coagulate (Allman and Lawrence 1972).

2.2.3 Chemical separation

An alkali dissolution technique, described by Rose *et al* (1996) was also tried. This treatment worked well in most cases but didn't always remove all of the biogenic silica (see SEM micrograph Figure 2.3). Dyson (1996) also used this procedure on Antarctic tephra from lake sediments but had even less success. Although this technique concentrated the glass through the removal of biogenic material, the detrital lithic grains and crystals were unaffected. Additionally, there are concerns over element mobility and compositional contamination, Rose *et al* (1996) do not recommend the use of this procedure prior to probe analyses.

The over-riding conclusion resulting from the trial of these methods of tephra concentration is that, due to the small sample size and particle size of the microtephra, few of the techniques worked sufficiently well to justify the additional resources and time required. Point counting smear slides was sufficient to identify potential ash layers, and even impure samples were amenable to shard specific electron microprobe analyses.
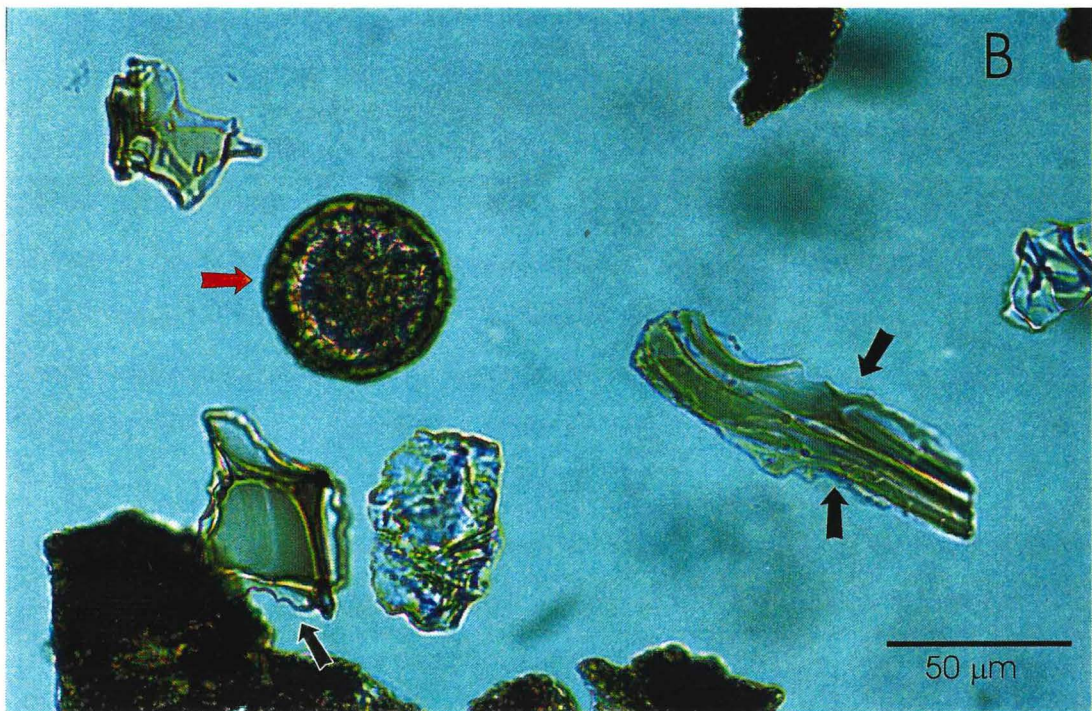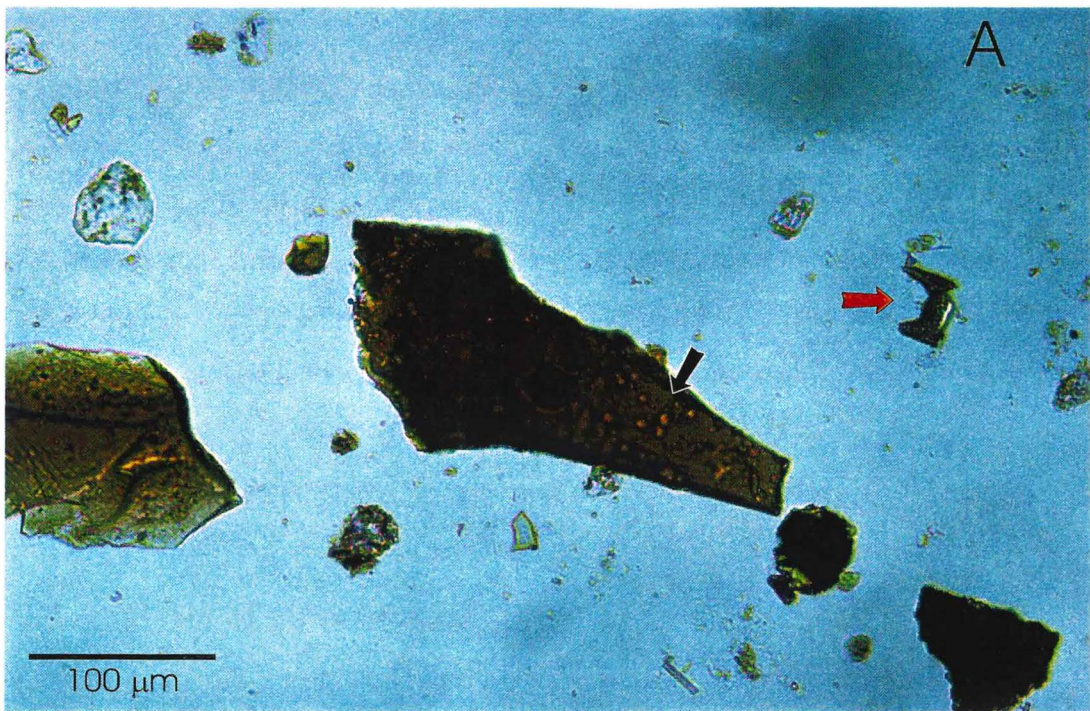
Figure 2.3 Attempted concentration of glassy tephra through the selective chemical attack, resulted in damage to the surface of the tephra prior to the complete removal of biogenic silica. (A) Surface pitting on a basaltic shard (black arrow). (B) Dissolution of the edges of basaltic shards (black arrows). Red arrows indicate partially dissolved biogenic siliceous tests.

2.3 Sample preparation for analytical determinations

After wet sieving, sample grains were mounted in epoxy resin (Araldite) and hand-lapped with loose carborundum powder before being machine polished using a suspension of $0.3\mu m$ alumina (Allen 1984). Most samples had an acceptable polish after three 20 minute polishing cycles. However, some required four cycles whilst others were polished after only two, although there was no clear reason why this should be so. After each cycle the sample surface was examined using a light microscope under reflected light to check for remaining surface scratches.

2.4 Analyses of glass shards

Colour, morphology and vesicularity were recorded during the point counting. Additional information on surface features was gathered using a scanning electron microscope (Leica Cambridge S360).

2.4.1 Major Element Determinations

The chemical composition of glass shards in this project was determined primarily by Electron Probe Microanalysis (EPMA) at the University of Edinburgh, Department of Geology and Geophysics, utilising a Cambridge Instruments Microscan Mk V. This two-spectrometer probe was set up to analyse nine major elements (Na, K, Si, Ti, Mg, Mn, Fe, Ca and Al) in pairs with a repeat analysis of sodium making up the final pair.

It is possible to set the electron microprobe to analyse additional elements with atomic weights greater than 20 but the analytical time would be extended accordingly. Each individual shard could, therefore, be analysed more accurately. However, it would not be possible to analyse as many different glass shards from each ash layer in the time available and the overall composition of the ash layer would be less well constrained. This is especially important given the acknowledged compositional variability of shards in the tephra layers examined.

Individual glass shards were analysed under beam conditions tailored to minimise the effect of alkali mobility (Hunt and Hill 1993, Hunt unpublished, P.G. Hill pers. comm.). These are: a 1 μm focused beam, accelerating voltage of 20 kV and beam

current of 15 nA. Counting times were 10 seconds per pair of elements. Repeated experimentation (e.g. Hunt (1997) has established that sodium and potassium become highly unstable under the heating effect of the beam and tend to migrate away from the point of beam incidence. This effect continues for as long as the sample is exposed to the beam (Autefage and Couderc 1980; Keller 1991; Hunt and Hill 1993; Hunt unpublished) and is particularly noticeable in the more evolved shards. The purpose of the repeat analysis of Na is, therefore, to gauge the stability of the shards.

During the analytical period, the beam position and X-ray emission peak position were checked daily. Pure metal and stable mineral standards were used for calibration at the beginning of every analytical session and regularly during sessions. Raw X-ray counts were converted into the equivalent weight percent oxide stoichiometrically using the ZAF correction procedure (Sweatman and Long 1969, Reed 1975, Potts 1987, Hunt unpublished).

In recent years, there have been several attempts to develop a set of idealised EPMA conditions for glass shard analysis and debate is far from settled. A detailed discussion of proposed analytical conditions are found in Froggatt (1992), Hunt and Hill (1993, 1994), and Bennett (1994).

Contrary to the approach suggested by INQUA (Froggatt 1992), analyses were not recalculated to 100 %. This was in large part due to the restricted range of elements analysed. The nine elements selected make up the bulk of the composition but, in addition to undetermined amounts of water, other elements, such as chlorine and phosphorus, can also be present in quantities up to several tenths of a weight-percent oxide. Therefore, any recalculation that did not take account of the undetermined elements would produce misleading and potentially erroneous correlations.

Another INQUA recommendation that has not been adopted in this thesis is the routine acceptance of low totals. Hunt and Hill (1993) give reasons why low totals should not be accepted, and in this thesis individual analyses where the total weight percent of the oxides is less than 95 % were rejected. If a wide range of analytical totals is accepted, a

greater data scatter will result, it will become harder to correlate accurately the individual ash layers and less confidence can be placed in such correlations.

2.4.2 The use of other analytical equipment

Some experimental analyses were conducted on an Oxford Isis 300 Energy Dispersive Spectrometer fitted to the Leica Cambridge S360 scanning electron microscope at the British Antarctic Survey. Probe conditions were again designed to minimise damage caused by the heating effect of the beam. These conditions were: a 5 μm rastered beam, accelerating voltage of 20 kV and beam current of 3.9 nA. Elemental spectra were collected simultaneously over a 20 second live count time. Initially the results from the Oxford Isis probe seemed promising based on analyses of a fragment of Lipari Obsidian (obtained from J.B.Hunt) and on duplicate analyses of one of the tephra samples previously analysed on the Edinburgh microprobe and on obsidian samples from Deception Island, South Shetland Islands, that had previously been analysed by XRF (courtesy of J.L.Smellie). Results for the Lipari obsidian and Deception Island obsidian were compared to published analyses (J.L. Smellie pers. comm., Hunt *et al.* 1995) and results of the tephra were compared with analyses of the same sample obtained from the Cambridge Instruments Mk V. Despite initial success in obtaining comparable results between the SEM and the EMP, mechanical and software problems meant that the SEM results were not as repeatable as those of the EMP. In particular the overall higher totals and lower precision in determining the concentration of the elements present in lower concentrations (total oxide weight percent less than 0.15%) led to unacceptable results compared with those obtained on the Edinburgh instrument. Therefore, for the sake of comparability; all the results reported in this thesis are those obtained on the Cambridge Instruments Mk V at Edinburgh.

NB It should be noted that this discrepancy does not imply that the Edinburgh results are 'right' and those obtained at BAS were 'wrong'. However, as the compositional differences between individual ash layers are subtle, it was important to maintain the same probe conditions for all samples during this first attempt to characterise systematically the composition of the Scotia Sea ash layers. It should also be noted that the Lipari analyses conducted at BAS would plot amongst the 'most accurate' laboratories in Figure 1D of Hunt and Hill (1996) and are a close compositional match for previously published Lipari Obsidian analyses (Hunt *et al.* 1995). During the course of this work, further analyses

of samples of Lipari obsidian were conducted at Edinburgh. Results of these analyses reveal consistent variations (lower SiO_2 and lower Na_2O) from results reported by Hunt and Hill, suggesting that as a unit the Lipari obsidian might not be as homogeneous as was originally thought (pers. comm. P. G. Hill, A. Dugmore; Hunt and Hill 1996 c.f. Hunt *et al.* 1995). Another important observation in Hunt and Hill (1996 p236) is that the calculation of SiO_2 content in rhyolitic glass shards can differ by up to 1 % depending on which correction procedure is applied to the raw data.

2.4.3 Ion Microprobe Analysis.

Some ash layers were also selected for additional analysis for a wider range of elements. Ion Microprobe analyses were conducted on several samples using a Cameca ims-4f microprobe at the Department of Geology and Geophysics, University of Edinburgh. The ion probe was used to determine the concentration of 9 minor and trace elements that were identified as being of particular importance in determining the source of individual eruptions.

2.5 Dating tephra layers

Beside making use of previously obtained proxy dating methods such as sediment Ba/Al ratios and previous and concurrent biostatigraphical dating, several samples were submitted for $^{40}Ar/^{39}Ar$ and ^{14}C dating.

2.5.1 $^{40}Ar/^{39}Ar$ Dating

Six samples of volcanic ash from the sediment drifts were sent to Lamont Doherty Earth Observatory, Columbia University, Palisades, New York where a new Argon-Argon chronology facility has recently been commissioned. Although the initial age estimate of 'last interglacial' based on the stratigraphical position of the tephra layer is at the upper limit of this dating technique the high potassium content of the glass (see Chapter 4 - analytical results) was considered sufficiently high to increase the chance of a successful result. Microlites are rare in the northern Bellingshausen Sea tephras and no sanidines were observed with adhering glass to suggest that they were contemporaneous with the glassy tephra. Individual sanidines could not therefore be submitted for $^{40}Ar/^{39}Ar$ dating.

2.5.2 ^{14}C Dating

The low potassium content and considerably younger age of the Scotia Sea tephra required an alternative dating method. As calcareous organisms are absent from the sediments under investigation, the total organic carbon content of the sediments was dated. Seventeen bulk sediment samples were sent for ^{14}C analysis at the NERC Radiocarbon Laboratory, East Kilbride, UK. The samples comprised material from core tops and sediment from immediately above or below ash layers. All of the samples contain at least 0.5% organic matter (C. J. Pudsey pers. comm.).

In addition to the assumptions and constraints involved in radiocarbon dating terrestrial material, dating marine-derived samples is subject to further complications. The oceans' carbon reservoir is up to sixty times greater than that of the atmosphere (Skirrow 1975). Due to the increased reservoir capacity, the residence time of ^{14}C in the ocean is much greater than in the atmosphere, and a considerable amount of ^{14}C decay occurs in the oceans. That results in a natural ^{14}C deficiency in marine specimens relative to their terrestrial counterparts (Gordon and Harkness 1992). Additionally, global ocean waters are not equally mixed. Vertical and lateral variations in ^{14}C concentration leads to geographical variations in the apparent age of water masses (Linick 1978, Gordon and Harkness 1992).

Analysis of bulk sediment samples are further constrained as oceanic sediments receive contemporaneous inputs of material derived from a variety of sources which may exhibit a range of ages. Post-depositional reworking, such as bioturbation, may also mix recently deposited organic carbon with older material. The average age of material arriving at the sea bed can be calculated by the analysis of bulk samples collected in sediment traps suspended above the sea floor. The effect of bioturbation can be a deduced by comparing the age of core top samples with sediment trap ages.

3. Results I – The Bellingshausen Sea

Systematic sampling of the Bellingshausen Sea cores was not undertaken during this study. Megascopic ash layers were identified visually by examination of the split core sections and confirmed by examination of smear slides taken directly from each suspected layer. Potential tephra layers were identified through microscopic examination of smear slides made from samples taken at systematic intervals down core. Descriptions of the colour, vesicularity and morphology of the glass shard types were made. Glass rich samples were then subject to grain discrete electron probe micro-analysis (EPMA). Additionally some shards were analyzed by ion microprobe analysis.

3.1 Northern Bellingshausen Sea

Geophysical surveys of the continental rise west of the Antarctic Peninsula have identified nine large mounds elongated roughly perpendicular to the shelf edge and interpreted as sediment drifts (Rebesco *et al* 1996; 1997, Pudsey and Camerlenghi 1998, Camerlenghi *et al* 1997). The mounds are separated by turbidity current channels and a further channel separates them from the continental slope (Figure 1.8). Figure 1.12 shows the positions of the drifts relative to the Antarctic Peninsula and the locations from which cores were obtained (core locations also listed in Table 3.1). No systematic search for disseminated tephra was conducted on the northern Bellingshausen Sea cores and only megascopic ash layers were investigated.

3.1.1 Existing core material

Two perpendicular transects on drift 7 were cored by the Osservatorio Geofisco Sperimentale during the cruise SEDANO -1 aboard RV *OGS-Explora* (Jan-Feb 1995). Detailed examination of these cores is still in progress. A 2–5 cm-thick ash layer was observed in three of the cores (SED04, SED06 and SED07). The ash was identified by colour and textural differences with the surrounding sediment. One sample was taken from each of SED04 and SED07, and two samples were taken from SED06 to investigate colour variations between the upper and lower part of the ash layer. Each of the samples were examined optically before being subject to grain discrete EPMA.

One sample of an ash layer found in piston core E5-24 recovered during the September-November 1962 cruise of USNS *Eltanin* (Goodell 1964) was also provided for examination in this project. At the time of core collection the sediment drifts had not been identified, however, the latitude and longitude (63° 58' S, 71° 07' W) locate this core on the northern tip of drift 4 (figure 1.12).

3.1.2 Newly acquired cores

During the course of this project, the British Antarctic Survey undertook Marine Geosciences cruise JR19 aboard RRS *James Clark Ross*. During this cruise 9 days were spent piston and gravity coring in the Bellingshausen Sea. Thirteen gravity and piston cores were recovered from the sediment drifts (Figure 1.12 and Table 3.1). A single ash layer up to 5cm thick was observed in 7 of those cores. The remaining cores are currently under investigation for the presence of diseminated tephra layers.

Table 3.1 Location of cores from the northern Bellingshausen Sea drifts.

Core	Latitude	Longitude	Water depth	Comments
SED04	67° 37.0' S	76° 58.1' W	3066	Drift 7 (medial)
SED06	67° 16.6' S	77° 45.2' W	3606	Drift 7 (distal)
SED07	67° 29.3' S	77° 21.1' W	3266	Drift 7 (medial)
E5-24	63° 58' S	71° 07' W	1058	Drift 4 (distal)
PC101	63° 05.7' S	65° 30.8' W	2930	Drift 1 (proximal)
PC102	64° 35.2' S	69° 24.8' W	2787	Drift 4 (proximal)
PC103	66° 48.4' S	75° 56.8' W	2941	Drift 6 (proximal)
PC104	65° 9.2' S	77° 22.6' W	3832	Drift 6 (distal)
GC105	65° 42.5' S	76° 31.5' W	3986	Drift 6 (distal)
PC106	66° 18.8' S	76° 58.7' W	3662	Drift 6 (medial)
PC107	65° 54.0' S	72° 39.9' W	3080	Drift 5 (medial)
PC108	65° 42.0' S	73° 38.1' W	3601	Drift 5 (distal)
PC109	65° 14.5' S	70° 20.0' W	2729	Drift 4a (proximal)
PC110	65° 08.8' S	70° 35.3' W	3025	Drift 4a (medial)
PC111	64° 19.0' S	70° 26.2' W	3357	Drift 4 (proximal)
GC112	64° 41.0' S	70° 32.5' W	3337	Drift 4 (medial)
PC113	63° 27.3' S	68° 58.0' W	3552	Drift 3 (distal)
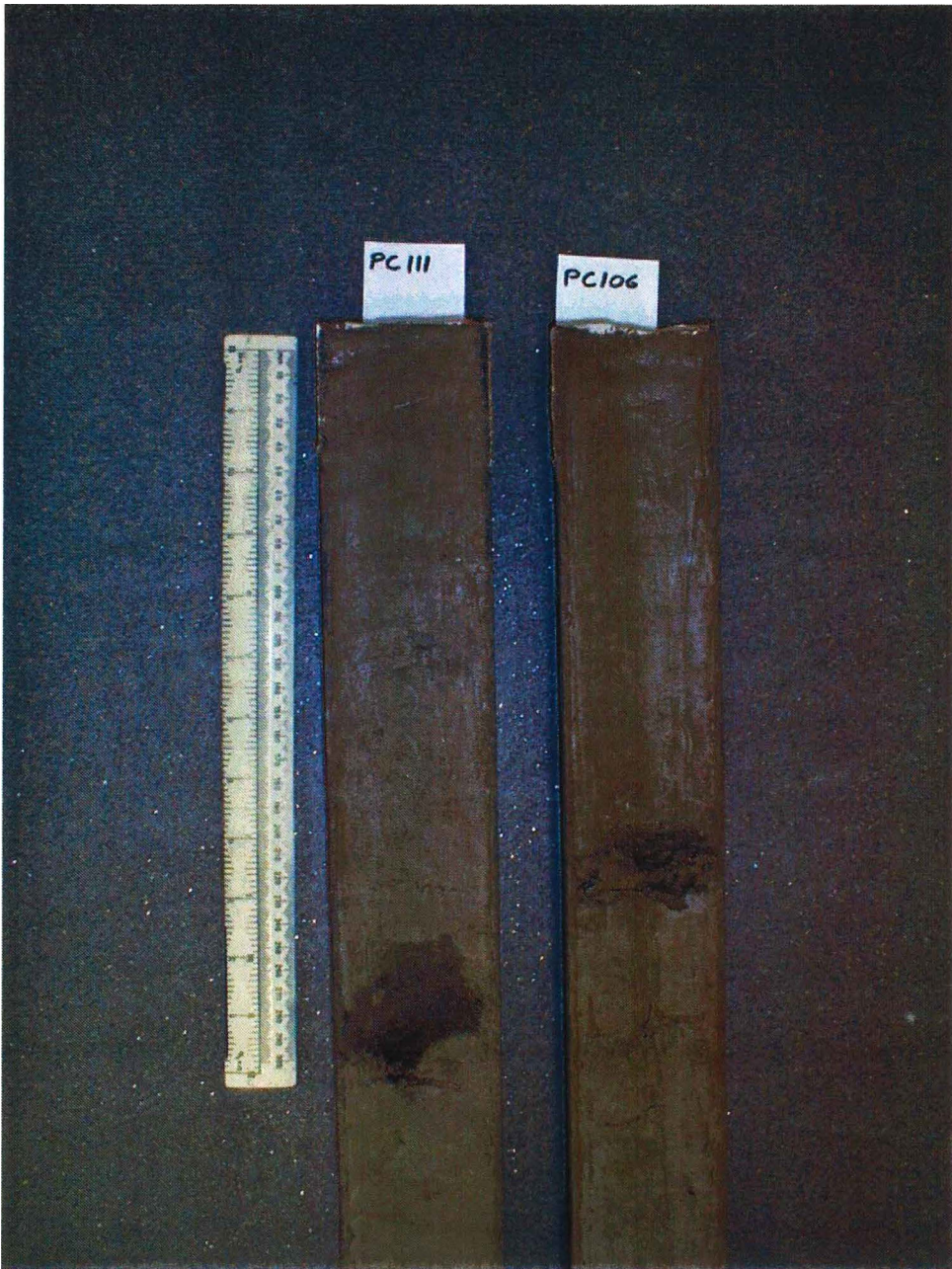
Figure 3.1 Unlike several of the Scotia Sea cores, the tephra layers in the northern Bellingshausen Sea sediment drift cores are clearly marked by colour and textural differences with the surrounding sediment.

3.1.3 Optical examination of the samples

Macroscopic examination of the cores show that each of the tephra layers were marked by an obvious colour and textural change (Figure 3.1). The basal contacts are sharply defined in many of the cores, whereas the upper contacts are more diffuse due to bioturbation. No obvious grading was visible in any of the ash layers. The disturbance caused during coring is evident from the appearance of the ash layers in Figure 3.1.

Sieved samples from the centre of each layer contain up to 95 % glass with minor lithic and crystal components (4 - 5 %) and small quantities of biogenic material (less than 0.5 %). The tephras are coarse and poorly sorted, with vitric shards ranging from 35 μm up to 620 μm across. The shards are equant to elongate and consist of colourless, highly vesicular glass (Figure 3.2) (c.f. glass shards from the other study areas described below e.g. figures 3.5, 4.2 and 4.5). Occasional spherical to sub-rounded vesicles are present but the majority of shards contain elongate pipe-like vesicles (coefficient of sphericity $C_s = 0.0$ (Sheridan and Marshall 1987)). The shards appear fresh and the surfaces are largely free from signs of abrasion, although the twisted shard and vesicle shapes suggest that they were subject to deformation during magmatic fragmentation (Figure 3.3 C + D). Crystals are not present within the glass, but many of the shards show adhering dust (Figure 3.3 A + B).

The long axes of 100 randomly chosen shards from each of ten of the ash layers were measured to investigate whether there was any variation in mean shard size either between sediment drifts or between proximal and distal locations on the drifts. The mean long axis values are summarized in Table 3.2 and shown in Figure 3.4. The whole data set is reproduced as Appendix 3.
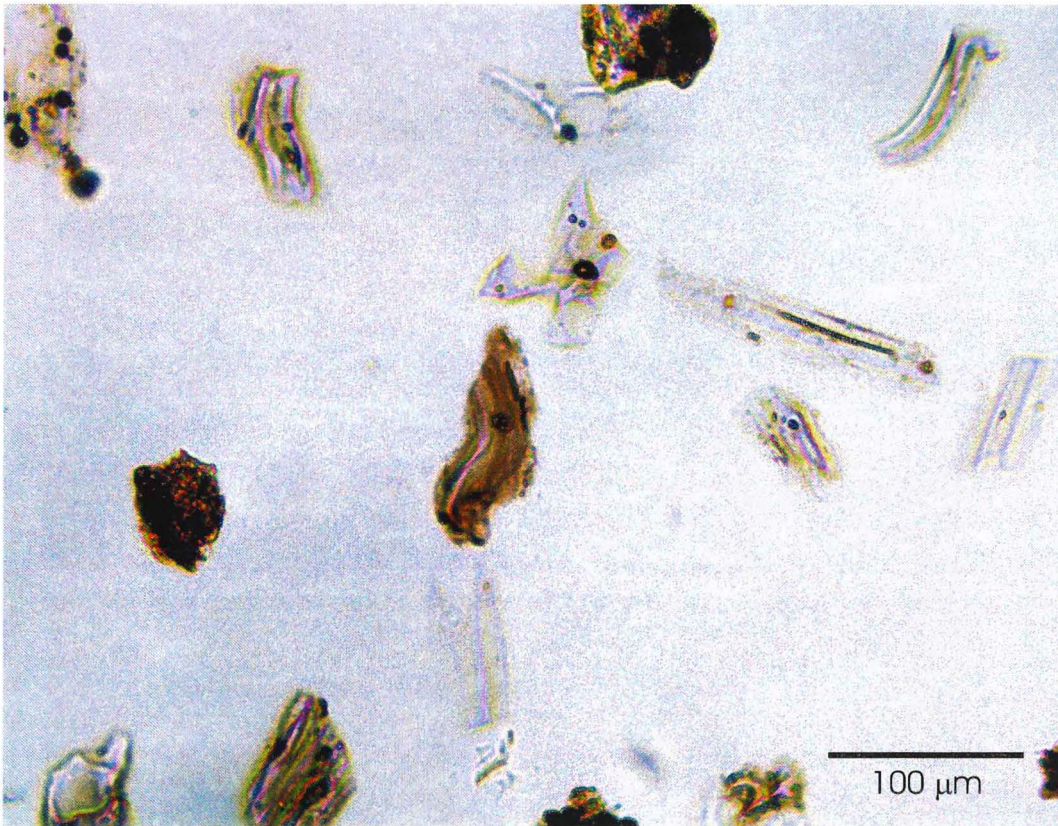
Figure 3.2 Highly vesicular shards with elongate vesicles from PC108. Some shards exhibit twisted morphologies indicating plastic deformation before cooling. Shards appear darker in this image than under normal light microscopes due to the lighting conditions demanded for the photomicrograph. These shards should be compared with the basaltic shards from the Scotia and southern Bellingshausen seas.
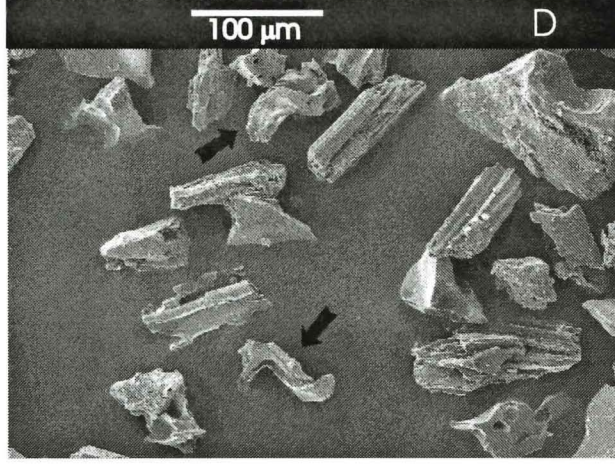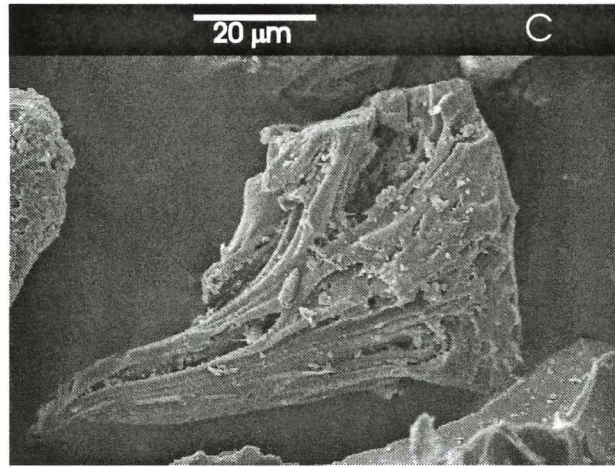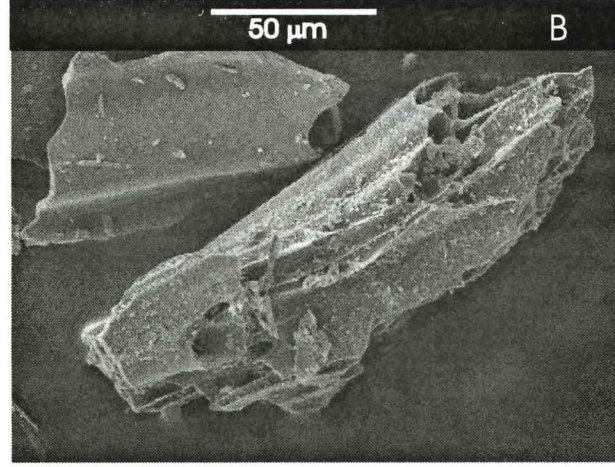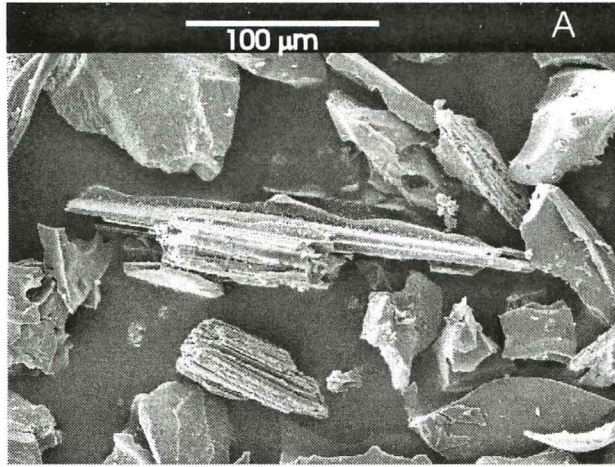
Figure 3.3 Scanning electron micrographs of northern Bellingshausen Sea tephra. (A) Elongate pipe-like vesicles. (B) Adhering dust particles. (C) Post-fragmentation deformation of glass shard. (D) Distorted, plastically deformed shards (arrowed).
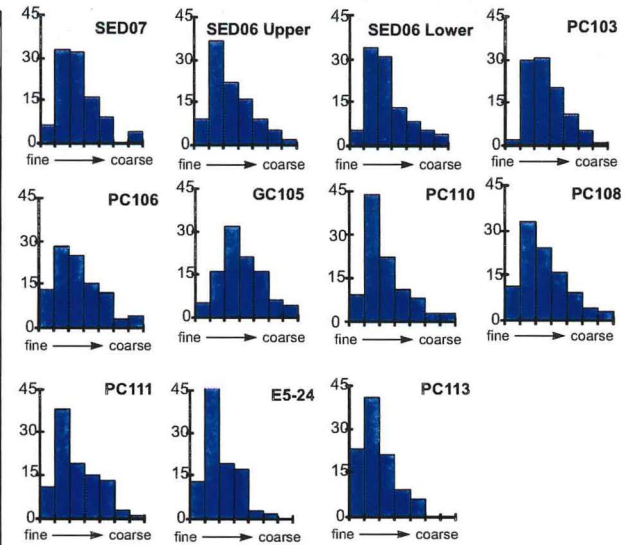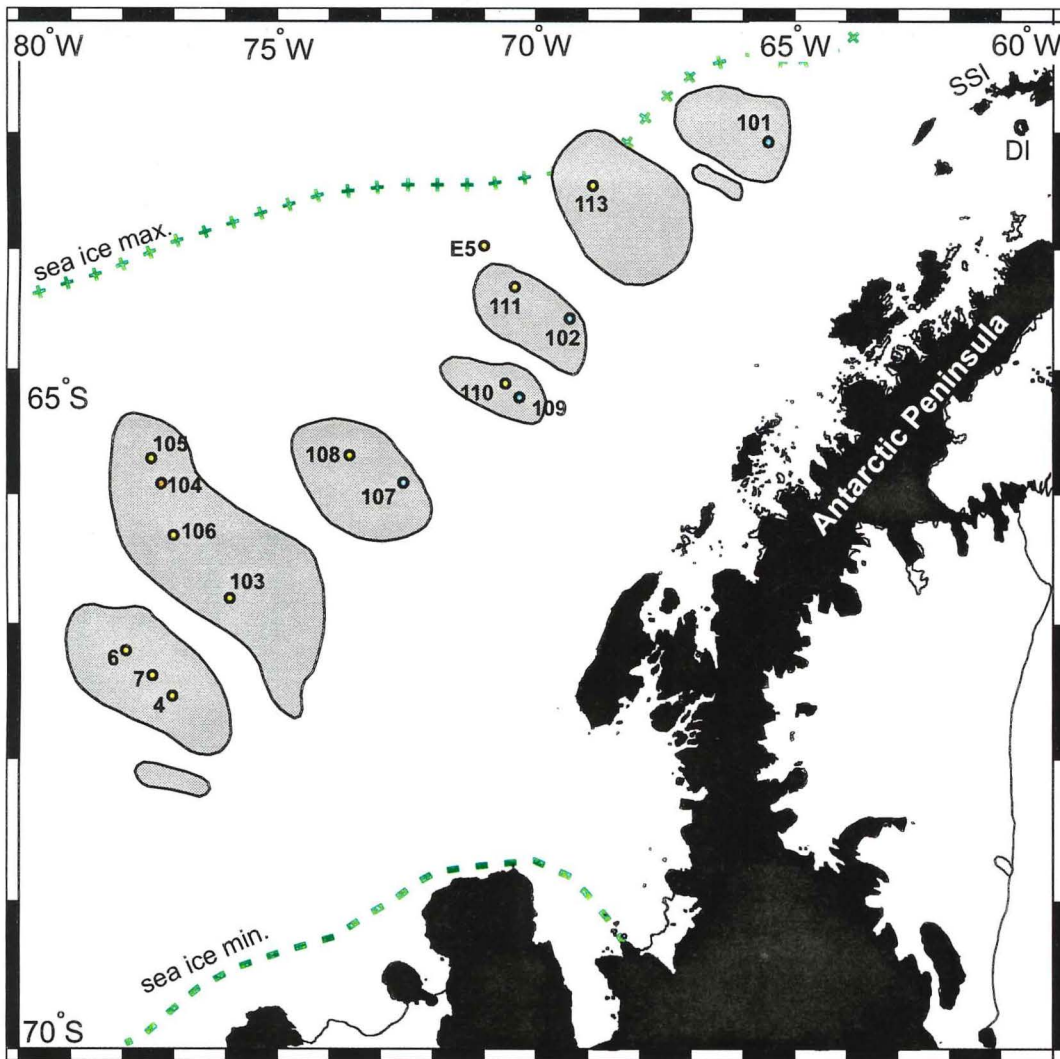
Figure 3.4 Grain size histograms for the northern Bellingshausen Sea cores investigated (yellow symbols on map). The x-axes indicate grain size classes in 32μm divisions from 32μm to +224 μm. Frequency is shown on the y-axes. Cores containing disseminated ash are represented by blue symbols and can be separated geographically from the cores containing the megascopic tephra layer.

Table 3.2 Summary of glass shard length showing the number of shards in each size category and the mean shard length. For each sample $n = 100$. SD = standard deviation.

	SED06 Lower	SED06 Upper	SED07	PC103	GC105	PC106	PC108	PC110	PC111	E5-24	PC113
32-63 μm	5	9	6	2	5	13	11	9	11	13	23
64-95 μm	34	37	33	30	16	28	33	44	38	46	41
96-127 μm	31	22	32	31	32	25	24	22	19	19	21
128-159 μm	13	16	16	20	21	15	16	11	15	17	9
160-191 μm	8	9	9	11	16	12	9	8	13	3	6
192-223 μm	5	5	0	5	6	3	4	3	3	2	0
>223 μm	4	2	4	1	4	2	3	3	1	0	0
Mean (μm)	119.6	110.5	113.5	120.9	130.2	117.1	113.0	107.4	111.9	97.7	91.0
(SD)	(69.9)	(44.2)	(42.1)	(38.6)	(45.4)	(56.5)	(47.7)	(48.8)	(46.53)	(33.5)	(38.9)

During microscopic examination of the SEDANO and JR19 cores it was noted that in the majority of cores the ash layer occurred at the base of a 1 metre thick unit, named Unit C by Pudsey and Camerlenghi (1998). Unit C is brown, rich in diatom valves, and has a low susceptibility to an induced magnetic field. It can be traced across all of the drifts and has been used as a correlatable stratigraphic horizon.

On going microscopic investigation of the cores collected during JR19 revealed significant quantities of disseminated ash in cores PC107, PC109, PC102 and PC101 (C.J. Pudsey pers. comm.). Examination of these tephra layers reveals that glass shards in cores PC102, PC107 and PC109 bear a striking similarity to those seen in the megascopic ash layers described above. This morphological similarity is augmented by stratigraphic data which suggest that these three disseminated tephra occur in the same sedimentary unit as the megascopic ash (i.e. Unit C).

There are a few exceptions to this conjuction of ash layer and diatom-bearing brown mud unit. In core SED06 two ash layers were identified by Pudsey and Camerlenghi (1998). The upper ash layer, which occurs at the base of Unit C, is a thin disseminated ash that was only recognized after microscopic examination of smear slides. This glass-rich layer has not yet been analysed. The lower ash layer is visible and occurs below base of Unit C. It was sampled and analysed as part of this thesis.

The megascopic ash from SED06 varied in colour from the base to the upper surface and a sample of each was taken for optical and EPMA analysis. The long axes of shards from the upper and lower samples from the ash layer were also counted separately.

Detailed investigation of the cores revealed two further ash layers that may prove to be significant but which were not fully explored during this thesis. One of these is an ash layer identified by a concentration of glass shards (16.8 % of the sieved sediment) in the sand fraction. It is located at a depth of 5.20 m below sea floor (mbsf) in core SED04. As SED04 did not completely recover Unit C this ash may be a correlative of the upper ash layer in SED06 rather than the visible ash layer seen lower down in that core. In core PC101, recovered from drift 1, no megascopic ash layer was found and although Unit C is present, it is thin and examination of sand fraction smear slides have failed to locate any concentrations of volcanic glass within that unit. Recent detailed microscopic examination of PC101, however, has revealed a concentration of vitric shards at a depth of 5.40 m (mbsf), 1.70 m below the base of Unit C. The shards appear dark brown in transmitted light. They contain crystals and have spherical to elliptical vesicles. These shards were found too late to be analysed by EPMA as part of this thesis. However, based on morphology, colour and stratigraphic position they clearly represent a different ash layer from that found at the base of Unit C and may possibly emanate from an entirely different volcanic source.

Morphologically these shards resemble basaltic shards seen in the southern Bellingshausen Sea, Scotia Sea and near Smith Island (see below and Chapter 4). Stratigraphically this brown glass layer lies below the unit which elsewhere contains the clear glass. The detailed analysis of this ash layer should be seen as an urgent objective for continuing research into the Bellingshausen Sea sediment drifts.

3.1.4 Note on analytical results and presentation

Early results obtained from electron probe microanalysis indicated that vitric shards from individual tephra layers are compositionally very variable. Therefore, wherever possible at least 15 shards were analyzed to characterize fully the tephra and avoid

compositional bias through over-representation of single shards (c.f. Hunt 1996 unpublished Ph.D. thesis).

Of the nine oxides routinely analysed, manganese oxide (MnO) and aluminium oxide (Al_2O_3) appear to vary by insignificant amounts even between source regions. They are therefore largely excluded from subsequent comparisons of ash layers either within or between study areas in this and subsequent chapters. As silica is the most abundant oxide it has the greatest scope for showing variation between tephra layers. In igneous classifications, silica is frequently plotted against Na_2O, K_2O or total alkalis (e.g. Wilson (1989)). This classification is of limited use in distinguishing between compositionally similar eruptions from a single source, but K_2O: Na_2O ratios plotted against SiO_2 provide a good discriminator of source region (see below).

3.1.5 Compositional analysis - Major oxides

Analyses of all the samples reveal a trachytic composition with little variation within or between samples (Table 3.3; Appendix 1). Silica shows the greatest variance (mean SiO_2 contents of the samples range from $60.54 \pm 1.07\%$ to $62.07 \pm 0.73\%$). K_2O values are high ($4.84 \pm 0.13 \%$ to $5.08 \pm 0.17 \%$), whereas MgO and CaO values are low. Both samples from the lower ash layer located below Unit C in SED06 (representing colour variations between the top and base of this tephra) were very similar and correlate well with the other samples of megascopic ash from the drifts within the error of the analysis.

Shards from SED04, which were presumed to represent a different ash layer due to the lower percentage of glass present and its stratigraphic position, are also compositionally very similar to the megascopic tephra. Although the overall mean composition of that ash is within the range and error of the other samples, it shows the greatest variance from the mean composition with either the highest mean value or the lowest mean value for 6 of the 9 major oxides (Table 3.3).

Table 3.3 Mean values and standard deviations (in parentheses) of major oxide geochemical compositions of glass shards from from the northern Bellingshausen Sea sediment drifts as determined by EPMA. Probe conditions 1 μm focused beam, 20 kV accelerating voltage, 15nA beam current, 10 second count times. * All iron calculated as FeO.

	SiO_2	TiO_2	Al_2O_3	FeO^*	MnO	MgO	CaO	Na_2O	K_2O	Total	*n*
E5-24	62.24 (0.52)	0.68 (0.04)	14.53 (0.18)	7.47 (0.21)	0.28 (0.04)	0.27 (0.02)	1.27 (0.07)	6.22 (0.33)	4.96 (0.11)	97.92	24
SED04	60.74 (0.36)	0.53 (0.04)	15.14 (0.28)	7.64 (0.39)	0.33 (0.04)	0.16 (0.05)	1.14 (0.11)	6.82 (0.42)	4.87 (0.14)	97.37	28
SED06/U	61.67 (0.80)	0.65 (0.04)	14.64 (0.29)	7.48 (0.19)	0.28 (0.04)	0.29 (0.02)	1.24 (0.07)	6.75 (0.32)	4.97 (0.15)	97.97	15
SED06/L	61.87 (0.93)	0.67 (0.03)	14.61 (0.18)	7.23 (0.33)	0.26 (0.03)	0.30 (0.02)	1.18 (0.08)	6.67 (0.19)	4.94 (0.16)	97.73	10
SED07	62.07 (0.73)	0.66 (0.04)	14.64 (0.18)	7.30 (0.18)	0.28 (0.05)	0.28 (0.03)	1.22 (0.07)	6.50 (0.56)	4.97 (0.09)	98.20	12
PC103	61.39 (0.51)	0.69 (0.06)	14.77 (0.14)	7.34 (0.18)	0.27 (0.03)	0.28 (0.05)	1.23 (0.0.7)	6.20 (0.33)	4.99 (0.14)	97.16	16
GC105	61.37 (0.54)	0.64 (0.05)	14.71 (0.38)	7.32 (0.36)	0.26 (0.04)	0.28 (0.03)	1.21 (0.08)	6.10 (0.53)	4.87 (0.13)	96.76	15
PC106	60.63 (0.64)	0.65 (0.04)	14.72 (0.98)	7.27 (0.18)	0.25 (0.03)	0.27 (0.04)	1.18 (0.08)	6.25 (0.24)	4.84 (0.13)	96.06	12
PC108	61.53 (0.91)	0.65 (0.05)	14.82 (0.56)	7.25 (0.47)	0.25 (0.05)	0.26 (0.02)	1.24 (0.09)	6.16 (0.32)	5.08 (0.17)	97.24	23
PC110	61.13 (0.73)	0.67 (0.06)	14.85 (0.39)	7.38 (0.21)	0.27 (0.03)	0.27 (0.03)	1.24 (0.05)	6.21 (0.25)	4.89 (0.16)	96.91	13
PC111	61.55 (0.56)	0.65 (0.04)	14.75 (0.24)	7.34 (0.20)	0.26 (0.05)	0.28 (0.03)	1.24 (0.08)	6.11 (0.32)	4.94 (0.14)	97.12	25
PC113	60.54 (1.07)	0.66 (0.06)	15.20 (0.95)	7.30 (0.16)	0.26 (0.03)	0.28 (0.03)	1.20 (0.09)	6.03 (0.29)	4.96 (0.22)	96.43	10

3.1.6 Compositional Analysis - Trace elements

Trace elements were determined by ion microprobe for two representative samples of the ash, from cores PC108 and PC111.

The abundance of each of the elements was calculated relative to silica. Mean silica contents of 61.53 % and 61.55 % were assumed for shards in PC108 and PC111 respectively (Table 3.4). The results of the analyses are shown in Table 3.4 and Appendix 2. The analyses show a high degree of uniformity.

Table 3.4 Mean and standard deviation values (in parentheses) of selected trace elements from two of the sediment drift tephra layers. All values are given in parts per million (ppm). *excludes one highly discrepant Ni analysis.

	Ni	Rb	Sr	Y	Zr	Nb	Ba	Ce	n
PC108	72 (±11)	122 (±7)	10 (±1)	62 (±1)	971 (±17)	169 (±4)	40 (±1)	234 (±6)	16
PC111	79 (±24)*	120 (±5)	10 (±2)	61 (±1)	960 (±19)	166 (±4)	40 (±3)	233 (±5)	10

The composition of the shards and in particular the levels of zirconium, barium, strontium and cerium contrast strongly with the composition of bulk sediment samples taken from the drifts. Unpublished data shows selected typical values of the composition of bulk samples from core SED06 (Table 3.5). These data suggest that the presence of tephras could be detected through trace element analyses of bulk sediment samples.

Table 3.5. Previously unpublished bulk sediment analyses (analysis by XRF). All values are parts per million. It should be noted that barium is a proxy of biological productivity and increases in Ba have been taken to indicate climatic amelioration (data from C.J. Pudsey).

Depth (mbsf)	Ni	Rb	Sr	Y	Zr	Nb	Ba	Ce
3.49	35	97	248	28	138	10	954	47
4.20	38	90	248	27	183	13	2082	57
4.86	27	96	248	28	156	10	815	64
5.52	28	93	241	30	137	8	535	61

3.2 Southern Bellingshausen Sea

Four samples of visible ash layers found in three cores recovered between 80 and 150 km from Peter I Island (a shield volcano) during USNS *Eltanin* cruises 11 and 42, southern Bellingshausen Sea (Figure 1.12). The samples were collected from the University of Florida marine core repository in Tallahassee, USA, by C. J. Pudsey. Two ash layers occur in core E11–21 at depths of 5cm and 150cm. Neither ash layer in this core was identified in the original core description, they were both identified by C.J.Pudsey. One ash layer was identified in each of cores E11–22 (9.13-9.20 mbsf) and E42–11 (0.20-0.45 mbsf). Both ash layers were described originally as black sands (Goodell 1965).

3.2.1 Optical examination of the ash

Optical examination of the tephras revealed lithic fragments, large brown glass shards and scoriaceous glass up to 4 mm across. The glass is transparent and contains large crystals (up to 320 µm) and microlites (1-3 µm) (figure 3.5). The morphology of the shards contrasts strongly with those from the sediment drifts (Figure 3.4).

Only loose samples of the tephra were examined, although copies of the original core descriptions were also available. For core E11-21-1 no mention is made of the presence of either volcanic ash layer in the core. The sample taken from 0.05 mbsf occurs in a 0.12 m thick unit described as poorly sorted sand with a sharp basal contact. Similarly the ash from 1.50 mbsf occurs in a unit described as a sand with irregular contacts, containing red mineral grains and foraminifera.

The ash layer in core E11-22 (9.13 – 9.20 mbsf) was noted and described as 'Volcanic sand. Angular mineral fragments and glass shards. Some grains show very good conchoidal fracture. Lower color [sic] and texture contact is very sharp'(Goodell 1965). The upper boundary of the ash layer is not mentioned.

The basal contact in core E42-11 is similarly sharp, although it is deformed while the upper contact is described as 'gradational, burrowed and mottled' (core description of C.J. Pudsey 1996).
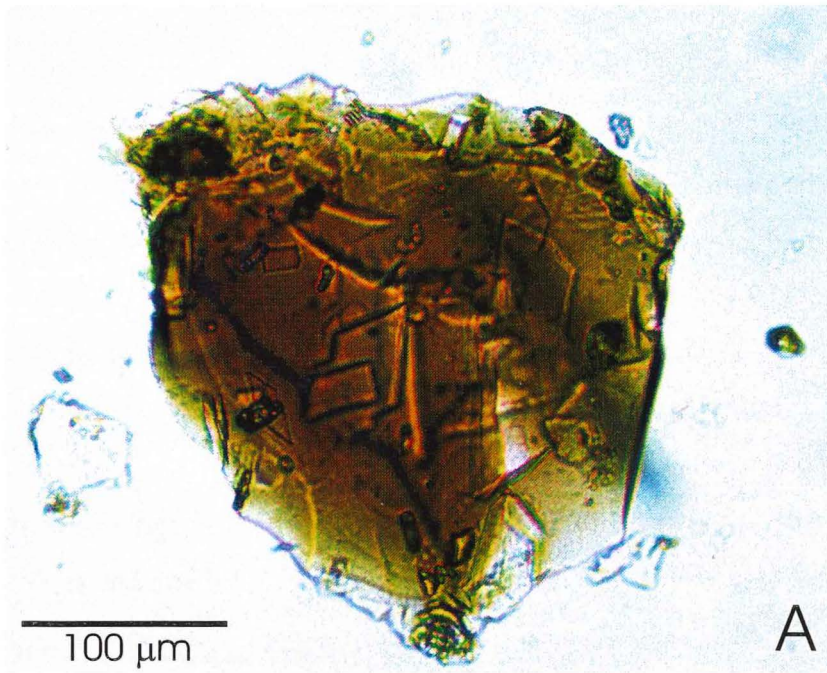
Figure 3.5 (A)Light micrograph of blocky, basaltic tephra from core E11-22. The large microlites are clearly visible in the image. The chipped edges typical of southern Bellingshausen Sea tephra are also visible at the top and bottom of this shard. (B) Shard from the same tephra layer showing conchoidal fractures and chipped edges. Surface pits are also present but difficult to pick out at this level of magnification.
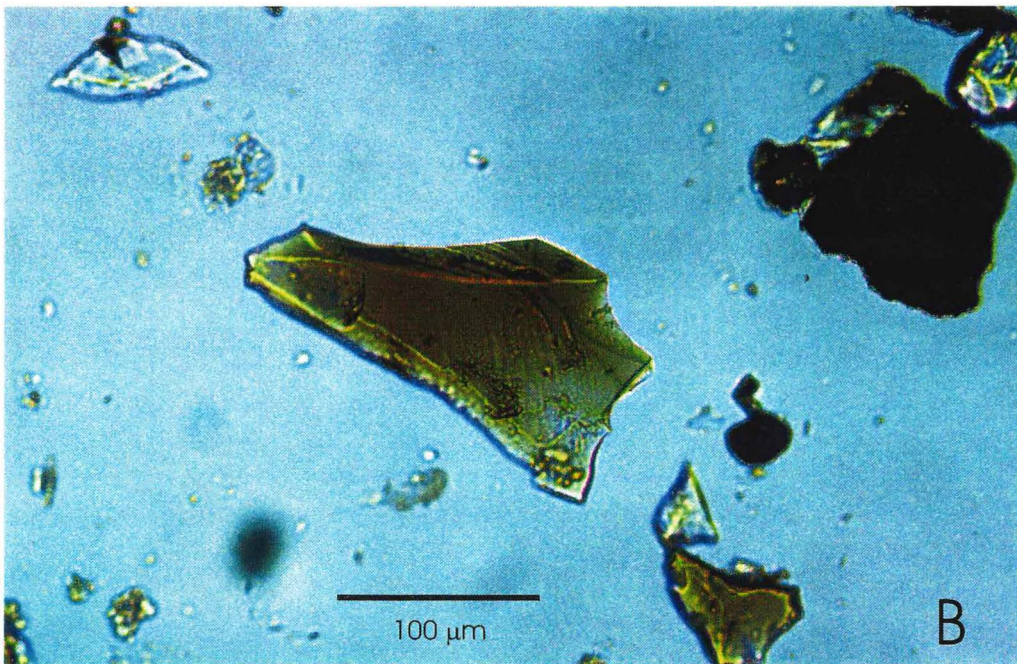
Microscopic examination of each of the four tephras shows that they consist of large, crystal-rich, blocky glass shards. Under transmitted light the glass colour ranges from pale yellow-brown to dark brown. Vesicles are rare, spherical and vary in size between samples (Figure 3.5). Vesicles from glass found at 5cm depth in core E11-21 are small, typically 5-25 μm in diameter, as are those in core E11-22 (9.13 mbsf). However, vesicles from the ash layer at 1.50 mbsf in core E11-21 are most commonly 40-50 μm in diameter. Some shards have cuspate edges, indicating that large vesicles were present during fragmentation. Many of the shards have chipped, fractured and pitted surfaces (e.g. Figure 3.5). Several scoriaceous fragments up to 2 mm across were present in each of the tephras and one lithic fragment 4 mm across with adhering glass shards was also found.

3.2.2 Analytical Results

The shards are compositionally variable but predominantly basaltic and all samples have elevated levels of FeO_T and TiO_2 c.f. the northern Bellingshausen Sea and Scotia Sea tephras (Appendix 1). Silica contents are much lower and more variable than in shards from the sediment drifts. TiO_2 values (2.98 ± 0.43 to 3.83 ± 0.47 wt. %) are much higher than in any of the sediment drift and Scotia Sea tephras (see below). Mean compositions are shown in Table 3.6. The ratio of K_2O/Na_2O can be used to distinguish between the northern and southern Bellingshausen Sea tephras (Figure 3.6).

Table 3.6 Mean values and standard deviations (in parentheses) of major oxide geochemical compositions of glass shards from the southern Bellingshausen Sea tephra layers as determined by EPMA. Probe conditions 1 μm focused beam, 20 kV accelerating voltage, 15nA beam current, 10 second count times. * All iron calculated as FeO. † = basaltic shards only, †† = basaltic andesite shards.

	SiO_2	TiO_2	Al_2O_3	FeO*	MnO	MgO	CaO	Na_2O	K_2O	Total	n
E42-11/42	48.61 (2.23)	3.58 (0.56)	14.02 (1.69)	10.95 (0.37)	0.13 (0.03)	5.25 (0.55)	9.45 (0.56)	3.35 (0.22)	1.14 (0.36)	96.48	16
E11-21/5	48.28 (1.53)	3.83 (0.47)	13.68 (0.39)	10.89 (0.52)	0.14 (0.04)	5.08 (0.46)	9.56 (0.48)	3.72 (0.29)	1.37 (0.41)	96.55	28
E11-21/150	49.24 (1.03)	3.64 (0.35)	13.91 (0.77)	10.74 (0.77)	0.14 (0.03)	5.01 (0.33)	9.51 (0.54)	3.68 (0.20)	1.37 (0.33)	97.25	23
E11-22/193	49.82 (0.91)[†]	3.08 (0.43)	14.03 (0.54)	10.61 (0.56)	0.14 (0.03)	5.17 (0.56)	8.92 (0.50)	3.50 (0.12)	1.19 (0.29)	96.47	21
	52.43 (0.33)[††]	2.68 (0.43)	14.49 (0.76)	9.49 (0.62)	0.12 (0.03)	4.43 (0.56)	7.97 (0.78)	3.55 (0.11)	1.42 (0.32)	96.63	5
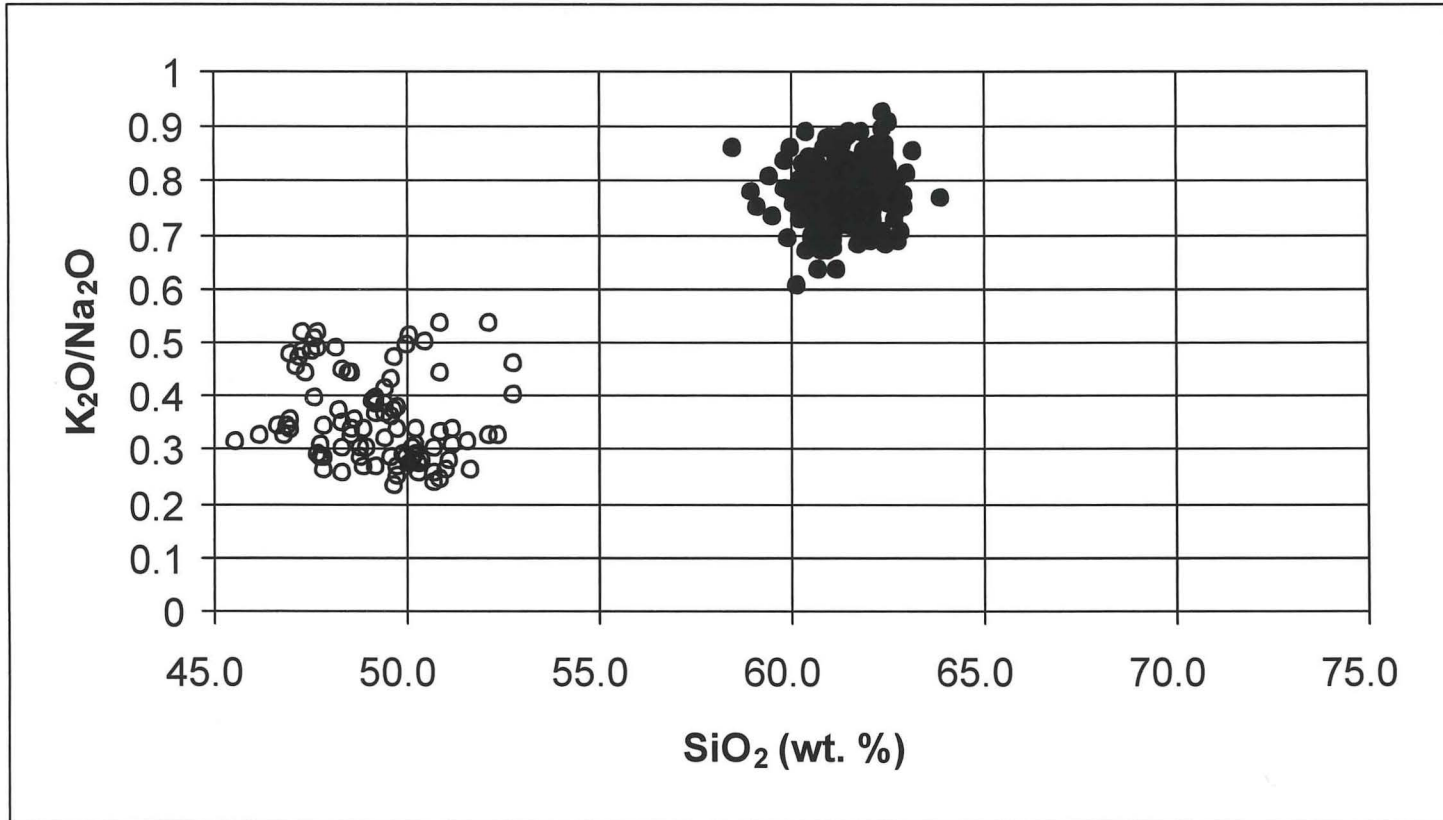
Figure 3.6 Comparison of K_2O/Na_2O ratios in the visible ash layers from the southern Bellingshausen Sea (open circles) and northern Bellingshausen Sea (filled circles).

4. Results II – The Scotia Sea and The Jane Basin

4.1 Identification of disseminated ash layers

No core from the Scotia Sea or Jane Basin or the Weddell Sea was found to contain more than 1 megascopic tephra layer.

Disseminated tephra layers were found to be fewer and with much lower glass shard concentrations than was anticipated. Moreover, there was a high background level of tephra between ash layers. Virtually every smear slide contained at least a few shards of glass. In the Scotia Sea cores background levels of tephra were usually about 1-2% glass in the sieved sediment. An arbitrary minimum value of 4% glass (roughly corresponding to a glass/lithic ratio of 1:10 or more) was adopted as the minimum value for potential tephra layers.

4.1.1 Weddell Sea

Only one core (GC057) was examined from the Weddell Sea. The sediments in core GC057 are dominated by clay and fine silt to the extent that from a dried sample weighing approximately 2.0 g, typically less than 0.01 g of material remained after sieving. Examination of the sieved sediment revealed very few vitric shards anywhere in the core and no concentration of glass at all.

This core was therefore excluded from any further investigation.

4.1.2 Northern Scotia Sea

Core PC063 is the most northerly examined in this project (53° 56.0' S). At that latitude the sea bed (3956 m) lies close to the Carbonate Compensation Depth. Core-top sediment contains about 15 % carbonate, mainly in the form of fragmentary foraminifera tests within the fine fraction (Pudsey and Howe 1998). However, carbonate preservation only occurs in Holocene age sediments meaning that older tephra layers cannot be dated by comparison with the oxygen isotope record.

No visible ash layers were found. Possible, disseminated tephra layers occur but with very low glass shard concentrations (less than the adopted minimum value of 4%). The greatest concentration of glass was 3.2% of the sieved sediment and only 7 samples contained >2.0% glass. Most samples contained between 0.4 and 1.4 % glass (Figure 4.1). Although they didn't contain as much as 4% glass the 7 samples with the greatest concentration of glass were selected for further investigation. Most of the glass shards are blocky and many shards show signs of hydration (surface rinds and cracks) and abrasion.

The uppermost potential tephra layer is located within the Upper Biogenic Unit as defined by Pudsey and Howe (1998) and the next two (which form a double peak) occur at a depth (0.62 – 0.70 mbsf) which corresponds to the beginning of magnetic susceptibility peak P2, at the boundary between the Upper Biogenic Unit and the Terrigenous Unit of Pudsey and Howe (1998). The fourth and fifth potential ash layers also occur within the Terrigenous Unit. The sixth peak with highest glass abundance, and a seventh peak lower down in the core occur at depths that have not been described in the literature. The magnetic susceptibility peak P1 is not seen in core PC063 (Howe and Pudsey 1999).

During the examination of the smear slides it was observed that between the first and second potential ash layers two slides contained a number of large shards (> 150 μm) of two distinct types. One type of glass was brown and the other was colourless. Both types were blocky and poorly vesicular to non-vesicular. They constitute only 1.2 % of the sample.

4.1.3 Central Scotia Sea cores

Only one megascopic ash layer was observed in cores PC029, PC079 and KC081 at depths of were 0.80 m, 1.79 m and 0.21 m respectively. The depths correlate with the first magnetic susceptibility peak (P1) in all three cores. The P1 peak is not seen in core PC078 (Figure 2.1) and no megascopic ash layer was visible in PC078.
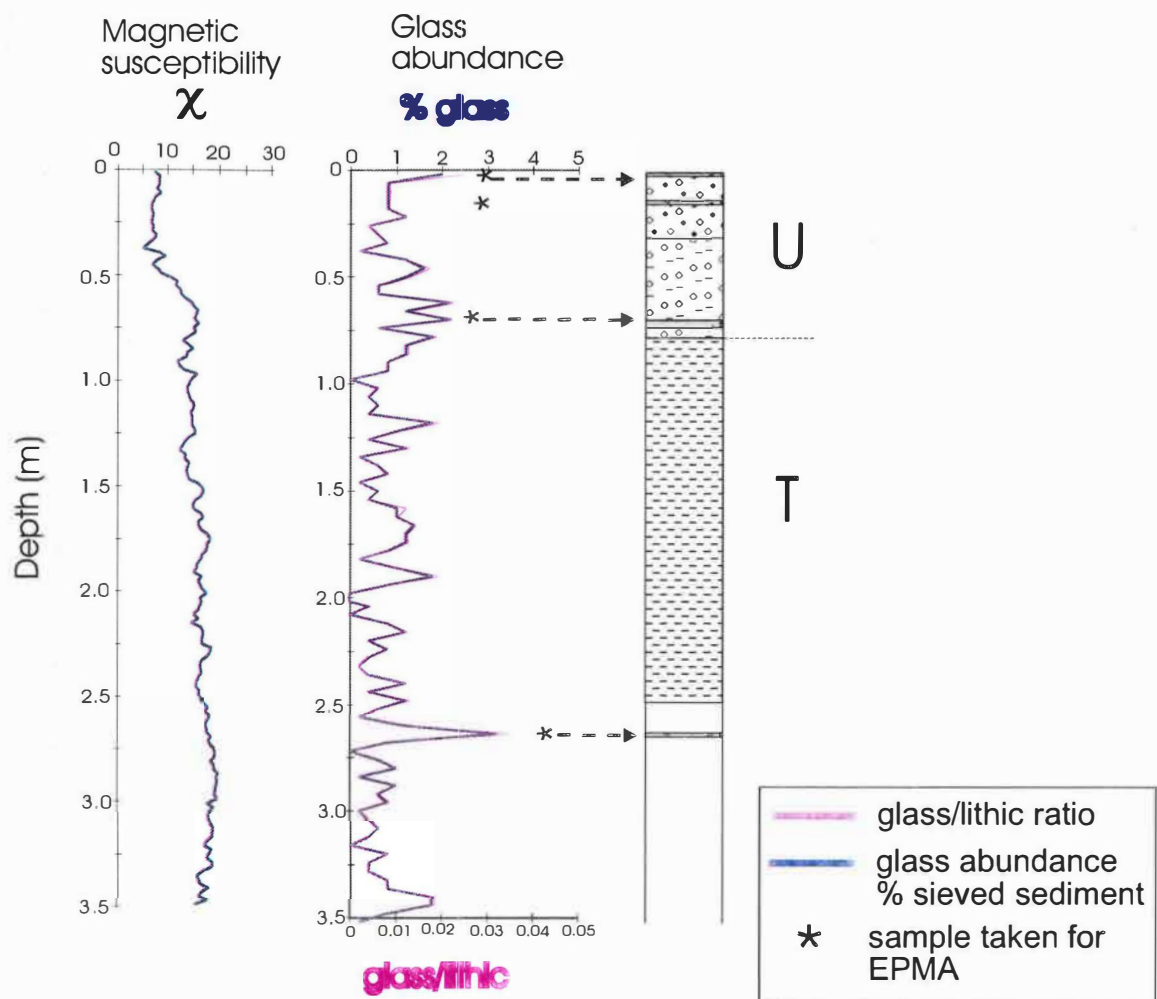
Figure 4.1 Magnetic susceptibility and glass abundance curves for core PC063
Asterisks mark location of potential ash layers. Ash layers investigated by EPMA
are indicated on the sediment log. Sedimentary units U and T identified by
Pudsey and Howe (1998) are also indicated.

Macroscopic examination of the cores showed the lower contact of the ash is fairly sharp with limited downward reworking to a depth of 1cm. The upper boundary in cores PC029 and PC079 is considerably more diffuse. The uppermost 17 cm of core KC081was recovered as a bag sample and is stored separately from the split core sections. The ash layer therefore represents the uppermost undisturbed part of this core, so the upper contact could not be observed.

Examination of smear slides taken from the megascopic ash layer reveal the presence of at least two distinct glass populations in all three cores (Figure 4.2). One population (accounting for 25–30% of the glass total) consists of colourless glass with elongate pipe-like vesicles. Unlike the colourless glass from the Bellingshausen Sea sediment drifts (Chapter 3), the Scotia Sea samples do not show evidence for plastic deformation. The second and dominant glass population (accounting for 70–75% of the glass) consists of cuspate to platy, brown shards and fragments of bubble walls. The larger shards contain rounded vesicles. Many of the brown shards contain small prismatic microcrystals between 5 μm and 10 μm in length, occasionally reaching 25 μm in length.

A crystal-rich very dark brown to black (opaque) glass was also seen in the megascopic ash layer. As many of the brown glass shards vary in the intensity of their colour, as well as in the degree of vesicularity and proportion of crystals, it is unclear whether the darkest shards represent a third glass population, or whether they are an end member of a continuously variable population. This ambiguity has led to initial descriptions of this ash layer as being bimodal (Moreton and Smellie 1998).

The maximum abundance of glass reaches 25.6 %, 55.5 % and 40.5 % in cores PC029, PC079 and KC081 respectively. Glass abundance decreases gradually above the ash layer and several subsidiary shard concentrations occur in cores PC029 and PC079. In core PC079 the volumetric abundance of glass does not drop below 4% for another 36 cm above the main peak and remains above the nominal background level of 2 % for virtually the whole of the upper 1.80 m of the core (Figure 4.3). The abundance of glass drops almost to zero in all three cores immediately below the base of the ash layer.
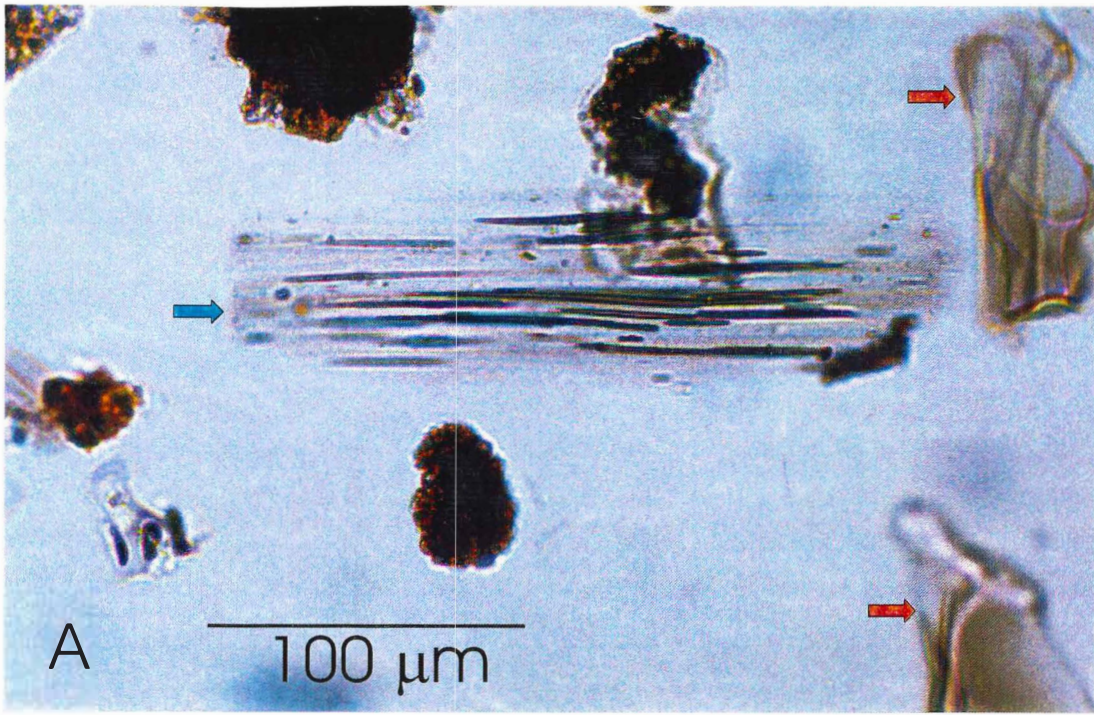
Figure 4.2 A and B. The bimodal tephra from the megascopic tephra layer..
Examples of the more numerous brown glass are indicated by red arrows, blue
arrows indicate less numerous colourless glass with elongate vesicles.
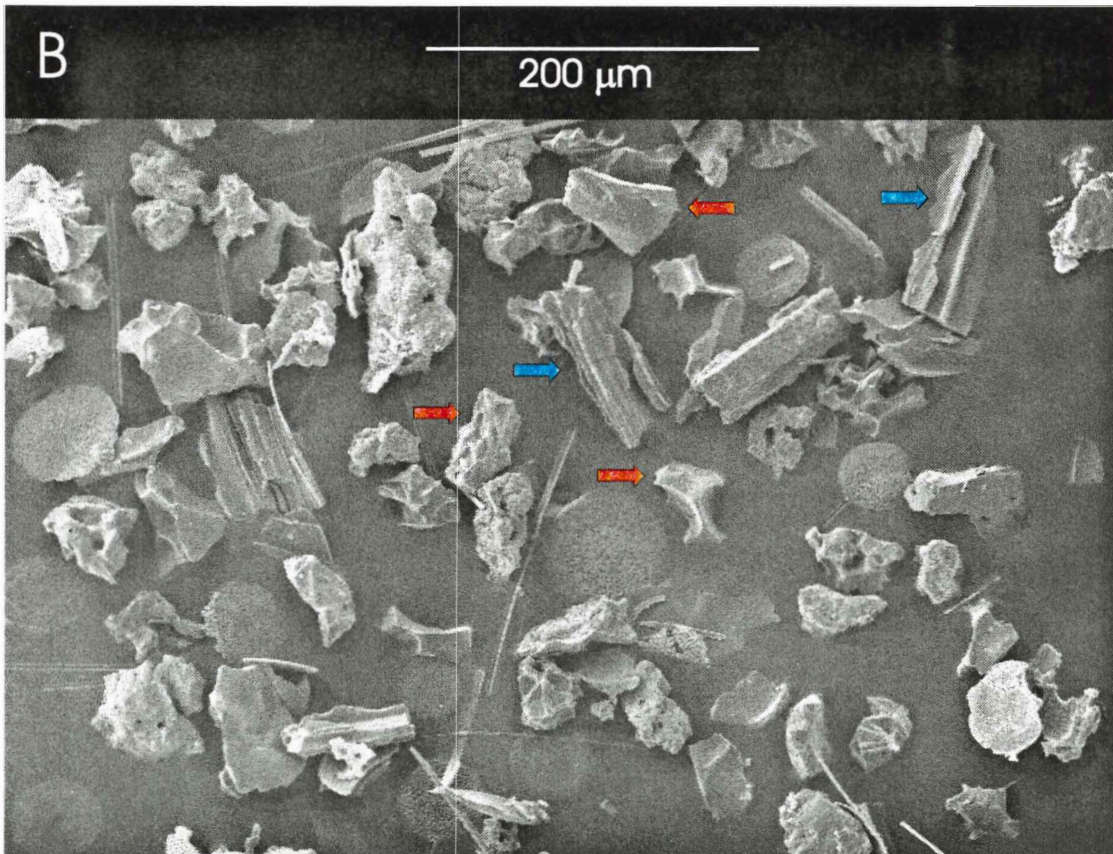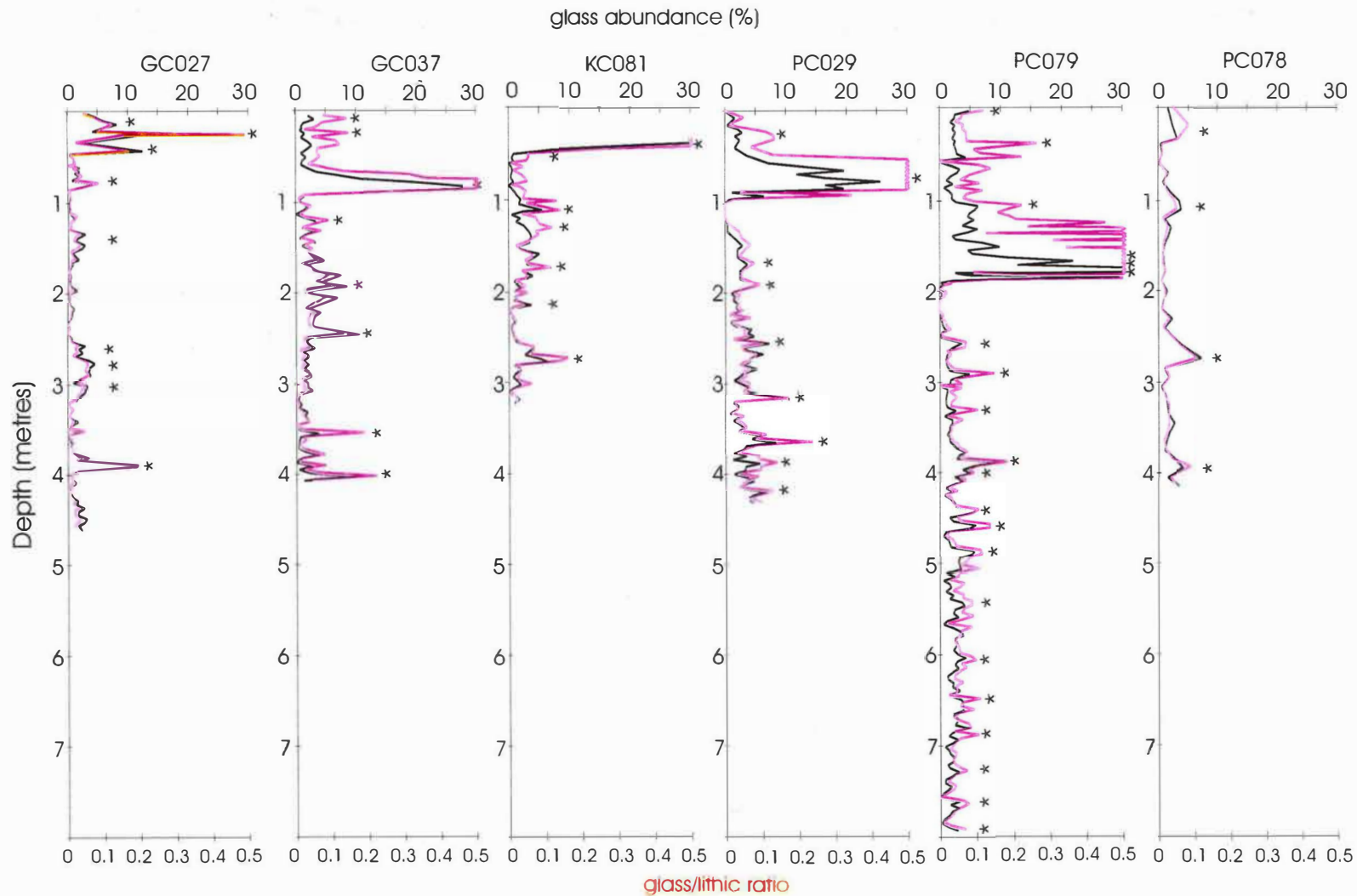
Figure 4.3 Glass abundance and glass-lithic ratio for the cetral Scotia Sea cores. Peak abundances of the visible ash have been truncated for scale. *= ash analysed by EPMA.

Detailed investigation of the megascopic ash layer in core PC079 reveals that the ratio of colourless to brown glass does not alter significantly for a distance of 15cm above the base of the ash layer.

Although no ash layer was visible in core PC078, a bimodal disseminated tephra containing both colourless and brown glass strongly resembling the visible ash layer found in the other three cores was observed at a depth of 0.35 m during examination of smear slides. However, whereas the glass contributed 25 – 55 % of the sieved sample in the three adjacent cores, the bimodal glass in PC078 only accounted for 3.2 %. This disseminated ash was also observed at 0.16 m in the trigger core (TC078), from which samples were taken for radiocarbon dating (see below).

The number of disseminated tephra layers identified above and immediately below the megascopic ash shows a clear correlation between the relative depths of the visible ash layer and the terrigenous 'mud with diatoms' unit of Pudsey and Howe (1998). All four cores contained only one disseminated ash in the Terrigenous Unit (Unit T). Below Unit T the number of disseminated tephra varies as a function of the differing lengths of the cores (Figure 4.4).

The systematic microscopic examination of the four cores revealed a total of 43 disseminated tephras where the volume of glass in the sieved sediment exceeds 4 % or where the glass-lithic ratio is greater than 1:10. Five of these tephras contain in excess of 10 % glass. All of the tephras with > 4 % glass were subsequently subject to electron probe microanalysis (Figure 4.3).

Based on the morphology of the shards, the disseminated ash layers fall into two categories. Above the megascopic ash layer in cores PC029 and PC079 microlites are frequently found in the brown glass. Colourless glass and black glass shards are also present. Below the megascopic ash the disseminated tephras contained only occasional clear or black glass shards. All other potential ash layers are dominated by brown vesicular glass shards with spherical to elliptical vesicles. Microlites are rarely present.
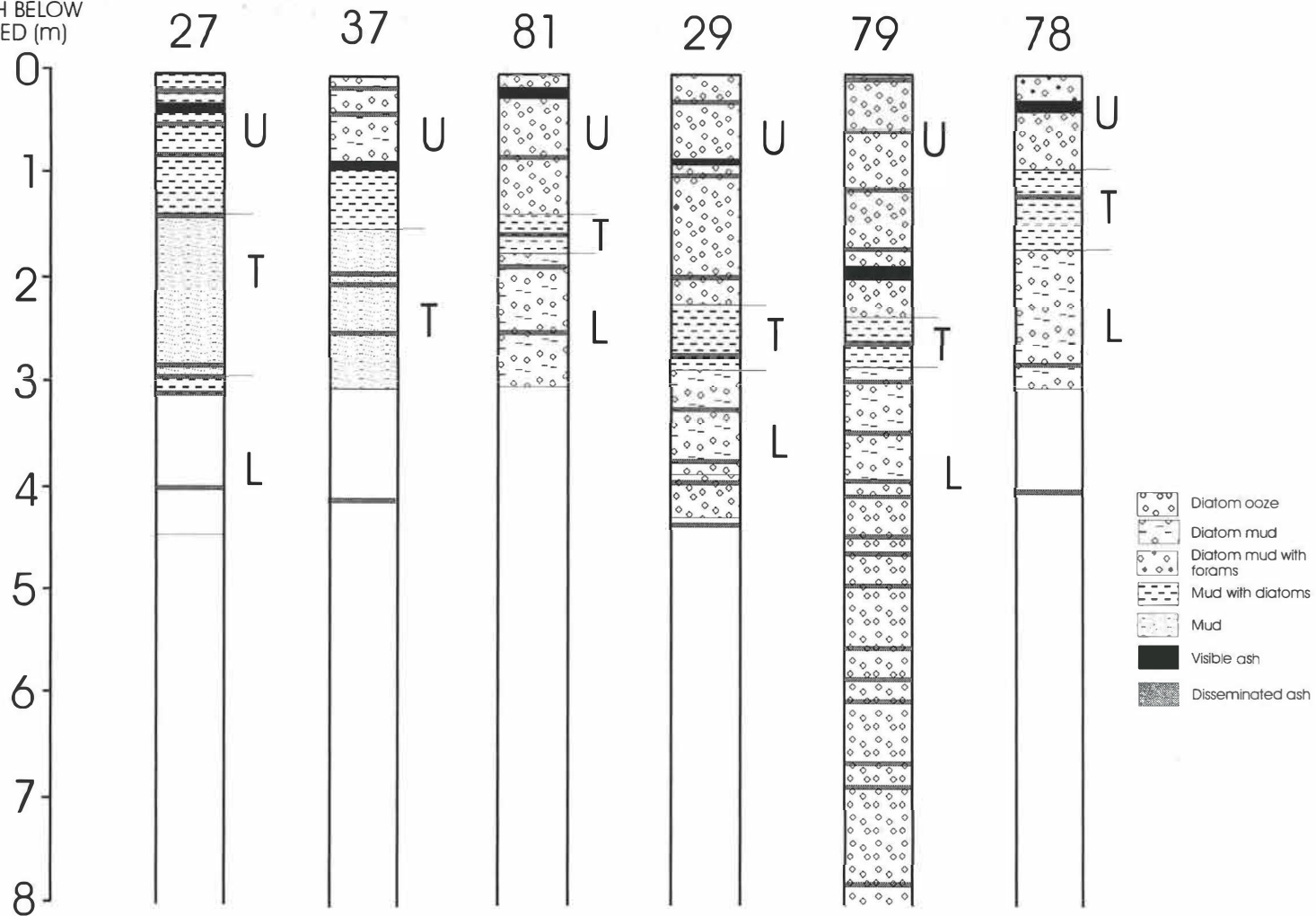
Figure 4.4 Visible and disseminated tephras identified in the Scotia Sea and Jane Basin Cores. The stratigraphic units are those identified by Pudsey and Howe (1998). U = Upper Biogenic Unit, T = Terrigenous Unit, L = Lower Biogenic Unit.

4.1.4 Jane Basin cores

Two gravity cores, GC027 and GC037, were examined from Jane Basin (Figure 1.6). One visible ash layer is present in each core. Microscopic examination of these ash layers revealed a mixed population of colourless and brown glass and rare black glass. Microlites are common in brown glass. The morphology of the different glass populations resemble those seen in the megascopic ash layer in the central Scotia Sea cores.

The megascopic ash layer has a sharp basal contact with very little glass present in the sediment below. Two possible ash layers were found above the megascopic ash in GC037 while only one was found in GC027. The visible ash layer occurs at a greater depth in core GC037 than in GC027 and the number of possible tephras found above the visible ash layer may be related to this difference in depth (figures 4.3 and 4.4).

The Jane Basin cores differ from those from the Scotia Sea in having a thicker terrigenous unit which is also largely devoid of diatoms (Figure 4.4). Three possible ash layers are identified within this unit in both Jane Basin cores, although their distribution is markedly different. In GC027 the potential ash layers are located at the top and base of the terrigenous unit whereas they occur toward the middle of the unit in GC037.

Overall GC027 contains less glass than GC037 and the peaks of glass abundance are less pronounced (Figure 4.3). Therefore several samples were taken for EPMA analyses where the volumetric abundance of glass did not quite reach 4 % of the sieved sediment as in other cores. The possible reasons for the lower abundance in core GC027 will be discussed in a later chapter.

The three uppermost ash layers in GC027 form a triple peak with one disseminated tephra either side of the visible ash layer. Both of the disseminated tephras contain bimodal populations of glass that resemble those of the visible ash layer. Brown glass with spherical vesicles is dominant over colourless glass with elongate vesicles, and crystal rich, black glass is also seen. Throughout the rest of core GC027 brown glass is the dominant glass type in all of the disseminated tephras. However, the microlites that

are common in the upper three peaks are not seen in shards elsewhere in the core. Colourless glass occurs only as isolated grains elsewhere.

In core GC037 the glass shards in the visible ash layer contain a mixed glass population with morphology and other characteristics similar to those in the visible ash layers described above. Both of the disseminated ash layers located above the visible ash layer showed similar mixed populations, but in the uppermost disseminated ash layer colourless glass was dominant. The remaining four ash layers in GC037 show some differences from the pattern seen elsewhere in Unit T and Unit L. The glass populations from the double peak at 1.91 m and 1.97 m depth are extremely similar. In both, the dominant glass type comprises thin platy brown glass with rare vesicles and common microlites. Some colourless glass with elongate vesicles and some black glass shards are present.

At 2.43 m depth the dominant glass type is colourless, thin and platy in appearance. Vesicles are rounded rather than elongate. The brown glass seen throughout all of the cores is not present in this ash layer. The lowest disseminated ash layer in core GC037 (at a depth of 4.01 m) is dominated by thin brown platy glass shards. Where the glass is thicker small round vesicles are abundant. Microlites are not common.

In all of the cores, the shards in the "background population" are dominated by vesicular brown glass. Figure 4.4 shows the location of all of the tephra layers identified with stratigraphical units after Pudsey and Howe (1998).

4.1.5 Boyd Strait Core

Despite the proximity of glaciated islands and Deception Island, the Boyd Strait core contained less relatively coarse sediment, ice-rafted debris and tephra than expected. Only two megascopic ash layers were observed, at depths of 2.98 m and 3.12 m. Glass shard abundances elsewhere in the core are only seen at background levels, and there are no disseminated tephra layers. Several smear slides were found to contain no glass at all.

The upper ash layer is the thicker of the two. Both have sharp basal contacts and sharp but less well defined upper contact surfaces. The upper ash layer exhibits normal grading with scoriaceous fragments up to 4 mm across at the base of the layer. Glass abundance reaches a peak of 76 % of the sieved sediment at a depth of 2.98 m but rapidly decreases to only 2.8 % at a depth of 2.92 m, suggesting that there has been little reworking of the tephra. By comparison, the lower of the two ash layers only reaches a peak glass abundance of 10.8 % and decreases gradually upward to the base of the overlying ash layer.

The glass in the upper ash layer consists of large, dark brown, vesicular shards with abundant large crystal inclusions. The dark colour may be a function of the size and thickness of the shards. The abundant vesicles ($C_v = 0.6 - 1.0$) are spherical to slightly ovoid ($C_s = 0.8$ to 1.0) (Figure 4.5). Optically the shards, although larger, bear some similarities to the dark brown to black crystal rich shards of the megascopic ash layer from the Scotia Sea.

4.1.6 Mount Hudson Ash

The tephra sample obtained from the 1991 eruption of Mt. Hudson, Chile, was prepared differently from the sediment core tephra described above. This sample was not wet sieved due to the small size of the shards, which were predominantly smaller than 32 µm, and because the tephra already represented a pure sample.

Examination of the tephra using a light microscope shows that the ash is light brown in colour and consists almost entirely of pale, angular glass shards. Shard morphology ranges from cuspate, through angular to equant. Vesiculation is extensive (coefficient of vesicularity $C_v = 0.8$ to 1.0 (Sheridan and Marshall 1987)) and vesicle shapes range from spherical to pipe-like ($C_s = 1.0$ to 0.0). (Figure 4.6).

Samples examined without any prior wet sieving or ultrasonic treatment show microparticles adhering to the larger shards filling vesicles and (Figure 4.6). The shards show a high degree of sorting.
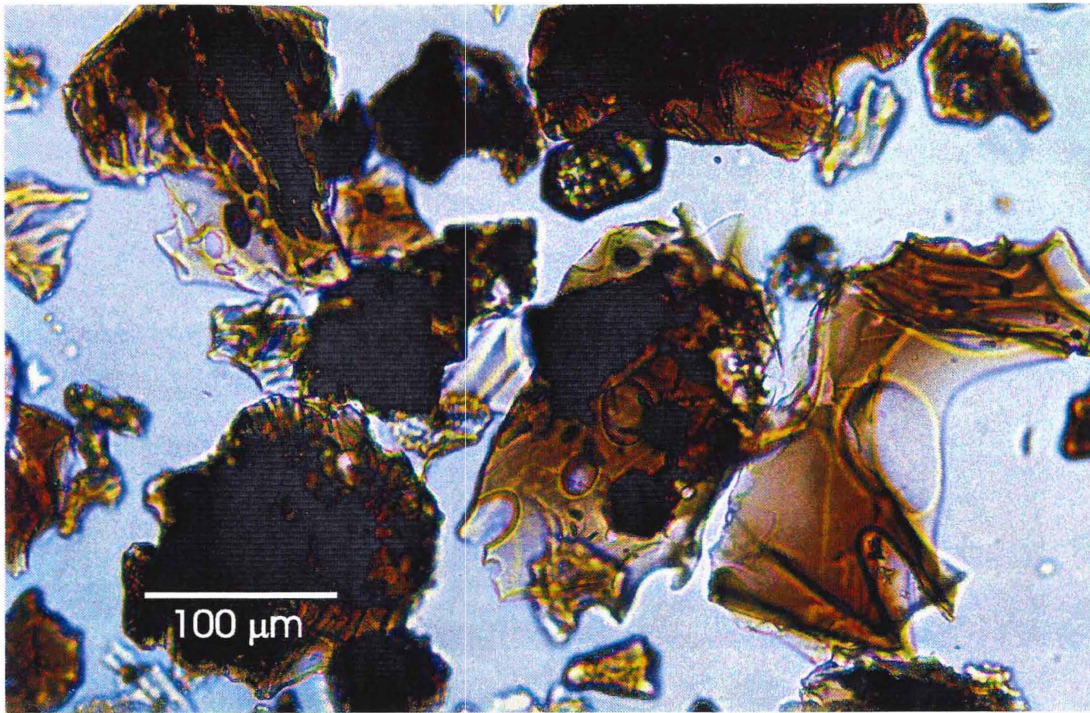
Figure 4.5 Boyd Strait tephra. The highly variable vesicle morphology ranges from spherical to pipe-like. Vesicle size ranges from 4 μm to 96 μm. Vesicle abundance varies between $C_v = 0.1$ and $C_v = 0.6$.
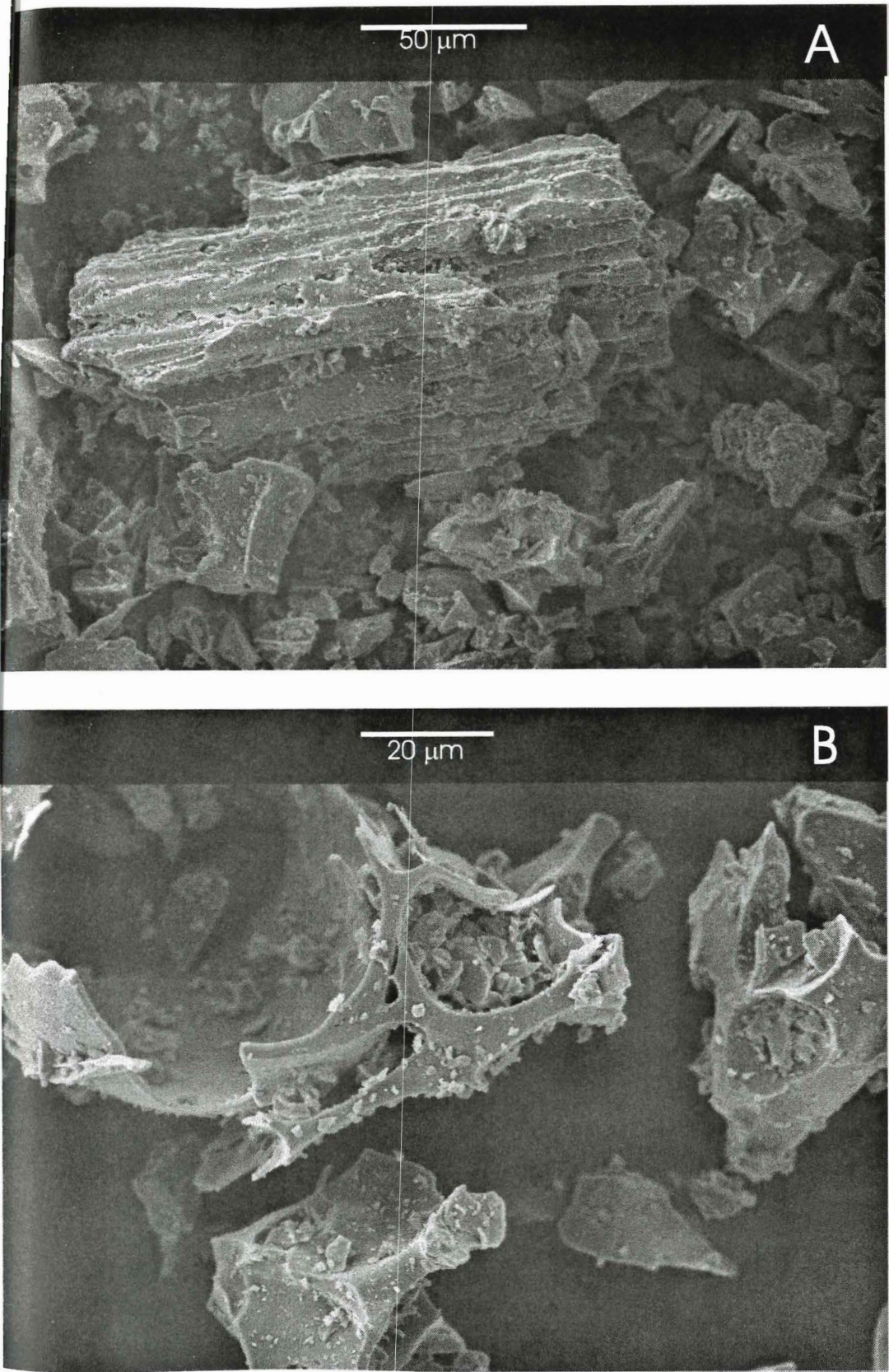
Figure 4.6 Scanning electron micrographs of tephra from the 1991 eruption of Mt. Hudson, Chile, which fell on the Falkland Islands. (A) Shard with elongate vesicles and adhering dust. (B) Fragmented walls of spherical vesicles and and the in filling of vesicles by dust particles.

4.2 EPMA analyses

4.2.1 Northern Scotia Sea

Only three of the potential ash layers (the first, third and sixth), and, a sample of the mixed population of brown and clear glass found between the first and second potential ash layers were analysed by EPMA to determine the geochemical compositions of the glass. The low abundance of glass created problems obtaining sufficient glass shards to obtain a reliable characterisation of each ash layer. Many of the shard analyses had low totals (i.e. less than 95 %) but these analyses are included in Table 4.1. The results reveal a very broad range of compositions within each sample (Table 4.1 and Appendix 1).

4.2.2 Central Scotia Sea and Jane Basin

A total of 58 disseminated ash layers were investigated by EPMA. To facilitate comparison with likely correlative tephras the ash layers have been grouped stratigraphically, based on the previously established stratigraphy discussed in chapter 1. Unit U has been further divided into i) tephras above the visible ash layer, ii) the visible ash layer plus the uppermost disseminated ash layer from PC078, iii) tephras which occur immediately below the visible ash. The ash layers from Unit L have also been divided into groups, based on bivariate graphs, depending on whether they produced i) scattered data, ii) data with a linear trend, iii) clustered data.

The tephras have a limited range of compositions (mainly basalt – basaltic andesite). Differences between tephra layers are slight but tephras can be distinguished mainly by iron, titanium, magnesium and calcium. Of these elements it was found that plotting iron against magnesium shows to best advantage the subtle compositional differences between the tephra layers.

4.2.2.1 The visible tephra layer

As the visible ash layer is an obvious marker horizon it is appropriate to compare the compositional analyses of this ash layer from all six of the cores before describing the other disseminated ash layers.

Table 4.1 Mean values and standard deviations (in parentheses) of major oxide geochemical compositions of glass shards from disseminated tephras found in core PC063 as determined by EPMA. Probe conditions 1 μm focused beam, 20 kV accelerating voltage, 15nA beam current, 10 second count times. Glass phases: a = andesite, b = basalt, ba = basaltic–andesite, r = rhyolite. * All iron calculated as FeO.

Depth (mbsf)	glass phase	SiO_2	TiO_2	Al_2O_3	FeO*	MnO	MgO	CaO	Na_2O	K_2O	Total	n
0.02	a	62.64	1.41	15.55	5.53	0.20	1.55	3.03	5.20	2.62	97.73	2
0.02	r	72.51	0.17	11.74	1.45	0.05	0.21	1.40	3.07	2.67	93.27	4
0.18	b	51.07	2.54	14.28	10.92	0.22	4.82	8.74	4.53	0.57	97.69	2
0.18	ba	54.30	2.20	16.25	8.66	0.17	3.32	7.52	4.92	0.64	97.98	2
0.18	r	59.50	0.97	14.87	8.14	0.27	1.37	3.36	5.82	2.94	97.24	6
0.74	b	48.59	2.06	16.41	8.84	0.19	4.79	8.62	4.32	1.53	95.35	3
0.74	ba	52.71	2.19	15.07	8.99	0.20	3.80	7.65	4.06	0.67	95.34	2
0.74	r	67.66	0.31	13.15	1.64	0.08	0.31	1.25	2.95	4.34	91.69	4
2.64	b	47.25	2.28	16.88	8.92	0.22	5.41	9.30	4.42	1.82	96.50	2
2.64	ba	53.18	1.67	15.89	8.15	0.20	3.94	7.77	4.95	0.66	96.41	1

Table 4.2. Mean compositions for the basaltic and rhyolitic clusters of the visible ash layer from the Scotia Sea. Dacites, andesites and basaltic-andesites omitted from the table. Standard deviations given in parentheses. *All iron calculated as FeO. Number of glass shards upon which mean is based are show in column n. Probe conditions: accelerating voltage 20kV, beam current 15nA, 1 μm focused beam. Elements were analysed in pairs with 10 second count times per pair.

Core number and sample depth (mbsf)	SiO2	TiO$_2$	Al$_2$O$_3$	FeO*	MnO	MgO	CaO	Na$_2$O	K$_2$O	Total	n
Basalt											
GC027 – 0.31	50.99 (0.58)	2.22 (0.22)	15.61 (0.50)	10.07 (0.65)	0.19 (0.02)	4.64 (0.59)	8.48 (0.72)	4.41 (0.27)	0.52 (0.09)	97.13	17
GC037 – 0.82	51.18 (1.13)	2.37 (0.22)	15.79 (0.76)	10.55 (0.88)	0.18 (0.04)	3.88 (0.48)	9.54 (0.80)	4.26 (0.30)	0.48 (0.07)	98.23	8
PC029 – 0.78	50.80 (0.65)	2.33 (0.09)	15.89 (0.81)	10.27 (0.29)	0.16 (0.03)	4.21 (0.33)	8.25 (0.33)	4.43 (0.34)	0.53 (0.06)	96.87	24
PC078 – 0.35	51.37 (0.46)	2.35(0.08)	15.56 (0.56)	9.98 (0.38)	0.15 (0.02)	4.63 (0.55)	8.66 (0.49)	4.03 (0.34)	0.75 (0.30)	97.48	5
PC079 – 1.80	51.39 (0.40)	2.39 (0.07)	15.73 (0.20)	10.30 (0.31)	0.14 (0.03)	4.18 (0.13)	8.22 (0.37)	4.52 (0.31)	0.50 (0.06)	97.37	16
KC081 – 0.21	50.51 (0.57)	2.44 (0.18)	15.48 (0.36)	10.23 (0.54)	0.21 (0.03)	4.42 (0.37)	8.44 (0.51)	4.55 (0.24)	0.53 (0.06)	96.81	25
Dacite/Rhyolite											
GC027 – 0.31	70.58 (1.39)	0.46 (0.13)	14.25 (0.49)	3.48 (0.62)	0.13 (0.03)	0.29 (0.21)	0.91 (0.37)	5.29 (0.33)	2.34 (0.22)	97.73	13
GC029 – 0.82	69.48 (1.83)	0.52 (0.23)	15.05 (1.05)	3.56 (0.28)	0.14 (0.04)	0.45 (0.28)	1.12 (0.56)	4.95 (0.53)	2.20 (0.34)	97.47	9
PC037 – 0.78	69.46 (1.24)	0.56 (0.18)	13.92 (0.45)	3.30 (0.13)	0.14 (0.06)	0.20 (0.14)	0.92 (0.13)	6.39 (0.54)	2.07 (0.25)	96.96	10
PC078 – 0.35	71.56 (0.44)	0.41 (0.10)	14.28 (0.44)	3.24 (0.13)	0.13 (0.05)	0.24 (0.09)	0.72 (0.22)	5.71 (0.25)	2.36 (0.22)	98.65	5
PC079 – 1.80	71.81 (0.82)	0.37 (0.05)	14.17 (0.15)	3.26 (0.14)	0.17 (0.04)	0.21 (0.03)	0.71 (0.07)	5.33 (0.52)	2.49 (0.12)	98.52	9
KC081 – 0.21	70.64 (1.16)	0.42 (0.14)	14.10 (0.36)	3.39 (0.17)	0.14 (0.03)	0.25 (0.14)	0.74 (0.24)	5.61 (0.45)	2.48 (0.23)	97.77	7

Mean compositions for the brown and colourless glass are given in Table 4.2, the complete data set is reproduced as Appendix I. In each of the cores the silica content of the brown glass falls within the range $SiO_2 = 50.48 \pm 0.57$ to 51.85 ± 0.93. Sodium values are high (4.13 % ± 0.42 to 4.55 % ± 0.74) whereas potassium values are low (0.48 % ± 0.06 to 0.71 % ± 0.25). The compositions are basaltic. In each of the cores the titanium contents are also high (2.20 % ±0.21 to 2.44 % ±0.23). The colourless glass has a completely different composition and ranges from dacite to rhyolite (herein referred to as rhyolitic). $SiO2 = 68.44$ % ± 2.44 to 71.81 % ± 0.82; $Na_2O = 5.18$ % to 6.39 %; $K_2O = 2.02$ % to 2.54 %.

Both glass types show a greater range of compositions than the sediment drift tephra described above (Chapter 3). Despite the variability in the glass chemistry both the rhyolitic glass and the basaltic glass are remarkably similar in all six cores. This correlation can be seen graphically by plotting FeO against MgO (Figure 4.7).

Only in the sample from PC079 were the black shards analysed. The analyses produced high totals (often >100 %) and widely varying compositions (indicated by high standard deviations). The Cambridge Instruments Mk. V. compositional totals rarely exceed 98 % due to the presence of volatiles which cannot be detected and the presence of elements not analysed. The most likely reason for the high totals is that crystal phases have been included in the volume of glass analysed. Figure 4.8 shows the differences between the black, brown and colourless glass from the visible ash layer in core PC079.

One of the notable characteristics of the megascopic tephra layer is the low potassium and relatively high sodium in all the glass types present. When these two values are combined to give the value of total alkalis these characteristics tend to cancel each other out and the impact of the distinctiveness of this ash layer compared to those already described in this thesis is lost. However, Figure 4.9 shows that, on a plot of K_2O/Na_2O against SiO_2, the Scotia Sea visible ash layer can be clearly distinguished from analyses of the basaltic tephra from the southern Bellingshausen Sea and trachytic tephra in the sediment drifts in the northern Bellingshausen Sea.
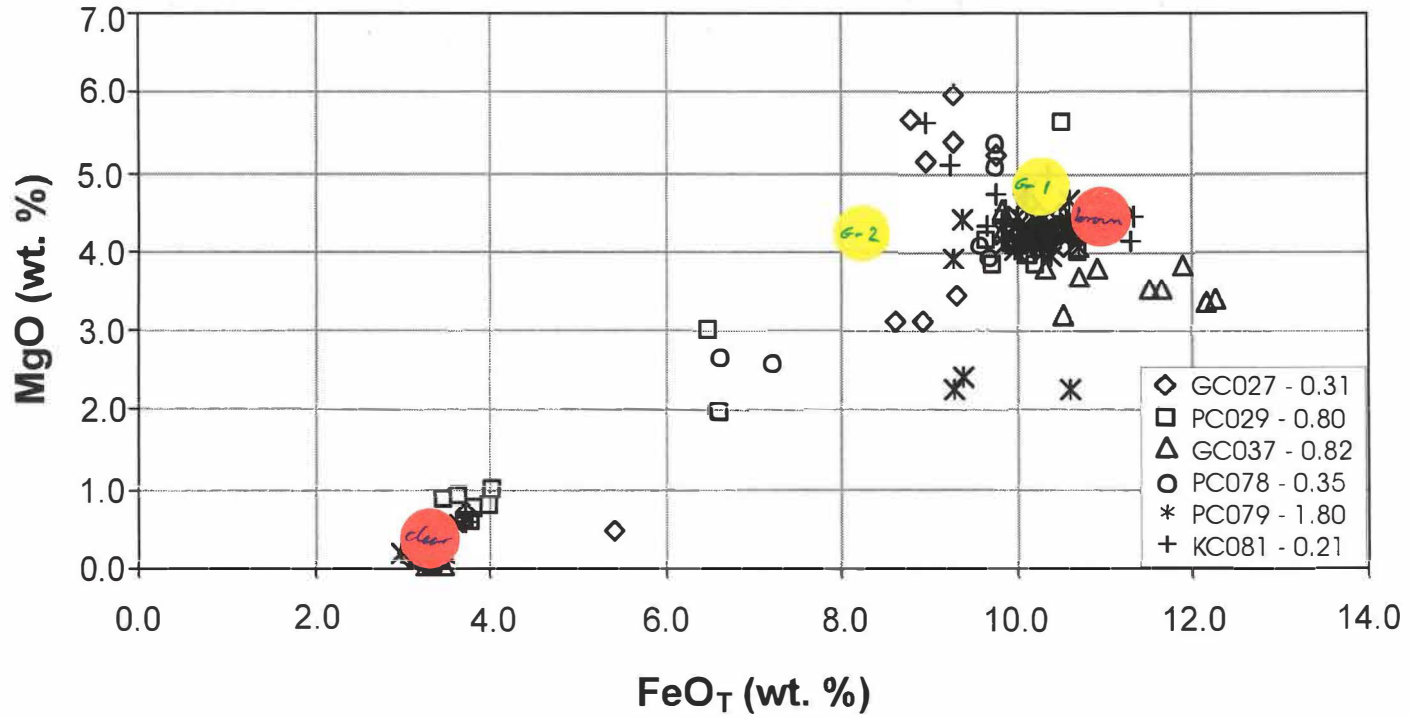
Figure 4.7 FeO$_T$–MgO plot of the colourless and brown glass shards from the visible ash layer from the Scotia Sea cores and the uppermost disseminated tephra from PC078.
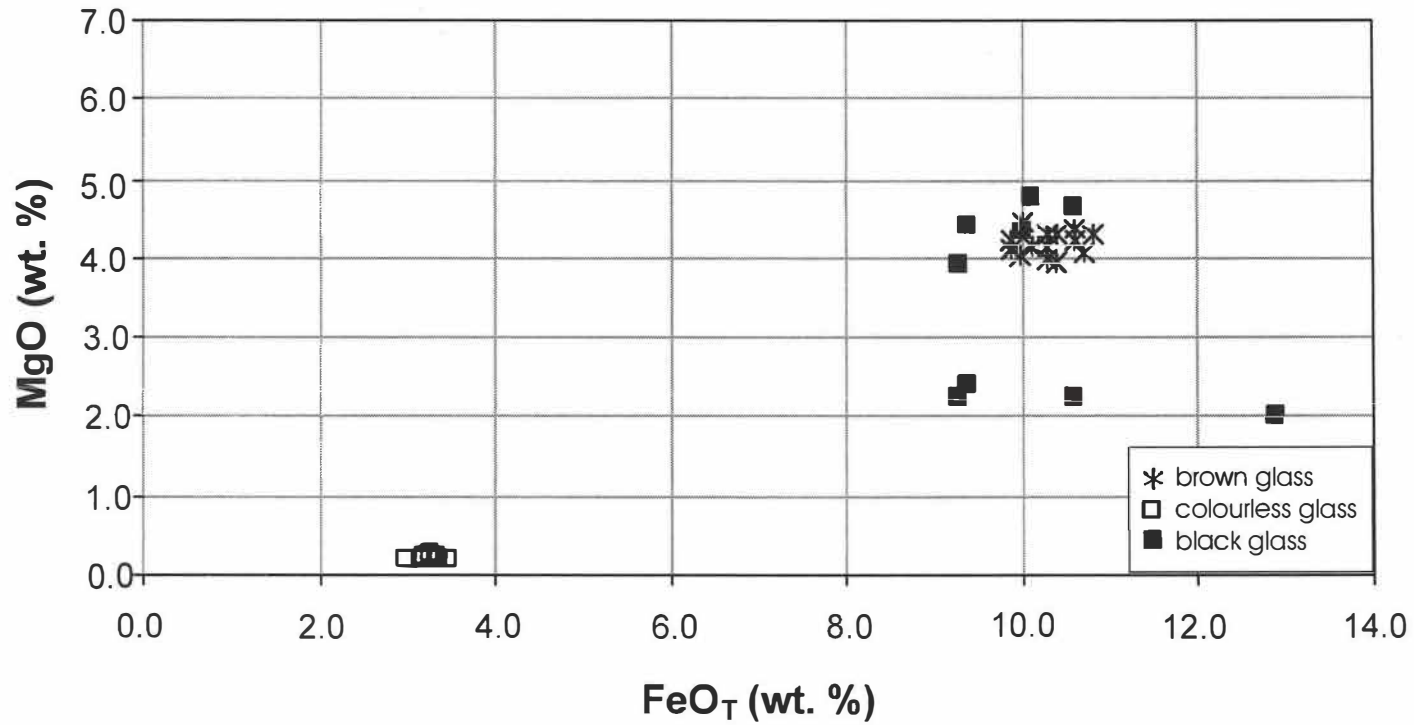
Figure 4.8 Comparison of the coulourless, brown and black glass shards present in the visible tephra layer in core PC079. Note the clustering of the colourless and brown glass analyses compared with the scatter of the black glass.
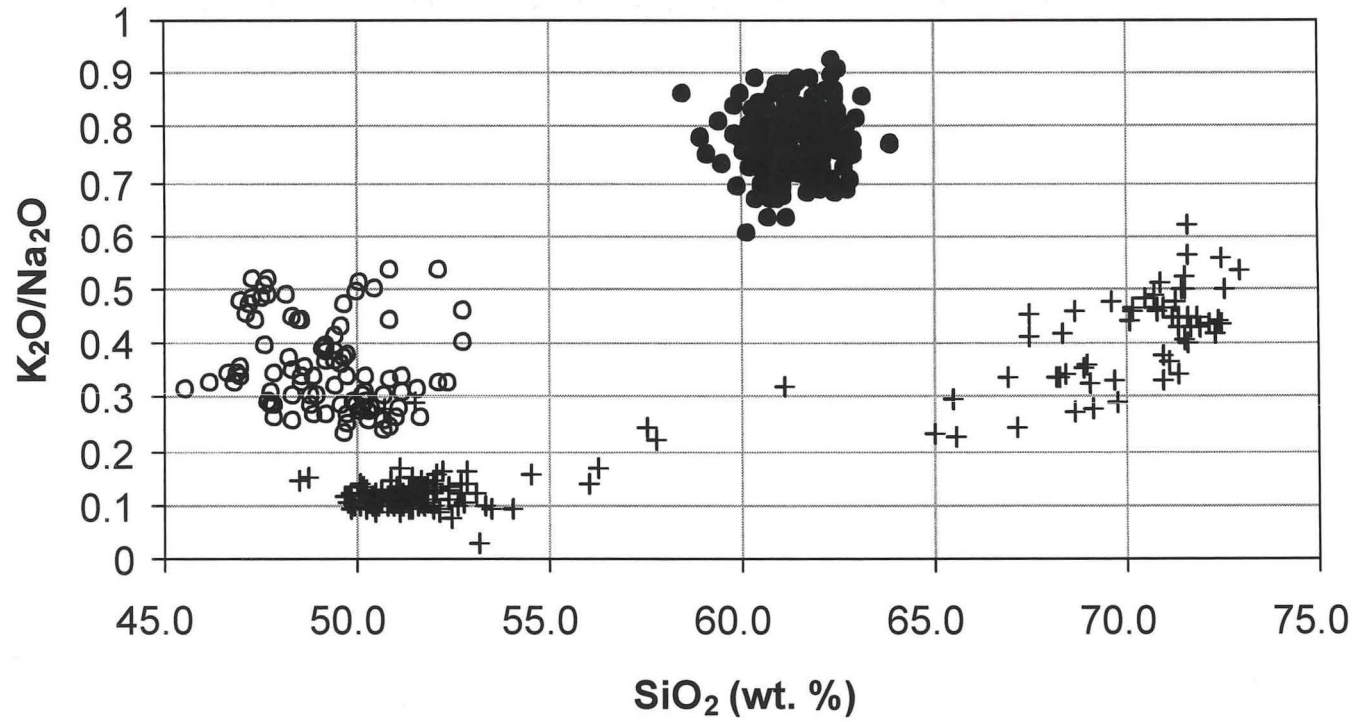
Figure 4.9 Comparison of the K2O/Na2O ratio in the visible ash layers from the Scotia Sea (crosses) with those of the southern Bellingshausen Sea (open circles) and the northern Bellingshausen Sea (filled circles)

4.2.2.2 Disseminated ash layers above the megascopic tephra

Shards in all of the disseminated ash layers located above the visible ash layer were found to have almost identical chemical compositions to shards in the megascopic ash, although the lower glass abundances meant that few colourless glass shards were available for analyses. The patterns of scatter away from the main clusters of rhyolitic and basaltic glass compositions (Figure 4.10) are essentially the same as for the megascopic tephra layer (Figure 4.7). The mean values for each of the ash layers are given in Table 4.3 and the full dataset is given in Appendix 1.

4.2.2.3 Unit U tephra below megascopic ash

Shards in ash layers at GC027–0.43 m, PC029–0.92 m and PC079–1.85 m, situated immediately below the megascopic ash in their respective cores, strongly resemble shard compositions of the megascopic tephra (Figure 4.11). Mean values for these tephras are shown in Table 4.4 (c.f. Table 4.2). Tephra from KC081-0.91 m show an inverse correlation between FeO_T and MgO and has low SiO_2. The ash layer at PC029–1.92 m is poorly characterised (only three analyses), but they all plot in the rhyolite field of the megascopic ash. Despite a considerable number of analyses, KC081–1.19 m shows no compositional homogeneity.

4.2.2.4 Ash layers from the Terrigenous unit.

Within the Terrigenous Unit, three basaltic tephras (PC029–2.68 m, PC079–2.91 m and KC081–1.59 m) form a cluster where most analyses contain < 9.5% FeO. This plots outside the field of the megascopic ash in which most anayses contain >10.0% FeO (c.f. Figure 4.7). All three datasets correlate well across a range of combinations of elements (Figure 4.12, Table 4.5 and Appendix 1).

Although they exhibit considerable scatter, data for tephra layers at PC078–1.12 m and PC079–2.57 m follow a similar linear trend. Both tephras have similar K_2O/Na_2O ratios and they contain outlying points with similar compositions. The correlation of these two tephras is not in stratigraphical conflict with the above cluster. However, when the outlying analyses are considered the mean values for these ash layers are very different.

Table 4.3 Mean values and standard deviations (in parentheses) of major oxide geochemical compositions of glass shards from disseminated tephras found above the megascopic ash as determined by EPMA. Probe conditions 1 μm focused beam, 20 kV accelerating voltage, 15nA beam current, 10 second count times. * All iron calculated as FeO.

Core Number and sample depth (mbsf)	SiO_2	TiO_2	Al_2O_3	FeO*	MnO	MgO	CaO	Na_2O	K_2O	Total	n
basalts											
GC027 – 0.16	50.51 (0.78)	2.33 (0.16)	15.65 (0.22)	9.80 (0.39)	0.22 (0.04)	4.32 (0.38)	8.48 (0.49)	4.46 (0.27)	0.50 (0.06)	96.27	6
PC029 – 0.24	50.35 (–)	2.26 (–)	15.25 (–)	9.92 (–)	0.18 (–)	4.39 (–)	8.29 (–)	4.55 (–)	0.51 (–)	95.70	1
GC037 – 0.06	51.32 (0.69)	2.12 (0.52)	15.93 (0.25)	9.41 (1.27)	0.21 (0.01)	4.67 (0.72)	8.61 (0.79)	4.49 (0.22)	0.52 (0.09)	97.28	3
GC037 – 0.34	50.39 (–)	2.07 (–)	15.60 (–)	9.79 (–)	0.21 (–)	4.84 (–)	8.70(–)	4.45 (–)	0.46 (–)	96.51	1
PC079 – 0.04	49.72 (1.64)	2.50 (0.27)	14.99 (0.68)	10.54 (0.61)	0.21 (0.04)	4.80 (0.44)	8.66 (0.77)	4.43 (0.19)	0.68 (0.46)	96.52	6
PC079 – 0.54	50.55 (0.68)	2.38 (0.18)	15.73 (0.33)	9.92 (0.29)	0.21 (0.02)	4.17 (0.10)	8.07 (0.21)	4.51 (0.19)	0.50 (0.04)	96.04	4
PC079 – 1.10	51.00 (0.40)	2.37 (0.26)	15.48 (0.31)	10.04 (0.80)	0.22 (0.02)	4.46 (0.38)	8.30 (0.53)	4.55 (0.23)	0.50 (0.02)	96.92	5
PC079 – 1.62	50.60 (0.72)	2.27 (0.25)	15.67 (0.28)	9.90 (0.65)	0.22 (0.02)	4.53 (0.59)	8.54 (0.68)	4.44 (0.25)	0.48 (0.07)	96.65	18
Rhyolite											
GC027 – 0.16	69.39 (1.25)	0.44 (0.18)	14.16 (0.67)	3.44 (0.34)	0.17 (0.03)	0.33 (0.24)	0.89 (0.46)	5.19 (0.28)	2.28 (0.31)	96.29	4
GC037 – 0.06	71.55 (–)	0.43 (–)	14.38 (–)	3.34 (–)	0.12 (–)	0.21 (–)	0.64 (–)	5.12 (–)	2.35 (–)	98.14	1
GC037 – 0.34	72.00 (–)	0.36 (–)	14.16 (–)	3.26 (–)	0.12 (–)	0.23 (–)	0.67 (–)	3.32 (–)	2.39 (–)	96.51	1
PC079 – 0.04	70.38 (–)	0.44 (–)	13.88 (–)	3.08 (–)	0.14 (–)	0.19 (–)	0.77 (–)	5.46 (–)	2.52 (–)	96.86	1
PC079 – 0.54	71.70 (–)	0.37 (–)	13.78 (–)	3.31 (–)	0.19 (–)	0.24 (–)	0.55 (–)	4.84 (–)	2.41 (–)	97.39	1
PC079 – 1.62	70.96 (0.74)	0.35 (0.06)	13.99 (0.39)	3.22 (0.15)	0.15 (0.02)	0.21 (0.04)	0.39 (0.10)	5.25 (0.12)	2.38 (0.17)	96.90	3
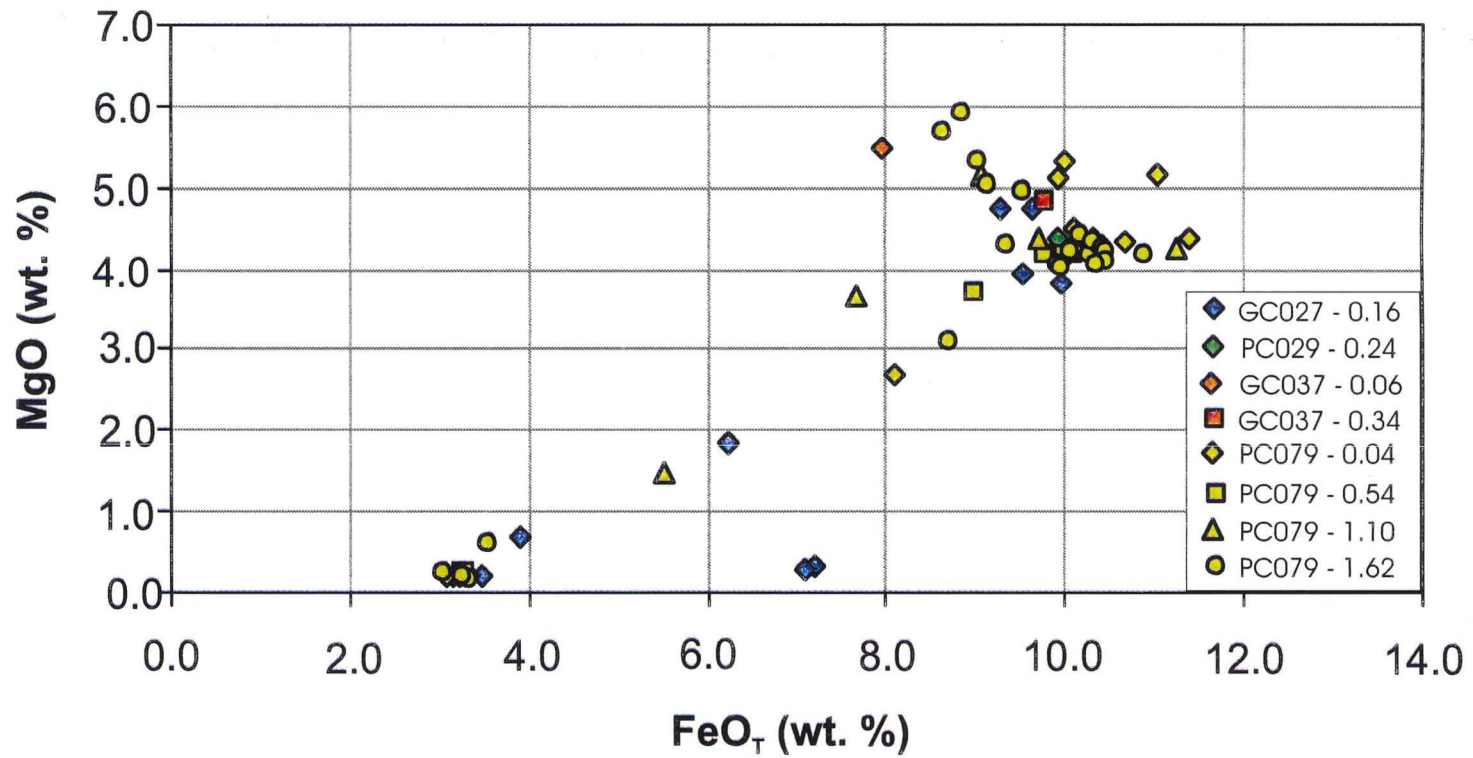
Figure 4.10 Plot of MgO – FeO$_T$ for ash layers found above the visible ash layer.

Table 4.4 Mean values and standard deviations (in parentheses) of major oxide geochemical compositions of glass shards from disseminated tephra layers identified in Unit U below the visible ash layer. Probe conditions 1 μm focused beam, 20 kV accelerating voltage, 15nA beam current, 10 second count times. * All iron calculated as FeO.

Core number and sample depth (mbsf)	SiO_2	TiO_2	Al_2O_3	FeO*	MnO	MgO	CaO	Na_2O	K_2O	Total	n
Basalts											
GC027 – 0.43	51.30 (0.11)	2.30 (0.21)	15.54 (0.14)	9.96 (0.06)	0.22 (0.10)	4.47 (0.35)	8.65 (0.79)	4.48 (0.09)	0.47 (0.01)	97.39	2
GC027 – 0.79	48.91 (–)	2.33 (–)	15.83 (–)	10.70 (–)	0.20 (–)	5.23 (–)	9.19 (–)	4.21 (–)	1.42 (–)	98.01	1
PC029 – 0.92	50.73 (0.47)	2.31 (0.18)	15.53 (0.15)	9.99 (0.51)	0.22 (0.04)	4.32 (0.43)	8.47 (0.54)	4.54 (0.21)	0.49 (0.07)	96.60	11
PC079 – 1.85	50.33 (0.61)	2.34 (0.16)	15.39 (0.31)	9.91 (0.53)	0.23 (0.04)	4.23 (0.22)	8.26 (0.35)	4.60 (0.21)	0.54 (0.09)	95.83	10
KC081 – 0.91	49.37 (0.36)	2.09 (0.29)	15.44 (0.51)	10.59 (0.74)	0.13 (0.05)	5.47 (0.66)	9.51 (0.91)	4.24 (0.14)	0.70 (0.31)	97.54	8
Rhyolites											
GC027 – 0.43	73.39 (–)	0.41 (–)	13.67 (–)	3.25 (–)	0.11 (–)	0.26 (–)	0.68 (–)	5.07 (–)	2.38 (–)	99.22	1
PC029 – 1.92	70.15 (0.99)	0.47 (0.02)	14.82 (0.25)	3.31 (0.13)	0.13 (0.02)	0.45 (0.01)	1.41 (0.10)	5.06 (0.31)	2.08 (0.08)	97.88	3
PC079 – 1.85	69.46 (1.29)	0.35 (0.05)	13.85 (0.22)	3.16 (0.06)	0.16 (0.02)	0.24 (0.02)	0.65 (0.10)	5.14 (0.18)	2.56 (0.14)	95.57	3
KC081 – 0.91	68.67 (–)	0.66 (–)	15.42 (–)	4.07 (–)	0.12 (–)	0.82 (–)	2.19 (–)	3.67 (–)	1.58 (–)	97.20	1
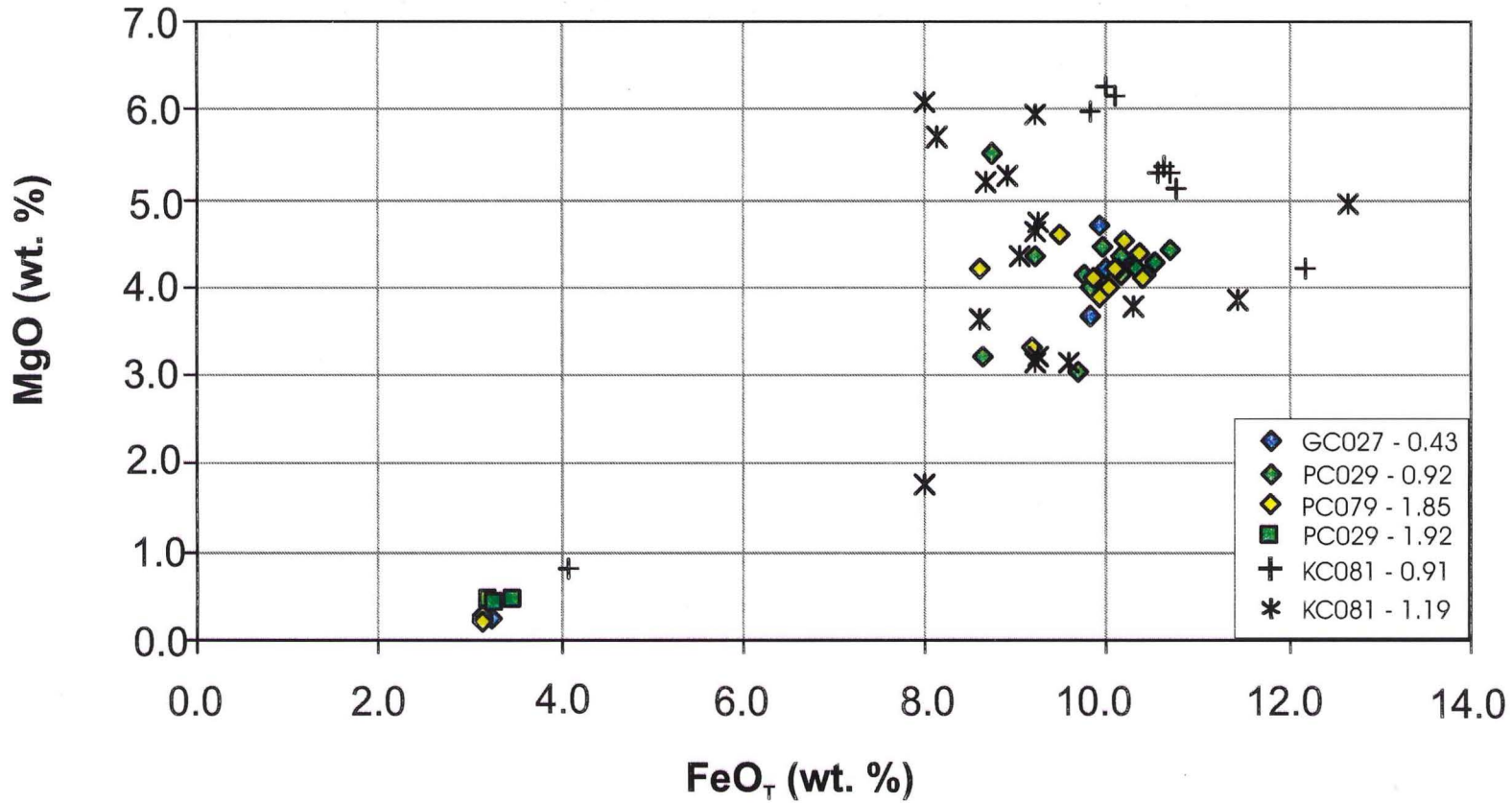
Figure 4.11 PLot of MgO – FeOT for disseminated tephra from Unit U below the visible ash layer. The diamond symbols form a distinct cluster in the same field as the analyses from the megascopic ash.

Table 4.5 Mean values and standard deviations for selected tephras from the terrigenous unit (Unit T). *All iron calculated as FeO. Number of glass shards upon which mean is based are show in column *n*. Probe conditions: 20kV accelerating voltage, 15nA beam current, 1 μm focused beam, 10 second count time.

Core number and sample depth (mbsf)	SiO_2	TiO_2	Al_2O_3	FeO*	MnO	MgO	CaO	Na_2O	K_2O	Total	*n*
PC079 – 2.57	53.65 (2.76)	1.77 (0.59)	16.13 (1.92)	8.68 (1.27)	0.16 (0.04)	3.48 (1.66)	7.51 (2.75)	4.68 (1.33)	1.04 (1.37)	97.10	*9*
PC078 – 1.12	56.29 (2.60)	1.66 (0.72)	15.25 (0.75)	8.54 (0.83)	0.18 (0.11)	2.65 (1.45)	5.55 (2.54)	5.35 (1.31)	1.63 (1.59)	97.10	*14*
GC037 – 1.97 b	51.12 (0.75)	2.21 (0.12)	16.03 (0.19)	9.88 (0.17)	0.17 (0.04)	4.37 (0.13)	8.56 (0.26)	4.55 (0.15)	0.49 (0.07)	97.38	*5*
GC037 – 1.97 r	69.12 (1.52)	0.54 (0.20)	15.26 (1.31)	3.49 (0.38)	0.14 (0.06)	0.48 (0.28)	1.13 (0.56)	5.85 (0.33)	2.17 (0.35)	98.18	*4*
PC029 – 2.68	52.66 (2.14)	1.85 (0.10)	15.26 (0.68)	9.46 (0.33)	0.16 (0.03)	4.30 (0.61)	8.13 (0.82)	4.35 (0.16)	0.63 (0.34)	96.80	*18*
PC079 – 2.91	53.19 (1.79)	1.86 (0.14)	15.87 (0.64)	9.05 (0.72)	0.16 (0.04)	4.36 (0.61)	8.33 (0.93)	4.51 (0.26)	0.55 (0.32)	97.88	*25*
KC081 – 1.59	52.18 (1.29)	1.99 (0.32)	15.82 (0.76)	9.41 (0.77)	0.19 (0.03)	4.53 (0.75)	8.63 (0.96)	4.45 (0.39)	0.52 (0.21)	97.72	*15*
GC037 – 2.43	68.15 (2.83)	0.37 (0.1)6	12.53 (0.91)	4.13 (1.26)	0.11 (0.05)	0.54 (0.34)	2.78 (0.84)	3.67 (0.32)	1.21 (0.16)	93.49	*10*
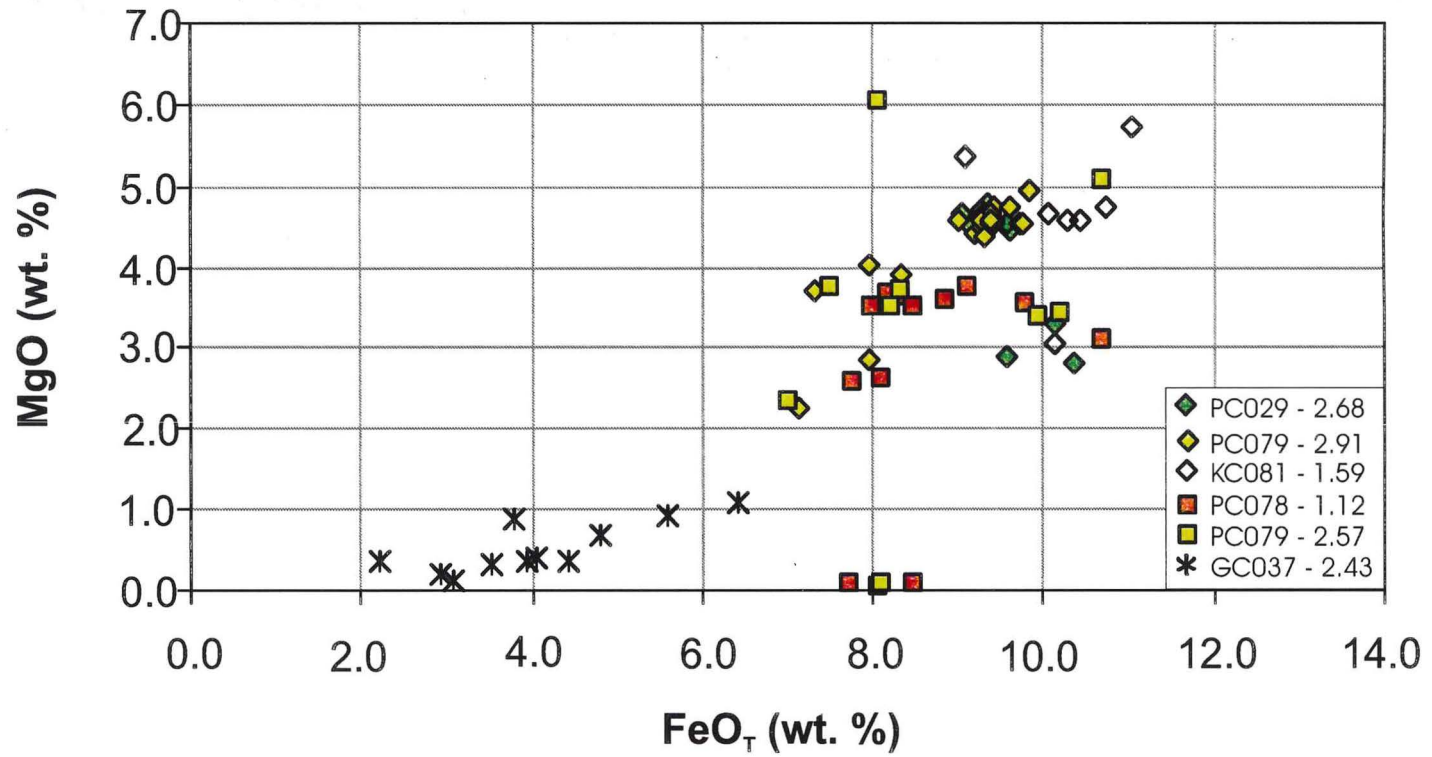
Figure 4.12. Plot of MgO - FeOT for tephras in the terrigenous unit.

One disseminated tephra (GC037–1.97 m) contains shards with geochemical data falling in the same fields as both the basaltic and the rhyolitic glass of the megascopic ash, which is situated over 1m higher up in that core. Many shards in this tephra layer returned low compositional totals. Those shards with low totals fall into two groups. In the basaltic shards with low totals, only silica contents are low relative to shards with totals >95%. In the basaltic-andesite shards all elements are present in reduced concentrations, relative to shards with totals >95%.

The ash layer GC037–2.43 m contains only dacitic to rhyolitic shards. Both potassium and sodium contents are low in this tephra, whilst calcium contents are high (Table 4.5). Many of these analyses returned low totals, which have been retained here as they clearly show the same trend as the analyses with totals of 95 % or more. The slope of this trend is different to that seen in other Scotia Sea tephra. Recalculating the composition of the shards to 100% does not alter the slope of the trend.

4.2.2.5 Ash in sedimentary Unit L

The largest group of ash layers are located in Unit L or at lower depths in units not yet described in the literature. With a few notable exceptions tephra was less abundant at these depths and finding sufficient glass shards to characterise each ash layer was achieved only with considerable difficulty and occasionally not at all. Several ash layers showed no compositional homogeneity and have been omitted from the following figures and tables. Only ash layers which produce tightly clustered data or linear trends can be confidently correlated at this stage.

The ash layers which could not be characterised predominantly came from core GC027, where the abundance of tephra was generally low throughout the core, as noted above. For the present these ash layers will be retained but must remain questionable. The ash layers concerned are GC027–1.35 m, GC027–2.78 m, GC027–2.90 m, GC027–3.02 m and GC037–3.54 m.

Ash layers with clustered data which do not correspond compositionally with any other tephras within Unit L are presented in Figure 4.13. These tephras have a high potential
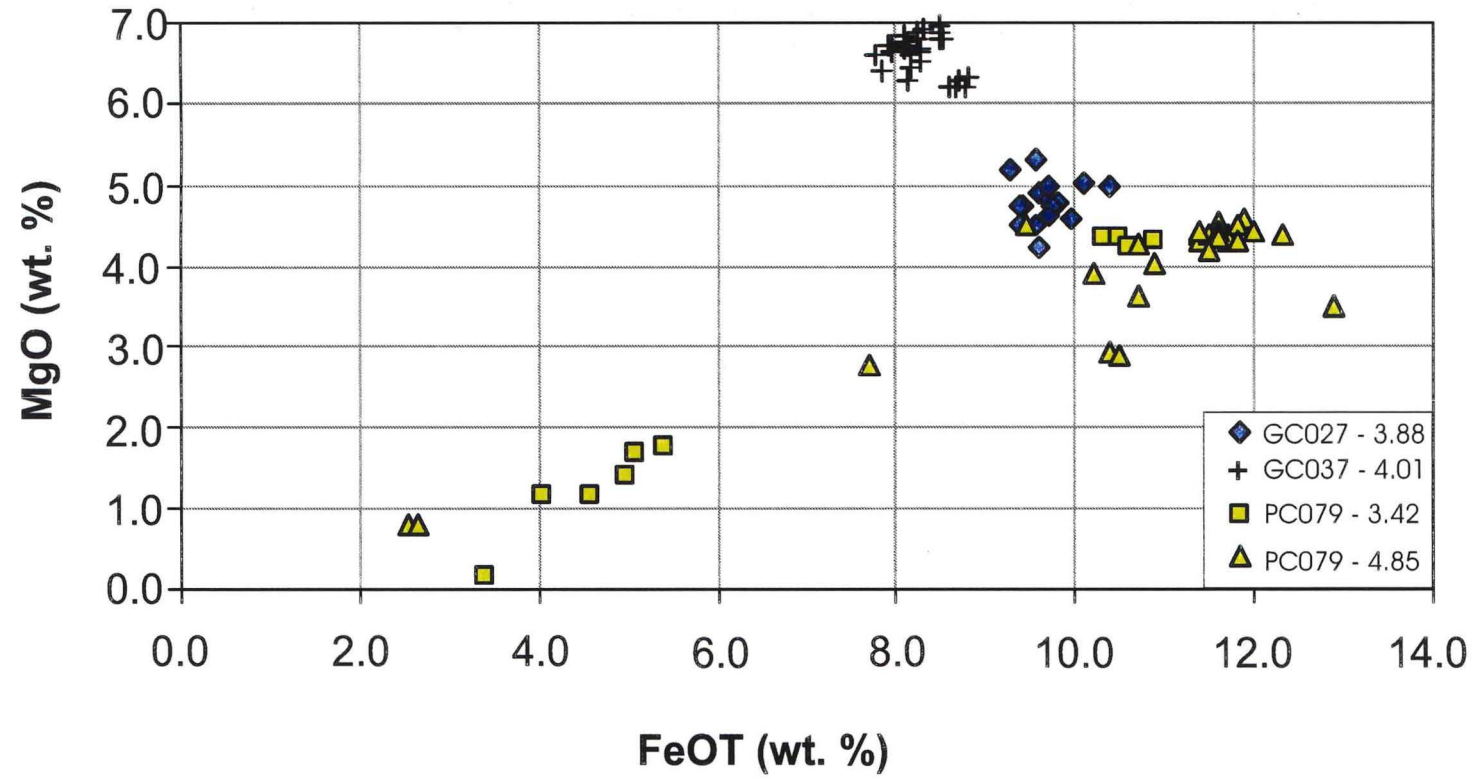
Figure 4.13 FeO$_T$ – MgO plot of tephras with unique clusters.

Table 4.6. Tephras from Unit L which show uniquely clustered data. These tephras have the potential for correlation with as yet undiscovered tephras in the region. Tephra PC079 – 3.42 may be bimodal with basaltic (b) and a trachyandesitic (t) modes. **Mean and standard deviation include both basalts and basaltic-andesites. Probe conditions: 20kV accelerating voltage, 15nA beam current, 1 μm focused beam, 10 second count time. * All iron shown as FeO.

Core Number and sample depth (mbsf)	SiO_2	TiO_2	Al_2O_3	FeO_T*	MnO	MgO	CaO	Na_2O	K_2O	Total	n
Unique clusters											
GC027 – 3.88	51.04 (0.60)	2.11 (0.10)	15.34 (0.19)	9.68 (0.29)	0.21 (0.03)	4.84 (0.23)	8.81 (0.34)	4.23 (0.15)	0.50 (0.04)	96.76	16
PC079 – 3.42 b	51.43 (0.21)	2.40 (0.04)	16.15 (0.18)	10.57 (0.31)	0.17 (0.03)	4.33 (0.02)	8.49 (0.24)	4.72 (1.15)	0.50 (0.01)	98.76	3
PC079 – 3.42 t	64.14 (1.39)	1.22 (0.06)	16.04 (0.20)	4.82 (0.52)	0.18 (0.04)	1.44 (0.29)	2.99 (0.69)	4.00 (0.95)	2.62 (0.73)	97.45	5
PC079 – 4.85	51.30 (0.35)	3.00 (0.18)	13.65 (0.57)	11.52 (0.55)	0.24 (0.03)	4.28 (0.27)	7.36 (0.32)	4.49 (0.15)	0.66 (0.08)	96.49	23
Coincident clusters											
PC029 – 3.64**	52.83 (0.60)	1.59 (0.16)	15.92 (0.44)	8.26 (0.44)	0.18 (5.24)	5.24 (0.26)	9.37 (0.48)	4.23 (0.17)	0.52 (0.09)	98.14	15
PC078 – 2.73**	51.73 (0.56)	1.61 (0.16)	15.74 (0.42)	8.54 (0.66)	0.19 (0.04)	5.34 (0.22)	9.28 (0.35)	4.21 (0.15)	0.51 (0.07)	97.15	14
PC079 – 3.89**	51.49 (0.61)	1.72 (0.37)	15.42 (0.91)	8.74 (1.16)	0.18 (0.04)	5.09 (0.52)	9.11 (0.82)	4.14 (0.24)	0.54 (0.10)	96.43	19
KC081 – 2.46**	52.63 (1.01)	1.73 (0.16)	15.95 (0.67)	8.68 (0.68)	0.18 (0.03)	4.98 (0.46)	9.00 (0.90)	4.28 (0.26)	0.58 (0.12)	98.01	9
PC027 – 3.88	50.92 (0.66)	1.79 (0.15)	14.99 (0.29)	9.59 (0.58)	0.19 (0.04)	5.57 (0.38)	9.73 (0.38)	4.25 (0.23)	0.42 (0.23)	97.45	15
PC078 – 3.93	51.05 (0.63)	1.79 (0.26)	14.74 (0.73)	9.50 (0.64)	0.17 (0.04)	5.24 (0.22)	9.26 (0.50)	4.03 (0.17)	0.48 (0.12)	96.26	8
PC079 – 5.47	50.92 (0.54)	1.81 (0.18)	14.87 (0.35)	9.58 (0.67)	0.22 (0.03)	5.01 (0.49)	9.25 (0.70)	4.32 (0.22)	0.40 (0.04)	96.47	11
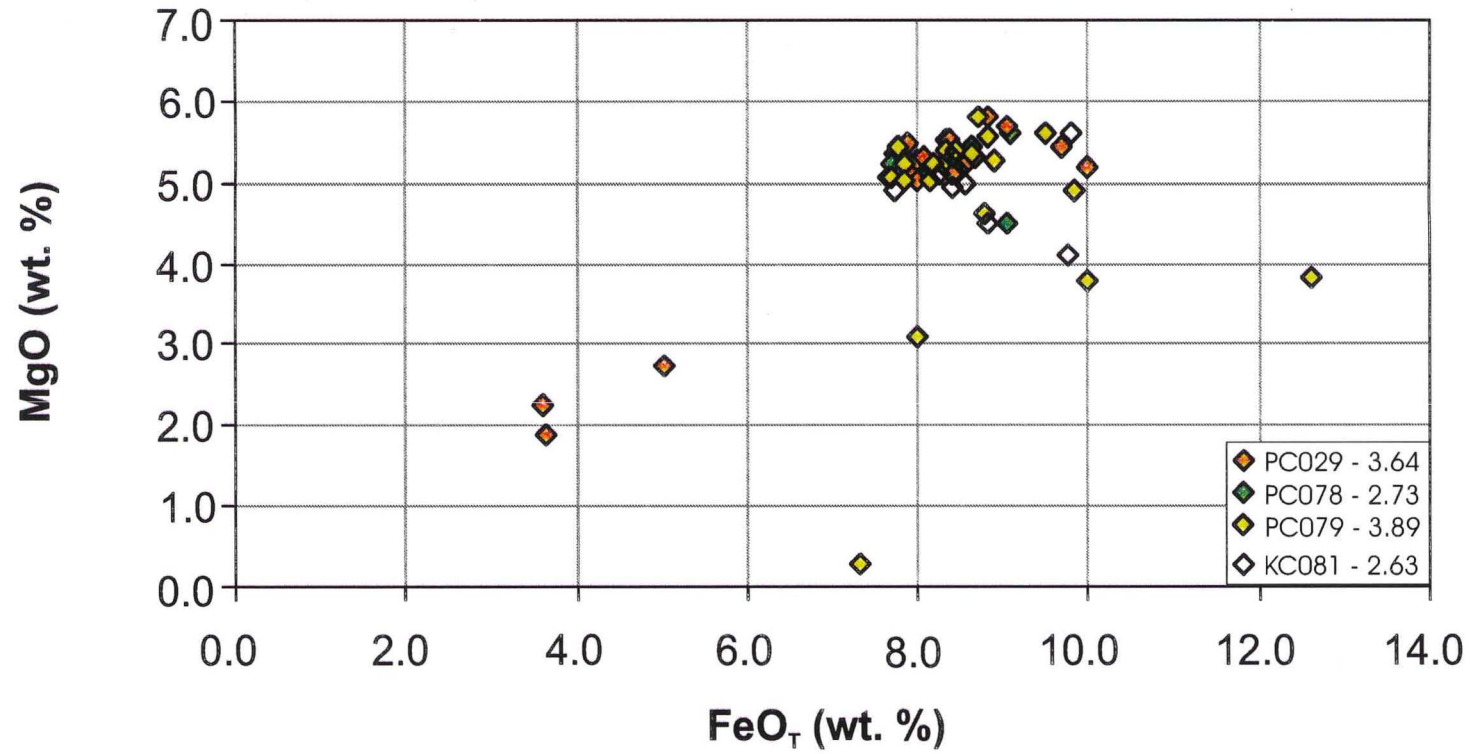
Figure 4.14 Plot of MgO – FeO$_T$ for tephras from Unit L which show coincident clustering of analyses.
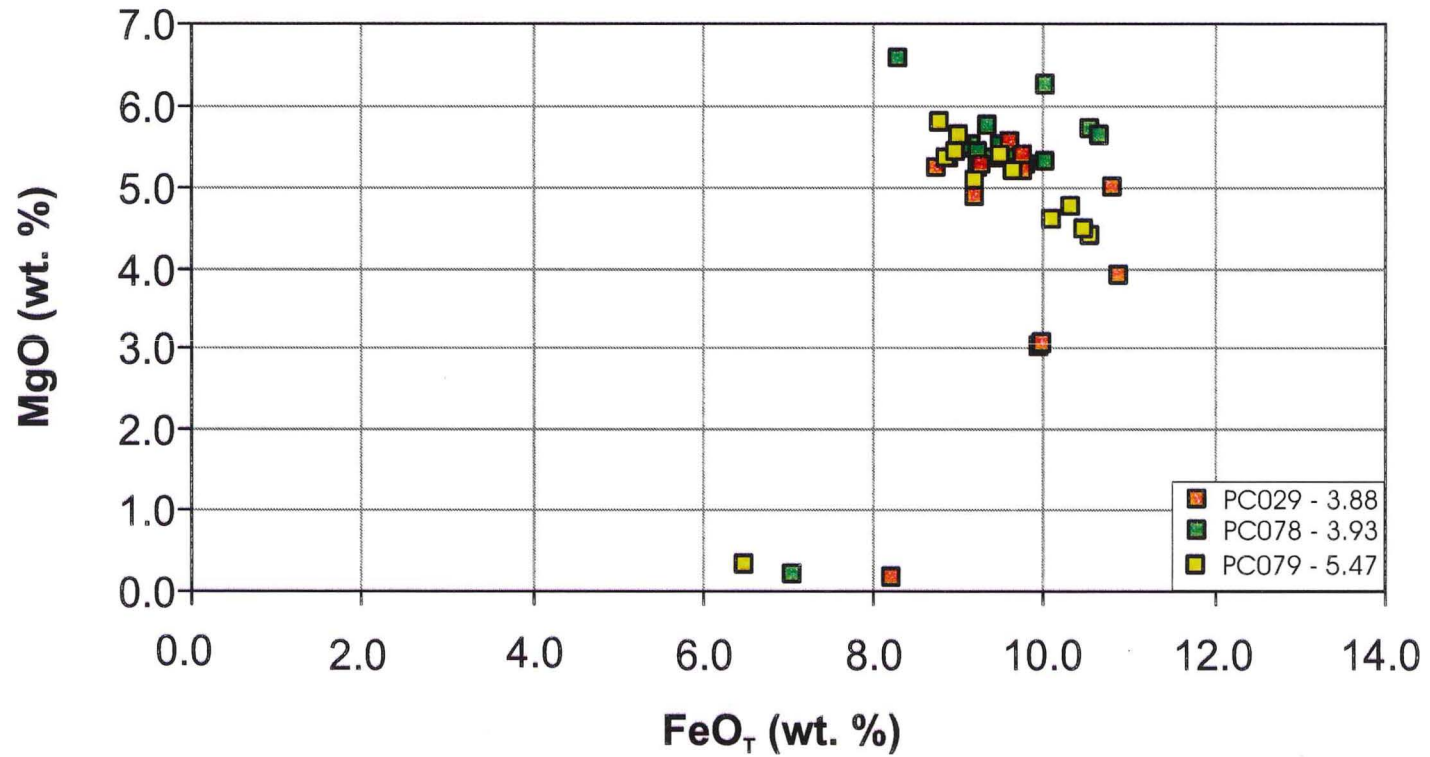
Figure 4.15. MgO – FeO$_T$ plot for the second group of tephras from Unit L which show coincident clusters.
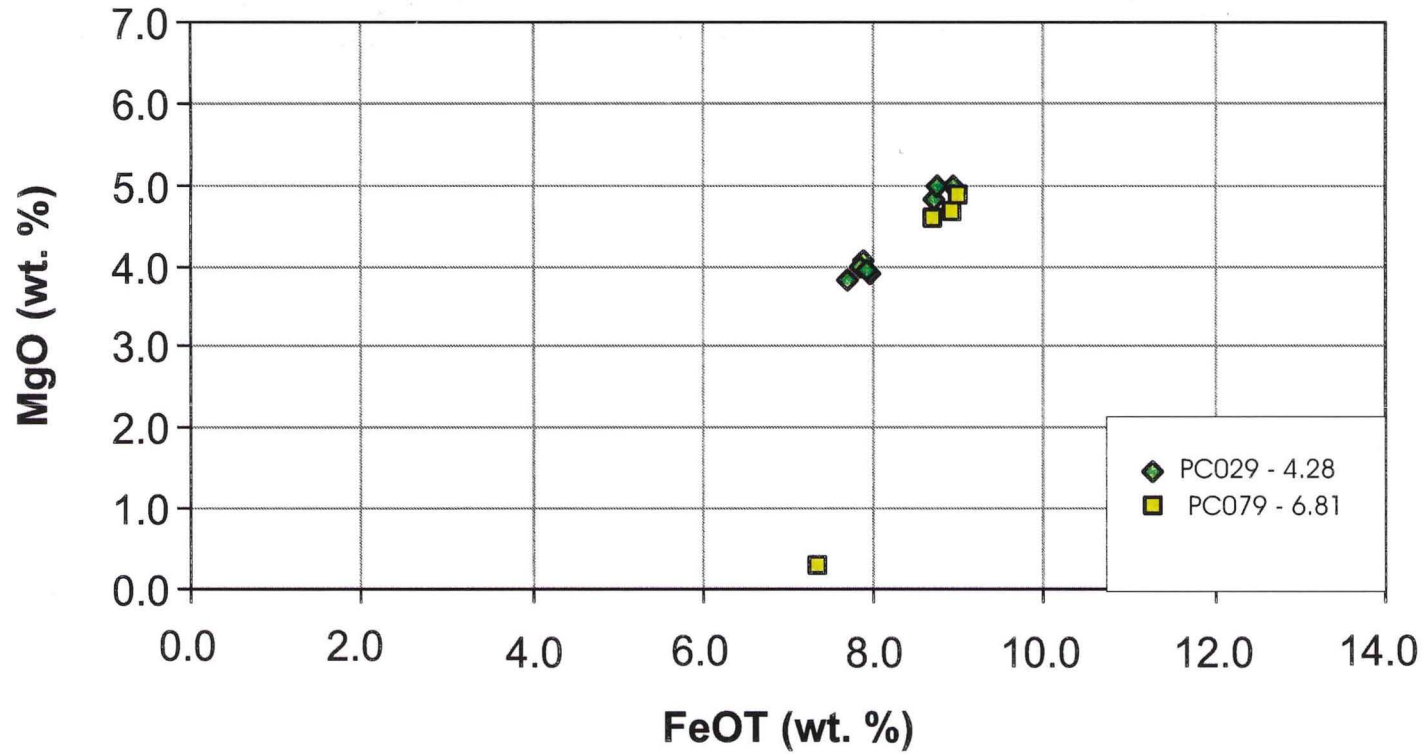
Figure 4.16 MgO – FeOT plot of a partial correlation of tephras from Unit U. These tephras are the closest match to the Boyd Strait tephras (core GC114).
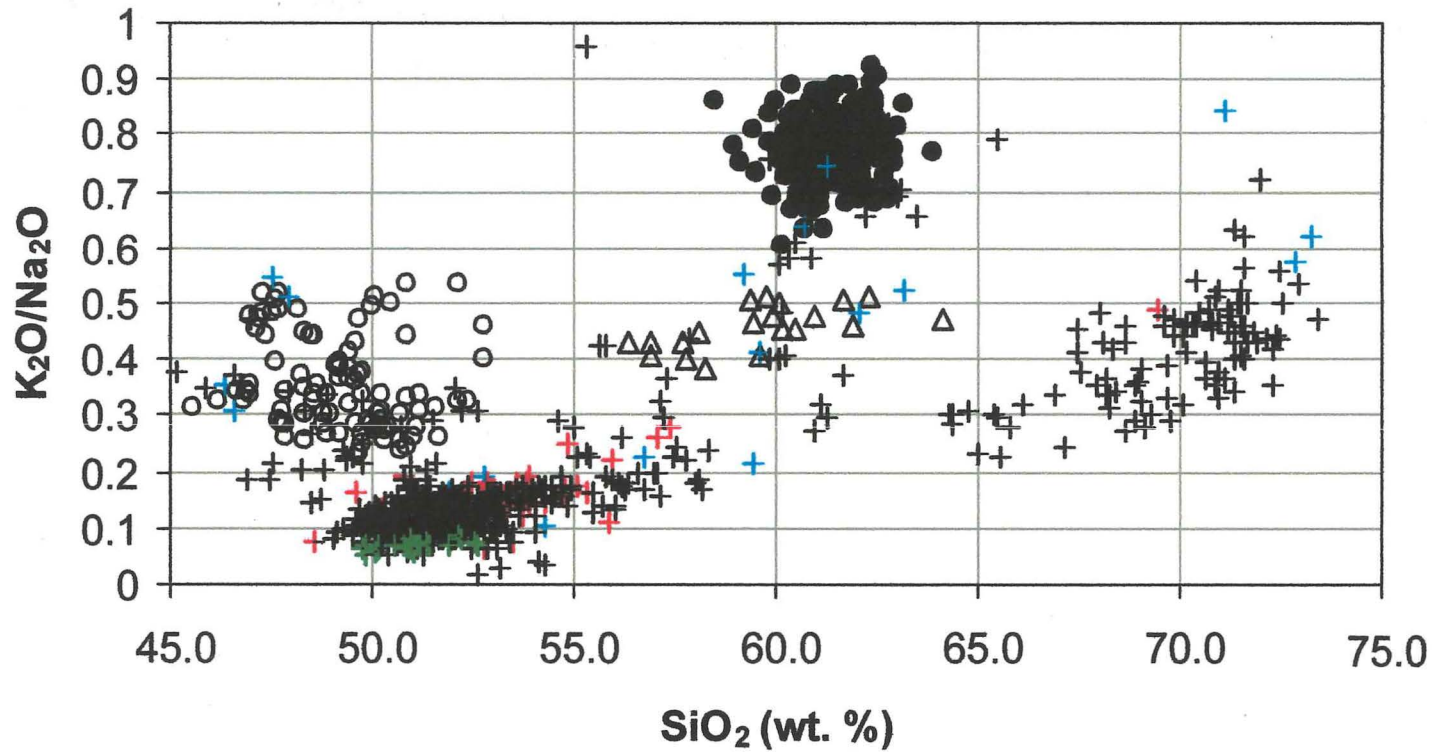
Figure 4.17. K_2O/Na_2O - SiO_2 data for all tephra analysed in this project. The northern Bellingshausen Sea tephra (filled circles), Southern Bellingshausen Sea (open circles), Mt. Hudson (Open triangles) and the bulk Scotia Sea tepras (crosses) can be clearly distinguished from one another. The tephras from core GC114 from Boyd Strait (red crosses) show a clear affinity with the bulk of the Scotia Sea tephra which have been identified as having a Deception Island origin. However the tephra from the northern Scotia Sea, core PC063 (blue crosses) show no clear affinity and appear to contain tephras from a variety of sources. Tephra from GC037 – 4.01 (green crosses) can be seen to plot at the extreme margin of the Scotia Sea analyses and suggest a possible South Sandwich Island source.

for correlation with as yet undiscovered tephras in other Scotia Sea cores. The remaining ash layers fall into two groups (Figures 4.14 and 4.15) which show coincident clusters, and are therefore, potential correlations. A third partial correlation between two tephras in the unit is shown in Figure 4.16. All coincident clusters shown in figures 4.14, 4.15 and 4.16, and in Table 4.6 take into account relative stratigraphic position of the different ash layers.

In Figure 4.13, ash layer GC027–3.88 m can be seen to produce a cluster that plots in the same field as analyses from tephras in the terrigenous unit (Figure 4.12). However, the lower limit of the terrigenous unit in GC027 is currently placed at a depth of 2.90 m below sea bed based on magnetic susceptibility and Ba/Al ratios (Shimmield *et al* 1993, Pudsey and Howe 1998, C. J. Pudsey pers. comm.).

Throughout core GC037, several ash layers contain populations of glass that give low totals. These ash layers contain both colourless and brown glass, and both types were responsible for the low totals suggesting that post-depositional alteration rather than chemical composition may be significant.

One tephra layer (GC037–4.01 m), close to the bottom of the core, has the highest mean MgO concentration (6.62 %) of any tephra examined in this thesis. The 4.01 m tephra can also be distinguished by the values of TiO_2, FeO_T and SiO_2 (Figure 4.13). Figure 4.17. reproduces Figure 4.9 but with all of the Scotia Sea data added. The analyses from GC037–4.01 m can be seen at the extreme limit of the Scotia Sea field.

4.2.3 Boyd Strait

None of the glass was analysed for trace elements, but the major oxide geochemistry summarised in Table 4.7 shows the glass has basaltic to basaltic-andesite compositions. Na_2O is relatively high while K_2O is low, as it is in the Scotia Sea tephras.

Table 4.7 Mean and standard deviations (in parentheses) of the major oxide geochemistry of the two ash layers found in core GC114. * All iron calculated as FeO. Probe conditions: accelerating voltage 20kV, beam current 15nA, 1 μm focused beam. Elements were analysed in pairs with 10 second count times per pair.

Depth (mbsf)	SiO$_2$	TiO$_2$	Al$_2$O$_3$	FeO *	MnO	MgO	CaO	Na$_2$O	K$_2$O	Total	n
2.98	53.50	1.81	15.54	8.33	0.19	4.08	7.62	4.61	0.74	96.42	46
	(2.90)	(0.46)	(1.01)	(1.35)	(0.04)	(1.12)	(1.46)	(0.32)	(0.32)		
2.98	69.44	0.37	13.68	3.09	0.14	0.18	0.54	5.30	2.60	95.35	1
3.12	53.53	2.00	15.41	8.81	0.18	3.91	7.58	4.58	0.70	96.70	22
	(1.28)	(0.62)	(1.55)	(1.88)	(0.04)	(0.72)	(0.80	(0.31)	(0.13)		

In the upper ash layers a single rhyolitic shard was found. Although this shard was morphologically similar to those seen in the mixed bimodal ash found in the Scotia Sea, chemically it shows several significant differences.

Boyd Strait tephra analyses from both ash layers form a positive FeO–MgO trend but with a large scatter of data (Figure 4.18). The pattern of scatter is similar to that for the black shards from the visible Scotia Sea tephra (Figure 4.8). The slope and position of the trend most closely matches the partial correlation of ash layers PC029–4.28 m and PC079–6.81 m.
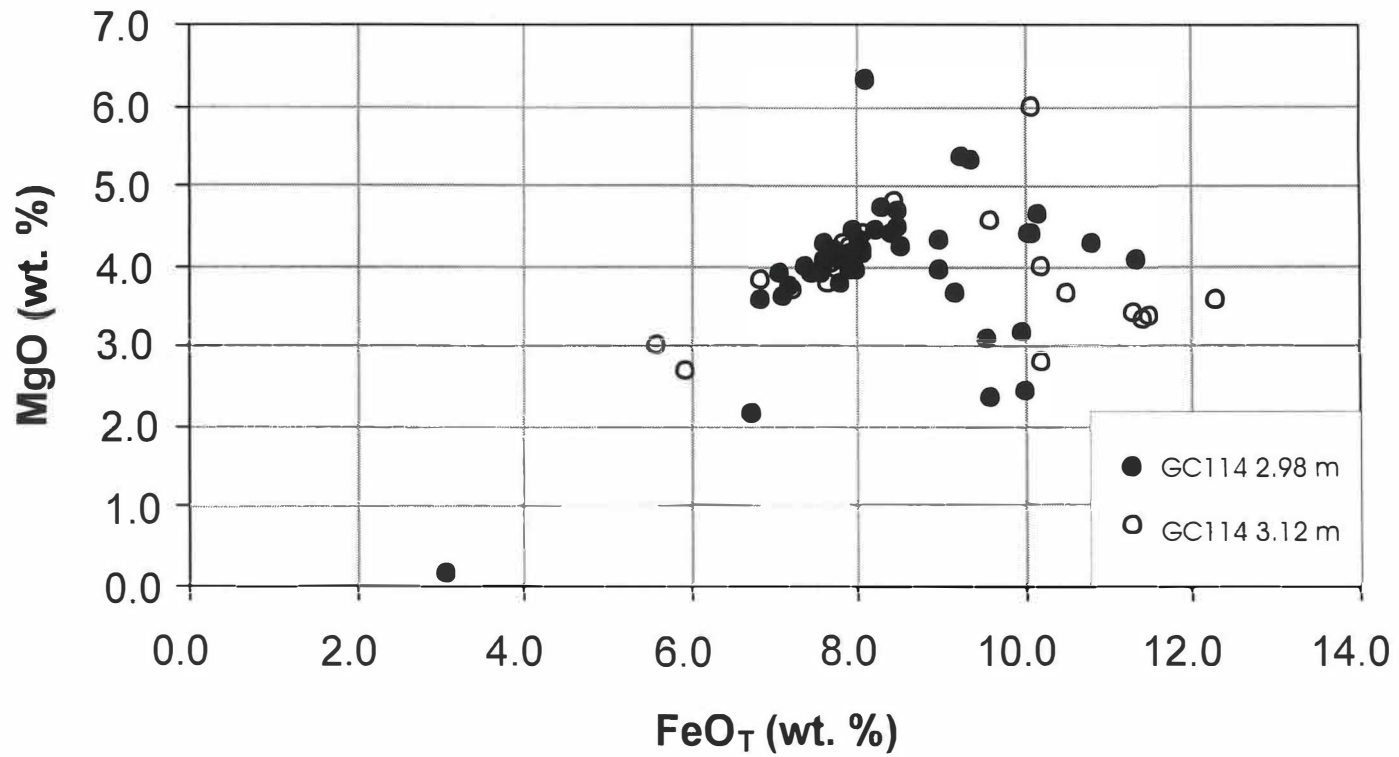
Figure 4.18 MgO – FeO$_T$ plot of tephras from the Boyd Strait core (GC114).

4.2.4 Mt. Hudson ash

The major element composition of the ash was determined by electron-probe microanalysis. The results of the EPMA shown in Table 4.8 and Figure 4.17 indicate that the Mt. Hudson tephra forms a well defined trend rather than a tight cluster. Compositionally the tephra range from trachyandesite to marginally dacitic with SiO_2 ranging from 56.38 to 64.11 % and total alkalis ranging from 6.42 to 8.29 %.

Table 4.8. Mean major oxide composition of vitric shards from the 1991 eruption of Mt. Hudson, Chile. Standard deviations are given in parentheses.

	SiO_2	TiO_2	Al_2O_3	FeO	MnO	MgO	CaO	Na_2O	K_2O	Total	n
Mt.	59.59	1.49	15.81	6.18	0.21	2.12	4.31	4.97	2.27	96.95	*20*
Hudson	(2.00)	(0.19)	(0.24)	(0.83)	(0.03)	(0.42)	(0.74)	(0.26)	(0.25)		

The mean SiO_2 of 59.59 % is similar to that of the sediment drift tephra. However, the Mt. Hudson tephra can confidently be distinguished from the sediment drift tephra by comparison of the alkali metals, as well as TiO_2, MgO and CaO contents.

4.3 Ion Microprobe results

Trace element abundances were determined for selected Scotia Sea tephra by ion-microprobe analysis, primarily to constrain the possible source volcano(es) (Table 4.9).

Two samples of the megascopic ash layer (PC079–1.80 m and KC081–0.21m) were analysed along with one tephra from Unit L (PC079–3.41m) which stratigraphically could not be the same as the megascopic ash but which has a similar composition. Two ash layers from Unit L (PC029–3.64 m and KC081–2.63 m), which have similar major element compositions and an ash layer with a broad range of major element composition (PC029–3.16 m, also in Unit L) were also analysed.

Both samples of the megascopic ash have similar trace element contents but the ash layer (PC079–3.41 m) which has similar major element composition to the megascopic ash could be distinguished from it by its trace elements. Ash layers PC029–3.64 m and

Table 4.9 Mean trace element determinations of selected ash layers from the Scotia Sea cores. All values shown in parts per million (ppm). Standard deviations shown in parentheses. b = basalt , r = rhyolite.

Core number and sample depth (mbsf)		Ni	Rb	Sr	Y	Zr	Nb	Ba	Ce	*n*
PC079 – 1.80	b	371 (±42)	4 (±1)	337 (±56)	27 (±7)	180 (±41)	6 (±1)	71 (±8)	27 (±6)	*18*
KC081 – 0.21	b	351 (±34)	4 (±1)	302 (±29)	28 (±3)	189 (±22)	6 (±1)	67 (±8)	28 (±4)	*12*
PC079 – 1.80	r	59 (±22)	37 (±11)	24 (±13)	67 (±4)	890 (±62)	26 (±3)	224 (±37)	83 (±11)	*4*
KC081 – 0.21	r	52 (±18)	32 (±1)	59 (±59)	59 (±6)	822 (±75)	25 (±2)	226 (±51)	74 (±5)	*3*
PC079 – 3.42	b	347 (±31)	15 (±5)	277 (±88)	15 (±5)	120 (±42)	3 (±1)	140 (±22)	23 (±7)	*2*
PC029 – 3.16	b	432 (±51)	6 (±6)	335 (±119)	21 (±3)	134 (±25)	4 (±2)	95 (±43)	26 (±11)	*8*
KC081 – 2.46	b	399 (±26)	4 (±2)	325 (±44)	21 (±2)	157 (±23)	5 (±1)	71 (±18)	23 (±4)	*6*
PC029 – 3.64	b	398 (±19)	4 (±1)	384 (±51)	17 (±4)	128 (±27)	4 (±1)	68 (±12)	20 (±4)	*6*

KC081–2.63 m, which have similar major oxide compositions, also show similar trace element concentrations. However, ash layer PC029–3.16 m, which does not correlate with any other tephra layer and which has a very varied major element composition, also shares several similarities with KC081–2.63 m, although the higher standard deviations show that the similarities are not as close as they immediately appear.

4.4. Radiocarbon dating

Following the publication of preliminary results from the investigation of the Scotia Sea tephra layers (Moreton and Smellie 1998), several samples of sediment rich in organic carbon were submitted for ^{14}C radiocarbon dating. The results of the radiocarbon dating are given in Table 4.10. A ^{14}C reservoir age of 1300 years was used. This reservoir age is a mean value calculated from various published ages (Berkmann *et al.* (1998). It is also the reservoir age of deep waters currently upwelling around Antarctica (Michel and Druffel 1983, Struvier *et al.* 1983). This reservoir age was preferred over a 1430 year reservoir age (Pudsey and King 1997) calculated from analyses of organic carbon from two sediment traps deployed in the Jane Basin. Although this latter age is calculated from contemporary sediments in the water column close to two of the core localities used in this study, it is the mean of only two published ages which show considerable variation (965 ± 50 and 1895 ± 55).

Core top ages, as an indicator of the effect of reworking through bioturbation, were not taken into account due to the problems of recovering sediments at the sediment-water interface (Andrews *et al.* 1999, see also section 5.4.1.3.) However, analysis of a piston core recovered from Andvord Bay, Antarctic Peninsula produced near-identical results from paired radiocarbon analyses of foraminifera and organic matter indicating that little reworking of significantly 'old' carbon had occurred (Domack *et al.* 1993).

After accounting for the marine ^{14}C reservoir effect the radio-carbon ages were converted to calendar ages through calibration with the U-Th ages calculated for Barbados corals (Bard *et al.* 1990a). By applying U-Th and ^{14}C dating to the same coral samples and comparing the results with independent derived, dendrochronological, dating of the corals, Bard *et al.* (1990a) showed that U-Th ages are accurate as they

accord with the dendrochronological calibration. U-Th dating can, therefore, be used to calibrate the ^{14}C ages beyond the range of dendrochonology. As the two correction factors used to calibrate the calendar ages are arithmetic rather than statistical the original 1 σ standard deviations have been retained.

Table 4.10 Radiocarbon ages of Scotia Sea cores. Reservoir age of 1300 years used for corrected ^{14}C age (Berkman *et al.* 1998). Calendar age calibrated using U–Th (Bard *et al.* 1990a). *The bimodal ash layer that occurs at 35cm below sea bed in PC078 occurs at 16 cm depth in trigger core TC078.

NERC Publication Code	Core and sample depth (mbsf)	Conventional Radiocarbon age (years BP ± 1σ)	Reservoir corrected age	Age in calendar years	Comments
AA-28116	PC029-0.05 m	13,925 ± 80	12,625 ± 80	14,380 ± 80	Core top
AA-28117	PC029-0.68 m	9,245 ± 65	7,945 ± 65	9,100 ± 65	Above visible ash
AA-28118	PC029-0.88 m	12,550 ± 80	11,250 ± 80	12,825 ± 80	Below visible ash
AA-28119	PC029-2.68 m	23,440 ± 210	22,140 ± 210	25,100 ±210	Below ash in Unit T
AA-28120	PC029-3.24 m	29,360 ± 360	28,060 ± 360	31,790 ± 360	Below ash in Unit L
AA-28104	TC078-0.12 m	9,570 ± 70	8,270 ± 70	9,465 ± 70	Above visible ash*
AA-28105	TC078-0.20 m	14,740 ± 100	13,440 ± 100	15,300 ± 100	Below visible ash*
AA-28106	PC078-1.20 m	20,590 ± 180	19,290 ± 180	21,900 ± 180	Below ash in Unit T
AA-28107	PC078-276 m	32,560 ± 180	31,260 ± 180	35,400 ± 180	Below ash in Unit L
AA-28108	PC079-0 m	7,690 ± 65	6,390 ± 65	7,350 ± 65	Core top
AA-28109	PC079-1.64 m	8,745 ± 65	7,445 ± 65	8,540 ± 65	Above visible ash
AA-28110	PC079-1.84 m	10,020 ± 75	8,720 ± 75	9,975 ± 75	Below visible ash
AA-28111	PC079-2.63 m	20,160 ± 75	18,860 ± 75	21,410 ± 75	Below ash in Unit T
AA-28112	PC079-2.96 m	25,530 ± 250	24,230 ± 250	27,470 ± 250	Below uppermost ash in Unit U
AA-28113	KC081-0 m	7,615 ± 65	6,315 ± 65	7,260 ± 65	Core top
AA-28114	KC081-0.23 m	12,645 ± 85	11,345 ± 85	12,930 ± 85	Below visible ash
AA-28115	KC081-1.59 m	24,790 ± 220	23,490 ± 220	26,630 ± 220	Below ash in Unit T

5 Discussion

5.1 The Northern Bellingshausen Sea (sediment drift) tephras

5.1.1 Sedimentary context of the tephra

Multi-channel seismic reflection profiles have shown the presence of 9 sediment drifts on the continental rise on the western Antarctic Peninsula margin. Piston and gravity cores from the sediment drifts were recovered during cruises *Eltanin* 05, SEDANO -1 and JR19. Most recently, two of the drifts were drilled during ODP Leg 178. The drifts are asymmetrical with the proximal slope being steeper and rougher than the distal slope (Camerlenghi and Rebesco 1994) indicating that along-slope currents have a greater erosive effect on the sediments closer to the continental margin. Sediments in the drifts show strong glacial - interglacial cyclicity, with brown, diatom-rich highly burrowed, silty clay units corresponding with interglacials and thicker, grey, terrigenous laminated units representing glacials (Pudsey and Camerlenghi 1998, Pudsey and Strobl in prep). Five sedimentary units have been identified in these cores corresponding to Holocene, last glacial, last interglacial and earlier glacial/interglacial sequences, and have been labeled Units A to E respectively (Pudsey and Camerlenghi 1998). A combination of biogenic barium abundance, beryllium and uranium-thorium dating have been used alongside biostratigraphy in order to date the sediments. Unit A consists of Holocene cover, whereas Unit B represents glacial stages 2-4. Unit C is defined as $\delta^{18}O$ stage 5 based on diatom abundance and Ba/Al ratios. Unit D has been identified as glacial stage 6 and Unit E has been dated to $\delta^{18}O$ stage 7 through the presence of *Hemidiscus karstenii* frustules (Burckle *et al*. 1978, Pudsey and Strobl in prep). Detailed stratigraphic interpretations of these cores have previously been published by Camerlenghi *et al*. (1997) and Pudsey and Camerlenghi (1998).

Unit C was described as a diatom-bearing silty clay layer, frequently including or topped by a deposit containing abundant foraminifera. It was originally defined on the basis of downcore variation in sediment colour and texture and was thought to correlate with the occurrence of a brown diatomaceous silty-clay (Pudsey and Camerlenghi 1998). However, a recent reappraisal of the sediments has placed increased emphasis on

the percentage abundance of diatoms (all species), as well as chemical and stable isotope signals (Pudsey and Strobl in prep). This re-examination of the sediments indicated that the climatically controlled factors governing biogenic productivity were happening in concert over the whole of the area covering sediment drift formation, whereas sedimentary processes leading to the colour and textural variations were diachronous, although the reasons for this remain unclear. It is posible, however, that the colour changes are the result of early stages of diagenesis.

Examination of the cores from the sediment drifts has shown that at least three ash layers, one megascopic tephra layer and two disseminated tephras, are present. The megascopic ash is 2 to 5 cm thick and contains highly vesicular clear glass. It occurs towards the base of Unit C in 11 cores (E5-24, SED04, SED06, SED07, PC103, GC105, PC106, PC108, PC110, PC111 and PC113 (this study - Chapter 3, see also Goodell 1964, Pudsey and Camerlenghi 1998, Pudsey and Strobl in prep)). All of these cores are from medial or distal locations on the drifts. Disseminated tephras have been found in four cores (PC101, PC102, PC107 and PC109) these cores are all from proximal to medial locations on the drifts. Core SED06 is the only core found to contain two ash layers. In that core, a disseminated tephra was identified above the megascopic ash layer. Both ash layers occur in Unit C and both contain pumiceous clear glass with abundant elongate vesicles. The disseminated tephra from PC101 is morphologically distinct from that found in the other cores. In that core, glass shards are dark brown with spherical to elliptical vesicles. Microcrystals are also present. The dark brown glass shards occur in Unit D, 1.35 m below the base of Unit C in that core. No tephra was found in Unit C in core PC101. The megascopic ash layer is the only sediment drift tephra to be subjected to geochemical investigation.

Subsequent examination of the base of the diatom-bearing silty clay unit from the proximal cores revealed thin, disturbed or disseminated ash layers in cores PC102, PC107 and PC109. In these cores the lower part of $\delta^{18}O$ stage 5 is more coarse grained than in the distal cores. It has been suggested that increased slope current flow along the upper continental rise was responsible for winnowing the fine fraction (C.J. Pudsey pers. comm.). Due to their high vesicularity, the glass shards have similar

hydrodynamic properties to smaller, lighter terrigenous sediment grains and are likely to have suffered preferential removal under conditions of more vigorous bottom currents. All of these, cores along with PC101 in which the Unit C ash layer has not been observed, are located on the proximal side of the drifts.

5.1.2 Dating the northern Bellingshausen Sea tephra

The brown biogenic unit which contains the megascopic tephra was identified as having been formed during $\delta^{18}O$ stage 5 by Pudsey and Camerlenghi (1998). Despite this inferred young age (c 75 – 128 ka), the high potassium content of the glass shards prompted attempts to directly date the ash layer itself using $^{40}Ar/^{39}Ar$ measurements of glass separates. This technique is still being refined as several problems have arisen due, in part, to the difficulty in separating the glass from the potential sources of extraneous argon (Chapter 2). Problems with inherited argon from feldspar crystals from basement rock entrained during violent explosive volcanism have long been recognised (Curtis 1966). Here, the problems are exacerbated by the potential deposition of glacially eroded rock fragments of substantially greater age and post-depositional reworking by bioturbation. As it was not possible to separate the glass from crystalline fragments (Chapter 2), the potential exists for contamination by excess argon trapped in crystals during their growth in the magma (Singer *et al.* 1998). Step heating of the samples showed that many of the glass samples were contaminated by radiogenic argon (S. Hemming pers. comm., B. Turrin pers. comm.), probably inherited from detrital feldspars eroded from the Antarctic continental margin and incorporated into the drift sediments. The inherited argon gives old ages for the glass that are in conflict with statigraphic evidence (see Pudsey and Camerlenghi 1998). In this case initial $^{40}Ar/^{39}Ar$ results yielded ages of about 2 Ma. The highest temperature steps have ages in the 20 – 40 Ma range, suggesting that the contaminant minerals are of that age. However, one sample did not appear to be significantly contaminated (B. Turrin pers. comm.) and produced an age of <216 ka. Much more experimental work needs to be done, in particular to refine methods of concentrating tephra, before $^{40}Ar/^{39}Ar$ can be applied to late Quaternary glass separates with any confidence.

5.1.3 Correlation of the northern Bellingshausen Sea tephra

Only the megascopic ash layer was analysed. Electron microprobe analysis reveals little compositional variation either within or between samples from different cores. A comparison of the composition of 203 glass shards analysed shows that the most abundant oxide, SiO_2, has a standard deviation of only 0.84 %. The glass is trachytic in composition. None of the samples can be distinguished from one another on the basis of major oxide geochemistry. There is no discernible difference in the geochemical composition between the top and base of the ash layer in core SED06 despite colour variations observed in that ash layer (see chapter 3). The two samples of megascopic ash that were analysed by ion microprobe (from cores PC108 and PC111) also show no significant compositional differences. As only samples of the megascopic tephra layer were analysed, there are no analyses from demonstrably different ashes with which to compare the megascopic tephras. It is not possible, therefore, to state unambiguously that all samples of megascopic ash are from the same eruption because the inherent inter-eruption variability is not known. However, the lack of compositional variation in either major oxide or trace element analyses, together with morphological and stratigraphical evidence, support the hypothesis that they are the product of a single eruptive event. The megascopic ash layer is therefore identified as an isochron and its use as a datum supports the revised definition of Unit C (Pudsey and Strobl in prep c.f. Pudsey and Camerlenghi 1998). The lack of compositional variation over a horizontal distance in excess of 650 km indicates that the megascopic ash is a useful marker horizon and its composition is likely to be representative of the source magma geochemistry.

Disseminated tephras with highly vesicular clear glass shards also occur within Unit C in cores PC102, PC107 and PC109. As none of the disseminated tephras were analysed, it is unknown whether the tephras in the latter three cores correlate with the disseminated or the megascopic ash in SED06. The colour, morphological and stratigraphic evidence are ambiguous although the spatial distribution of these cores, i.e. present in more proximal locations with higher along-slope current velocities, suggest that these disseminated tephras could be correlatives of the megascopic ash.

No ash layer was identified in Unit C in core PC101. A disseminated tephra containing pale brown glass was found in core PC101 but it occurs well below the base of Unit C, at a depth of 5.4m. Therefore, it can be discounted as a correlative of either of the two ashes found in Unit C in the other cores on stratigraphical and morphological grounds. Until the composition of the pale brown glass has been determined its source cannot be identified. The gradual decrease in shard size from south to north across the drifts (chapter 3) suggests an airfall distribution. Shards with a mean length >80 μm had the potential to reach PC101 but none were found in Unit C in that core. As Unit C shows no signs of winnowing it is unlikely that tephra was deposited and then subsequently removed by current action. It can therefore be surmised that tephra was never deposited at this site suggesting that the leading edge of the volcanic plume was situated to the west of this location, or else that this locality was covered by ice at the time of the eruption. At present it is not possible to say which scenario is the more likely.

5.1.4 Identification of the source of the tephra

As is the case with the Scotia Sea, several potential sources of tephra surround the Bellingshausen Sea (Chapter 1). The closest volcanoes lie in Palmer Land and Ellsworth Land at the base of the Peninsula, the volcanic edifice of Peter I Island, the South Shetland Islands and the string of seamounts described by Vanney and Johnson (1976). Marie Byrd Land is located farther to the southwest but is upwind of both the northern and southern Bellingshausen Sea study areas in the prevailing westerly winds (Mullan and Hichman 1990).

Little is known about the volcanoes of Palmer Land and Ellsworth Land. They are poorly exposed and many may be entirely covered by ice (Rowley *et al* 1990). Access to these volcanoes is extremely difficult, consequently they have rarely been visited and most investigations remain at a reconnaissance level. Most of the cones are heavily eroded, leading to the suggestion that they are pre-Quaternary and, except for inconclusive reports of steam and freshwater pools at a couple of localities, all appear to be extinct (the youngest K-Ar date reported so far is <1Ma). Furthermore, all the volcanoes are situated in a within-plate setting with low silica lavas (42-51 wt. %). On

the basis of published and unpublished compositional data and published whole-rock ages, both Palmer Land and Ellsworth Land can be discounted as potential sources of the sediment drift ash layer (Rowley *et al.* 1990, J.L. Smellie unpublished data).

The most recently active volcano in the South Shetland Islands (Deception Island) lies in excess of 800 km down-wind of the furthest (southwestern-most) sediment drift. Drake Passage forms the central axis of storm systems tracking clockwise around the Antarctic, and therefore the South Shetland Islands would experience north-easterly winds as the anticyclones pass through Drake Passage. However, dispersal of tephra from the South Shetland Islands under this wind regime is not consistent with the largest glass shards being located on the southwestern-most drifts. The extensive published and unpublished datasets of Deception Island lava and tephra compositions (Smellie 1990, Moreton and Smellie 1998, unpublished data of J.L.Smellie and S.G. Moreton (this thesis)) are also incompatible with a South Shetland source for the northern Bellingshausen Sea tephra.

Peter I Island is situated in a preferential location for the source of the sediment drift tephra - located a little over 1000 km to the southwest of the most northeasterly drift (Figure 1.12). However, published data for Peter I Island lavas are compositionally very different from the sediment drift tephra (Prestvik *et al.* 1990, Verwoerd *et al.* 1990). Therefore, Peter I Island can also be excluded as the tephra source.

Although relatively few geochemical analyses have been published for the individual volcanoes of Marie Byrd Land (MBL), all of the Bellingshausen Sea tephra analyses fit onto published fractionation trends for MBL volcanoes (LeMasurier 1990). The intermediate composition of the glass (Table 3.3), in particular high K_2O and low CaO and MgO, suggest Marie Byrd Land as a likely source region for the tephra (LeMasurier 1990). Prevailing atmospheric circulation flowing clockwise around the Antarctic would disperse volcanic plumes northeastward toward the drifts (Figure 1.5). This plume dispersal direction is consistent with the south to north decrease in mean shard size across the drifts that is evident from the measurement of 100 randomly chosen shards from each megascopic ash layer. Marie Byrd Land is therefore confirmed

as the source region of the megascopic tephra. However, major element compositions alone are insufficient to distinguish unambiguously which volcano was the source. Five volcanoes are thought to have been active during the Quaternary (Mt. Berlin, Mt. Siple, Mt. Takahe, Mt. Waesche and Toney Mountain (LeMasurier 1990)). Several volcanoes in the MBL volcanic province are difficult to access and published data on lava types is limited. There are no published analyses of intermediate rocks from Mt. Siple or Mt. Waesche. However, comparison between the results of this study and unpublished data of J.L. Smellie show that neither volcano provides a compositional match for the sediment drift tephra. The trace element composition of the tephra (Table 3.4) shows similarities with published data for both Mt. Berlin and Mt. Takahe (LeMasurier 1990, unpublished data of J.L. Smellie) but is dissimilar to published analyses of intermediate lavas from Toney Mountain (LeMasurier *et al.* 1990, unpublished data of J.L. Smellie). Mt. Berlin is the only confirmed active volcano in Marie Byrd Land and large pumice clasts found at Mt. Moulton and correlated to Mt. Berlin are evidence for highly explosive eruptions of Mt. Berlin (Wilch and McIntosh in press).

5.1.5 Transport and deposition of the tephra

The mean shard size of the glassy tephra show an imperfect northward fining trend from southwest to northeast. SED06 is the only core where samples were taken from the top and base of the megascopic ash layer. Stokes' Law predicts tephra layers originating as air-fall deposits in marine sediments should be normally graded, as larger grains have higher settling velocities through the water column. In core SED06 the base of the ash layer is coarser than the top but the differences are slight. The greatest variability occurs in the size of the largest shards. The largest shard from the base of the ash layer is 620 μm. This individual shard considerably skews the data as the next largest shard in that sample is 290 μm. The largest shard at the top of the ash layer is 250 μm. Additionally, the top of the ash layer has fewer shards in the 96-127 μm fraction but more in the 128-159 μm and 160-191 μm fractions (Figure 3.4). The results can be explained by the observation that while the extremes in the particle size range most closely follow the predictions of Stokes's Law, this is mainly the result of particle shape. The largest grains are greatly elongated in one axis only and therefore do not conform with the hypothetical spherical shape but will settle more quickly due to their

relatively streamlined shape. Furthermore, modelling and water tank experiments on simulated ash falls settling through water columns show that tephra particles tend to form density currents and plumes and therefore the hydrodynamic properties of individual shards are less significant than initial loading at the water surface and turbulence in the water column (Carey 1997). Particle aggregation may also be an important factor in introducing variable grading characteristics to a deposit (Wiesner *et al*. 1995).There is no clear trend in grain size between medial and distal locations on the drifts which suggests that the eruption plume was well mixed and there was no selective reworking by bottom currents at the time of deposition which would otherwise have selectively removed the smaller shards. It is noticeable however, that the cores with disseminated tephra (PC101, PC102, PC107 and PC109) can be separated geographically from the remaining cores which contain a megascopic tephra by a virtually straight line (Figure 3.4). Two possible explanations could account for this observation. Either the dividing line between the megascopic ash and the disseminated ash represents the edge of the volcanic plume, with cores located to the east of this line receiving little or no tephra, or there could have been a physical barrier preventing deposition to the east of this line. The most obvious example of the latter would be the presence of seasonal sea ice. Assuming that the seasonal growth and decay of sea ice was similar during the last interglacial (δ^{18}O stage 5) as it is today, the limit to the extent of the macroscopic ash layer would suggest that the eruption occurred during spring before the ice had fully melted back to its minimum position.

The diminishing size of the glass shards with increased distance from the source is evidence that the tephra was deposited directly from the volcanic plume passing over the core locations rather than from irregular dumping from sea ice. The distance from Mt. Berlin to the northernmost megascopic ash layer so far identified (core PC113 on sediment drift 3) is in excess of 2000 km. This observation highlights the potential for long-distance transport of tephra in the Antarctic where the troposphere is lower and it is easier for eruption columns to reach fast-moving tropospheric and stratospheric winds (Smellie in press). However, the large distance between source and depocentre and the coarse size of the glass shards found in the drifts do not conform with theoretical models of tephra dispersal (Fisher 1964, Shaw et al. 1974), especially for the

anomalously large (620 µm) shard from core SED06. In order to account for such long distance atmospheric transport, two conditions may have influenced the volcanic plume. Firstly, the top of the eruption column may have attained extreme altitude (> 40 km). Secondly, wind speeds may have exceeded those used in the models, which are based on mid-latitude (50° N) winter-season velocities.

Although the troposphere is lower over the poles (as low as 8km (Sparks *et al.* 1997)) this serves to inhibit the ascent height of the plume as the eruption plume has to ascend through a thicker region of more intensely stratified air (Sparks *et al.* 1997). However, for a large Plinian eruption the gas thrust region, in which the eruption column is propelled by the explosive force of the expanding gas, can extend from several hundred metres to a few kilometres. Thereafter, the plume continues to rise under the influence of thermal convection which gives the plume positive buoyancy compared to the surrounding air. The convective region of the plume can extend tens of kilometres into the atmosphere, especially in eruptions of highly fragmented tephra, in which the rapidly cooling fine-grained material heats the surrounding air, causing enhanced buoyancy (Sparks *et al.* 1997, Woods 1998). Thus, a large-magnitude eruption containing highly fragmented tephra, such as may have caused the deposition of the sediment-drift tephra layer, would have an improved chance of reaching the stratosphere.

Around the Antarctic, ground-level windspeeds frequently exceed 80 mph for several days at a time as storm systems track around the continent following the Polar Front. In the troposphere above the poles, upper-air westerly winds blow continuously westward creating a vortex around the Polar Low. These trosposeric winds complete a circuit of the South Pole every 12-14 days (Lally and Lichfield 1969). The westerly winds are centered around a latitude of 60° S. Dust from an eruption plume injected into the troposphere close to the edge of this zone of westerly winds would probably be capable of circling Antarctica several times, and even relatively large pyroclasts may be transported over considerable distances. In order for a volcanic plume from an eruption at Mt. Berlin (76° 03' S) to become entrained in the Polar Westerlies it may first require the plume to be transported northward away from the volcano. The fact that only one

substantial tephra layer originating from a Marie Byrd Land volcano has been found in the sediment drifts of the northern Bellingshausen Sea suggests that the conjunction of eruption style and atmospheric conditions necessary for such long distance tephra transport are rare.

5.2 Southern Bellingshausen Sea

The tephra layers from the Southern Bellingshausen Sea show a high degree of compositional heterogeneity both within and between samples (Table 3.5). Due to the highly variable compositions of the tephras, it was not possible to determine whether any of the ash layers are correlatives. The major oxide chemistry is similar to published analyses of lavas from both Peter I Island and Marie Byrd Land volcanoes (Prestvik *et al.* 1990, Verwoerd *et al.* 1990, LeMasurier 1990). It is thought that Peter I Island formed in response to the same post-subduction, rift-related volcanism that occurred in nearby Marie Byrd Land and the Antarctic Peninsula (Prestvik *et al* 1990). However, while the southern Bellingshausen Sea tephra plots on the fractionation trend of MBL lavas for several elements (e.g. SiO_2, FeO and MgO) the overall composition also matches that of Peter I Island, and the elevated TiO_2 values favour Peter I Island as the source of the tephra (c.f. Prestvik 1990; Verwoerd *et al* 1990).

The southern Bellingshausen Sea cores were all collected within 100 km of Peter I island, which has a basal diameter of 64 km (Verwoerd *et al* 1990). The large clast size of the tephra (up to 4 mm across) suggests a local provenance for the tephra. Although the tephra is scoriaceous, the largest clasts are not buoyant in water even after oven drying. Therefore, long distance rafting of the tephra similar to that seen in pumiceous clasts from the South Sandwich Islands (Gass *et al.* 1963) is unlikely although ice-rafting is possible.

The Southern Bellingshausen Sea ash layers exhibit sharp basal contacts and normal grading (personal communication from C.J. Pudsey). The large shards, heterogeneous composition of the ash layers, and proximity to the submerged flanks of the Peter I Island volcano strongly suggest that these ash layers may have been emplaced by

turbidity currents. The cyclical and graded nature of the cores as a whole suggests that turbidity currents occur frequently on the flanks of Peter I Island (Goodell 1964, 1965).

Although no attempt was made to directly date these tephras, published K-Ar ages for lavas on Peter I Island are less than 327 ± 88 Ka (Prestvik 1990). (This is considerably younger than the 12.5 ± 1.5 Ma originally reported by Bastien and Craddock 1976). These revised young ages suggest that the ash layers were probably emplaced during the Middle Pleistocene.

5.3 The Northern Scotia Sea tephras

The broad range of geochemical compositions present in glass shards from core PC063 (Figure 4.17, Table 4.1) is indicative that multiple volcanic sources have contributed tephra to this region of the Scotia Sea. Neither the shards themselves nor the surrounding sediment have been dated. The morphology of some of the shards includes surface features such as crusts and cracks that are not seen in any other shards from the Scotia or northern Bellingshausen seas. These features are indicative of the early signs of hydration (Wohletz 1987). Chipped edges and rounded shard morphology can be indicative of increased abrasion during saltation in pyroclastic flow and surge deposits, whereas shards within airfall tephra deposits show minimal modification during transport (Wohletz 1987). It is likely that saltation during bottom current transport would produce similarly chipped and rounded shards. The shard morphology and geochemical compositions indicate that none of the glass shards concentrations are the product of primary air-fall tephra deposition.

5.4 The Central Scotia Sea and Jane Basin tephra

5.4.1 The megascopic ash

5.4.1.1 Identification of source

The major element compositions of both the basaltic and rhyolitic components of the megascopic tephra from the Scotia Sea and Weddell Sea are the same, within analytical error, in all six cores (Chapter 4). The high sodium content of the dominant basaltic glass

shards correlate well with published geochemical data obtained for Deception Island tephras and lavas (Hawkes 1961; Weaver *et al*. 1979, Smellie 1990 and unpublished data of J.L. Smellie). Elevated Na_2O is a regionally unique characteristic of Deception Island magmas, and is not found in other Antarctic and South American volcanoes, nor in the South Sandwich Islands (c.f. Smellie 1990). Additional characteristics of Deception Island tephras that distinguish them from other potential Bransfield Strait sources are high TiO_2 and low K_2O (Weaver *et al*. 1979, Keller *et al*. 1991). The composition of the rhyolitic glass in the megascopic ash layer also plots on the fractionation trend of Deception Island magma. However, the rhyolitic glass is more evolved than any previously published analyses from that island. The trace element compositions determined by ion microprobe analyses closely match unpublished trace element compositions previously obtained by XRF analyses of lava bombs from Deception Island (unpublished data of J.L.Smellie). Deception Island, situated almost 800km upwind of the nearest core examined here, is therefore identified as the source of megascopic tephra.

The megascopic bimodal ash layer can be traced across the Scotia Sea and Weddell Sea from core PC078 in the north to GC027 in the south, a distance in excess of 600 km. Correlation of the ash layer is confirmed by stratigraphic position, magnetic susceptibility, morphological characteristics (basaltic and rhyolite shards), major and trace element composition and radiocarbon dating. The low abundance of glass shards (<5 % of the sieved sediment) in core PC078 and the complete absence of glass from this eruption in core PC063 suggest that the northernmost limit of dispersal of this tephra lies somewhere between these two locations. However it should be noted that faster bottom current speeds at core PC063, which is situated near to the axis of the ACC, may have removed tephra by winnowing as the highly vesicular shards have hydrodynamic properties comparable to much smaller terrigenous grains. The southern limit of dispersal probably lies to the south of core GC027. The fact that the megascopic ash is not seen in core GC057 cannot be taken as evidence that the ash did not travel as far south as this location, as this core site is frequently covered by annual and multi-year sea-ice (Figure 1.7) (Gilbert *et al*. 1998).

In core PC079, the ratio of basaltic and rhyolitic glass is invariant over a vertical distance of 15 cm (this study, section 4.1.3), indicating that the two glass phases were thoroughly mixed prior to deposition. The two glass phases also share a common spatial distribution over a 600 km transect perpendicular to the axis of dispersal (Figure 1.6). The ubiquitous co-occurrence and complete mixing of two compositionally distinct glass populations prior to deposition indicates that the two phases were co-erupted and are not the product of post-depositional mixing. Although this is not the first example of multiple glass populations in ash layers from Deception Island (Matthies 1988; Dyson (1996 unpublished MRes thesis University College London)), the range of compositions is more extreme than previously reported.

5.4.1.2 Transport and deposition of the megascopic tephra

The main axis of iceberg migration is southwest to northeast. The majority of icebergs leave the Weddell Sea to the west of the South Orkney Islands and follow a northeasterly trajectory that takes them toward South Georgia (Figure 1.6). The densest concentration of icebergs passes over the location of cores PC029, PC079 and KC081. Relatively few icebergs are recorded over the site of PC078, which would account for the glass concentration distribution in the Scotia Sea if the tephra was ice-rafted. However, few icebergs leave the Weddell Sea through Jane Basin where glass abundance in the megascopic ash exceeds 25 % of the sieved sediment. If the megascopic ash in the Scotia Sea was transported to the core locations by ice-rafting then the same ash layer in Jane Basin would be considerably thinner. If the initial dispersal of the plume was toward Jane Basin then it could be expected that the megascopic ash layer there would be thicker than the subsequently ice-rafted and dispersed tephra in the Scotia Sea cores. It is therefore unlikely that ice-rafting has been a significant factor in the transport and deposition of the megascopic ash.

Evidence for the atmospheric dispersal of the megascopic ash can be seen in the wide geographical dispersal of the ash. As the ash layer is not seen in any cores recovered by the British Antarctic Survey between core stations KC081 and GC037, it is possible that the tops of these cores have not been completely recovered. Alternatively, shifting wind directions during the course of the eruption or differential wind-shear at different
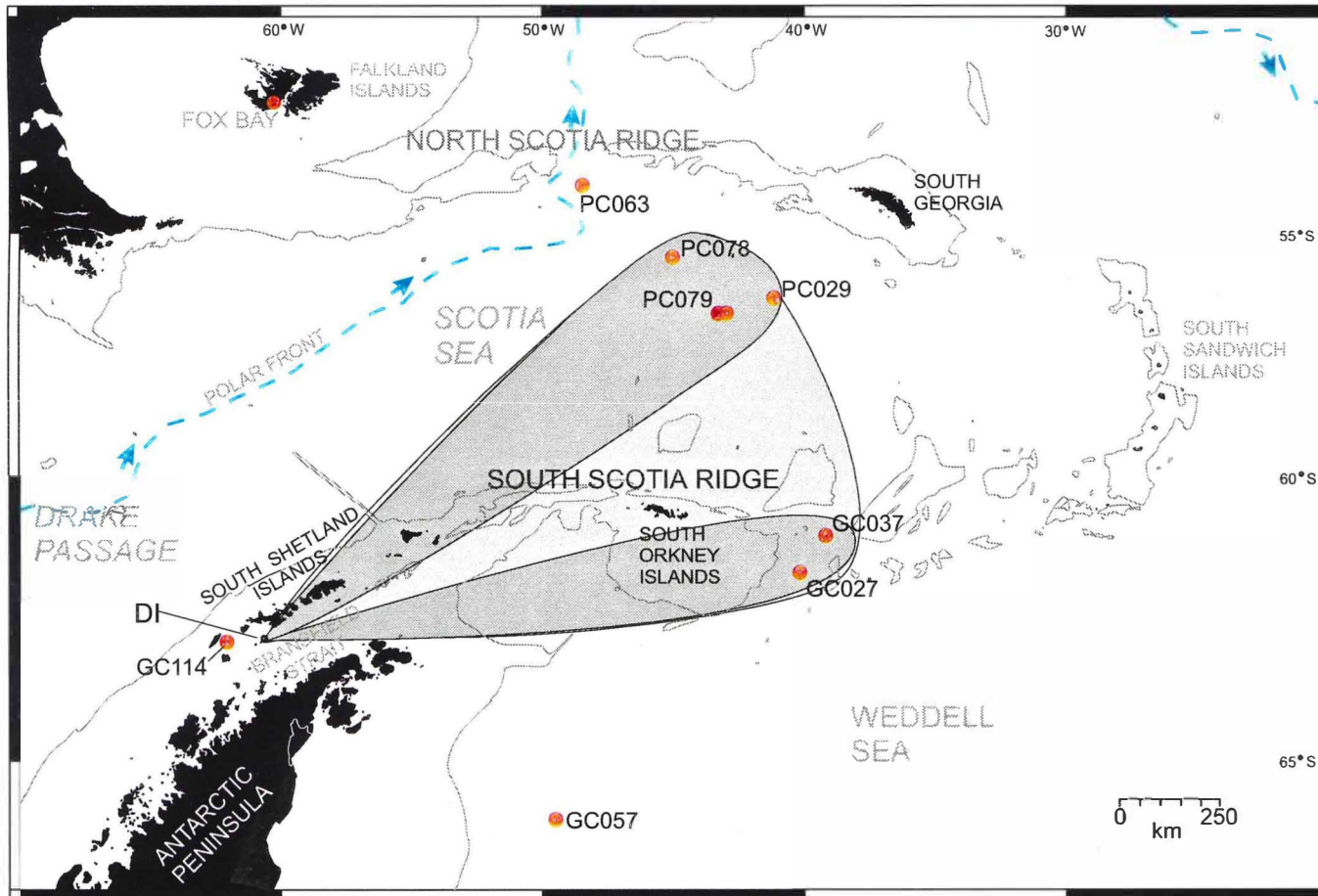
Figure 5.1 Map of the Scotia Sea and surrounding region showing possible, simplified, trajectories of the volcanic plume responsible for the deposition of the megascopic tephra. As no megascopic ash layer has been observed between cores GC037 and PC029 a bifurcated plume (darker shading) may be more a more likely scenario than a single broard plume (stippled shading). The 2000 metre bathymetric contour is shown by a thin pecked line. Blue arrows = path of the ACC (after Orsi *et al*. 1995). DI = Deception Island, PI = Penguin Island, BI = Bridgeman Island.

altitudes may have bifurcated the plume, as happened following the eruption of Augustine volcano, Alaska, 1986 (Sparks *et al.* 1997). It is proposed that a bifurcated plume was a possible cause of the megascopic ash distribution seen in the Scotia and Weddell seas. If this interpretation is correct, the simplest extrapolation of the flight paths of the respective plumes would take one axis over the South Shetland Islands and the other axis close to the South Orkney Islands (Figure 5.1). A further extrapolation of what appears to be the main axis of the plume over the Scotia Sea would carry it over South Georgia 400 km to the north east of PC079. The potential therefore exists for this same unusual ash layer to be deposited on South Georgia, South Shetland Islands and throughout Bransfield Strait. The fact that no comparable ash layer has yet been reported from numerous studies of lake sediments, moss banks, ice cores or peat bogs on these islands may in part be related to the lack of suitable ice-free terrestrial depocentres at the time of the eruption.

Cores containing numerous ash layers were recovered from Bransfield Strait during Polarstern cruise ANT XV/2 (1998). Investigation of these ash layers is ongoing. At least one core (PS47/068) contains a compositionally mixed ash layer including colourless, brown and dark brown-black glass (S. Fretzdorff pers. comm.). The brown glass contains spherical vesicles and abundant microlites. The highly vesicular colourless glass is subordinate to the brown glass and contains elongate vesicles (S. Fretzdorff pers. comm.). Both brown and colourless glass types are morphologically similar to glass types observed in the Scotia Sea and Weddell Sea cores. Investigation of these glass populations by EPMA shows very similar compositions to both the brown basaltic and colourless rhyolitic tephra described from the Scotia Sea above (Table 5.1 unpublished data reproduced courtesy of S.Fretzdorff). Although the Bransfield Strait tephra compositions reproduced in Table 5.1 and the Scotia Sea tephra compositions reproduced in Table 4.2 are in very good agreement they are not directly comparable as the data of Dr. S. Fretzdorff includes analyses for three additional oxides/elements (P_2O_5, F and Cl) which were not analysed for in the analyses in this study. These elements/oxides account for up to 0.6 % of the normalised total. The data have also been normalised to 100 %, contrary to the results given in this thesis. Recalculating the totals of the data in this study to 100 % without taking into

Table 5.1 Mean and standard deviation (in parentheses) for electron microprobe analyses of glass shards from core PS47/068 collected during R/V *Polarstern* cruise ANT XV/2 to Bransfield Strait. All totals have been recalculated to 100%. All analyses are from a mixed composition ash layer at 2.63 m depth. One population of brown glass shards and possibly two separate sub-populations of colourless glass have been identified. (The data are previously unpublished data reproduced here with the kind permission of Dr. S. Fretzdorff, Christian-Albrechts-Universität, Germany). *All iron calculated as FeO.

	SiO_2	TiO_2	Al_2O_3	FeO_*	MnO	MgO	CaO	Na_2O	K_2O	F	P_2O_5	Cl	n
Brown glass	52.84 (0.58)	2.30 (0.22)	15.23 (0.28)	11.16 (0.65)	0.24 (0.03)	4.49 (0.49)	8.29 (0.67)	4.47 (0.14)	0.42 (0.05)	0.06 (0.02)	0.42 (0.04)	0.07 (0.02)	33
Colourless glass 1	70.73 (0.82)	0.53 (0.02)	15.42 (0.37)	3.60 (0.18)	0.16 (0.05)	0.51 (0.15)	1.60 (0.58)	4.92 (0.40)	2.16 (0.23)	0.06 (0.02)	0.14 (0.03)	0.18 (0.61)	11
Colourless glass 2	72.58 (0.19)	0.36 (0.02)	14.62 (0.14)	3.30 (0.09)	0.16 (0.03)	0.20 (0.02)	0.67 (0.03)	5.17 (0.19)	2.57 (0.08)	0.09 (0.03)	0.08 (0.02)	0.19 (0.01)	9

account the three elements not analysed would produce erroneous results. However, as the compositional totals for the megascopic ash are high (averaging 97.69 %) the only significant difference between the normalised Bransfield Strait analyses and the non-normalised Scotia Sea analyses would be in the most abundant elements, in particular SiO_2 and Al_2O_3. As these (and all other elements) are in broad agreement between the two regions it is suggested that the Bransfield Strait tephra analyses are correlatable with the megascopic ash from the Scotia and Weddell Seas. On the basis of the basalt-rhyolite bimodal composition, the dominance of basaltic glass over rhyolitic glass, morphological similarities and correlatable major oxide compositional analyses, it is proposed here that the Bransfield Strait bimodal ash layer can be correlated with the megascopic ash layer found in the Scotia Sea and northern Weddell Sea. Proposed research for the near future involving the determination of trace element compositions of the Bransfield Strait tephra and the mutual exchange of sample material between BAS and GEOMAR to allow EPMA to be cross-checked on the different electron probes, will enable this hypothesis to be validated.

5.4.1.3 Age of the megascopic ash.

The ^{14}C age of the visible tephra layer has determined from organic carbon in sediments bracketing the ash layer. Allowing for a 1300 year reservoir age and calibrating the ^{14}C ages to the U/Th timescale (Bard *et al*. 1990a, Berkman *et al*. 1998), indicates the tephra layer can be dated to approximately 10,670 calendar years BP (Table 4.10 and Figure 5.2).

The ^{14}C derived age of the megascopic ash is, however, in disagreement with the position of the base of the Holocene and the last glacial maximum (LGM) (figures 2.1 and 5.2) calculated from the Ba/Al ratio and the abundance of the radiolaria *Cycladophora davisiana* respectively (Pudsey and Howe 1998). If the positions of these two time planes are correct, then the ^{14}C age of the sediments are too old. An 'old' age for the sediments would result from the presence of old reworked carbon in the sediments (forming a sedimentological reservoir age that would need to be taken into account). Omitting the core top age from PC029 due to the age inversion in that core (Table 4.10), the core top ages from PC079 and KC081 give a mean calibrated ^{14}C age

of c. 7,300 BP Slightly older core top ages of 10,500 and 13,000 years BP were calculated for cores in the Jane Basin (Pudsey and King 1997). Both sets of core top ages suggest that the ^{14}C reservoir age for sediments is considerably greater than that for the open ocean. Taking a sediment carbon reservoir age of c. 7,300 years into account would imply that the megascopic ash dates from 3,370 years BP. This younger age would be stratigraphically consistent with the position of the base of the Holocene and the LGM.

However, the apparent age of the core tops is more likely to be the result of incomplete sediment recovery. Observations by Stow (1994) show that, in mud-rich areas, sediments at the sediment-water interface have a soft spongy texture with a 70–80% water content and a full interchange of the superjacent fluid. Disturbance to core top sediments during coring operations has long been appreciated, this is particularly pronounced in the case of piston cores (Piggot 1941, Ross and Riedel 1967, McCoy and Von Herzen 1971). Graphic evidence suggests that up to 1m of surficial sediments may be lost from a piston core during core recovery (McCoy and Von Herzen 1971). The re-suspension of surficial sediments and subsequent loss during core retrieval was similarly observed during recent coring programmes (personal observation of S.G. Moreton, BAS marine geosciences cruise JR19). The recovered core tops, therefore, represent the youngest consolidated sediments in the sediment pile and give age estimates for the consolidation and compaction of abyssal sediments. Incomplete core recovery would also account for the absence of the megascopic tephra (dated at c. 10,670 year BP) in the Jane Basin cores described by Pudsey and King (1997) where the core top sediments were dated to 10,500 and 13,000 years BP (based on a 1430 year reservoir age).

It is proposed that the radiocarbon dating of the megascopic ash is correct and the positions of the base of the Holocene and the LGM in the Scotia Sea and Jane Basin cores are erroneous. This study, therefore, highlights the need for further investigation of palaeo-ecological processes operating in and the proxy dating methods applied to this region of the Southern Ocean. Additional ^{14}C dating of core top sediments and sediments bracketing the visible ash layer will greatly aid such investigations.
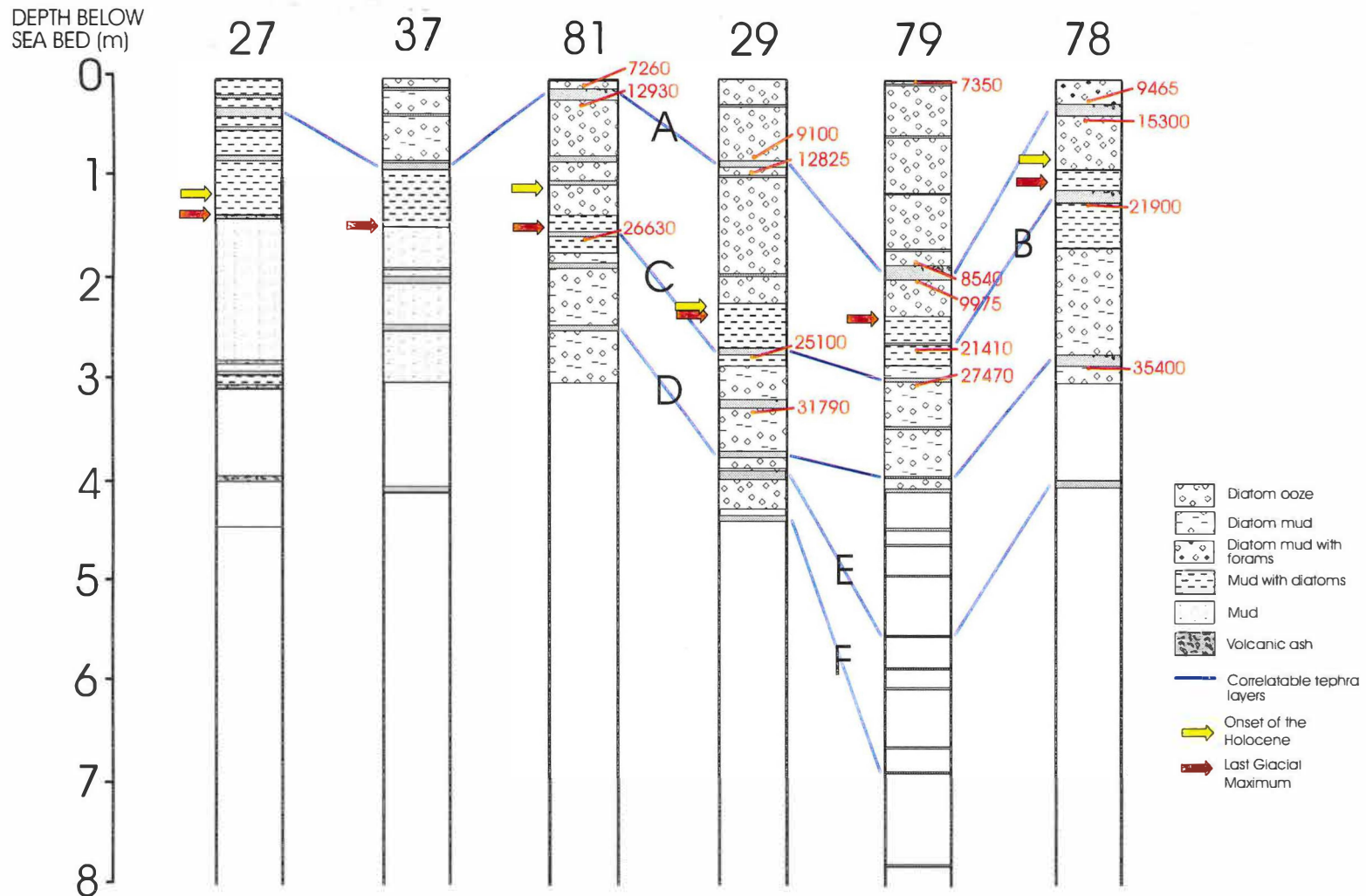
Figure 5.2 Six tephra layers (labeled A to F) can be correlated across the Scotia Sea. Corrected radiocarbon ages in calender years BP are shown in red. These ages are in disagreement with the positions of the onset of the Holocene and the Last Glacial Maximum calculated by Pudsey and Howe (1998)

5.4.1.4 Implications of an early Holocene age for future correlation of the megascopic ash

It has been suggested that the onset of deglaciation occurred later in the southern hemisphere than it did in the northern hemisphere (possibly as late as 9,000 BP) and that the retreat of land-based glaciers progressed only slowly during the first half of the Holocene until about 5000 BP (Hjort *et al.* 1998). It is therefore unlikely that, at this early stage of deglaciation, many terrestrial depositional environments were totally ice free and capable of trapping tephra. Conversely, none of the temperate ice-caps (which experience melting of basal ice) in the Antarctic Peninsula region are currently thought to retain ice of sufficient age to contain the megascopic tephra layer (R. Mulvaney pers. comm.).

5.4.2 Tephra above the megascopic ash layer

All glass analysed from tephra concentrations found above the megascopic ash layers is compositionally identical to the megascopic ash layer. It is possible that the tephra concentrations reflect discrete eruptive events fed by a magma chamber which had not undergone significant fractionation since the megascopic ash was erupted. However, historical activity of Deception Island has produced predominantly intermediate lavas and tephras dissimilar to the megascopic ash layer (Barker *et al.* 1975) indicating that this cannot be the case. Alternatively, the tephra concentrations may be artifacts of bioturbation caused by changes in the depth or rate of biological mixing of the sediments or the effect of changing rates of biogenic productivity. The latter explanation is favoured as the outlying data points from the analyses of these tephra concentrations (Figure 4.10) correlate well with similar outlying data points from the megascopic ash layer (Figure 4.7).

The above interpretation means that the cataclysmic eruption which resulted in the deposition of the bimodal megascopic ash was the last eruption of sufficient magnitude to distribute tephra in the central Scotia Sea. Eruptive activity is still continuing on Deception Island, as is evident from historical eruptions and recent eruptions and the presence of at least 9 tephras that post-date the megascopic ash in the Bransfield Strait cores (S. Fretzdorff unpublished data). The cessation of Deception Island tephra input

to the central Scotia Sea, despite continued activity on that island, suggests that there has been a change in style and/or magnitude of eruptions since the megascopic ash-forming eruption.

5.4.3 Ash layers below the megascopic ash

Besides the megascopic ash layer five other ash layers can be correlated to varying extents between Scotia Sea cores PC029, PC078, PC079 and KC081 (Figure 5.2). Correlations are based on glass chemistry, stratigraphy and magnetic susceptibility measurements. Where possible, correlatable tephras have been radiocarbon dated.

5.4.3.1 Tephra in Unit U

Concentrations of disseminated tephra immediately below the megascopic ash layer in cores GC027, PC029 and KC081 have shard compositions (both basaltic and rhyolitic) which strongly resemble those of the megascopic ash layer. As glass abundance drops to virtually zero directly below these tephra concentrations they represent the maximal downcore reworking of the megascopic ash by bioturbation.

The significance of the poorly characterised disseminated tephra from PC029–1.92 m remains enigmatic. Only three acceptable analyses were obtained from that tephra. All of the analyses were rhyolitic and match the composition of the rhyolitic glass in the megascopic ash layer. The complete absence of glass shards from 1.00 m to 1.24 m in this core (Figure 4.3) and the fact that this concentration of tephra occurs 1 metre below the established downcore maxima of the bioturbated megascopic ash indicates that the presence of these shards is not the result of normal bioturbation. The most likely explanation for the presence of these shards is disturbance at the edge of the core during core barrel penetration into the sediment followed by poor sample point selection during the sediment processing stage.

The ash layer KC081–0.91 m has a unique geochemical composition when compared to tephras from the surrounding cores. The overall composition of glass is indicative of a Deception Island source. Why this tephra has not been found in the adjacent cores is not

clear, although it is possible that the 4 cm sampling interval may not sufficiently small to locate all disseminated tephras.

5.4.3.2 Tephra in Unit T

The disseminated tephra layers in Unit T in cores PC078 (1.12 m) and PC079 (2.57 m) both plot along the same linear trend. The outlying analyses (Figure 4.12, Chapter 4), account for the difference in the mean values (Table 4.5). These two tephra layers are dated at $21,900 \pm 180$ calendar years BP and $21,410 \pm 220$ calendar years BP respectively (Table 4.10). Although the tephras have not been analysed for trace element composition, they can be correlated on the basis of major oxide composition and radiocarbon age, and they thus form the second correlatable tephra layer in this region. The underlying tephra in PC079 (2.91 mbsf), located immediately below the base of Unit T (*sensu* Pudsey and Howe 1998), can be correlated compositionally with the tephra from Unit T in cores PC029 (2.68 m) and KC081 (1.59 m) (Figure 4.12). These three tephra layers are radiocarbon dated to $27,470 \pm 250$ calendar years BP, $25,100 \pm 210$ calendar years BP and $26,630 \pm 220$ calendar years BP respectively (Table 4.10), giving a mean age for this ash layer of c.26,400 years BP. The correlation of these three tephra layers, the third tephra isochron, requires that Unit T in core PC079 may have to be redefined to include the tephra at a depth of 2.91 m. All of the tephras in Unit T are identified as having a Deception Island origin based on their geochemical composition.

5.4.3.3 Tephra in Unit L

Tephra layers PC029–3.64 m, PC078–2.73 m, PC079–3.89 m, and KC081–2.63 m can be correlated on major oxide compositions. Trace element compositions from glass samples from PC029–3.64 m and KC081–2.63 m are also comparable. These four tephras therefore form the fourth tephra isochron from the Scotia Sea. Only one of these tephras has been radiocarbon dated (PC078 – 2.73 m). The corrected calendar age of $35,400 \pm$ 180 years BP (allowing for a 1300 year reservoir age (Berkman *et al.* 1998) and correlation to the U–Th timescale (Bard *et al.* 1990a)) is in good agreement with a sample taken from 3.24 m in core PC029 immediately below a compositionally dissimilar and uncorrelated tephra layer. That dated sample, from 40 cm above the correlatable tephra, gave a radiocarbon age of $31,790 \pm 360$ calendar years BP.

Compositional analyses from glass shard concentrations at PC029–3.88 m, PC078–3.93 m and PC079–5.47 m show considerable similarities although there are notable differences in MgO and CaO. Despite these differences these tephras are tentatively correlated as the fifth Scotia Sea tephra layer. None of these tephras have been dated directly. Attempts to date the tephra by extrapolation of the mean sedimentation rates to the fourth tephra isochron proved to be untenable due to the rapid changes in sediment accumulation between cores below the fourth tephra (see section 5.4.5 below).

Some similarities in major oxide composition (Figure 4.16) suggest that tephras PC029–4.28 m and PC079–6.81 m may be correlatives. However, few analyses were obtained for either of these tephra layers and the major oxide analyses from PC029–4.28 m show a potential bimodal composition for this tephra layer. Only one of these modes correlates with the tephra layer PC079–6.81 m. No trace element analyses or radiocarbon dating have been undertaken for these tephra layers. Further analyses of these tephras will be necessary before they can be confirmed to be true correlatives.

Tephra layers PC027–3.88 m, PC078–3.93 m and PC079–5.47 m all have geochemical compositions indicative of Deception Island. Each produced tightly clustered EPMA results (Figure 4.15) but none of them can be correlated to any other Scotia Sea tephra so far identified. However, their compositional distinctiveness suggests that there is good potential for using these tephras for correlating ash layers found during future investigations.

The disseminated tephra at the base core GC037 (at a depth of 4.01mbsf) can be distinguished from other tephras in the Scotia Sea and northern Weddell Sea by subtle but consistent variations in four of the most significant major oxides (MgO, CaO, TiO_2 and SiO_2). The trace element composition for this tephra has not yet been determined. The major oxide composition of the glass plots at the extreme margins of known Deception Island lava and tephra compositions (Figure 4.17). However, this tephra shows broad compositional similarities with other potential Bransfield Strait sources as well as similarities to several South Sandwich Island sources. In the absence of trace element

data, this tephra cannot be assigned to any specific source, but it possibly represents the only non-Deception Island tephra found in the central Scotia Sea and northern Weddell Sea cores.

5.4.4 Observations of the Scotia Sea and Weddell Sea tephra distribution

In general, the abundance of glass found in cores GC027 and PC078 is very much lower than it is elsewhere. This suggests that these core locations may lie close to the limits of eruption plume dispersal for Bransfield Strait volcanoes and in particular for Deception Island. These limits identify a region extending from Deception Island potentially as far as South Georgia and including Powell Basin, Protector Basin, the South Orkney Islands and the South Shetland Islands as having the highest potential for furthering the Scotia Sea tephrostratigraphy proposed in this study.

One observation from the glass abundance curves of the central Scotia Sea cores (PC029, PC078, PC079 and KC081) and the Jane Basin Cores (GC027 and GC037) is that in all six cores the background level of glass drops to some of its lowest concentrations immediately below the bimodal ash layer. This is particularly evident in the cores that show the greatest concentrations of vitric tephra (Figure 4.3). This phenomenon is unlikely to be an artifact of bioturbation. Bioturbation tends to displace tephra upward from the point of original deposition as the zone of mixing keeps pace with continued sediment accrual (Watkins *et al.* 1978). Thus small scale eruptions preceding the megascopic ash would have been reworked upward toward the point of deposition of the megascopic ash. Ruddiman and Glover (1982) also noted that the peak abundance of tephra is displaced downward from the point of deposition by mixing in the active bioturbation zone. One possibility is that the deposition of the megascopic ash acted as a barrier to bioturbation, preventing the downward transmission of tephra. However, ash layers up to, at least, 0.7 cm thick had no inhibiting effect of the mixing of sediments (Ruddiman and Glover 1982).

N.B. In this study it was not possible to reconstruct the original thickness of the tephra due to the coarseness of the sampling resolution and because several key parameters were not recorded or could not be determined (e.g. the abundance of glass in the <32 μm size fraction and the percentage of lithic fragments which were part of the tephra).

Dilution of the glass abundance signal by rapid deposition of biogenic silica or large influxes of terrigenous material can be ruled out as a cause of the decreased abundance of glass below the megascopic tephra. The relative amounts of both of these sedimentary components are essentially unchanged below and above the megascopic ash layer. A more likely explanation lies in the mechanics of the volcano and its conduit system. The drop in glass abundance may represent a true reduction in tephra output, representing a quiescent period in the volcano's history. Supporting evidence for a quiescent period can be seen in the rhyolitic population of glass which accounts for approximately 30 % glass volume of the megascopic ash, but which does not occur in significant proportions in any of the earlier eruptions. A quiescent period would allow a small magma chamber time to fractionate to produce a more evolved tephra.

A quiescent period in the history of Deception Island would also partially account for the magnitude of the subsequent eruption, which is the largest eruption from that volcano seen in the distal tephra record. The increased viscosity of the evolved magma could become a significant factor in producing a cataclysmic eruption. This in turn would result in increased tephra input into the stratosphere. The ongoing investigation of the Bransfield Strait sediment cores also suggests a decrease in the volcanic activity in the region prior to the eruption of the correlative of the megascopic ash (S. Fretzdorff pers. comm.). The occurrence of abundant microlites in the megascopic ash layer is also worth considering in relation to the magnitude of that eruption. The formation of crystals within the magma has been identified as an important factor in explosive eruptions from lava domes (Dingwall 1998) . Even though the crystal sizes and volume in the megascopic ash are small (c. 10–30 % of the glass volume), the presence of crystals serves to increase the viscosity of the melt, as the deformation of the mass must be taken up entirely by the decreased fraction of the flow cross-section of the magma occupied by the liquid (Dingwell 1998). The formation of crystals will also release volatiles and latent heat that would contribute to the energy available for explosive activity (Cas and Wright 1987). A further consideration for the magnitude of the megascopic ash layer is the dating of that ash to approximately 10,670 BP. As deglaciation is thought to have occurred later in the southern hemisphere than in the

north (9000-5000 BP (Hjort *et al.* 1998)), it is likely that Deception Island would still have been largely covered by ice at that time. Contact with ice or water during an eruption can lead to intense explosive activity due to the expansion of steam and greater fragmentation which produces a larger volume of fine-grained tephra (Walker and Crossdale 1972, Houghton and Nairn 1991, Sparks *et al.* 1997).

5.4.5 Calculation of sedimentation rates based on tephrostratigraphy and ^{14}C dating

One of the objectives of identifying datable tephra isochrons is to constrain estimates of sedimentation rates. As only one correlatable tephra was found in each of the Jane Basin cores (GC027 and GC037) and no core-top ages were obtained from either of these cores, no estimations of sediment rates for Jane Basin can be made.

Incomplete core recovery above the megascopic ash layers means that calculation of sedimentation rates above that horizon remain questionable. The calibrated core-top ^{14}C ages from cores PC079 and KC081 are remarkably similar (7350 ± 65 and 7260 ± 65). On the assumption that these ages are typical for the central Scotia Sea region, a mean core-top age of c. 7300 years BP can be applied to all four central Scotia Sea core tops. The obvious age inversion from the top of core PC029 has been disregarded. Calculating the sedimentation rates from the core tops to the 10,670 BP megascopic ash produced widely varying rates for early Holocene sedimentation, ranging from 7 cm / ka to 53 cm / ka (Figure 5.3).

Below the visible tephra sedimentation rates for each core have been calculated using the mean age of each correlatable tephra present. The results show a much more uniform sedimentation rate for all of the central Scotia Sea cores. In cores PC078 and PC079 the sedimentation rate from the megascopic tephra to second tephra layer is 7 cm / ka. Between the megascopic tephra and the third tephra in cores PC029, PC079 and KC081 the sedimentation rates are 12, 8 and 9 cm / ka respectively. Sedimentation rates between the third and fourth tephras in those same cores are more uniform at 11, 11 and 12 cm / ka respectively.
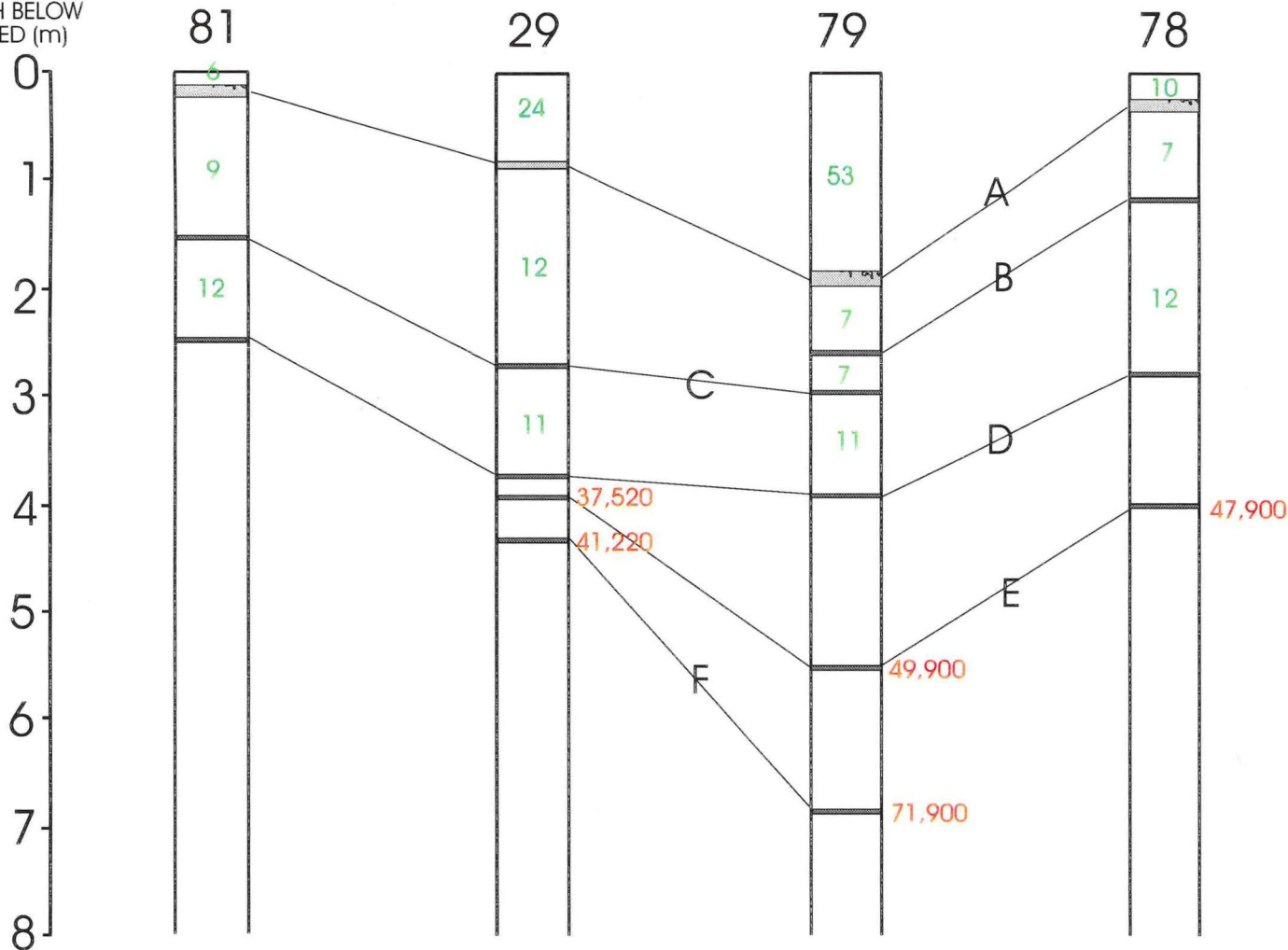
Figure 5.3 Schematic of the central Scotia Sea cores showing the calculated sedimentation rates in cm/ka (green figures). Red figures are ages of tephra layers based on extrapolation of the mean sedimentation rates for each tephra layer.

Thus mean sedimentation rates from the megascopic tephra to the fourth tephra layer (approximately a 24,730 year time span) in each of the cores are 11, 10, 8 and 8 cm / ka for cores PC029, PC078, PC079 and KC081. However, it has been noted that below the megascopic tephra in cores PC078, PC079 and KC081 sedimentation rates increase with depth. In core PC029 there is a slight reduction in the sedimentation rate below the third tephra from 12 to 11 cm / ka. This trend is amplified below the fourth tephra (Figure 5.3), although the reason for this pattern is not clear.

Extrapolation of the mean sedimentation rate below the fourth tephra dates the fifth tephra variously at 37,580 BP (PC029), 47,900 BP (PC078) and 55,150 BP (PC079). Similar extrapolation to the sixth tephra produces dates of 41,220 BP (PC029) and 71900 BP (PC079) (Figure 5.3). These dates are clearly untenable. Further investigation of direct or proxy dating of tephras beyond the range of ^{14}C dating, therefore, needs to be undertaken before a complete tephrochronology can be constructed for the northern Antarctic Peninsula region.

5.4.6 The case for the caldera-forming eruption on Deception Island being the source of the megascopic ash layer.

The cataclysmic eruption which preceded caldera collapse on Deception Island is estimated to have produced 30 ± 10 km^3 of tephra (Smellie in press). The central Scotia Sea and northern Weddell Sea core sites are situated downwind of Deception Island and form a transect perpendicular to the likely axis of tephra dispersal from that island. The megascopic ash layer recovered from six sediment cores from the Scotia and Weddell seas is the most extensive late Quaternary tephra known to be deposited in the region. It was also the last eruption to contribute tephra to the Scotia Sea and northern Weddell Sea sediments. Deception Island has unambiguously been identified as the source of the megascopic ash. No megascopic Quaternary ash layers from Deception Island have yet been identified in either continental shelf or deep-sea sediments west of Boyd Strait (core GC114), despite extensive investigation of the western Antarctic Peninsula margin (This study, Pudsey et al.1994, Barker, Camerlenghi et al. in press).

Two other studies have independently inferred a late Pleistocene or early Holocene age for the formation of the caldera on Deception Island (Birkenmajer 1995, Smellie in prep.). The megascopic tephra layer has been ^{14}C dated to approximately 10,670 years BP (this study). The dating of the megascopic ash and potentially, therefore, the caldera-forming eruption to the early Holocene has significant implications for the extent of ice-cover on Deception Island at the time of the eruption.

A recent re-evaluation of lake sediments from the South Shetland Islands (Hjort *et al*. 1998) suggested that the retreat of land-based glaciers was out of phase with the northern hemisphere and did not begin until as late as 9,000 BP. This later deglaciation means that the pre-caldera volcanic edifice in Deception Island is likely to have been covered by extensive valley and cirque glaciers, and possibly even a small ice-cap. Several of the volcanic islands in the South Sandwich Islands arc (e.g. Visokoi Island, Saunders Island) at the eastern margin of the Scotia Sea are smaller than or similar in size to the pre-caldera Deception Island and they still support small ice-caps under current interglacial conditions (J.L. Smellie pers. comm.). The presence of overlying ice that can interact with the rising fragmented magma layer in the conduit can increase the violence of an eruption as the ice vaporises explosively. Increased magmatic fragmentation will produce a greater volume of fine-grained tephra, which is more easily transported for long distances. However, although land-based glaciers were not in full retreat by 10,670 BP, a sharp warming of the Southern Ocean occurred at about 13-12 ka, roughly synchronous with the North Atlantic (Bard *et al*. 1990 b). Eustatic sea-level rise resulting from northern hemisphere deglaciation and thermal expansion of the ocean would have floated the termini of previously grounded glaciers, leading to increased thermal erosion of the glacier bases and increased calving. Loss of mass from glacier termini should be accompanied by compensation thinning at the head of the glacier if the glaciers remain in equilibrium. Thinning and subsequent loss of ice mass would result in a reduction in confining pressure over the underlying magma chamber. This effect would be even greater if the magma chamber was at a shallow depth and the hydraulic pressure in the chamber is finely balanced by the overlying lithostatic load.

Ice removal has been identified elsewhere as a trigger for explosive volcanism (Hall 1982, Sigvaldason *et al.* 1992, Zielinski *et al.* 1995). Where the lithosphere is thin or magma chambers are at shallow depths, the explosive volcanic response to decompressive unloading can be extremely rapid (on timescales of days to years (J. Maclennan pers. comm.)).

If the megascopic ash layer is attributed to the eruption which immediately preceded caldera formation on Deception Island, this would explain the decreased magnitude of the post megascopic ash eruptions (which did not disperse tephra as far as the Scotia Sea). If caldera collapse occurred soon after the megascopic ash was formed, the subsequent loss of mass and lowered topography would lead to a significant reduction in the volume of ice covering the island, which would reduce the confining pressure on the underlying magma chamber facilitating lower energy eruptions. Alternatively, if sometime between the megascopic ash eruption and successive eruptions, the onset of deglaciation removed sufficient ice volume from the island to prevent the occurrence of phreatomagmatic eruptions, both the explosivity of the eruptions and the degree of fragmentation of the tephra would be reduced. Consequently, the volume of tephra input into the Scotia Sea would decrease.

When the circumstantial evidence is considered; the age of both the megascopic ash and the proposed age of the Deception Island caldera formation; the volume of the megascopic ash from the Scotia and Weddell seas; and the fact that no other voluminous Late Quaternary Deception Island tephra has been discovered in either the Weddell Sea, Scotia Sea or Bellingshausen Sea; it may be hypothesised that the megascopic ash layer stems from the cataclysmic eruption that predated and ultimately led to the collapse of the Deception Island volcanic edifice. This hypothesis is further strengthened by the characteristics of the Scotia and Weddell sea tephra records which indicate a quiescent period in the volcano's history followed by a large input of glassy tephra (the megascopic ash layer). The glassy tephra has all the characteristics (highly evolved population of glass, high vesicularity, high microlite content and a large volume of highly fragmented fine-grained tephra) of being caused by a large and violent eruption. The age of the tephra is also consistent with known eustatic sea level changes and a conjectured level of ice

coverage on Deception Island which combine to provide a potential trigger mechanism for the eruption.

The ground truth from Deception Island, however, does not support this hypothesis. J.L. Smellie (unpublished data) has identified two compositionally distinctive basaltic magmas involved in the eruption which immediately preceded caldera formation, whereas only one is found in the megascopic ash (see also Smellie *et al.* 1992). Moreover, the most highly evolved component of the caldera-forming eruption is dacitic. This indicates compositional incompatibility of the megascopic ash and the caldera-forming eruption recognised on the island. Furthermore, tephra deposition from that eruption blankets much of Deception Island with a mean depth of 70 m indicating that Deception Island was largely ice-free at the time of the eruption (J.L. Smellie pers. comm.). This physical evidence from Deception Island is in agreement with one of the current theories on the immediate pre-caldera eruption, which is, that the eruption was triggered by the influx of a new batch of juvenile magma into the magma chamber (Smellie *et al.* 1992).

The hypothesis that the pre-caldera eruption and the megascopic ash forming eruption are synonymous is at odds with the current state of knowledge of the geological sequence on Deception Island and therefore remains conjectural.

5.5 Boyd Strait

The large grain size, normally graded bedding and heterogeneous composition of the shards in core GC114 are features similar to those in ash layers from the southern Bellingshausen sea (discussed above). They suggest that both of the ash layers in core GC114 were emplaced by turbidity currents rather than pyroclastic fallout from the an eruption column. It is thought that each of the Boyd Strait tephras are not the product of a single eruptive event. However, it has not proved possible to separate individual component tephras from the ash layer, nor can either of the ash layers be correlated with any of the Scotia Sea tephras. Deception Island has been identified as the source of both tephra layers.

Unfortunately, at present, no independent dating method has been applied to any sedimentological unit in core GC114. It is therefore not possible to determine directly the age of the proposed turbidity currents nor link their deposition to any external mechanism. A sedimentation rate of c. 24 cm/1000yr has been calculated, based on the correlation of the 2.63 m deep ash layer in nearby Bransfield Strait with the 10,670 year BP megascopic ash layer in the Scotia Sea. This yields approximate ages of 12,240 BP and 12,800 BP for the emplacement of the two tephras near Smith Island. As the upper turbidity current is almost exclusively composed of volcanigenic material from Deception Island, it is possible that the turbidity current may have followed shortly after or been triggered during a violent volcanic eruption on that island. The calculated ages of the these tephras makes it unlikely that they are from the same eruption(s) as the one(s) that produced the tephra layers PC029–4.28 and PC079–6.81 which they are geochemically similar to but which are dated at > 35,400 years BP.

5.6 The Mount Hudson Ash

The Mt. Hudson ash was the only historical tephra examined and the only tephra in which the source and depositional history were known prior to examination. This tephra indicates the variation in composition that can occur during a short-duration eruption. It also highlights the potential for mis-correlation of tephras if the whole range of compositions are not analysed or if variable wind directions during plume dispersal separate different sub-populations of the evolutionary series.

The Mt. Hudson tephra is also representative of magmas erupted in southern Andean volcanoes. On the basis of this tephra, South America can be ruled out as a significant source for the late Quaternary Scotia Sea tephras examined in this project.

6. Summary and Conclusions

6.1 Northern Bellingshausen Sea

One megascopic tephra layer was observed in 11 cores recovered from the northern Bellingshausen Sea sediment drifts. Major oxide and trace element analyses of glass shards combined with stratigraphic position of the tephra confirm that it is a single correlatable horizon. This tephra isochron has been dated by Ba/Al ratios and palaeontological assemblage analyses to $\delta^{18}O$ substage 5e. It was not possible to independently verify the age of the tephras by $^{39}Ar/^{40}Ar$ dating due to contamination of the samples with 'old' argon contained within detrital minerals incorporated into the tephra layers through bioturbation and contemporaneous deposition. Major oxide and trace element compositions combined with the late Quaternary age of the tephra identify Mt. Berlin, Marie Byrd Land, as the most likely source of the tephra. Diminishing shard size from south-west to north-east is consistent with a source volcano being situated to the south and west (i.e. upwind in the prevailing west wind drift).

Two disseminated tephras were found, but not investigated, in the northern Bellingshausen Sea sediment drifts. The identification of disseminated tephras within these sediments indicates that there is a very high probability that further (disseminated) tephras will be found and correlated between the sediment drifts. The potential exists, therefore, for a late Quaternary tephrostratigraphy to be erected for the northern Bellingshausen Sea region in future investigations. Such a tephrostratigraphy will greatly aid palaeoecological, palaeoceanographic and palaeoclimatic studies in the region.

6.2 Southern Bellingshausen Sea.

Each of the four tephras (from three cores) showed a highly variable major oxide composition. The high compositional variance of the tephras meant that none of the four tephras could be correlated with or discriminated against any other tephra. None of the tephras were analysed for trace element composition, and none of the tephras were

dated. The ratio of $K_2O : Na_2O$ when plotted against SiO_2 clearly distinguishes the southern Bellingshausen Sea tephras from the northern Bellingshausen Sea tephra. The overall major oxide composition identified Peter I Island as the source of all four southern Bellingshausen Sea tephras. The proximity of the cores to the base of the volcanic island and the large size of the glass shards are consistent with the geochemical identification of Peter I Island as the source.

Shard size and shape, the grading and sharp basal contact of the tephra layers and the heterogeneity of shard compositions suggests that turbidity currents are the most likely mechanism for the deposition of the tephras.

6.3 Scotia Sea and Weddell Sea.

6.3.1 The northern Scotia Sea

The northern Scotia Sea core PC063 contained fewer glass shards than were found elsewhere in the Scotia Sea and Jane Basin. The maximum concentration of glass shards in the sieved sediments is only 3.2%. Major oxide compositional analyses of glass from potential tephra layers in this core show that the glass shards came from a variety of volcanic source regions. Concentrations of glass within this core therefore represent reworked and redeposited shards rather than primary tephra deposits.

6.3.2 The Weddell Sea

Only one core (GC057) was examined from the Weddell Sea. The sediments were almost exclusively clay and no concentrations of glass were found. This site is frequently covered by ice and the absence of tephra indicates that it has been similarly covered for much of the late Quaternary.

6.3.3 The central Scotia Sea and Jane Basin.

One megascopic ash layer was identified in the central Scotia Sea and Jane Basin cores. The megascopic tephra can be correlated between all six cores (GC027, PC029, GC037, PC078, PC079 and KC081). It is morphologically and geochemically bimodal.

The glassy fraction of tephra layer comprises c.70-80% brown, vesicular, basaltic glass with rounded vesicles and microlites, and c.20-30% colourless, highly vesicular, rhyolitic glass with pipe-like vesicles but no microlites. Lesser amounts of opaque, black glass shards of basaltic composition with microlites are also present. Further examination of the black glass shards may show them to be the third fraction of a trimodal composition. Deception Island, South Shetland Islands has been identified as the source of this tephra. The megascopic tephra has been ^{14}C dated to c. 10,670 B.P. As such it forms a major regional isochron for the earliest Holocene marine sediments.

As the megascopic ash layer is the only voluminous Deception Island tephra known anywhere in the Antarctic Peninsula region it is proposed that the eruption which led to the formation of the megascopic ash also preceded and directly led to caldera collapse on that island. No primary air-fall tephras in the Scotia Sea post-date the megascopic tephra. All tephra rich horizons above the megascopic tephra can be attributed to upward reworking of that tephra by bioturbation.

Below the megascopic tephra five other tephras can be correlated to varying extents between the central Scotia Sea cores. Deception Island has been identified as the source of all correlatable tephras. Three of these tephras have been radiocarbon dated to 21,660 BP, 26,400 BP and 35,400 BP. The two oldest correlatable tephras have not been directly dated.

Incomplete core-top recovery indicates that surficial sediments in the Scotia Sea remain poorly consolidated for up to 7,000 years after initial deposition. This finding is important for understanding the effect that changes in bottom current velocity have on the reworking and removal of deep-sea sediments. Estimates of sedimentation rate based on dated tephra horizons indicate that rates were high but variable (6 to 53 cm / ka) between c.10,670 BP and c.7,300 BP Core sites PC078, PC079 and KC081 show a gradual decrease in sedimentation rate between c.35, 400 BP and c.10,670 BP. Core PC029 shows the inverse of this.

A further 23 individual tephra layers were found that could not be correlated. Geochemical plots of three of these tephras produce unique clusters which have a high potential for future correlation with as yet undiscovered tephras. The main reason for the lack of positive correlation among the remaining tephras was the generation of insufficient geochemical analyses with acceptably high analytical totals. With the exception of one tephra (GC037–4.01 mbsf), which was identified as having a South Sandwich Island origin, Deception Island, South Shetland Islands, was identified as the source of all central Scotia Sea and Jane Basin tephras. Deception Island has, therefore, been by far the most active volcano in the Antarctic Peninsula region over at least the last 35,400 years.

6.4 Meeting the Aims of the project.

This thesis has successfully demonstrated the utility and potential of disseminated and megascopic tephra isochrons as an aid to investigation of Antarctic deep-marine sedimentary environments.

It was not possible to correlate the marine tephra record with any terrestrial tephra discovered to date due to:

i)   lack of published geochemical data from previous research.

ii)   the pre-Holocene age of most of the marine tephras, which pre-date the existence of many of the terrestrial depositional sites so far investigated in the region.

The source volcano for most of the individual tephra layers has been identified in both study areas. No tephra was found that spanned both the Bellingshausen and Scotia Sea sediment record, but the potential for such key tephras being found in the future remains high.

Although the lack of suitable core material meant that it was not possible to fully investigate changes in volcanicity over a full glacial–interglacial cycle, it is noted that the largest tephra producing volcanic eruption in both of the study areas coincided with the onset of a climatically warm period.

A substantial database comprising in excess of 1200 individual major oxide or trace element geochemical analyses has been constructed.

[14]C dating of tephras has yielded valuable information on the sedimentation rates in the region as well as the timing of significant volcanic activity. Experimental work of the application of $^{40}Ar - ^{39}Ar$ is still in progress.

6.5 Naming the tephra layers

No formal procedure has been followed for naming the tephra layers but the following names are proposed for the two correlatable megascopic tephras.

The term SEDANO ASH is proposed for the northern Bellingshausen Sea sediment drift tephra. This is in honour of the research program of the Osservatorio Geofisco Sperimentale which first recognised that ash layer. Incidentally 'sedano' is Italian for celery, but that's by-the-by.

The term DOCTORATE ASH is proposed for the Scotia Sea and Jane Basin megascopic tephra, as it is hoped that this will be the result of four years of intensive study of this tephra.

7. References

Allen, D. (1984) A one-stage precision polishing technique for geological specimens. *Mineralogical Magazine*, **48**, 298-300.

Allman, M. and Lawrence, D.F. (1972) Geological Laboratory Techniques, Blandford, London. 335 pp

Anderson, J.B. (1975) Factors controlling $CaCO_3$ dissolution in the Weddell Sea from foraminiferal distribution patterns. *Marine Geology* **19**, 315-332.

Andrews, J.T., Domack, E.D., Cunningham, W.L., Leventer, A., Licht, K.J., Jull, A.J.T., DeMaster, D.J. and Jennings, A.E. (1999). Problems and possible solutions concerning radiocarbon dating of surface marine sediments, Ross Sea, Antarctica. *Quaternary Research*, **52**, 206-216.

Autefage, F. and Couderc, J.-J. (1980): Étude du mecanisme de la migration du sodium et du potassium au cours du leur analyse a la microsonde electronique. *Bulletin of Mineralogy,* **103**, 623-629.

Baker, P.E. (1990). South Sandwich Islands. In: LeMasurier, W.E. and Thomson, J.W., (eds) *Volcanoes of the Antarctic plate and Southern Oceans*. Antarctic Research Series , vol.48, American Geophysical Union, Washington, D.C., 361-395

Baker, P.E., Davies, T.G. and Roobol, M.J. (1969) Volcanic activity at Deception Island in 1967 and 1969. *Nature*, **224**, 553-560.

Baker, P.E., McReath, I. Harvey, M.R. Roobol,, M.J. and Davies, T.G. (1975) The geology of the South Shetland Islands, V, Volcanic evolution of Deception Island, *British Antarctic Survey Scientific Report.* **78**, pp 81

Bard, E., Hamelin, B., Fairbanks, R.G. and Zindler, A., (1990 a) Calibration of the 14C timescale over the past 30,000 years using mass spectrometric U-Th ages from Barbados corals. *Nature*. **345**, 405-410.

Bard, E., Labeyrie, L.D., Pichon, J.-J., Labracherie, M., Arnold, M., Duprat, J., Moynes, J. and Duplessy, J.-C. (1990 b) The last deglaciation in the Southern and Northern Hemispheres: a comparison based on oxygen isotope, sea surface temperature estimates, and accelerator ^{14}C dating from deep-sea sediments, *In*: Thiede (ed) *Geological History of the Polar Oceans: Arctic Versus Antarctic*. Kluwer Academic Press, Netherlands, 405-415.

Barker, P.F. (1976) The techtonic framework of Cenozoic volcanism in the Scotia Sea region – A review. *In*: González-Ferrán, O. (ed) *Preceedings of the international symposium on Andean and Antarctic Volcanology Problems*. International Association of Volcanology and Chemistry of the Earth's Interior, 330-346.

Barker, P.F. (1982) The Cenozoic subduction history of the Pacific margin of the Antarctic Peninsula: Ridge crest-trench interactions. *Journal of the Geological Society of London*, **139**, 787-801.

Barker, P.F. (1992) The sedimentary record of Antarctic climate change. *Philosophical Transactions of the Royal Society, London.* **Series B, 388**, 259-267.

Barker, P.F., and Burrell, J. (1982) The influence upon Southern Ocean circulation, and climate of the opening of Drake Passage. *In*: Craddock, C. *Antarctic Geoscience*, University of Wisconsin Press, Madinson, 377-385.

Barker, P.F. and Dalziel, I.W.D. (1983) Progress in geodynamics in the Scotia Arc region. *In*: Cabre, R. (ed*) Geodynamics of the eastern Pacific region, Caribbean and Scotia Seas*. Geodynamics Series 9, American Geophysical Union, Washington, D.C. 137-170.

Barker, P.F., McReath, I., Harvey, M.R., Roobol, M.J. and Davies, T.G. (1975) The geology of the South Shetland Islands. V. Volcanic evolution of Deception Island. *British Antarctic Survey Scientific Reports*, **78**, 81 pp.

Barrett, P.J., Adams, C.J., McIntosh, W.C., Swisher III, C.C. and Wilson, G.S., (1992). Geochronological evidence supporting Antarctic deglaciation three million years ago. *Nature*, **359**, 816-818.

Bastien, T.W. and Craddock, C., (1976) The geology of Peter I Island. *In:* Hollister, C.D., Craddock, C., *et al. Initial Reports of the Deep Sea Drilling Project*, **35**. Washington, DC: US Government Printing Office, 341-357.

Bennett, K.D. (1994) Tephra Geochemistry: a comment on Hunt and Hill. *The Holocene*, **4** (4), 435-436.

Berger, W. and Heath, G.R. (1968) Vertical mixing of pelagic sediments. *Journal of Marine Research*, **27**, 135-143.

Berkman, P.A., Andrews, J.T., Björck, S., Colhoun, E.A., Emslie, S.D., Goodwin, I.D., Hall, B.L., Hart, C.P., Hirakawa, K., Igarashi, A., Ingólfsson, Ó., López-Martínez, J., Lyons, W.B., Mabin, M.C.G., Quilty, P.G., Taviani, M. and Yoshida, Y. (1998). Circum-Antarctic coastal environmental shifts during the Late Quaternary reflected by emerged marine deposits. *Antarctic Science.* **10** (3), 345-362.

Birkenmajer, K. (1992) Evolution of the Bransfield Basin and rift, West Antarctica. *In*: Yoshida, Y. (ed*) Recent progress in Antarctic Earth Science.* Terra Scientific Publishing Company, Tokyo. 405-410.

Birkenmajer, K. (1995) Volcano-structural Evolution of the Deception Island Volcano, West Antarctica. *Terra Antartica.* **2** (1), 33-40.

Björck, S., Malmer, N., Hjort, C., Sandgren, P. Ingólfsson, Ó., Wallén, B., Smith, R.I.L. and Jönsson, B.L., (1991a). Stratigraphic and Palaeoclimatic studies of a 5500-year-old moss bank on Elephant Island, Antarctica. *Arctic and Alpine Research*. **23** (4), 361-374.

Björck, S., Håkansson, H., Zale, R., Karlén, W. and Jönsson, B.L., (1991b) A late Holocene lake sediment sequence from Livingston Island, South Shetland Islands, with palaeoclimatic implications. *Antarctic Science*, **3** (1) 61-72.

Björck, S., Sandgren, P. and Zale, R., (1991c) Late Holocene tephrochronology of the northern Antarctic Peninsula. *Quaternary Research*, **36**, 322-328.

Brasier, M.D. (1995) Fossil indicators of nutrient levels. 1: Eutrophication and climate change. In Bosence, D.W.J. and Allison, P.A. (eds), *Marine Palaeoenvironmental Analysis from Fossils*. Geol. Soc. Spec. Pub. No. 83. 113-132.

Broecker, W.S., (1992) Upset for Milankovitch theory. *Nature*, **359**, 779-780

Broecker, W.S and Peng, T.-H. (1982). *Tracers in the Sea*. Eldigio Press, New York. 689 pp

Broecker, W.S., Peteet, D.M. and Rind, D., (1985) Does the ocean-atmosphere system have more than one stable mode of operation? *Nature*, **315**, 21-26.

Burckle, L.H., Clarke, D.B. and Shackleton, N. (1978) Isochronous last appearance datum of the diatom *Hemidiscus karstenii* in the subantarctic. *Geology*, **6**, 243-246.

Burckle, L.H. and Mortlock, R., (1998) Sea-ice extent in the Southern Ocean during the Last Glacial Maximum: another approach to the problem. *Annals of Glaciology*, **27** 302-304

Calvet, J., Pallàs, R., Sàbat, F. and Vilaplana, J.M. (1997) Los niveles de cenizas de los glaciares de Livingston. Criterios para su datación. In: Settat, D. (ed), *Quinto Simposio Español de Estudios Antarcticos, 1993, Barcelona. Actas*. Madrid, Comisión Interministerial de Ciencia y Tecnología, 195-208.

Camerlenghi, A. and Rebesco, M. (1994) Bottom current-controlled sedimentation on the continental rise of the Antarctic Peninsula Pacific Margin. Abstract only, 15° IAS Regional Meeting, Ischia 13-14 April 1994.

Camerlenghi, A., Rebesco, M. and Pudsey, C.J., (1997) High resolution terrigenous sedimentary record of a sediment drift on the Antarctic Peninsula Pacific margin (initial results of the 'SEDANO' program). In Ricci, C.A. (ed) *The Antarctic region: Geological evolution and processes*. Siena Museo Nazionale dell' Antartide, 705-710.

Canals, M., Gràcia, E., Prieto, M.J. and Parson, L.M., (1997) The very early stages of seafloor spreading: The central Bransfield Basin, NW Antarctic Peninsula. In

Ricci, C.A. (ed) *The Antarctic region: Geological evolution and processes*. Siena Museo Nazionale dell' Antartide, 669-673

Carey, S., (1997) Influence of convective sedimentation on the formation of widespread tephra fall layers in the deep sea. *Geology*. **25** (9), 839-842.

Cas, R.A.F and Wright, J.V., (1987) Volcanic successions modern and ancient. Chapman and Hall, London. Ch. 3. 33-57

Cooper, A.P.R., Smellie, J.L. and Maylin, J. (1998) Evidence for shallowing and uplift from bathymetric records of Deception Island, Antarctica. *Antarctic Science*. **10** (4), 455-461.

Curtis, G. H., (1966). The problem of contamination in obtaining accurate dates of young geologic rocks, *In:* Schaeffer, O.A. and Zahringer, J. (eds.), *Potassium-argon dating*. Springer Verlag, New York, 15-162.

Deacon, G.E.R. (1963). The Southern Ocean. In: *The Sea*, Hill, M.N. (ed). Interscience, New York, 281 pp.

Deacon, G.E.R, and Moorey, J.A. (1975). The boundary region between currents from the Weddell Sea and Drake Passage. *Deep-Sea Research*, **22**, 265-268.

Deacon, G.E.R, and Foster, T.D. (1977). The boundary region between the Weddell Sea and Drake Passage currents. *Deep-Sea Research*, **24**, 505-510.

De Batist, M., Bart, P.-J. and Vanneste, K., (1997) Belantostrat Belgian contribution to the "Antarctic offshore acoustic stratigraphy project (Antostrat)". In Caschetto (ed*) Belgian Programme on the Antarctic. Scientific Results of Phase III (1992–1996)*. Volume 2. Federal Office for Scientific, Technical and Cultural Affairs. Brussels, Belgium.

del Valle, R.A., Fourcade, N.H. and Medina, F.A. (1983). Interpretacion preliminar de las edades K/Ar y de los analisis quimicos de las rocas volcánicas y de los disques de los nunataks Foca, Antártida. *Contrib. Inst. Antart. Argent*. **287**, 13 pp

Denton, G.H., Bockheim, J.G., Wilson, S.C. and Struiver, M. (1998) Late Wisconsin and Early Holocene glacial history, inner Ross embayment, Antarctica, *Quaternary Research*, **31**(2), 151-182.

Dingwell, D.B. (1998) Recent experimental progress in the physical descripton of silicic magma relevent to explosive eruptions. *In:* Gilbert, J.S. and Sparks R.S.J. (eds) *The Physics of Explosive Eruptions*. Geological Society, London, Special Publication, **145**, 9-26.

Domack, E. W., Mashiotta, T.A., Burkley, L.A. and Ishman, S.E. (1993). 300-Year cyclicity in organic matter preservation in Antarctic fjord sediments. *In:* Kennett, J. P. and Warnke, D.A. (eds) *The Antarctic Paleoenvironment: A*

perspective on global change. Antarcic Research Series, **60**, American Geophysical Union, Washington, D.C., 265-272.

Drewry, D. J., Barker, P.F., Curry, F.C., Gardiner, B.G., Heywood, R.B., Jarvis, M.J., Paren, J.G., Priddle, J., Smith, G.J., Thomson, M.R.A. and Walton, D.W.H. (1993). *Antarctic Science: A British Perspective. Interdisciplinary Science Reviews*, **18** (1)

Dunbar, N.W., Kyle, P.R., McIntosh, W.C. and Esser, R.P. (1995) Geochemical composition and stratigraphy of tephra layers in Antarctic blue ice: Insights into glacial tephrochronology. *Antarctic Journal of the United States*, **30** (5), 76-78.

Dymond, J., Suess, E., and Lyle, M., (1992) Barium in deep-sea sediment: a geochemical proxy for palaeoproductivity. *Palaeoceanography*, **7**, 63-181.

Dyson, C.L. (1996) Antarctic tephrochronological studies at Midge Lake, Livingston Island, South Shetland Islands and at Sombre Lake, Signy Island, South Orkney Islands. Unpublished MRes. dissertation, University College London.

Echols, R.J. (1971) Distribution of foraminifera in sediments of the Scotia Sea area, Antarctic waters. American Geophysical Union, *Antarctic Research Series*, **15**, 93-168.

Echols, R.J. and Kennett, J.P. (1973). Distribution of foraminifera in the surface sediments. In: Goodell, H.G.(ed). *Marine Sediments of the Southern Oceans*. Antarctic Map Folio Series. **17**. American Geographical Society. New York. 13-17.

Federman, A.N., Watkins, N.D. and Sigurdsson, H. (1982) Scotia Arc volcanism recorded in abyssal piston cores downwind from the islands. In: Craddock, C. (ed), *Antarctic Geoscience*, University of Wisconsin Press, Madison, 223-228.

Fisher, R.V. (1964) Maximum size, median diameter, and sorting of tephra. *Journal of Geophysical Research*, **69** (2), 341-355.

Foldvik, A. and Gammelsrod, T. (1988) Notes on Southern Ocean hydrography, sea-ice and bottom water formation. *Palaeogeography, Palaeoclimatology, Palaeoecology*, **67**, 3-17.

Frakes, L.A. (1971) *USNS Eltanin core descriptions, cruises 32 to 45*. Antarctic Core Facility, Department of Geology, Florida State University.

Fretzdorff, S. (1997) The Réunion hotspot: history of explosive activity and geochemical evolution. *Geologisch-Paläontologisches Institut und Museum Berichte*, **81**. 98 pp.

Froggatt, P.C. (1992) Standardisation of the chemical analysis of tephra deposits. Report on the ICCT working group. *Quaternary International,* **13/14**, 93-96.

Froggatt, P.C., Nelson, C.S., Carter, L., Griggs, G. and Blank, K.P. (1986), An exceptionally large late Quaternary eruption from New Zealand. *Nature*, **319**, 578-582.

Gass, I.G, Harris, P.G and Holdgate, M.W. (1963) Pumice eruption in the area of the South Sandwich Islands. *Geological Magazine.* **100** (4). 321-330.

Gilbert, I.M., Pudsey, C.J. and Murray, J.W. (1998) A sediment record of cyclic bottom current variability from the northwest Weddell Sea. *Sedimentary Geology*, **115**, 185-214.

González-Ferrán, O. (1983). The Seal Nunataks: An active volcanic group on the Larsen Ice Shelf, West Antarctica. *In*: Oliver, R. L., James, P.R. and Jago, J.B. *Antarctic Earth Science*, Cambridge University Press, New York. 334-337.

González-Ferrán, O. (1991) The Bransfield rift and its active volcanism. In: Thomson, M.R.A., Crame, J.A. and Thomson, J.W. (eds) *Geological Evolution of Antarctica*. Cambridge University Press, Cambridge. 505-509

Goodell, H.G., (1964) Marine geology of the Drake Passage, Scotia Sea and South Sandwich Trench (USNS *Eltanin* cruises 1-8). Florida State University, Tallahassee.

Goodell, H.G., (1965) Marine geology: USNS *Eltanin* cruises 9-15. Florida State University, Tallahassee.

Goodell, H.G., Houtz, R., Ewing, M., Hayes, D., Naini, B., Echols, R.J., Kennett, J.P. and Donahue, J.G. (1973) Marine sediments of the Southern Oceans. *Antarctic Map Folio Series*, **17**, 18 pp

Gordon, J.E. and Harkness, D.D. (1992). Magnitute and geographical variation of the radiocarbon content in marine life: Implications foor reservoir corrections in radiocarbon dating. *Quaternary Science Reviews*, **11**, 697-708.

Gow, A.J., Ueda, H.T. and Garfield, D.E. (1968). Antarctic ice sheet: Preliminary results of the first core to bedrock. *Science*, **161**, 1011-1013.

Gow, A.J. and Williamson, T. (1971). Volcanic ash in the Antarctic ice sheet and its possible climatic implications. *Earth and Planetary Science Letters*, **13**, 210-218.

Grobe, H., Mackensen, A., Hubberten, H.-W., Spiess, V. and Fütterer, D.K. (1990) Stable isotope record of late Quaternary sedimentation rates at the Antarctic continental margin. In: Bleil, U. and Thiede, J. (eds) *Geological History of the Polar Oceans: Arctic versus Antarctic*, Kluwer Academic Publishers, 539-572.

Grönvold, K., Óskersson, N., Johnsen, S.J., Clausen, H.B., Hammer, C.U., Bond, G. and Bard, E. (1995) Ash layers from Iceland in the Greenland GRIP ice core

correlated with oceanic and land sediments. *Earth and Planetary Science Letters*, **135**, 149-155.

Grovtov, A.S., Nechaev, D.A., Panteleev, G.G. and Yaremchuk, M.I. (1998). Large scale circulation in the Bellingshausen and Amundsen seas as a variational inverse of climatological data. *Journal of Geophysical Research: Oceans,* **103**, 13,011-13,022.

Guinasso, N.L. Jr. and Schink, D.R. (1975) Quantitative estimates of biological mixing rates in abyssal sediments. *Journal of Geophysical Research*, **80**, 3032-3043.

Hall, K.V. (1982). Rapid deglaciation as an initiator of volcanic activity: an hypothesis. *Earth Surface Processes and Landforms*, **7**, 45-51

Harland, R., Pudsey, C.J., Howe, J.A. and Fitzpatrick, M.E.J. (1998) Recent dinoflagellate cysts in a transect from the Falkland Trough to the Weddell Sea, Antarctica. *Palaeontology,* **41** (6), 1093-1131.

Hawkes, D.D., (1961), The geology of the South Shetland Islands: II. The geology and petrology of Deception Island, *Falkland Islands Dependency Survey Scientific Report.,* **27**, London

Hays, D., Lozano, J.A., Shackleton,N.J., and Irving, G., (1976) Reconstruction of the Atlantic and western Indian Ocean sectors of the 18,000B.P. Antarctic Ocean. In: *Investigation of Late Quaternary Paleoceanography and Paleoclimatology.* Geol. Soc. Am. Mem. **145**. 337-372

Hjort, C., Björck, S., Ingólfsson, Ó. and Möller, P. (1998). Holocene deglaciation and climate history of the northern Antarctic Peninsula region: a discussion of correlations between the Southern and Northern Hemispheres. *Annals of Glaciology*, **27**, 110-112.

Hodgson, D.A., Dyson, C.L., Jones, V.J. and Smellie, J.L. (1998). Tephra analysis of sediments from Midge Lake (South Shetland Islands) and Sombre Lake (South Orkney Island), Antarctica. *Antarctic Science*, **10** (1), 13-20.

Hofmann, A., Kipfstuhl, J., Fütterer, D., Gersonde, R., Grobe, H. and Kuhn, G. (1997 - unpublished) Rapid climate variations and calving events during the last Glacial in the Scotia Sea, Antarctica, In: *Antarctica and Global Change: Interactions and Impacts, Symposiums Programme and Abstracts.* (abstract only).

Holtedahl, O. (1929). On the geology and physiography of some Antarctic and sub-Antarctic islands. *Scientific Results of the Norwegian Antarctic Expedition, No.3.* 172 pp

Houghton, B.F. and Nairn, I.A. (1991) The 1976–1982 Strombolian and phreatomagmatic eruptions of White Island, New Zealand: eruptive and depositional mechanisms of a wet volcano. *Bulletin of Volcanology*, **54**, 35-49.

Howe, J.A. and Pudsey, C.J. (1999) Antarctic Circumpolar Deepwater: a Quaternary palaeoflow record from the northern Scotia Sea, South Atlantic Ocean. *Journal of Sedimentary Research*, **64** (4), 847-862.

Huang, T.C. and Watkins, N.D. (1982) Explosive volcanic eruptions in the vicinity of Balleny Islands recorded in the abyssal sediments of the Southern Oceans. In: Craddock, C. (ed), *Antarctic Geoscience*, University of Wisconsin Press, Madison, 787. Abstract only.

Huang, T.C., Watkins, N.D., Shaw, D.M. and Kennett, J.P. (1973). Atmospherically transported volcanic dust in South Pacific deep-sea sedimentary cores at distances over 3,000 km from the eruptive source. *Earth and Planetary Science Letters*, **20**, 119-124.

Hubberten, H.W, Morche, W., Westall, F., Fütterer, D.K. and Keller, J. (1991). Geochemical investigations of volcanic ash layers from southern Atlantic legs 113 and 114. *In* Ciesielski, P.F., Kristoffersen, Y., *et al*., 1991. Proc *ODP, Sci Results*, 114: College Station TX (Ocean Drilling Program).

Hunt, J.B. (1996). Quaternary Tephrology and Tephrochronology of the North Atlantic Region. Ph.D. thesis, University of Edinburgh. Unpublished.

Hunt, J.B., and Hill, P.G., (1993) Tephra geochemistry: a discussion of some persistent analytical problems, *The Holocene* **3** (3), 271-278

Hunt, J.B., and Hill, P.G., (1994) Geochemical data in tephrochronology: a reply to Bennet, *The Holocene* **4** (4) 435-438.

Hunt, J.B., and Hill, P.G., (1996) An Inter-laboratory comparison of the electron probe microanalysis of glass geochemistry, *Quaternary International*, **34-36**, 229-241.

Hunt, J.B., Fannin, N.G.T., Hill, P.G. and Peacock , J.D. (1995) The tephrochronology and radiocarbon dating of the North Atlantic, Late-Quaternary sediments: an example from the St. Kilda Basin. In Scrutton, R.A., Stoker, M.S., Shimmield, G.B and Tudhope,A.W. (eds*) The Tectonics, Sedimentation and Palaeoceanography of the North Atlantic Region*, Geological Society Special Publication No. 90, 277-248

Jackson, M.L. Levelt, T.W.M. Syers, J.K, Rex, R.W., Clayton, R.N., Sherman, G.D. and Uehhara, G. (1971) Geomorphological relationship of tropospherically derived quartz in the soils of the Hawaiian Islands. *Proceedings of the Soil Science Society of America*, **35**, 515-525.

Jeffers, J.D., Anderson, J.B. and Lawver, L.A. (1991) Evolution of the Bransfield Basin, Antarctic Peninsula. In: Thomson, M.R.A., Crame, J.A. and Thomson, J.W. (eds) *Geological Evolution of Antarctica*. Cambridge University Press, Cambridge. 481-485.

Jones, R.W. and Pudsey, C.J. (1994). Recent benthic foraminifera from the Western Antarctic Ocean. *Journal of Micropalaeontology,* **13**, 17-23.

Jordan, R.W., Priddle, J., Pudsey, C.J., Barker, P.F. and Whitehouse, M.J. (1991) Unusual diatom layers in Upper Pleistocene sediments from the northern Weddell Sea. *Deep-Sea Research*, **38** (7), 829-843.

Jordan, R.W. and Pudsey, C.J. (1992) High-resolution diatom stratigraphy of Quaternary sediments from the Scotia Sea. *Marine Micropalaeontology*, **19**, 201-237.

Keller, R.A. and Fisk, M.R. (1992) Quaternary marginal basin volcanism in the Bransfield strait as a modern analogue of the southern Chilean ophiolites. In: Parson, L.M., Murton, B.J. and Brownin, P. (eds). *Ophiolites and their modern oceanic analogues*. Geological Society, London, Special Publication, **60**, 155-169

Keller, R.A. and Fisk, M.R., White, W.M. and Birkenmayer, K. (1992) Isotope and trace element constraints on mixing and melting models of marginal basin volcanism, Bransfield Strait, Antarctica. *Earth and Planetary Science Letters*, **111**, 287-303.

Kennett, J.P. and Warnke, D.A. (1992) *The Antarctic Palaeoenviroment: a perspective on global Change part I*. Antarctic Research Series **56**, American Geophysical Union, Washington, D.C. pp385.

Keys, J.R. (1990). Ice. *In*: Glasby, G.P. (ed) *Antarctic Sector of the Pacific*. Elsevier Oceanography Series **51**, Elsevier, Amsterdam, 95–123.

Kyle, P.R. and Seward, D. (1984). Dispersed rhyolitic tephra from New Zealand in deep-sea sediments of the Southern Ocean. *Geology*, **12**, 487-490.

Kyle, P.R. and Jezek, P.A. (1978). Compositions of three tephra layers from the Byrd Station ice core, Antarctica. *Journal of Volcanology and Geothermal Research*, **4**, 225-232.

Kyle, P.R. Jezek, P.A., Mosely-Thompson, E. and Thompson, L.G. (1981). Tephra layers in Byrd Station ice core and the Dome C ice core, Antarctica and their climatic importance. *Journal of Volcanology and Geothermal Research*, **11**, 29-39.

Kyle, P.R., Palais, J.M. and Delmas, R. (1982). The volcanic record of Antarctic ice cores: preliminary results and potential for future investigations. *Annals of Glaciology*, **3**, 172-177.

Lally, V.E. and Lichfield, E.W. (1969). A summary of the status and plans for the GHOST Balloon Project. *American Meterological Society Bulletin*. **50**, 868-874.

Larson, C.A. (1894) The voyage of the *Jason* to the Antarctic regions, *Geographical Journal*, **4**, 333-344.

Larter, R.D. and Barker, P.F. (1991) Neogene interaction of tectonic and glacial processes at the Pacific margin of the Antarctic Peninsula. In: Macdonald, D.I.M., (ed) *Sedimentation, tectonics and ecstasy.* International Association of Sedimentologists Special Publication, **12**, 165-186.

Larter, R.D. and Cunningham, A.P. (1993) The depositional pattern and distribution of glacial-interglacial sequences on the Antarctic Peninsula Pacific margin. *Marine Geology*, **109**, 203-219.

Ledbetter, M.T. and Elwood, B.B. (1976). Selection of sample intervals in deep-sea sedimentary cores. *Geology*, **4**, 303-304.

Ledbetter, M.T. and Ciesielski, P.F. (1986). Post-Miocene disconformities and palaeoceanography in the Atlantic sector of the Southern Ocean. *Palaeogeography, Palaeoclimatology, Palaeoecology*, **52**, 185-214.

LeMasurier, W.E. (1990). Marie Byrd Land. In: LeMasurier, W.E. and Thomson, J.W., (eds) *Volcanoes of the Antarctic plate and southern Oceans.* Antarctic Research Series , vol.48, American Geophysical Union, Washington, D.C. 147-163.

LeMasurier, W.E. and Wade, F.A., (1976) Volcanic history in Marie Byrd Land: Implications with regard to Southern Hemispere tectonic reconstructions. *In*: Gonzalez-Ferran, O., (ed) *Andean and Antarctic Volcanology Problems*, International Association of Volcanology and Chemistry of the Earth's Interior, Rome.

LeMasurier, W.E. and Rex, D.C. (1989). Evolution of linear volcanic ranges in Marie Byrd Land, West Antarctica. *Journal of Geophysical Research*, **94 B6**, 7,223-7,236.

Linick, T.W. (1978). La Jolla measurements of radiocarbon in the oceans, *Radiocarbon*, **20**, 333-359.

Lowe, J.J. and Turney, C.S.M. (1997) Vedde Ash layer discovered in a small lake basin on the Scottish mainland. *Journal of the Geological Society*, **154** (4), 605-612

McCoy, F.W. and Von Herzen, R.P. (1971) Deep-sea corehead camera photography and piston coring. *Deep-Sea Research*, **18**, 361-373

Maksimov, I.V. and Vorob'ev, V.N. (1964) Contribution to the study of deep currents in the Southern Ocean. *Inf. Bulletin of Soviet Antarctic Expedition*, **4**, 17-19.

Mangerud, J., Lie, S.E., Furnes, H., Kristiansen, I.L. and Lømo, L. (1984) A Younger Dryas ash bed in western Norway, and its possible correlations with tephra in cores from the Norwegian Sea and the North Atlantic. *Quaternary Resaerch*, **21**, 85-104

Mantyla, A.W. and Reid, J.L. (1983). Abyssal characteristics of the World Ocean waters. *Deep-Sea Research*, **30** (8), 805-833.

Marchant, D.R., Denton, G.H. and Swisher III, C.C. (1993). Miocene-Pliocene-Pleistocene glacial history of Arena Valley, Quatermain Mountains, Antarctica. *Geografiska Annaler*, **75 A**, 269-303.

Marchant, D.R., Denton, G.H., Swisher III, C.C. and Potter Jr., N. (1996). Late Cenozoic Antarctic palaeoclimate reconstructed from volcanic ashes in the Dry Valley region of southern Victoria Land. *Geological Society of America Bulletin*, **108** (2), 181-194.

Marti, J., Vila, J. and Rey, J. (1996) Deception Island (Bransfield Strait, Antarctica): an example of a volcanic caldera developed by extensional tectonics. In: McGuire, W.J., Jones, A.P. and Neuberg, J. (eds) *Volcano instability on the Earth and other planets*. Geological Society, London, Special Publication, **110**, 253-265.

Matthies, D., Storzer, D. and Troll, G. (1988), Volcanic ashes in Bransfield Strait sediments: geochemical and stratigraphical investigations (Antarctica). *Proceedings of the Second International conference on Natural Glasses. Prague.* 139-147

Matthies, D., Mäusbacher, R. and Storzer, D., (1990) Deception Island tephra: a stratigraphic marker for limnic and marine sediments in the Bransfield Strait area, Antarctica. *Zbl. Geol. Paläont.*, **1**, 153-185.

McGinnis, I.N. and Hayes, D.E. (1994). Sediment drift formation along the Antarctic Peninsula. *Terra Antartica*, **1** (2), 275-276.

McGinnis, I.N. and Hayes, D.E. (1995). The roles of down-slope and along-slope depositional processes: southern Antarctic Peninsula margin. *Antarctic Research Series*, **68**, 141-156.

McGinnis, I.N., Hayes, D.E. and Driscoll, N.W. (1997) Sedimentary processes across the continental rise of the southern Antarctic Peninsula. *Marine Geology*, **37**, 1-18.

McGuire, W.J., Howarth, R.J., Firth, C.R., Solow, A.R., Pullens, A.D., Saunders, S.J., Stewart, I.S. and Vita-Finzi, C. (1997). Correlation between rate of sea-level change and frequency of explosive volcanism in the Mediterranean. *Nature*, **389**, 473-476.

Michel, R.L. and Druffel, E.M. (1983) Radiocarbon in the Weddell Sea as observed in a deep-sea coral and in a krill. *Geophysical Research Letters*, **10**, 190-192.

Middleton, N.J. (1989) Desert Dust. *In*: Thomas, D.S.G. (ed) *Arid Zone Geomorphology*, Belhaven Press, London, 262-283.

Moreton, S.G. and Smellie, J.L. (1998). Identification and correlation of distal tephra layers in deep-sea sediment cores, Scotia Sea, Antarctica. *Annals of Glaciology*, **27**, 285-289.

Mullan, A.B. and Hickman, J.S. (1990). Meteorology. In: Glasby, G.P. (ed) *Antarctic Sector of the Pacific*. Elsevier Oceanography Series **51**, Elsevier, Amsterdam, 21–54.

Murray, J.W. (1995) Ocean Water Masses, Circulation and Climate. In Bosence, D.W.J. and Allison, P.A. (eds), *Marine Palaeoenvironmental Analysis from Fossils*. Geol. Soc. Spec. Pub. No. **83**. 245-264.

Nicholls, K. W., Makinson, K. and Robinson, A.V. (1991) Ocean circulation beneath the Ronne Ice Shelf, *Nature* **354**, 221-223.

Ninkovich, D., Heezen, B.C., Conolly, J.R. and Burckle, L.H. (1964). South Sandwich tephra in deep-sea sediments. *Deep-Sea Research*, **11**, 605-619.

Nowlin, W.D. and Klinck, J.M.. (1986) Physics of the Antarctic Circumpolar Current, *Reviews of Geophysics*, **24**, 469-491.

Nowlin, W.D. and Zenk, W. (1988) Westward bottom currents along the margin of the South Shetland Island Arc. *Deep-Sea Research*, **35**, 269-301.

Orheim, O. (1972) Volcanic activity on Deception Island, South Shetland Islands. In Adie, R.J. (ed*) Antarctic geology and Geophysics*, 117-120.

Orsi, A.H., Nowlin Jr. W.D. and.Whitworth III, T. (1992) On the circulation and stratification of the Weddell Gyre. *Deep-Sea Research*, **40** (1), 169-203.

Orsi, A.H., Whitworth III, T. and Nowlin Jr. W.D. (1995) On the meridional extent and front of the Antarctic Circumpolar Current. *Deep-Sea Research*, **42**, 641-673.

Palais, J.M. and Kyle, P.R., (1988). Chemical composition of ice containing tephra layers in the Byrd Station ice core, Antarctica. *Quaternary Research*, **30**, 315-330.

Palais, J.M., Kyle, P.R., Mosely-Thompson, E. and Thomas, E. (1987). Correlation of a 3,200 year old tephra in ice cores from Vostok and South Pole stations, Antarctica. *Geophysical Research Letters*, **14**, 804-807.

Palais, J.M., Kyle, P.R. McIntosh, W.C. and Seward, D. (1988). Magmatic and phreatomagmatic volcanic activity at Mt. Takahe, West Antarctica, based on tephra layers in the Byrd ice core and field observations at Mt. Takahe. *Journal of Volcanology and Geothermal Research*, **35**, 295-317.

Paramor, T.J. (in prep.). The Antarctic Circumpolar Current: oceanographic and climatic significance in the late Quaternary. University College London, Ph.D. Thesis.

Pearce, J.A., Baker, P.E., Harvey, P.K. and Luff, I.W. (1995). Geochemical evidence for subduction fluxes, mantle melting and fractional crystallization beneath the South Sandwich Island Arc. *Journal of Petrology*, **36** (1), 1,073-1,109.

Pierce, R.B. and Fairlie, T.D.A. (1993). Chaotic advection in the stratosphere: implications for the dispersal of chemically perturbed air from the polar vortex. *Journal of Geophysical Research*, **98**, 18,589-18,595.

Piggott, C.S. (1941) Factors involved in submarine core sampling. *Bulletin of the Geological Society of America*, **52**, 1,513-1,524.

Pilcher, J.R and Hall, V.A. (1992) Towards a tephrachronology for the Holocene of the north of Ireland. *The Holocene*, **2** (3), 255-259.

Potts, P.J. (1987) *A Handbook of Silicate Rock Analysis*. Blackie, London.

Prestvik, T., Barnes, C.G., Sundvoll, B. and Duncan, R.A. (1990) Petrology of Peter I Øy (Peter I Island), West Antarctica. *Journal of Volcanology and Geothermal Research*, **44**, 315-338.

Pudsey, C.J. (1992) Late Quaternary changes in Antarctic Bottom Water velocity inferred from sediment grain size in the northern Weddell Sea. *Marine Geology*, **107**, 9-33.

Pudsey, C.J., Barker, P.F. and Hamilton, N. (1988) Weddell Sea abyssal sediments: a record of Antarctic Bottom Water flow. *Marine Geology*, **81**, 289-314.

Pudsey, C.J., Barker, P.F. and Larter, R.D. (1994) Ice sheet retreat from the Antarctic Peninsula shelf. *Continental Shelf Research.* **14** (15) 1,647-1,675.

Pudsey, C.J. and Camerlenghi, A. (1998) Glacial-interglacial deposition on a sediment drift on the Pacific margin of the Antarctic Peninsula. *Antarctic Science*, **10**, 286-308.

Pudsey, C.J. and Howe, J.A., (1998) Quaternary history of the Antarctic Circumpolar Current: evidence from the Scotia Sea. *Marine Geology*, **148**, 83-112.

Pudsey, C.J. and King, P. (1997) Particle fluxes, benthic processes and the palaeoenvironmental record in the northern Weddell Sea, *Deep-Sea Research*, **44** (11), 1,841-1,876.

Pudsey, C.J. and Strobl, C., (in prep.) Sedimentation on the continental rise west of the Antarctic Peninsula over the last three glacial cycles.

Quartermain, L.B. (1964) *The Balleny Islands: A descriptive and historical outline, compiled for the use of the New Zealand Antarctic Research Expedition Balleny Islands Reconnaissance Party 1963-1964*. Antarctic Division New Zealand Department of Science and Industrial Research. Wellington. 42pp.

Rebesco, M., Larter, R.D., Barker, P.F., Camerlenghi, A. and Vanneste, L.E. (1994) The history of sedimentation on the continental rise west of the Antarctic Peninsula. *Terra Antartica*, **1** (2), 277-279.

Rebesco, M., Larter, R.D., Camerlenghi, A. and Barker, P.F. (1996) Giant sediment drifts on the continental rise west of the Antarctic Peninsula. *Geo-Marine Letters*, **16**, 65-75.

Rebesco, M., Larter, R.D., Barker, P.F., Camerlenghi, A. and Vanneste, L.E. (1997) The history of sedimentation on the continental rise west of the Antarctic Peninsula. *Antarctic Research Series*, **71**, 29-49.

Reed, S.J.B. (1975) *Electron Microprobe analysis*, Cambridge University Press, Cambridge

Reed, S.J.B. (1993) *Electron Microprobe analysis*, 2nd edition Cambridge University Press, Cambridge.

Reed, S.J.B. (1996) *Electron Microprobe analysis and Scanning electron Microscopy in Geology*. Cambridge University Press, Cambridge. pp 201.

Rey, J., Somoza, L. and Martínez-Frías, J. (1995) Tectonic, volcanic and hydrothermal event sequence on Deception Island (Antarctica). *Geo-marine Letters*, **15**, 1-8.

Robinson, S.G. (1990) Applications for whole-core magnetic susceptibility measurements of deep-sea sediments: Leg 115 results. *In:* Duncan, R.A., Backman, J., Peterson.L.C. *et al., Proceedings of the Ocean Drilling Program, Scientific Results, Vol. 115*. College Station, TX (Ocean Drilling Program).

Rose, N.L. Golding, P.N.E. and Battarbee, R.W. (1996) Selective concentration and enumeration of tephra shards from lake sediment cores. *The Holocene*, **6** (2), 243-246

Ross, D.A. and Riedel, W.R. (1967) Comparison of upper parts of some piston cores with simultaneously collected open-barrel cores. *Deep-Sea Research*, **14**, 285-294.

Rowley, P.D., Thomson, J.W., Smellie, J.L., Laudon, T.S., La Prade, K.E. and LeMasurier, W.E. (1990) Alexander Island, Palmer Land and Ellsworth Land. In: LeMasurier, W.E. and Thomson, J.W (eds) *Volcanoes of the Antarctic plate and southern Oceans*. Antarctic Research Series , **48**, American Geophysical Union, Washington, D.C. 257-301

Ruddiman, W.F. and Glover, L.K. (1972) Vertical mixing of ice-rafted volcanic ash in North Atlantic sediments. *Geological Society of America Bulletin*, **83**, 2817-2836.

Ruddiman, W.F. and Glover, L.K. (1982) Mixing of volcanic ash zones in subpolar North Atlantic sediments. *In*: Scrutton, R.A. and Talwani, M. (eds) *The Ocean Floor*, Chichester, John Wiley and Sons.

Saunders, A.D. and Tarney, J. (1982). Igneous activity in the southern Andes and northern Antarctic Peninsula: A review. *Journal of the Geological Society of London*, **139**, 691-700.

Saunders, A.D., Tarney, J., Weaver, S.D. and Barker, P.F. (1982). Scotia Sea floor: Geochemistry of basalts from the Drake Passage and South Sandwich Spreading Centres. In: Craddock, C. (ed), *Antarctic Geoscience*, University of Wisconsin Press, Madison, 213-222.

Scasso, R. A., Corbella, H. and Tiberi, P. (1994). Sedimentological analysis of the tephra from the 12-15 August 1991 eruption of Hudson volcano. *Bulletin of Volcanology*, **56**, 121-132.

Shane, P.A.R. and Froggatt, P.C. (1992). Composition of widespread volcanic glass in deep-sea sediments of the Southern Pacific Ocean: an Antarctic source inferred. *Bulletin of Volcanology*, **54**, 595-601.

Shaw, D.M., Watkins, N.D. and Huang, T.C. (1974). Atmospherically transported volcanic glass in deep-sea sediments: theoretical considerations. *Journal of Geophysical Research*, **79** (21), 3087-3094.

Sheridan, M.F. and Marshall, J.R. (1987) Comparative charts for quantitative analysis of grain-textural elements on pyroclasts. *In*. Marshall, J.R. (ed) *Clastic Particles: Scanning Electron Microscopy and Shape analysis of Sedimentary and Volcanic Clasts*. Van Nostrand Reinhold, New York

Shimmield, G.B. (1992), Can sediment geochemistry record changes in coastal upwelling palaeoproductivity? Evidence from northwest Africa and the Arabian Sea. In: Summerhayes, C.P., Prell, W., and Emeis, K.C., (eds*)* *Upwelling Systems since the early Miocene*. Spec. Publ. Geol. Soc. London, **64**, 29-46

Shimmield, G. B., Derrick, S., Pudsey, C.J., Barker, P.F., Mackensen, A., and Grobe, H. (1993) The use of inorganic chemistry in studying the palaeoceanography of the Weddell Sea. *Antarctic Special Topic*. 99-108.

Shimmield, G. B., Derrick, S., Mackensen, A., Grobe, H. and Pudsey, C.J., (1994) The history of biogenic silica, organic carbon and barium accumulation in the Weddell Sea and Antarctic Ocean over the last 150,00 years. In: Zahn *et al* (eds) *Carbon cycling in the Glacial Ocean: constraints on the ocean's role in global change*. Proc. NATO ARW, **I 17**, 555-574

Sigvaldason, G.E., Annertz, K. and Nilsson, M. (1992). Effect of glacier loading/unloading on volcanism: Postglacial volcanic production rate of the Dyngjufjöll area, central Iceland. *Bulletin of Volcanology*, **54**, 385-392.

Simpkin, T. and Siebert, L. (1994). *Volcanoes of the World*. 2nd Edition. Geoscience Press, Tucson. pp 349.

Singer, B.S., Wijbrans, J.R., Nelson, S.T., Pringle, M.S, Freeley, T.C. and Dungan, M.A., (1998). Inherited argon in a Pleistocene andesite lava: $^{40}Ar/^{39}Ar$ incremental-heating and laser-fusion analyses of plagioclase. *Geology*, **26** (5), 427-430.

Skirrow, G. (1975). The dissolved gases – carbon dioxide. *In:* Riley, J.P. and Skirrow, G. (eds), *Chemical Oceanography*, Vol. 1. Academic press, London, 1-192.

Smellie, J.L., (1988) Recent observations on the volcanic history of Deception Island, South Shetland Islands. *British Antarctic Survey Scientific Report*, **81**, 83-85.

Smellie, J.L. (1990) Graham Land and South Shetland Islands. In: LeMasurier, W.E. and Thomson, J.W., (eds) *Volcanoes of the Antarctic plate and southern Oceans*. Antarctic Research Series , **48**, American Geophysical Union, Washington, D.C. 303-359

Smellie, J.L. (in press). The upper Cenozoic tephra record in the South Polar region: review. *Quaternary Science Reviews*.

Smellie, J.L. (in prep). Eruptive history of a large marginal basin volcano with a restless caldera: Deception Island, Bransfield Strait, Antarctica.

Smellie, J.L. and Hole, M.J. (1997). Products and processes in Pliocene-Recent, subaqueous to emergent volcanism in the Peninsula: examples of englacial surtseyan volcano construction. *Bulletin of Volcanology*, **58**, 628-646.

Smellie, J.L, López-Martínez, J., Rey, J. and Serrano, E. (1997) Maps of Deception Island, South Shetland Islands. In Ricci, C.A. (ed) *The Antarctic region: Geological evolution and processes*. Sienna Museo Nazionale dell' Antartide, 1,195-1,198.

Smellie, J.L. Pankhurst, R.J., Thomson, M.R.A. and Davies, R.E.S. (1984). The geology of the South Shetland Islands. VI. Stratigraphy, geochemistry and evolution. *British Antarctic Survey Scientific Report*, **87**, pp 85

Smith, D.G.W and Westgate, J.A. (1969) Electron probe technique for characterising pyroclastic deposits. *Earth and Planetary Science Letters*, **5**, 313-319.

Sparks, R.S.J., Bursik, M.I., Carey, S.N., Gilbert, J.S., Glaze, L.S., Sigurdsson, H. and Woods, A.W. (1997) *Volcanic Plumes*. John Wiley and Sons. Chichester. pp 574.

Stow, D.A.V. (1994) Deep-sea sediment transport. *In*: Pye, K. (ed) *Sediment transport and depositional processes*, Blackwell, London.

Straub, S.M., Schmincke, H-U. and Horn, S. (1996). Sandwich Tephra - Petrologie und Vulkanologie quarterer (<300 ka) vulkanischer Aktivitaet an der Sued Sandwich Konvergenz rekonstruiert anhand submariner Tephralagen. *Abschlußbericht Zu SCHM250/55-1/2 Sandwich Tephra*. (unpublished).

Struvier, M., Quay, P.D. and Ostlund, H.G. (1983) Abyssal water carbon-14 distribution and the age of the world oceans. *Science*, **219**, 849-851.

Sugden, D.E. (1982) *Arctic and Antarctic: A modern geographical synthesis*, Barnes and Noble.

Sweatman, T.R. and Long, J.V.P. (1969) Quantitative electron-prob microanalysis of rock-forming minerals. *Journal of Petrology*, **10**, 332-379.

Tarney, J., Saunders, A.D. and Weaver, S.D. (1977). Geochemistry of volcanic rocks from the island arcs and marginal basins of the Scotia arc region. In: Talwani, M. and Pitman III, W.C. (eds). *Island Arcs, Deep-Sea Trenches and Back-Arc Basins, Maurice Ewing Series, Volume 1.* American Geophysical Union, Washington, D.C. 367-377.

Tatur, A., del Valle, R. and Pazdur, M. (1991). Lake sediments in maritime Antarctic zone: a record of landscape and biota evolution: preliminary report. *Internationale Vereinigung für Theoretische und Angewandte Limnologie*, **24**, 3,022-3,024.

Vanney, J.R. and Johnson, G.L., (1976) Geomorphology of the Pacific continental margin of the Antarctic Peninsula. *In:* Hollister, C.D., Craddock, C., *et al. Initial Reports of the Deep Sea Drilling Project*, **35**. Washington, DC: US Government Printing Office, 279-289.

Verwoerd, W.J., Chevallier, L. and Thomson, J.W. (1990) Oceanic Islands on the Antarctic Plate. *In*: LeMasurier, W.E. and Thomson, J.W., (eds) *Volcanoes of the Antarctic plate and southern Oceans..* Antarctic Research Series , **48**, American Geophysical Union, Washington, D.C. 396-463

Walker, G.P.L. and Crossdale, R. (1972) Characteristics of some basaltic pyroclastics. *Bulletin of Volcanology*. **35**, 303-317.

Watkins, N.D., Sparks, R.J.S., Sigurdsson, H., Huang, T.C., Federman, A., Carey, S. and Ninkovich, D. (1978) Volume and extent of the Minoan tephra from Santorini volcano: new evidence from deep-sea cores. *Nature* **271**, 122-126.

Watkins, N.D. and Kennett, J.P. (1972). Summary of researches on the *Eltanin* deep-sea sedimentary cores and a discussion of sub-Antarctic volcanism, climate change and faunal extinction. *In*: Adie, R.J. (ed). Antarctic Geology and Geophysics. Universitetsforlaget, Oslo, (abstract only), 763.

Weaver, S.D., Saunders, A.D., Pankhurst,R.J., and Tarney, J. (1979) A geochemical study of magmatism associated with the initial stages of back-arc spreading: The Quaternary volcanics of Bransfield Strait, from the South Shetland Islands. *Contrib. Mineral.Petrol.*, **68**, 151-169

Whitham, A.G. and Sparks, R.J.S. (1986). Pumice. *Bulletin of Volcanology*, **48**, 209-223.

Whitworth, T., Orsi, A.H., Kim, S.-J., Nowlin, W.D. and Locarnini, R.A. (1998). Water masses and mixing near the Antarctic slope front. In: Jacobs, S. S., and Weiss, F. (Eds), *Ocean, Ice and Atmosphere: Interactions at the Antarctic Continental Margin*. Antarctic Research Series, **75**, American Geophysical Union, Washington, D.C. 1-27

Wiesner, M.G., Wang, Y. and Zheng, L. (1995) Fallout of volcanic ash to the deep South China Sea induced by the 1991 eruption of Mount Pinatubo (Philippines) *Geology*. **23** (10), 885-888.

Wilch, T.I and McIntosh, W.C. (in prep.). Late Pleistocene ^{40}Ar/^{39}Ar tephrochronology in Marie Byrd Land, West Antarctica: Potential time horizons in future West Antarctic ice and marine cores.

Williams, H. and McBirney, A.R. (1979). *Volcanology*. Freeman, Cooper, San Francisco, 397pp.

Wilson, M. (1989*) Igneous Petrogenesis: A Global Techtonic Approach*. Unwin Hyman, London, 466pp.

Wohletz, K.H. (1987) Chemical and textural surface features of pyroclasts from hydrovolcanic eruption sequences. *In*: Marshall, J.R. (ed) *Clastic Particles: Scanning Electron Microscopy and Shape analysis of Sedimentary and Volcanic Clasts*. Van Nostrand Reinhold, New York.

Woods, A.W. (1998) Observations and models of volcanic eruption columns. *In:* Gilbert, J.S. and Sparks R.S.J. (eds) *The Physics of Explosive Eruptions*. Geological Society, London, Special Publication, **145**, 27-50.

Zielinski, G.A., Mayewski, P.A., Meeker, L.D., Whitlow, S. and Twickler, M.S. (1996). A 110,000 -yr record of explosive volcanism from the GISP2 (Greenland) ice core. *Quaternary Research*, **45**, 109-118.

Zielinski, U. and Gersonde, R. (1997) Diatom distribution in the Southern Ocean surface sediments (Atlantic sector): Implications for palaeoenvironmental reconstructions. *Palaeogeography, Palaeoclimatology, Palaeoecology*, **129**, 213-250.

I. Appendix I – Major element compositions

Core section	depth (mbsf)	SiO_2	TiO_2	Al_2O_3	FeO_T	MnO	MgO	CaO	Na_2O	K_2O	Total
E42-11	0.20	43.39	4.46	19.06	10.28	0.14	3.96	8.79	3.20	1.75	95.03
E42-11	0.20	45.56	3.38	17.24	10.95	0.15	5.69	9.54	3.04	0.95	96.50
E42-11	0.20	47.16	3.92	13.84	10.37	0.08	5.04	10.08	3.58	1.63	95.70
E42-11	0.20	47.21	4.97	13.73	11.35	0.15	4.52	9.24	3.80	1.78	96.75
E42-11	0.20	47.84	3.62	13.31	10.95	0.12	5.46	10.03	3.38	1.15	95.86
E42-11	0.20	47.85	3.51	13.68	11.05	0.19	6.11	10.15	3.25	0.85	96.64
E42-11	0.20	48.35	3.45	13.82	11.19	0.15	6.10	9.95	3.22	0.98	97.21
E42-11	0.20	48.35	3.83	13.61	11.06	0.15	5.38	9.95	3.42	1.19	96.94
E42-11	0.20	48.57	3.69	13.29	11.37	0.13	5.56	10.06	3.64	1.22	97.53
E42-11	0.20	48.59	3.84	13.83	11.43	0.13	5.38	9.94	3.41	1.11	97.66
E42-11	0.20	49.14	3.60	14.15	10.26	0.15	4.66	8.98	3.57	1.39	95.90
E42-11	0.20	50.89	3.03	13.01	10.98	0.14	5.17	8.83	3.43	0.83	96.31
E42-11	0.20	51.03	2.85	13.22	11.12	0.10	5.30	8.89	3.15	0.83	96.49
E42-11	0.20	51.07	3.14	12.84	11.25	0.14	5.38	9.03	3.17	0.83	96.85
E42-11	0.20	51.13	2.97	12.79	10.83	0.08	5.11	8.91	3.16	0.89	95.87
E42-11	0.20	51.65	3.04	12.95	10.82	0.11	5.17	8.77	3.16	0.82	96.49

Core section	depth (mbsf)	SiO_2	TiO_2	Al_2O_3	FeO_T	MnO	MgO	CaO	Na_2O	K_2O	Total
E11-21/5	0.05	46.18	3.94	13.90	11.17	0.13	5.05	10.17	4.14	1.34	96.02
E11-21/5	0.05	46.66	3.78	13.82	11.49	0.13	5.11	10.26	4.14	1.43	96.82
E11-21/5	0.05	46.79	4.01	14.07	11.47	0.10	5.14	10.19	4.15	1.36	97.28
E11-21/5	0.05	46.93	3.99	13.97	11.23	0.18	5.09	10.27	4.06	1.40	97.12
E11-21/5	0.05	47.00	3.96	13.82	11.37	0.21	5.11	10.11	4.04	1.43	97.05
E11-21/5	0.05	47.02	4.18	14.40	11.25	0.23	3.71	9.40	3.97	1.89	96.05
E11-21/5	0.05	47.02	3.99	13.96	11.78	0.19	5.08	9.91	3.78	1.27	96.98
E11-21/5	0.05	47.29	4.21	13.78	10.10	0.12	5.58	9.81	3.76	1.82	96.47
E11-21/5	0.05	47.30	4.65	13.69	10.31	0.15	4.58	8.88	4.11	2.13	95.80
E11-21/5	0.05	47.37	4.48	13.84	11.37	0.13	4.66	9.36	3.86	1.71	96.78
E11-21/5	0.05	47.54	4.22	14.01	10.45	0.12	5.67	9.87	3.59	1.74	97.21
E11-21/5	0.05	47.65	4.54	13.85	10.58	0.14	4.52	8.76	4.04	2.05	96.13
E11-21/5	0.05	47.66	4.36	14.27	11.69	0.15	4.22	8.79	3.91	1.91	96.96
E11-21/5	0.05	47.73	4.54	13.86	10.26	0.08	4.47	8.92	3.94	2.04	95.84
E11-21/5	0.05	48.34	3.60	13.30	11.43	0.18	5.41	9.79	3.72	0.95	96.72
E11-21/5	0.05	48.62	3.39	13.76	10.59	0.12	5.70	10.18	3.37	1.20	96.93
E11-21/5	0.05	48.77	3.74	13.24	11.15	0.16	5.33	10.19	3.47	1.05	97.10
E11-21/5	0.05	48.81	3.70	13.48	11.12	0.13	5.32	9.69	3.56	1.01	96.82
E11-21/5	0.05	49.20	3.70	13.69	10.53	0.13	5.23	9.52	3.27	1.30	96.57
E11-21/5	0.05	49.47	3.79	13.97	11.15	0.12	4.87	9.38	3.46	1.26	97.47
E11-21/5	0.05	49.63	3.75	13.93	10.59	0.17	4.91	9.44	3.31	1.43	97.16
E11-21/5	0.05	50.07	3.47	13.32	10.86	0.07	5.36	9.42	3.23	0.89	96.69
E11-21/5	0.05	50.15	3.24	13.37	10.40	0.21	5.35	8.99	3.56	0.99	96.26
E11-21/5	0.05	50.30	3.05	12.52	10.96	0.13	5.15	9.39	3.49	0.96	95.95
E11-21/5	0.05	50.35	3.10	13.49	10.72	0.12	5.38	9.28	3.40	0.86	96.70
E11-21/5	0.05	50.38	3.05	13.34	10.90	0.11	5.33	9.23	3.40	0.95	96.69
E11-21/5	0.05	50.69	3.26	13.38	10.36	0.09	5.42	9.63	3.52	0.84	97.19
E11-21/5	0.05	50.74	3.39	13.52	10.53	0.13	5.39	9.08	3.60	0.93	97.31

Core section	depth (mbsf)	SiO$_2$	TiO$_2$	Al$_2$O$_3$	FeO$_T$	MnO	MgO	CaO	Na$_2$O	K$_2$O	Total
E11-21/150	1.50	47.66	3.72	13.58	11.49	0.12	5.42	10.24	3.85	1.11	97.19
E11-21/150	1.50	47.78	3.67	13.90	11.62	0.13	5.33	10.24	3.79	1.07	97.53
E11-21/150	1.50	47.78	3.67	13.61	11.58	0.16	5.13	10.22	3.72	1.14	97.01
E11-21/150	1.50	47.86	3.58	13.78	11.57	0.16	5.37	10.41	4.00	1.15	97.88
E11-21/150	1.50	48.18	4.16	14.05	10.45	0.14	4.90	9.55	3.87	1.89	97.19
E11-21/150	1.50	48.32	4.00	14.05	10.98	0.12	4.80	9.38	4.06	1.81	97.52
E11-21/150	1.50	48.51	3.96	14.16	10.76	0.13	4.84	9.42	3.87	1.70	97.35
E11-21/150	1.50	48.57	4.23	14.21	11.02	0.15	4.78	9.49	3.90	1.72	98.07
E11-21/150	1.50	48.87	3.58	13.26	11.39	0.14	5.14	9.44	3.64	0.97	96.43
E11-21/150	1.50	48.89	3.25	13.62	10.95	0.17	5.47	9.82	3.47	1.18	96.82
E11-21/150	1.50	49.24	3.41	13.53	10.43	0.14	5.28	9.37	3.48	1.34	96.22
E11-21/150	1.50	49.45	3.35	13.84	10.48	0.12	5.14	9.70	3.65	1.17	96.90
E11-21/150	1.50	49.45	3.45	13.64	10.68	0.13	5.13	9.26	3.38	1.30	96.42
E11-21/150	1.50	49.63	3.72	13.54	10.61	0.20	5.16	9.44	3.38	1.21	96.89
E11-21/150	1.50	49.67	3.39	13.64	10.56	0.16	5.06	9.46	3.49	1.30	96.73
E11-21/150	1.50	49.78	3.40	13.77	10.81	0.09	5.35	9.79	3.65	1.23	97.87
E11-21/150	1.50	49.80	3.38	13.66	11.29	0.13	5.14	9.64	3.59	1.35	97.98
E11-21/150	1.50	50.00	3.72	13.23	11.65	0.13	5.00	9.41	3.46	0.99	97.59
E11-21/150	1.50	50.23	3.63	13.81	11.05	0.18	5.03	9.37	3.62	1.22	98.14
E11-21/150	1.50	50.47	3.97	13.60	9.87	0.14	4.59	8.48	3.86	1.92	96.90
E11-21/150	1.50	50.73	2.67	17.14	8.48	0.11	4.13	9.89	3.54	1.07	97.76
E11-21/150	1.50	50.85	4.00	13.80	9.41	0.08	4.56	8.32	4.00	1.77	96.79
E11-21/150	1.50	50.90	3.87	14.62	9.95	0.14	4.57	8.41	3.71	1.99	98.16

Core section	depth (mbsf)	SiO$_2$	TiO$_2$	Al$_2$O$_3$	FeO$_T$	MnO	MgO	CaO	Na$_2$O	K$_2$O	Total
E11-22/193	9.13	47.63	3.38	13.52	10.79	0.15	5.97	9.65	3.31	1.30	95.70
E11-22/193	9.13	48.22	3.29	13.73	10.80	0.15	6.11	9.47	3.39	1.26	96.42
E11-22/193	9.13	48.96	3.57	14.00	10.20	0.16	5.28	8.72	3.38	1.02	95.29
E11-22/193	9.13	49.18	2.74	14.71	10.71	0.13	5.48	9.40	3.59	0.95	96.89
E11-22/193	9.13	49.19	3.72	13.77	11.63	0.17	4.55	9.03	3.57	1.31	96.94
E11-22/193	9.13	49.45	3.52	13.92	11.73	0.14	4.62	8.94	3.31	1.36	96.99
E11-22/193	9.13	49.64	2.66	14.48	10.24	0.18	5.71	9.40	3.63	1.04	96.98
E11-22/193	9.13	49.65	2.72	14.31	10.57	0.15	5.67	9.11	3.57	0.83	96.58
E11-22/193	9.13	49.68	3.26	13.80	11.84	0.14	4.60	8.61	3.73	1.38	97.04
E11-22/193	9.13	49.69	3.71	14.57	9.77	0.12	4.24	8.14	3.71	1.75	95.70
E11-22/193	9.13	49.74	2.57	14.39	10.85	0.16	5.56	9.12	3.29	0.83	96.51
E11-22/193	9.13	49.75	2.79	14.22	10.64	0.14	5.54	8.97	3.54	0.94	96.53
E11-22/193	9.13	49.93	2.58	14.22	10.31	0.09	5.37	9.16	3.52	1.02	96.20
E11-22/193	9.13	49.99	3.82	14.26	9.76	0.16	4.24	7.90	3.58	1.76	95.47
E11-22/193	9.13	50.07	3.65	14.42	9.96	0.12	4.21	7.84	3.62	1.86	95.75
E11-22/193	9.13	50.14	2.88	14.55	10.59	0.10	5.51	9.05	3.37	1.01	97.20
E11-22/193	9.13	50.22	2.92	14.49	10.26	0.16	5.27	9.33	3.43	1.00	97.08
E11-22/193	9.13	50.27	2.77	14.68	10.16	0.17	5.54	9.56	3.53	1.09	97.77
E11-22/193	9.13	50.85	2.87	13.41	10.65	0.12	5.04	8.70	3.45	1.15	96.24
E11-22/193	9.13	51.17	2.78	13.41	10.59	0.19	5.13	8.79	3.47	1.17	96.70
E11-22/193	9.13	51.17	2.65	12.78	10.69	0.13	5.11	8.69	3.46	1.06	95.74
E11-22/193	9.13	51.59	2.83	13.09	10.74	0.12	4.95	8.71	3.51	1.11	96.65
E11-22/193	9.13	52.12	2.72	13.91	10.28	0.16	5.06	8.79	3.52	1.15	97.71
E11-22/193	9.13	52.12	3.42	14.79	9.19	0.12	3.76	7.03	3.51	1.88	95.82
E11-22/193	9.13	52.36	2.47	13.46	10.01	0.12	4.95	8.76	3.49	1.14	96.76
E11-22/193	9.13	52.78	2.38	15.10	9.05	0.10	4.17	7.56	3.49	1.60	96.23
E11-22/193	9.13	52.78	2.45	15.18	8.90	0.08	4.20	7.70	3.75	1.51	96.55

Core section	depth (mbsf)	SiO_2	TiO_2	Al_2O_3	FeO_T	MnO	MgO	CaO	Na_2O	K_2O	Total
Mt. Hudson	n/a	62.32	1.19	16.11	4.98	0.25	1.49	3.22	5.19	2.67	97.42
Mt.Hudson	n/a	59.74	1.52	15.73	6.53	0.22	2.17	4.38	4.81	2.47	97.57
Mt. Hudson	n/a	59.40	1.31	15.36	5.50	0.17	1.63	3.72	4.75	2.40	94.24
Mt.Hudson	n/a	56.91	1.68	15.65	7.64	0.24	2.95	5.62	4.57	1.85	97.11
Mt. Hudson	n/a	64.11	1.11	16.22	4.97	0.24	1.57	3.24	5.64	2.65	99.75
Mt.Hudson	n/a	58.29	1.74	15.45	6.95	0.20	2.44	4.98	4.90	1.88	96.83
Mt. Hudson	n/a	61.65	1.46	16.02	5.52	0.19	1.81	4.00	5.01	2.52	98.18
Mt.Hudson	n/a	57.66	1.59	15.67	7.12	0.23	2.46	5.21	4.81	2.07	96.82
Mt. Hudson	n/a	57.80	1.79	15.61	7.20	0.26	2.60	5.11	4.88	1.95	97.20
Mt.Hudson	n/a	59.60	1.53	15.90	6.07	0.24	2.18	4.34	5.17	2.11	97.14
Mt. Hudson	n/a	56.38	1.79	15.61	7.18	0.16	2.72	5.34	4.68	2.02	95.88
Mt.Hudson	n/a	60.15	1.47	15.95	6.11	0.20	2.03	4.10	5.33	2.42	97.76
Mt. Hudson	n/a	60.93	1.31	16.02	5.29	0.22	1.76	3.70	5.10	2.42	96.75
Mt.Hudson	n/a	60.47	1.56	16.09	5.93	0.20	2.13	4.23	5.03	2.27	97.91
Mt. Hudson	n/a	60.11	1.33	15.78	5.48	0.17	1.71	3.83	4.85	2.42	95.68
Mt.Hudson	n/a	58.09	1.57	15.79	6.55	0.25	2.38	5.00	4.74	2.11	96.48
Mt. Hudson	n/a	59.91	1.43	15.77	5.93	0.20	2.06	3.81	4.85	2.32	96.28
Mt.Hudson	n/a	61.89	1.25	16.07	5.22	0.19	1.63	3.25	5.36	2.45	97.31
Mt. Hudson	n/a	59.46	1.43	15.87	6.12	0.19	2.08	4.15	4.96	2.32	96.58
Mt.Hudson	n/a	56.94	1.66	15.55	7.23	0.22	2.62	5.03	4.80	2.07	96.12

Core section	depth (mbsf)	SiO_2	TiO_2	Al_2O_3	FeO_T	MnO	MgO	CaO	Na_2O	K_2O	Total
E5-24	3.23	60.73	0.66	14.38	7.22	0.27	0.25	1.13	5.82	4.69	95.15
E5-24	3.23	61.26	0.74	14.45	7.49	0.28	0.28	1.29	6.37	4.97	97.13
E5-24	3.23	61.70	0.66	14.58	7.85	0.31	0.29	1.25	6.68	4.98	98.30
E5-24	3.23	61.90	0.72	14.50	7.19	0.27	0.31	1.23	6.27	5.03	97.42
E5-24	3.23	61.94	0.68	14.26	7.93	0.21	0.30	1.28	6.17	4.92	97.69
E5-24	3.23	61.98	0.69	14.39	7.68	0.34	0.25	1.32	5.79	4.94	97.38
E5-24	3.23	62.01	0.67	14.74	7.38	0.27	0.24	1.29	5.91	5.07	97.58
E5-24	3.23	62.06	0.64	14.49	7.49	0.31	0.25	1.28	6.57	4.99	98.08
E5-24	3.23	62.08	0.66	14.39	7.68	0.29	0.26	1.30	6.25	5.01	97.92
E5-24	3.23	62.12	0.69	14.62	7.25	0.21	0.26	1.19	6.50	4.72	97.56
E5-24	3.23	62.27	0.72	14.78	7.49	0.34	0.27	1.18	5.97	5.04	98.06
E5-24	3.23	62.29	0.72	14.62	7.25	0.27	0.31	1.19	5.81	4.93	97.39
E5-24	3.23	62.35	0.60	14.60	7.17	0.25	0.22	1.23	5.89	5.05	97.36
E5-24	3.23	62.36	0.69	14.70	7.49	0.26	0.25	1.37	6.09	5.06	98.27
E5-24	3.23	62.38	0.66	14.78	7.36	0.26	0.24	1.34	6.07	4.80	97.89
E5-24	3.23	62.49	0.65	14.52	7.64	0.30	0.28	1.46	5.81	5.03	98.18
E5-24	3.23	62.52	0.72	14.55	7.53	0.31	0.26	1.20	6.47	5.14	98.70
E5-24	3.23	62.56	0.68	14.44	7.77	0.29	0.29	1.36	6.63	5.00	99.02
E5-24	3.23	62.59	0.73	14.16	7.58	0.33	0.30	1.23	6.43	4.95	98.30
E5-24	3.23	62.59	0.65	14.36	7.35	0.36	0.27	1.30	6.52	4.91	98.31
E5-24	3.23	62.60	0.70	14.65	7.31	0.23	0.25	1.34	6.26	4.95	98.29
E5-24	3.23	62.78	0.59	14.37	7.31	0.26	0.25	1.20	6.54	4.85	98.15
E5-24	3.23	62.94	0.63	14.90	7.58	0.24	0.29	1.25	6.77	5.06	99.66
E5-24	3.23	63.19	0.76	14.39	7.31	0.31	0.29	1.28	5.71	4.88	98.12

Core section	depth (mbsf)	SiO_2	TiO_2	Al_2O_3	FeO_T	MnO	MgO	CaO	Na_2O	K_2O	Total
SED-4	5.18	60.37	0.50	14.61	8.25	0.39	0.12	0.92	7.19	4.79	97.14
SED-4	5.18	60.27	0.54	14.63	7.62	0.37	0.12	1.06	6.85	4.99	96.45
SED-4	5.18	60.18	0.47	14.66	8.50	0.31	0.10	0.94	7.48	4.53	97.17
SED-4	5.18	60.95	0.49	14.78	7.87	0.36	0.18	1.06	7.15	4.79	97.63

Core section	depth (mbsf)	SiO$_2$	TiO$_2$	Al$_2$O$_3$	FeO$_T$	MnO	MgO	CaO	Na$_2$O	K$_2$O	Total
SED-4	5.18	60.73	0.52	14.86	8.28	0.39	0.09	1.07	7.37	4.67	97.98
SED-4	5.18	61.15	0.52	14.93	7.95	0.33	0.11	1.10	7.09	4.91	98.09
SED-4	5.18	60.24	0.50	15.00	7.50	0.37	0.22	1.24	6.39	4.97	96.43
SED-4	5.18	60.60	0.55	15.00	7.12	0.26	0.23	1.21	6.35	5.23	96.55
SED-4	5.18	60.97	0.55	15.01	7.63	0.30	0.15	1.35	6.42	4.88	97.26
SED-4	5.18	61.01	0.55	15.01	7.99	0.37	0.12	1.12	7.00	4.83	98.00
SED-4	5.18	60.53	0.51	15.05	8.03	0.36	0.16	1.05	7.37	4.95	98.01
SED-4	5.18	60.59	0.51	15.08	7.89	0.28	0.14	1.14	7.21	5.04	97.88
SED-4	5.18	61.17	0.50	15.08	8.07	0.31	0.18	1.00	7.31	4.65	98.27
SED-4	5.18	60.97	0.60	15.10	7.70	0.28	0.23	1.38	6.80	4.91	97.97
SED-4	5.18	60.33	0.57	15.14	7.47	0.33	0.22	1.27	6.25	4.83	96.41
SED-4	5.18	60.54	0.51	15.16	7.36	0.34	0.21	1.20	6.35	4.84	96.51
SED-4	5.18	60.00	0.53	15.22	7.75	0.26	0.20	1.18	6.41	5.00	96.55
SED-4	5.18	61.23	0.45	15.25	7.92	0.34	0.09	1.05	7.32	4.62	98.27
SED-4	5.18	60.44	0.56	15.32	7.12	0.32	0.17	1.19	6.59	4.92	96.63
SED-4	5.18	60.77	0.57	15.33	7.20	0.33	0.25	1.13	6.17	4.88	96.63
SED-4	5.18	60.85	0.53	15.34	7.21	0.27	0.12	1.11	6.56	4.91	96.90
SED-4	5.18	61.30	0.59	15.34	7.28	0.33	0.12	1.18	6.69	4.78	97.61
SED-4	5.18	61.15	0.48	15.40	7.32	0.26	0.12	1.10	7.17	4.84	97.84
SED-4	5.18	60.75	0.52	15.41	7.31	0.41	0.24	1.21	6.28	4.96	97.09
SED-4	5.18	60.63	0.52	15.50	7.47	0.33	0.23	1.21	6.63	4.81	97.33
SED-4	5.18	60.86	0.57	15.53	7.54	0.29	0.19	1.22	6.55	4.84	97.59
SED-4	5.18	61.28	0.50	15.53	7.08	0.33	0.12	1.19	6.68	4.96	97.67
SED-4	5.18	60.80	0.55	15.71	7.41	0.34	0.09	1.15	7.37	4.93	98.35

Core section	depth (mbsf)	SiO$_2$	TiO$_2$	Al$_2$O$_3$	FeO$_T$	MnO	MgO	CaO	Na$_2$O	K$_2$O	Total
SED6U	4.73	59.91	0.65	14.36	7.26	0.28	0.32	1.28	6.74	4.67	95.47
SED6U	4.73	60.47	0.66	14.59	7.26	0.28	0.30	1.21	6.31	5.02	96.10
SED6U	4.73	61.06	0.66	14.45	7.34	0.23	0.27	1.17	6.74	5.01	96.93
SED6U	4.73	61.29	0.60	14.78	7.26	0.31	0.27	1.20	6.57	4.96	97.24
SED6U	4.73	61.42	0.60	14.38	7.46	0.38	0.29	1.17	6.78	4.88	97.36
SED6U	4.73	61.48	0.66	14.48	7.52	0.29	0.29	1.30	7.12	5.11	98.25
SED6U	4.73	61.64	0.70	14.62	7.36	0.33	0.29	1.22	7.02	5.17	98.35
SED6U	4.73	61.78	0.71	14.61	7.29	0.20	0.32	1.20	7.06	4.99	98.16
SED6U	4.73	61.83	0.61	14.56	7.77	0.26	0.25	1.29	6.95	5.05	98.57
SED6U	4.73	61.91	0.73	15.00	7.71	0.32	0.26	1.39	6.04	4.92	98.28
SED6U	4.73	62.14	0.69	14.86	7.60	0.23	0.31	1.13	6.87	5.10	98.93
SED6U	4.73	62.16	0.63	14.79	7.79	0.33	0.32	1.25	7.01	5.02	99.30
SED6U	4.73	62.39	0.67	14.53	7.69	0.29	0.27	1.23	6.40	5.13	98.60
SED6U	4.73	62.77	0.62	14.83	7.33	0.28	0.27	1.27	7.07	4.83	99.27
SED6U	4.73	62.87	0.62	14.75	7.51	0.23	0.32	1.31	6.62	4.67	98.90
SED6L	4.79	60.96	0.65	14.82	7.37	0.25	0.31	1.16	6.96	4.91	97.39
SED6L	4.79	60.97	0.72	14.57	7.55	0.27	0.30	1.29	6.73	4.95	97.35
SED6L	4.79	61.12	0.66	14.63	7.05	0.28	0.31	1.20	6.41	4.86	96.52
SED6L	4.79	61.30	0.63	14.79	6.76	0.22	0.33	1.18	6.46	4.62	96.29
SED6L	4.79	61.69	0.66	14.30	7.21	0.23	0.28	1.14	6.65	5.04	97.20
SED6L	4.79	61.74	0.71	14.57	7.39	0.26	0.27	1.23	6.97	4.74	97.88
SED6L	4.79	62.02	0.71	14.51	7.50	0.30	0.29	1.18	6.60	5.02	98.13
SED6L	4.79	62.10	0.68	14.84	7.49	0.27	0.29	1.28	6.77	5.13	98.85
SED6L	4.79	62.97	0.64	14.01	7.40	0.27	0.30	1.14	6.64	5.12	98.49
SED6L	4.79	63.87	0.67	15.03	6.57	0.22	0.29	1.01	6.51	4.99	99.16

Core section	depth (mbsf)	SiO$_2$	TiO$_2$	Al$_2$O$_3$	FeO$_T$	MnO	MgO	CaO	Na$_2$O	K$_2$O	Total
SED7	5.42	60.68	0.61	14.45	7.35	0.26	0.28	1.15	5.94	4.93	95.65
SED7	5.42	61.00	0.61	14.48	7.52	0.39	0.28	1.29	6.81	4.98	97.36
SED7	5.42	61.33	0.67	14.55	7.46	0.24	0.28	1.16	5.69	4.92	96.30
SED7	5.42	61.81	0.67	14.76	7.21	0.30	0.30	1.16	6.60	4.93	97.74
SED7	5.42	62.09	0.71	14.72	7.48	0.31	0.26	1.33	6.92	4.76	98.58
SED7	5.42	62.16	0.66	14.80	7.33	0.24	0.33	1.16	6.46	5.08	98.22
SED7	5.42	62.38	0.70	14.79	7.10	0.33	0.25	1.20	5.53	5.11	97.39
SED7	5.42	62.41	0.67	14.54	7.21	0.27	0.27	1.21	7.06	4.97	98.61
SED7	5.42	62.47	0.71	14.63	7.41	0.24	0.32	1.19	7.28	4.95	99.20
SED7	5.42	62.70	0.63	14.47	7.17	0.25	0.28	1.26	6.91	5.02	98.69
SED7	5.42	62.76	0.69	14.45	7.45	0.27	0.26	1.32	6.56	5.01	98.77
SED7	5.42	62.99	0.64	15.02	6.91	0.26	0.25	1.16	6.16	5.01	98.40

Core section	depth (mbsf)	SiO$_2$	TiO$_2$	Al$_2$O$_3$	FeO$_T$	MnO	MgO	CaO	Na$_2$O	K$_2$O	Total
PC103	8.82	60.42	0.70	14.88	7.29	0.25	0.27	1.24	5.57	4.95	95.57
PC103	8.82	60.47	0.67	14.95	7.09	0.26	0.26	1.20	5.89	4.97	95.76
PC103	8.82	60.82	0.69	14.81	7.35	0.25	0.27	1.14	6.54	4.93	96.80
PC103	8.82	61.02	0.63	14.72	7.42	0.28	0.32	1.28	5.87	4.80	96.34
PC103	8.82	61.04	0.68	14.83	7.23	0.29	0.30	1.24	6.59	4.83	97.03
PC103	8.82	61.23	0.62	14.68	7.43	0.27	0.27	1.23	6.69	5.13	97.55
PC103	8.82	61.43	0.87	14.72	7.59	0.26	0.40	1.42	6.62	4.98	98.29
PC103	8.82	61.44	0.71	14.84	7.52	0.31	0.28	1.25	6.54	5.29	98.18
PC103	8.82	61.45	0.67	14.70	7.53	0.31	0.29	1.27	6.06	4.97	97.25
PC103	8.82	61.56	0.68	14.58	7.21	0.30	0.25	1.27	6.15	4.96	96.96
PC103	8.82	61.58	0.63	14.82	7.27	0.26	0.25	1.12	6.35	4.87	97.15
PC103	8.82	61.79	0.71	14.68	7.59	0.29	0.32	1.21	6.05	4.92	97.56
PC103	8.82	61.81	0.69	14.60	7.49	0.24	0.22	1.23	5.86	5.20	97.34
PC103	8.82	61.81	0.73	14.65	7.01	0.24	0.19	1.25	6.31	5.14	97.33
PC103	8.82	62.09	0.65	14.78	7.11	0.27	0.25	1.22	5.96	4.83	97.16
PC103	8.82	62.33	0.64	15.11	7.32	0.21	0.26	1.19	6.10	5.03	98.19

Core section	depth (mbsf)	SiO$_2$	TiO$_2$	Al$_2$O$_3$	FeO$_T$	MnO	MgO	CaO	Na$_2$O	K$_2$O	Total
GC105	3.74	59.85	0.67	15.44	7.46	0.28	0.27	1.20	6.26	4.90	96.33
GC105	3.74	60.86	0.65	14.53	7.14	0.28	0.32	1.13	6.29	4.94	96.14
GC105	3.74	61.04	0.70	14.88	7.56	0.21	0.30	1.17	5.74	5.03	96.63
GC105	3.74	61.06	0.66	14.69	7.06	0.23	0.29	1.31	5.66	4.87	95.83
GC105	3.74	61.17	0.61	14.55	7.51	0.28	0.25	1.26	6.21	4.63	96.47
GC105	3.74	61.27	0.62	14.54	7.46	0.24	0.27	1.25	6.38	4.72	96.75
GC105	3.74	61.36	0.63	14.59	7.59	0.23	0.25	1.23	5.88	4.73	96.49
GC105	3.74	61.48	0.73	14.60	7.66	0.32	0.32	1.32	6.09	4.82	97.34
GC105	3.74	61.61	0.70	14.72	7.46	0.28	0.31	1.21	5.93	4.82	97.04
GC105	3.74	61.66	0.64	14.52	6.97	0.31	0.30	1.21	6.45	4.81	96.87
GC105	3.74	61.71	0.62	14.69	7.52	0.24	0.25	1.20	6.46	5.08	97.77
GC105	3.74	61.83	0.52	15.52	6.23	0.18	0.30	0.99	6.93	4.99	97.49
GC105	3.74	61.87	0.63	14.65	7.53	0.32	0.31	1.24	6.22	4.82	97.59
GC105	3.74	61.89	0.62	14.29	7.36	0.30	0.25	1.17	4.56	5.00	95.44
GC105	3.74	61.94	0.65	14.48	7.22	0.26	0.25	1.32	6.41	4.92	97.45

Core section	depth (mbsf)	SiO$_2$	TiO$_2$	Al$_2$O$_3$	FeO$_T$	MnO	MgO	CaO	Na$_2$O	K$_2$O	Total
PC106	6.16	58.99	0.75	17.81	7.13	0.23	0.24	1.08	6.28	4.88	97.39
PC106	6.16	60.06	0.65	14.65	7.31	0.25	0.27	1.19	6.20	4.70	95.28

Core section	depth (mbsf)	SiO₂	TiO₂	Al₂O₃	FeOₜ	MnO	MgO	CaO	Na₂O	K₂O	Total

Core section	depth	SiO2	TiO2	Al2O3	FeOT	MnO	MgO	CaO	Na2O	K2O	Total
PC106	6.16	60.38	0.65	14.49	7.47	0.28	0.22	1.08	6.52	4.87	95.96
PC106	6.16	60.49	0.69	14.52	7.20	0.20	0.30	1.15	6.28	4.56	95.39
PC106	6.16	60.61	0.58	14.35	7.20	0.27	0.33	1.29	6.56	4.72	95.91
PC106	6.16	60.78	0.64	14.32	7.01	0.27	0.29	1.27	6.19	4.96	95.73
PC106	6.16	60.81	0.62	14.35	7.33	0.30	0.21	1.16	6.35	5.06	96.19
PC106	6.16	60.81	0.67	14.41	7.04	0.25	0.26	1.09	6.23	4.91	95.67
PC106	6.16	60.85	0.60	14.35	7.31	0.27	0.29	1.27	6.34	4.81	96.09
PC106	6.16	61.15	0.66	14.54	7.29	0.24	0.30	1.22	6.32	4.90	96.62
PC106	6.16	61.27	0.66	14.47	7.67	0.19	0.30	1.26	6.13	4.85	96.80
PC106	6.16	61.38	0.67	14.40	7.27	0.29	0.24	1.14	5.59	4.89	95.87

Core section	depth (mbsf)	SiO₂	TiO₂	Al₂O₃	FeOₜ	MnO	MgO	CaO	Na₂O	K₂O	Total
PC108	4.65	59.48	0.60	16.84	6.95	0.26	0.26	1.20	6.06	4.88	96.53
PC108	4.65	59.85	0.66	15.53	7.16	0.27	0.26	1.10	5.86	4.89	95.58
PC108	4.65	60.29	0.60	14.32	7.38	0.30	0.25	1.25	5.85	4.86	95.10
PC108	4.65	60.62	0.65	14.63	7.13	0.25	0.27	1.22	6.35	5.35	96.47
PC108	4.65	60.72	0.63	14.41	7.45	0.20	0.26	1.30	6.26	5.20	96.43
PC108	4.65	61.00	0.62	15.19	7.09	0.28	0.27	1.23	6.16	4.85	96.69
PC108	4.65	61.13	0.60	14.44	7.35	0.20	0.26	1.24	6.29	5.03	96.54
PC108	4.65	61.16	0.73	14.61	7.48	0.26	0.26	1.24	5.76	5.04	96.54
PC108	4.65	61.22	0.68	14.50	7.19	0.33	0.28	1.30	5.92	5.07	96.49
PC108	4.65	61.26	0.73	14.54	7.61	0.22	0.25	1.25	6.52	5.29	97.67
PC108	4.65	61.30	0.55	14.71	7.24	0.28	0.28	1.23	6.37	5.22	97.18
PC108	4.65	61.56	0.68	14.61	7.58	0.26	0.25	1.28	6.41	5.18	97.81
PC108	4.65	61.89	0.70	14.76	7.29	0.28	0.29	1.33	6.42	4.87	97.83
PC108	4.65	62.15	0.62	14.56	7.59	0.18	0.25	1.23	6.10	5.04	97.72
PC108	4.65	62.16	0.67	14.54	7.14	0.28	0.28	1.22	6.66	5.19	98.14
PC108	4.65	62.19	0.68	14.58	7.70	0.28	0.28	1.31	5.91	5.13	98.06
PC108	4.65	62.28	0.61	14.73	7.43	0.35	0.27	1.34	6.16	5.04	98.21
PC108	4.65	62.32	0.64	14.74	7.50	0.22	0.23	1.31	6.18	5.11	98.25
PC108	4.65	62.38	0.65	14.64	7.48	0.27	0.30	1.31	6.25	5.04	98.32
PC108	4.65	62.41	0.72	14.81	7.26	0.28	0.29	1.34	5.59	5.01	97.71
PC108	4.65	62.47	0.67	14.77	7.01	0.20	0.25	1.05	5.99	5.01	97.42
PC108	4.65	62.54	0.65	14.52	7.46	0.25	0.26	1.13	5.74	5.19	97.74
PC108	4.65	62.78	0.58	15.79	5.31	0.15	0.18	1.01	6.90	5.54	98.24

Core section	depth (mbsf)	SiO₂	TiO₂	Al₂O₃	FeOₜ	MnO	MgO	CaO	Na₂O	K₂O	Total
PC110	3.25	59.50	0.69	14.60	7.29	0.33	0.25	1.20	6.49	4.77	95.12
PC110	3.25	60.47	0.64	15.01	7.57	0.29	0.27	1.25	5.95	4.83	96.28
PC110	3.25	60.57	0.62	14.51	7.56	0.27	0.32	1.22	6.85	4.75	96.67
PC110	3.25	60.92	0.69	15.74	7.23	0.25	0.26	1.26	6.07	4.74	97.16
PC110	3.25	61.03	0.56	14.53	7.06	0.28	0.29	1.12	5.97	4.76	95.60
PC110	3.25	61.05	0.64	14.88	7.42	0.27	0.25	1.22	6.36	4.98	97.07
PC110	3.25	61.08	0.66	14.56	7.55	0.25	0.24	1.30	6.18	4.89	96.71
PC110	3.25	61.11	0.69	15.32	7.75	0.24	0.27	1.23	6.09	4.84	97.54
PC110	3.25	61.39	0.78	14.62	7.28	0.24	0.30	1.20	6.02	5.27	97.10
PC110	3.25	61.50	0.65	15.25	7.13	0.27	0.23	1.32	6.28	4.84	97.47
PC110	3.25	61.54	0.60	14.45	7.12	0.21	0.25	1.27	6.14	4.79	96.37
PC110	3.25	61.94	0.69	14.59	7.47	0.27	0.28	1.21	6.18	5.03	97.66
PC110	3.25	62.53	0.77	14.93	7.48	0.33	0.31	1.25	6.15	5.07	98.82

Core section	depth (mbsf)	SiO$_2$	TiO$_2$	Al$_2$O$_3$	FeO$_T$	MnO	MgO	CaO	Na$_2$O	K$_2$O	Total
PC111	6.86	60.06	0.67	14.92	7.10	0.27	0.23	1.31	6.13	4.75	95.44
PC111	6.86	60.70	0.65	14.33	7.48	0.28	0.29	1.27	6.60	4.88	96.48
PC111	6.86	60.85	0.62	15.54	7.53	0.25	0.30	1.31	5.96	5.13	97.49
PC111	6.86	60.93	0.59	14.74	7.45	0.21	0.27	1.09	5.60	4.90	95.78
PC111	6.86	61.02	0.62	14.65	7.44	0.24	0.25	1.31	6.71	5.00	97.24
PC111	6.86	61.16	0.67	14.58	7.22	0.19	0.28	1.25	5.72	4.82	95.89
PC111	6.86	61.21	0.61	14.57	7.51	0.21	0.29	1.21	6.75	4.99	97.35
PC111	6.86	61.38	0.69	14.69	7.41	0.27	0.28	1.43	5.72	4.73	96.60
PC111	6.86	61.48	0.69	14.37	7.24	0.16	0.27	1.12	6.39	4.95	96.67
PC111	6.86	61.48	0.61	15.13	7.65	0.21	0.26	1.28	6.21	4.99	97.82
PC111	6.86	61.49	0.69	14.86	7.09	0.28	0.25	1.20	5.86	5.21	96.93
PC111	6.86	61.50	0.62	14.83	7.59	0.28	0.27	1.34	6.02	4.92	97.37
PC111	6.86	61.51	0.61	14.77	7.52	0.28	0.34	1.24	5.86	4.89	97.02
PC111	6.86	61.67	0.61	14.72	7.23	0.32	0.33	1.17	6.30	4.87	97.22
PC111	6.86	61.70	0.71	14.58	7.24	0.31	0.27	1.26	6.00	4.95	97.02
PC111	6.86	61.75	0.69	14.85	6.91	0.22	0.22	1.09	6.45	4.62	96.80
PC111	6.86	61.90	0.69	14.74	7.33	0.30	0.23	1.30	5.68	4.87	97.04
PC111	6.86	61.91	0.61	14.53	7.21	0.29	0.27	1.17	5.81	4.91	96.71
PC111	6.86	61.97	0.69	14.69	7.71	0.27	0.31	1.25	6.10	4.85	97.84
PC111	6.86	62.03	0.67	14.81	7.40	0.29	0.28	1.30	6.21	5.05	98.04
PC111	6.86	62.03	0.62	14.95	7.15	0.27	0.25	1.16	6.32	5.08	97.83
PC111	6.86	62.13	0.60	14.71	7.53	0.23	0.29	1.11	5.94	5.07	97.61
PC111	6.86	62.20	0.66	14.76	7.48	0.38	0.29	1.26	6.17	4.77	97.97
PC111	6.86	62.27	0.69	14.71	7.57	0.24	0.29	1.23	6.29	5.12	98.41
PC111	6.86	62.46	0.73	14.79	7.58	0.31	0.29	1.30	5.95	5.07	98.48

Core section	depth (mbsf)	SiO$_2$	TiO$_2$	Al$_2$O$_3$	FeO$_T$	MnO	MgO	CaO	Na$_2$O	K$_2$O	Total
PC113	5.55	58.49	0.65	17.52	7.05	0.25	0.22	1.23	5.75	4.95	96.11
PC113	5.55	59.12	0.61	16.12	6.99	0.23	0.28	1.11	6.20	4.66	95.32
PC113	5.55	59.99	0.74	15.13	7.29	0.26	0.27	1.20	5.84	5.04	95.76
PC113	5.55	60.23	0.63	14.50	7.44	0.28	0.28	1.09	6.14	4.94	95.53
PC113	5.55	60.68	0.73	14.53	7.28	0.25	0.26	1.06	5.63	4.65	95.07
PC113	5.55	61.07	0.62	14.99	7.45	0.23	0.30	1.24	6.35	4.76	97.01
PC113	5.55	61.21	0.64	15.15	7.38	0.34	0.30	1.35	5.87	5.17	97.41
PC113	5.55	61.38	0.67	14.65	7.37	0.24	0.25	1.20	6.53	5.32	97.61
PC113	5.55	61.53	0.59	14.86	7.37	0.26	0.30	1.18	5.80	5.12	97.01
PC113	5.55	61.70	0.75	14.54	7.39	0.26	0.32	1.32	6.17	5.00	97.45

Core section	depth (mbsf)	SiO$_2$	TiO$_2$	Al$_2$O$_3$	FeO$_T$	MnO	MgO	CaO	Na$_2$O	K$_2$O	Total
GC027/1/16	0.16	49.59	2.48	15.56	10.30	0.28	4.29	8.12	4.68	0.55	95.86
GC027/1/16	0.16	49.95	2.31	15.27	10.10	0.18	4.29	8.65	4.19	0.54	95.50
GC027/1/16	0.16	50.27	2.15	15.89	9.63	0.23	4.75	8.96	4.33	0.44	96.65
GC027/1/16	0.16	50.53	2.14	15.62	9.28	0.25	4.76	9.10	4.17	0.42	96.27
GC027/1/16	0.16	50.88	2.41	15.700	9.97	0.18	3.84	7.99	4.60	0.55	96.12
GC027/1/16	0.16	51.82	2.49	15.84	9.52	0.25	3.96	8.05	4.81	0.48	97.22
GC027/1/16	0.16	60.55	0.68	14.58	7.21	0.29	0.32	1.18	6.24	4.95	96.00
GC027/1/16	0.16	61.01	0.75	14.52	7.09	0.27	0.30	1.30	6.30	4.85	96.39
GC027/1/16	0.16	61.26	1.32	15.37	6.24	0.22	1.84	3.82	5.00	1.48	96.55
GC027/1/16	0.16	67.53	0.70	15.13	3.91	0.20	0.69	1.57	4.93	1.86	96.52
GC027/1/16	0.16	69.81	0.38	13.62	3.23	0.17	0.21	0.59	5.30	2.49	95.8
GC027/1/16	0.16	69.88	0.30	14.00	3.14	0.12	0.19	0.76	5.01	2.22	95.62
GC027/1/16	0.16	70.30	0.39	13.88	3.48	0.18	0.22	0.64	5.53	2.55	97.17

GC027/2/4	0.31	49.86	2.03	15.58	9.77	0.15	5.23	8.85	4.45	0.41	96.33
GC027/2/4	0.31	50.04	1.87	15.60	9.29	0.19	5.96	9.97	3.79	0.38	97.09
GC027/2/4	0.31	50.26	1.96	15.83	9.29	0.17	5.37	9.30	4.54	0.42	97.14
GC027/2/4	0.31	50.38	1.94	15.90	8.78	0.17	5.65	10.07	4.03	0.46	97.38
GC027/2/4	0.31	50.65	2.42	15.76	10.51	0.20	4.06	8.16	4.51	0.53	96.80
GC027/2/4	0.31	50.84	2.21	16.30	10.21	0.21	4.16	8.01	4.69	0.55	97.18
GC027/2/4	0.31	50.90	2.14	16.41	10.18	0.18	4.35	7.79	4.56	0.66	97.17
GC027/2/4	0.31	51.03	2.45	16.01	10.24	0.18	4.26	8.07	4.44	0.49	97.17
GC027/2/4	0.31	51.12	1.97	15.67	8.96	0.19	5.14	8.99	4.37	0.53	96.94
GC027/2/4	0.31	51.24	2.48	15.49	10.62	0.22	4.18	8.25	4.53	0.53	97.54
GC027/2/4	0.31	51.27	2.46	15.17	11.22	0.19	4.51	7.93	4.68	0.54	97.97
GC027/2/4	0.31	51.31	2.07	15.89	10.05	0.23	4.28	8.31	4.21	0.41	96.76
GC027/2/4	0.31	51.35	2.52	15.62	10.59	0.17	4.24	8.08	4.50	0.57	97.64
GC027/2/4	0.31	51.43	2.21	14.54	10.24	0.19	4.50	7.86	4.50	0.68	96.15
GC027/2/4	0.31	51.57	2.27	14.61	10.49	0.16	4.51	7.90	4.61	0.62	96.74
GC027/2/4	0.31	51.74	2.42	15.31	10.54	0.24	4.28	8.30	4.64	0.61	98.08
GC027/2/4	0.31	51.83	2.25	15.76	10.16	0.20	4.26	8.31	3.89	0.49	97.15
GC027/2/4	0.31	52.70	2.01	15.38	9.31	0.18	3.43	6.42	5.00	0.71	95.14
GC027/2/4	0.31	54.53	1.84	15.78	8.92	0.21	3.14	6.52	4.72	0.75	96.41
GC027/2/4	0.31	56.24	2.05	15.83	8.60	0.13	3.14	6.20	4.89	0.82	97.90
GC027/2/4	0.31	68.16	0.68	15.24	3.67	0.18	0.60	1.42	5.74	1.93	97.62
GC027/2/4	0.31	68.62	0.74	14.17	5.42	0.15	0.46	1.65	4.73	2.16	98.10
GC027/2/4	0.31	69.01	0.57	15.08	3.55	0.17	0.55	1.25	5.88	1.92	97.98
GC027/2/4	0.31	69.64	0.58	14.01	3.71	0.15	0.70	1.37	4.94	2.36	97.46
GC027/2/4	0.31	70.16	0.36	14.42	3.10	0.11	0.21	0.72	5.46	2.54	97.08
GC027/2/4	0.31	70.45	0.36	14.80	3.27	0.13	0.18	0.62	5.21	2.52	97.54
GC027/2/4	0.31	70.83	0.40	14.03	3.22	0.13	0.17	0.74	5.24	2.41	97.17
GC027/2/4	0.31	71.29	0.41	14.12	3.26	0.13	0.16	0.69	4.93	2.36	97.35
GC027/2/4	0.31	71.35	0.43	13.88	3.14	0.12	0.14	0.79	5.38	2.4	97.63
GC027/2/4	0.31	71.39	0.40	13.84	3.17	0.14	0.15	0.70	5.19	2.58	97.56
GC027/2/4	0.31	71.80	0.35	13.76	3.07	0.11	0.14	0.60	5.32	2.37	97.52
GC027/2/4	0.31	72.32	0.36	13.92	3.42	0.11	0.17	0.61	5.57	2.33	98.81
GC027/2/4	0.31	72.51	0.39	13.96	3.26	0.09	0.16	0.69	5.14	2.58	98.78
GC027/2/16	0.43	51.22	2.45	15.44	10.00	0.29	4.22	8.09	4.42	0.46	96.60
GC027/2/16	0.43	51.37	2.15	15.64	9.91	0.15	4.71	9.21	4.54	0.48	98.16
GC027/2/16	0.43	52.02	2.36	15.55	10.20	0.20	4.32	8.44	4.55	0.50	98.14
GC027/2/16	0.43	52.33	2.32	15.75	9.82	0.23	3.67	7.38	4.66	0.61	96.77
GC027/2/16	0.43	52.74	2.49	15.51	10.20	0.21	4.22	8.00	4.63	0.57	98.56
GC027/2/16	0.43	73.39	0.41	13.67	3.25	0.11	0.26	0.68	5.07	2.38	99.22
GC027/2/52	0.79	48.91	2.33	15.83	10.70	0.20	5.23	9.19	4.21	1.42	98.01
GC027/2/52	0.79	64.35	1.38	15.39	5.29	0.18	1.46	2.97	4.58	1.38	96.98
GC027/2/52	0.79	65.39	1.26	15.17	5.27	0.24	1.38	2.78	4.78	1.44	97.71
GC027/5/76	3.88	49.90	1.95	15.26	10.40	0.24	4.97	9.17	4.15	0.49	96.52
GC027/5/76	3.88	50.17	2.02	15.39	9.56	0.18	5.31	9.26	3.93	0.46	96.28
GC027/5/76	3.88	50.69	2.03	15.59	9.29	0.24	5.18	9.23	4.19	0.45	96.89
GC027/5/76	3.88	50.74	2.18	15.39	10.10	0.20	5.04	9.03	4.34	0.47	97.48
GC027/5/76	3.88	50.79	2.12	15.37	9.66	0.22	4.93	8.83	4.15	0.48	96.55
GC027/5/76	3.88	50.83	1.92	15.70	9.58	0.18	4.92	9.31	4.09	0.44	96.97
GC027/5/76	3.88	50.86	2.18	15.07	9.69	0.19	4.84	8.77	4.30	0.54	96.44
GC027/5/76	3.88	50.95	2.10	15.23	9.43	0.20	4.76	8.62	4.20	0.52	96.01
GC027/5/76	3.88	50.96	2.21	15.29	9.82	0.19	4.78	8.72	4.23	0.46	96.66
GC027/5/76	3.88	51.05	1.98	15.38	9.70	0.19	4.98	9.15	4.06	0.49	96.98

Core section	depth (mbsf)	SiO_2	TiO_2	Al_2O_3	FeO_T	MnO	MgO	CaO	Na_2O	K_2O	Total
GC027/5/76	3.88	51.17	2.20	15.19	9.73	0.24	4.74	8.74	4.45	0.54	97.0
GC027/5/76	3.88	51.31	2.11	15.66	9.56	0.26	4.51	8.43	4.43	0.52	96.79
GC027/5/76	3.88	51.64	2.26	15.09	9.69	0.22	4.63	8.31	4.09	0.55	96.48
GC027/5/76	3.88	51.71	2.07	15.38	9.37	0.24	4.76	8.49	4.36	0.52	96.9
GC027/5/76	3.88	51.90	2.22	15.35	9.97	0.25	4.59	8.54	4.24	0.52	97.58
GC027/5/76	3.88	51.94	2.14	15.14	9.38	0.18	4.51	8.43	4.46	0.56	96.74
GC027/5/76	3.88	53.13	2.16	15.01	9.58	0.25	4.22	7.63	4.72	0.72	97.42
Core section	depth (mbsf)	SiO_2	TiO_2	Al_2O_3	FeO_T	MnO	MgO	CaO	Na_2O	K_2O	Total
PC029/1/24	0.24	50.35	2.26	15.25	9.92	0.18	4.39	8.29	4.55	0.51	95.70
PC029/1/80	0.76	48.70	2.22	19.34	10.27	0.15	4.02	8.08	3.88	0.59	97.25
PC029/1/76	0.76	49.79	2.25	16.01	9.96	0.14	4.33	8.48	4.66	0.53	96.15
PC029/1/76	0.76	50.25	2.41	14.76	10.52	0.18	5.62	9.31	4.03	0.51	97.59
PC029/1/80	0.76	50.26	2.45	15.56	9.95	0.19	4.13	8.23	4.62	0.50	95.89
PC029/1/80	0.76	50.34	2.32	15.68	10.36	0.10	4.18	8.29	4.54	0.50	96.31
PC029/1/80	0.76	50.52	2.43	15.49	10.21	0.16	4.21	8.39	4.73	0.48	96.62
PC029/1/76	0.76	50.56	2.35	15.59	10.48	0.12	4.33	8.00	4.25	0.43	96.11
PC029/1/80	0.76	50.63	2.29	15.87	9.66	0.20	4.15	8.41	4.70	0.53	96.44
PC029/1/80	0.76	50.66	2.34	15.43	10.46	0.17	4.25	8.32	4.64	0.57	96.84
PC029/1/80	0.76	50.84	2.21	16.30	10.21	0.21	4.16	8.01	4.69	0.55	97.18
PC029/1/76	0.76	50.85	2.35	16.02	10.79	0.17	4.24	8.57	3.78	0.49	97.26
PC029/1/76	0.76	50.86	2.39	16.02	10.34	0.16	4.17	8.31	4.30	0.48	97.03
PC029/1/76	0.76	50.90	2.32	16.04	10.69	0.16	4.01	8.49	4.41	0.53	97.55
PC029/1/80	0.76	51.03	2.45	16.01	10.24	0.18	4.26	8.07	4.44	0.49	97.17
PC029/1/80	0.76	51.09	2.38	15.22	10.39	0.20	4.19	7.83	4.53	0.59	96.42
PC029/1/76	0.76	51.10	2.31	15.79	10.21	0.15	3.85	7.40	4.26	0.73	95.80
PC029/1/76	0.76	51.13	2.32	16.08	10.12	0.12	4.21	8.19	4.57	0.54	97.28
PC029/1/80	0.76	51.14	2.36	15.51	10.31	0.14	4.03	8.22	4.61	0.50	96.82
PC029/1/80	0.76	51.20	2.15	15.48	10.16	0.14	3.95	8.05	4.79	0.48	96.40
PC029/1/80	0.76	51.27	2.27	15.66	10.19	0.14	4.13	8.16	4.43	0.52	96.77
PC029/1/80	0.76	51.28	2.32	15.69	9.93	0.13	4.22	8.27	4.72	0.52	97.08
PC029/1/80	0.76	51.34	2.20	16.05	9.72	0.18	3.83	8.53	4.71	0.53	97.09
PC029/1/76	0.76	51.50	2.52	15.55	10.78	0.16	4.31	8.08	4.28	0.58	97.76
PC029/1/76	0.76	51.97	2.37	16.13	10.52	0.14	4.36	8.40	3.65	0.51	98.05
PC029/1/76	0.76	52.21	2.72	15.73	10.70	0.18	4.05	7.94	4.38	0.72	98.63
PC029/1/76	0.76	53.18	1.94	18.75	6.48	0.02	2.99	9.15	7.95	0.23	100.70
PC029/1/76	0.76	61.10	1.28	15.83	6.59	0.19	1.99	4.43	4.33	1.39	97.13
PC029/1/80	0.76	64.99	0.80	16.31	3.64	0.10	0.89	3.13	5.72	1.32	96.90
PC029/1/80	0.76	65.45	0.69	16.24	4.00	0.13	0.79	1.95	5.92	1.76	96.93
PC029/1/80	0.76	65.56	0.66	16.34	3.46	0.06	0.86	2.93	5.93	1.33	97.13
PC029/1/80	0.76	67.48	0.38	17.40	3.29	0.13	0.28	0.85	5.56	2.29	97.66
PC029/1/76	0.76	67.49	0.69	15.31	3.77	0.20	0.60	1.35	4.39	1.98	95.78
PC029/1/80	0.76	68.14	0.66	15.19	3.82	0.15	0.74	1.87	5.08	1.72	97.37
PC029/1/76	0.76	68.37	0.71	15.35	3.72	0.14	0.58	1.34	4.64	1.94	96.79
PC029/1/80	0.76	68.40	0.91	15.31	4.03	0.17	0.97	2.05	5.29	1.82	98.95
PC029/1/76	0.76	70.72	0.28	14.01	3.42	0.05	0.26	0.58	4.89	2.38	96.59
PC029/1/76	0.76	71.51	0.33	14.70	3.33	0.15	0.23	0.70	5.08	2.67	98.70
PC029/1/76	0.76	71.56	0.37	14.29	3.36	0.15	0.19	0.61	4.02	2.51	97.06
PC029/1/80	0.76	71.62	0.33	13.92	3.30	0.11	0.21	0.72	5.62	2.50	98.33
PC029/1/92	0.92	49.85	1.86	15.77	8.75	0.21	5.51	10.00	4.12	0.32	96.39
PC029/1/92	0.92	49.96	2.26	15.48	9.96	0.19	4.47	8.48	4.59	0.51	95.90
PC029/1/92	0.92	50.58	2.29	15.62	10.31	0.24	4.19	8.48	4.57	0.52	96.80
PC029/1/92	0.92	50.64	2.53	15.40	9.76	0.24	4.13	8.42	4.61	0.52	96.25

PC029/1/92	0.92	50.66	2.35	15.41	9.90	0.29	3.99	8.15	4.42	0.42	95.59
PC029/1/92	0.92	50.79	2.40	15.43	9.86	0.17	4.01	8.25	4.90	0.47	96.28
PC029/1/92	0.92	50.97	2.30	15.49	10.17	0.20	4.15	8.35	4.58	0.51	96.72
PC029/1/92	0.92	50.97	2.38	15.55	9.83	0.17	4.01	8.21	4.51	0.52	96.15
PC029/1/92	0.92	50.98	2.52	15.36	10.51	0.24	4.28	7.94	4.80	0.56	97.19
PC029/1/92	0.92	51.30	2.35	15.50	10.15	0.24	4.35	8.35	4.44	0.52	97.20
PC029/1/92	0.92	51.31	2.22	15.79	10.69	0.24	4.42	8.54	4.36	0.51	98.08
PC029/1/92	0.92	52.29	2.32	15.64	9.22	0.21	4.34	8.52	4.62	0.55	97.71
PC029/1/92	0.92	52.66	2.42	15.66	10.44	0.20	4.14	8.45	4.54	0.47	98.98
PC029/1/92	0.92	55.77	2.61	13.90	9.68	0.25	3.03	5.94	4.95	0.95	97.08
PC029/1/92	0.92	57.08	2.20	14.98	8.62	0.19	3.20	5.96	5.16	1.01	98.40
PC029/2/42	1.92	69.01	0.46	14.68	3.22	0.14	0.45	1.44	5.37	2.07	96.84
PC029/2/42	1.92	70.65	0.45	14.68	3.26	0.11	0.44	1.30	5.05	2.01	97.95
PC029/2/42	1.92	70.80	0.49	15.11	3.46	0.14	0.45	1.50	4.76	2.17	98.88
PC029/2/118	2.68	50.82	1.87	15.62	9.32	0.16	4.54	8.48	4.43	0.44	95.68
PC029/2/118	2.68	51.19	1.80	16.08	9.22	0.19	4.58	8.62	4.20	0.48	96.36
PC029/2/118	2.68	51.26	1.87	15.42	9.59	0.13	4.47	8.95	4.47	0.42	96.58
PC029/2/118	2.68	51.30	1.80	15.08	9.33	0.21	4.78	8.30	4.25	0.53	95.58
PC029/2/118	2.68	51.47	1.90	15.69	9.36	0.10	4.48	8.40	4.44	0.48	96.32
PC029/2/118	2.68	51.53	1.85	15.91	9.58	0.14	4.55	8.62	4.48	0.53	97.19
PC029/2/118	2.68	51.58	1.92	15.09	9.72	0.16	4.56	8.45	4.27	0.44	96.19
PC029/2/118	2.68	51.84	2.00	15.36	9.28	0.16	4.56	8.50	4.32	0.46	96.48
PC029/2/118	2.68	52.05	1.94	15.42	9.21	0.20	4.55	8.51	4.49	0.48	96.85
PC029/2/118	2.68	52.06	1.80	15.71	9.41	0.22	4.59	8.28	4.37	0.40	96.84
PC029/2/118	2.68	52.07	1.92	15.39	9.05	0.14	4.67	8.40	4.60	0.49	96.73
PC029/2/118	2.68	52.16	1.99	15.33	9.17	0.19	4.51	8.25	4.50	0.51	96.61
PC029/2/118	2.68	52.20	1.95	15.56	9.26	0.15	4.57	8.32	4.38	0.57	96.96
PC029/2/118	2.68	52.32	1.85	15.61	9.33	0.18	4.47	8.54	4.41	0.48	97.19
PC029/2/118	2.68	52.36	1.82	15.36	9.34	0.15	4.56	8.45	4.48	0.51	97.03
PC029/2/118	2.68	57.14	1.69	13.73	10.14	0.13	3.29	6.53	3.98	1.29	97.92
PC029/2/118	2.68	57.21	1.60	14.94	9.56	0.16	2.89	6.56	4.14	1.23	98.29
PC029/2/118	2.68	57.32	1.75	13.43	10.36	0.14	2.82	6.10	4.10	1.51	97.53
PC029/3/16	3.16	49.88	1.72	14.77	9.19	0.20	6.57	10.32	3.25	0.35	96.25
PC029/3/16	3.16	51.52	1.97	16.02	9.00	0.17	3.87	6.70	4.46	0.63	94.34
PC029/3/16	3.16	51.61	1.89	14.23	9.49	0.18	5.65	9.49	3.90	0.54	96.98
PC029/3/16	3.16	51.63	1.77	15.98	8.77	0.18	5.34	9.68	4.11	0.45	97.91
PC029/3/16	3.16	51.75	2.45	14.44	10.90	0.19	4.28	7.94	4.46	0.63	97.04
PC029/3/16	3.16	51.95	2.20	13.98	11.22	0.22	4.59	7.68	4.34	0.74	96.92
PC029/3/16	3.16	52.02	1.54	17.25	8.38	0.14	4.80	10.39	3.82	0.40	98.74
PC029/3/16	3.16	53.00	1.58	15.90	8.01	0.18	4.99	9.36	4.25	0.56	97.83
PC029/3/16	3.16	53.11	2.10	15.35	9.63	0.18	4.45	8.07	4.03	0.64	97.56
PC029/3/16	3.16	53.17	1.70	15.84	8.75	0.19	5.36	9.68	3.48	0.36	98.53
PC029/3/16	3.16	54.41	1.61	15.89	8.01	0.12	3.81	7.73	4.88	0.71	97.17
PC029/3/16	3.16	54.65	1.63	15.13	8.56	0.18	3.94	7.38	4.52	0.86	96.85
PC029/3/16	3.16	58.20	1.95	15.78	7.83	0.14	2.32	5.77	5.25	0.87	98.11
PC029/3/64	3.64	51.64	1.62	16.56	8.08	0.18	5.16	9.61	4.09	0.41	97.35
PC029/3/64	3.64	52.39	1.58	16.19	8.55	0.16	5.24	9.81	4.22	0.46	98.60
PC029/3/64	3.64	52.51	1.28	16.37	7.85	0.14	5.33	9.96	4.22	0.38	98.04
PC029/3/64	3.64	52.57	1.54	16.13	8.03	0.20	5.28	9.59	4.15	0.55	98.04
PC029/3/64	3.64	52.58	1.63	15.55	8.34	0.20	5.52	9.04	4.15	0.66	97.67
PC029/3/64	3.64	52.60	1.68	15.23	8.63	0.23	5.43	9.53	4.34	0.52	98.19
PC029/3/64	3.64	52.64	1.46	16.14	8.41	0.16	5.17	9.57	4.29	0.43	98.27

Core section	depth (mbsf)	SiO$_2$	TiO$_2$	Al$_2$O$_3$	FeO$_T$	MnO	MgO	CaO	Na$_2$O	K$_2$O	Total
PC029/3/64	3.64	52.76	1.55	16.42	7.96	0.18	5.18	9.60	4.14	0.42	98.21
PC029/3/64	3.64	52.85	1.70	15.63	8.46	0.14	5.41	9.51	4.23	0.55	98.48
PC029/3/64	3.64	52.95	1.86	15.20	9.10	0.14	5.59	8.91	4.00	0.59	98.34
PC029/3/64	3.64	53.00	1.52	15.89	7.74	0.21	5.35	9.62	4.04	0.50	97.87
PC029/3/64	3.64	53.01	1.58	16.16	7.98	0.11	5.05	9.09	4.42	0.56	97.96
PC029/3/64	3.64	53.21	1.46	15.82	8.04	0.17	5.11	9.27	4.14	0.52	97.74
PC029/3/64	3.64	53.26	1.53	16.20	7.68	0.16	5.21	9.51	4.39	0.54	98.48
PC029/3/64	3.64	54.45	1.91	15.33	9.05	0.25	4.49	7.97	4.64	0.69	98.78
PC029/3/88	3.88	49.36	2.09	14.91	10.53	0.20	5.70	9.43	4.18	0.93	97.33
PC029/3/88	3.88	49.53	1.92	14.90	10.65	0.16	5.65	9.34	4.63	1.04	97.82
PC029/3/88	3.88	50.57	1.78	15.16	9.57	0.26	5.42	9.69	4.11	0.34	96.90
PC029/3/88	3.88	50.81	1.42	15.38	8.28	0.17	6.57	10.78	3.76	0.30	97.47
PC029/3/88	3.88	50.85	1.72	15.00	9.64	0.27	5.37	10.16	4.51	0.27	97.79
PC029/3/88	3.88	51.06	1.81	14.09	10.02	0.18	6.23	9.71	4.17	0.36	97.63
PC029/3/88	3.88	51.12	1.76	15.17	9.49	0.17	5.53	9.56	4.33	0.28	97.41
PC029/3/88	3.88	51.14	1.89	15.06	9.81	0.19	5.29	9.36	4.54	0.38	97.66
PC029/3/88	3.88	51.15	1.93	15.03	9.33	0.20	5.77	10.06	3.99	0.34	97.80
PC029/3/88	3.88	51.19	1.71	14.92	9.28	0.10	5.34	9.71	4.32	0.33	96.90
PC029/3/88	3.88	51.22	1.82	15.27	9.16	0.16	5.50	9.72	4.19	0.29	97.33
PC029/3/88	3.88	51.28	1.81	14.93	10.03	0.22	5.30	9.48	4.41	0.33	97.79
PC029/3/88	3.88	51.43	1.69	14.98	9.22	0.23	5.44	9.81	4.15	0.33	97.28
PC029/3/88	3.88	51.52	1.74	14.88	9.65	0.22	5.24	9.76	4.31	0.33	97.65
PC029/3/88	3.88	51.63	1.71	15.19	9.22	0.19	5.22	9.35	4.10	0.44	97.05
PC029/3/88	3.88	52.02	1.75	15.06	9.41	0.15	5.35	9.49	4.29	0.35	97.87
PC029/3/88	3.88	52.14	1.63	15.08	8.99	0.24	5.49	9.58	4.07	0.38	97.60
PC029/3/88	3.88	52.15	1.75	15.11	9.03	0.18	5.52	9.22	4.33	0.37	97.66
PC029/3/88	3.88	52.51	1.79	15.32	9.26	0.20	5.28	9.71	4.34	0.34	98.75
PC029/3/88	3.88	62.78	0.52	15.67	7.07	0.31	0.20	1.10	6.27	5.13	99.05
PC029/3/128	4.28	51.71	1.56	15.01	8.93	0.15	4.98	8.81	4.06	0.46	95.67
PC029/3/128	4.28	51.85	1.62	15.15	8.69	0.18	4.83	8.82	4.00	0.42	95.56
PC029/3/128	4.28	52.27	1.66	16.07	7.90	0.18	4.06	7.86	4.67	0.65	95.32
PC029/3/128	4.28	52.35	1.60	16.00	7.85	0.16	3.97	7.86	4.47	0.78	95.04
PC029/3/128	4.28	52.42	1.56	15.24	8.74	0.24	4.99	8.33	4.14	0.44	96.10
PC029/3/128	4.28	53.14	1.69	16.09	7.95	0.20	3.92	7.52	4.72	0.76	95.99
PC029/3/128	4.28	53.40	1.60	15.92	7.93	0.21	3.95	7.26	4.79	0.76	95.82
PC029/3/128	4.28	53.54	1.69	15.70	7.69	0.19	3.82	7.28	4.38	0.72	95.01
Core section	depth (mbsf)	SiO$_2$	TiO$_2$	Al$_2$O$_3$	FeO$_T$	MnO	MgO	CaO	Na$_2$O	K$_2$O	Total
GC037/1/6	0.06	51.65	2.52	16.02	9.97	0.21	4.12	8.09	4.63	0.62	97.83
GC037/1/6	0.06	50.53	2.31	15.65	10.30	0.22	4.40	8.22	4.59	0.51	96.71
GC037/1/6	0.06	51.78	1.53	16.13	7.95	0.21	5.49	9.52	4.24	0.44	97.29
GC037/1/6	0.06	71.55	0.43	14.38	3.34	0.12	0.21	0.64	5.12	2.35	98.14
GC037/1/34	0.34	50.39	2.07	15.60	9.79	0.21	4.84	8.70	4.45	0.46	96.51
GC037/1/34	0.34	72.00	0.36	14.16	3.26	0.12	0.23	0.67	3.32	2.39	96.51
GC037/1/82	0.82	48.51	2.48	17.56	10.54	0.20	3.21	8.32	3.72	0.55	95.09
GC037/1/82	0.82	50.94	2.49	15.39	10.32	0.17	3.78	9.46	4.47	0.44	97.46
GC037/1/82	0.82	51.32	2.08	15.63	9.99	0.14	4.31	10.36	4.31	0.41	98.55
GC037/1/82	0.82	51.40	2.21	15.60	9.83	0.19	4.29	10.29	4.50	0.42	98.73
GC037/1/82	0.82	51.56	2.10	16.05	9.82	0.10	4.53	10.52	4.24	0.41	99.33
GC037/1/82	0.82	51.79	2.66	15.13	12.27	0.16	3.42	8.91	4.05	0.54	98.93
GC037/1/82	0.82	51.95	2.31	15.65	10.12	0.21	3.98	9.59	4.69	0.46	98.96

GC037/1/82	0.82	51.97	2.60	15.33	11.49	0.24	3.51	8.88	4.11	0.57	98.70
GC037/1/82	0.82	52.01	2.24	15.70	10.01	0.25	4.10	10.25	4.28	0.40	99.24
GC037/1/82	0.82	52.07	2.84	14.96	11.89	0.17	3.84	8.93	4.17	0.54	99.41
GC037/1/82	0.82	52.36	2.54	15.34	11.63	0.24	3.52	8.88	4.13	0.53	99.17
GC037/1/82	0.82	53.13	2.66	16.01	12.16	0.22	3.37	8.62	4.66	0.57	101.40
GC037/1/82	0.82	53.30	2.52	16.29	10.70	0.21	3.68	9.06	4.86	0.47	101.10
GC037/1/82	0.82	53.52	2.49	16.27	10.91	0.18	3.80	9.32	4.99	0.47	102.00
GC037/1/82	0.82	67.12	0.67	13.99	3.06	0.19	0.32	0.94	6.90	1.69	94.88
GC037/1/82	0.82	68.69	0.69	14.21	3.36	0.27	0.32	1.10	6.46	1.78	96.88
GC037/1/82	0.82	68.91	0.40	13.39	3.28	0.13	0.04	0.89	6.35	2.24	95.63
GC037/1/82	0.82	68.98	0.45	13.57	3.42	0.08	0.11	0.89	6.30	2.28	96.08
GC037/1/82	0.82	69.14	0.82	14.51	3.18	0.16	0.33	1.02	6.59	1.83	97.58
GC037/1/82	0.82	69.65	0.37	13.23	3.34	0.11	0.06	0.75	6.67	2.20	96.38
GC037/1/82	0.82	69.73	0.84	14.60	3.25	0.12	0.44	1.12	6.24	1.83	98.17
GC037/1/82	0.82	70.14	0.45	13.76	3.40	0.10	0.16	0.77	4.98	2.28	96.04
GC037/1/82	0.82	70.92	0.44	13.93	3.19	0.10	0.14	0.85	6.83	2.27	98.67
GC037/1/82	0.82	71.35	0.46	13.96	3.49	0.14	0.04	0.88	6.59	2.26	99.17
GC037/2/82	1.97	49.99	2.26	15.94	9.82	0.16	4.39	8.67	4.42	0.47	96.12
GC037/2/82	1.97	50.80	2.06	15.74	9.70	0.19	4.22	8.31	4.72	0.46	96.20
GC037/2/82	1.97	51.29	2.12	16.19	9.84	0.11	4.56	8.80	4.72	0.47	98.10
GC037/2/82	1.97	51.73	2.22	16.19	9.88	0.20	4.38	8.26	4.46	0.61	97.93
GC037/2/82	1.97	51.79	2.37	16.08	10.17	0.19	4.31	8.76	4.45	0.45	98.57
GC037/2/82	1.97	68.07	0.39	17.01	3.21	0.05	0.27	0.64	5.74	2.47	97.85
GC037/2/82	1.97	68.21	0.70	14.98	4.05	0.16	0.72	1.75	5.42	1.98	97.97
GC037/2/82	1.97	68.86	0.71	15.18	3.40	0.18	0.71	1.46	6.10	1.77	98.37
GC037/2/82	1.97	71.33	0.34	13.85	3.31	0.15	0.21	0.66	6.12	2.44	98.41
GC037/2/128	2.43	61.63	0.27	20.04	3.54	0.10	0.32	2.14	3.47	1.29	92.80
GC037/2/128	2.43	64.26	0.46	13.20	5.59	0.14	0.92	3.95	3.51	1.07	93.10
GC037/2/128	2.43	64.35	0.54	13.97	6.41	0.22	1.10	4.14	3.77	1.07	95.57
GC037/2/128	2.43	64.74	0.68	12.34	3.80	0.09	0.88	3.07	3.03	0.93	89.56
GC037/2/128	2.43	67.90	0.19	11.57	3.08	0.07	0.13	1.73	3.97	1.41	90.05
GC037/2/128	2.43	68.24	0.21	11.26	2.92	0.09	0.19	1.80	4.01	1.25	89.97
GC037/2/128	2.43	69.31	0.26	12.71	4.06	0.09	0.39	2.60	4.04	1.23	94.69
GC037/2/128	2.43	69.70	0.43	13.31	4.80	0.14	0.70	3.29	3.64	1.41	97.42
GC037/2/128	2.43	70.07	0.34	11.35	2.23	0.01	0.38	1.98	3.36	1.08	90.80
GC037/2/128	2.43	70.62	0.30	12.56	4.43	0.10	0.35	2.57	3.56	1.31	95.80
GC037/2/128	2.43	72.32	0.31	13.05	3.94	0.10	0.35	2.65	3.78	1.33	97.83
GC037/3/136	4.01	49.80	1.37	15.49	8.18	0.07	6.58	11.15	3.72	0.24	96.60
GC037/3/136	4.01	49.82	1.41	15.59	7.93	0.15	6.72	11.35	3.53	0.19	96.69
GC037/3/136	4.01	49.83	1.29	15.57	7.78	0.14	6.61	11.39	3.75	0.19	96.55
GC037/3/136	4.01	49.88	1.44	15.46	8.09	0.10	6.76	11.63	3.52	0.25	97.13
GC037/3/136	4.01	49.88	1.30	14.98	8.28	0.10	6.65	11.58	3.63	0.19	96.59
GC037/3/136	4.01	50.07	1.39	15.45	8.48	0.19	6.81	11.99	3.84	0.22	98.44
GC037/3/136	4.01	50.16	1.39	15.28	8.12	0.13	6.71	11.59	3.63	0.25	97.26
GC037/3/136	4.01	50.18	1.40	15.53	7.96	0.08	6.71	11.44	3.54	0.22	97.06
GC037/3/136	4.01	50.52	1.27	15.61	8.26	0.12	6.67	11.57	3.73	0.26	98.01
GC037/3/136	4.01	50.79	1.52	15.71	8.47	0.15	6.96	11.67	3.76	0.26	99.29
GC037/3/136	4.01	50.91	1.26	15.74	8.44	0.22	7.05	11.47	3.58	0.22	98.89
GC037/3/136	4.01	50.96	1.54	15.52	8.22	0.09	6.87	11.76	3.63	0.30	98.89
GC037/3/136	4.01	50.99	1.38	15.31	8.09	0.14	6.67	10.88	3.61	0.24	97.31
GC037/3/136	4.01	51.01	1.39	15.40	8.51	0.23	6.81	11.56	3.64	0.21	98.76
GC037/3/136	4.01	51.05	1.38	15.84	8.23	0.16	6.80	11.49	3.78	0.27	99.00
GC037/3/136	4.01	51.07	1.26	15.42	8.10	0.14	6.83	10.91	3.73	0.24	97.70

Core section	depth (mbsf)	SiO$_2$	TiO$_2$	Al$_2$O$_3$	FeO$_T$	MnO	MgO	CaO	Na$_2$O	K$_2$O	Total
GC037/3/136	4.01	51.08	1.27	15.40	8.16	0.12	6.44	10.60	3.73	0.25	97.05
GC037/3/136	4.01	51.18	1.33	15.40	7.84	0.15	6.40	10.24	3.51	0.24	96.29
GC037/3/136	4.01	51.20	1.45	14.85	8.65	0.14	6.21	10.33	3.88	0.26	96.97
GC037/3/136	4.01	51.22	1.31	15.22	8.50	0.22	6.88	11.05	3.60	0.25	98.25
GC037/3/136	4.01	51.32	1.35	15.18	8.28	0.12	6.50	10.42	3.81	0.28	97.26
GC037/3/136	4.01	51.38	1.39	15.98	8.32	0.14	6.93	11.52	3.59	0.26	99.51
GC037/3/136	4.01	51.41	1.35	15.49	8.14	0.10	6.29	10.66	3.90	0.27	97.61
GC037/3/136	4.01	51.88	1.50	16.03	7.95	0.19	6.62	11.40	3.59	0.26	99.42
GC037/3/136	4.01	52.11	1.49	14.94	8.61	0.12	6.20	10.59	3.83	0.33	98.22
GC037/3/136	4.01	52.24	1.55	15.25	8.81	0.19	6.30	10.34	4.13	0.34	99.15
GC037/3/136	4.01	52.52	1.50	15.05	8.79	0.14	6.21	10.57	3.87	0.30	98.95
GC037/3/136	4.01	52.64	1.52	15.18	8.71	0.12	6.26	10.29	4.05	0.29	99.06
Core section	depth (mbsf)	SiO$_2$	TiO$_2$	Al$_2$O$_3$	FeO$_T$	MnO	MgO	CaO	Na$_2$O	K$_2$O	Total
PC063/1/2	0.02	62.10	1.43	15.65	5.57	0.23	1.72	3.24	5.04	2.43	97.41
PC063/1/2	0.02	63.17	1.39	15.44	5.48	0.16	1.38	2.83	5.35	2.81	98.01
PC063/1/2	0.02	71.15	0.09	12.89	1.20	0.04	0.21	1.15	3.35	2.82	92.90
PC063/1/2	0.02	72.74	0.15	11.54	0.97	0.05	0.16	0.76	2.73	4.17	93.27
PC063/1/2	0.02	72.89	0.23	11.29	1.72	0.05	0.26	1.83	3.08	1.78	93.13
PC063/1/2	0.02	73.25	0.21	11.23	1.92	0.05	0.21	1.85	3.10	1.92	93.74
PC063/1/18	0.18	50.16	2.27	13.86	10.17	0.20	5.61	10.10	4.09	0.44	96.85
PC063/1/18	0.18	51.97	2.81	14.70	11.67	0.24	4.02	7.38	4.97	0.69	98.45
PC063/1/18	0.18	54.29	1.88	15.99	8.49	0.17	3.64	7.60	4.60	0.73	97.39
PC063/1/18	0.18	54.30	2.51	16.51	8.83	0.16	3.00	7.44	5.23	0.54	98.52
PC063/1/18	0.18	56.74	1.29	15.16	8.80	0.19	3.08	6.64	3.89	0.89	96.68
PC063/1/18	0.18	59.22	0.60	14.22	9.37	0.40	0.05	0.95	7.99	4.40	97.20
PC063/1/18	0.18	59.45	1.59	15.10	7.40	0.16	2.43	4.87	5.11	1.11	97.22
PC063/1/18	0.18	59.57	1.20	15.55	7.19	0.20	2.25	5.17	3.95	1.64	96.72
PC063/1/18	0.18	60.72	0.40	14.51	8.49	0.37	0.07	1.14	7.52	4.79	98.01
PC063/1/18	0.18	61.27	0.73	14.66	7.59	0.31	0.31	1.39	6.45	4.79	97.50
PC063/2/20	0.74	46.33	1.87	17.19	9.72	0.19	5.94	9.48	4.27	1.52	96.51
PC063/2/20	0.74	47.55	2.46	16.70	8.23	0.19	4.90	9.15	4.39	2.39	95.96
PC063/2/20	0.74	51.88	1.84	15.34	8.56	0.19	3.54	7.23	4.30	0.69	93.57
PC063/2/20	0.74	52.63	1.59	16.54	7.32	0.19	4.13	7.95	4.09	0.57	95.01
PC063/2/20	0.74	52.79	2.78	13.59	10.66	0.21	3.47	7.34	4.03	0.77	95.64
PC063/2/20	0.74	66.34	0.28	12.89	1.51	0.05	0.23	1.21	2.80	4.67	89.98
PC063/2/20	0.74	67.39	0.29	13.47	1.68	0.05	0.29	1.22	2.91	4.51	91.81
PC063/2/20	0.74	68.00	0.27	13.22	1.69	0.07	0.30	1.31	2.89	4.44	92.19
PC063/2/20	0.74	68.89	0.41	13.02	1.69	0.13	0.42	1.25	3.22	3.75	92.78
PC063/3/60	2.64	46.56	1.95	17.10	9.53	0.21	5.84	9.55	4.47	1.39	96.60
PC063/3/60	2.64	47.94	2.60	16.66	8.31	0.23	4.97	9.05	4.36	2.24	96.36
PC063/3/60	2.64	53.18	1.67	15.89	8.15	0.20	3.94	7.77	4.95	0.66	96.41
Core section	depth (mbsf)	SiO$_2$	TiO$_2$	Al$_2$O$_3$	FeO$_T$	MnO	MgO	CaO	Na$_2$O	K$_2$O	Total
PC078/1/35	0.35	50.71	2.21	14.95	9.77	0.14	5.34	9.07	3.84	1.08	97.11
PC078/1/35	0.35	51.22	2.37	16.13	10.50	0.16	4.34	8.45	3.99	0.49	97.62
PC078/1/35	0.35	51.43	2.39	15.98	10.30	0.15	4.34	8.27	4.12	0.49	97.47
PC078/1/35	0.35	51.53	2.37	14.97	9.75	0.13	5.08	9.29	3.65	1.06	97.83
PC078/1/35	0.35	51.97	2.43	15.76	9.60	0.19	4.06	8.23	4.54	0.63	97.41
PC078/1/35	0.35	52.10	2.54	15.76	10.60	0.13	4.22	7.87	3.93	0.62	97.80

PC078/1/35	0.35	52.67	2.54	15.84	9.68	0.21	3.93	7.84	4.86	0.59	98.16
PC078/1/35	0.35	57.52	1.35	15.37	6.65	0.05	2.64	5.59	4.60	1.12	94.89
PC078/1/35	0.35	57.74	1.39	15.82	7.24	0.18	2.58	5.41	5.10	1.13	96.59
PC078/1/35	0.35	71.08	0.56	15.03	3.41	0.13	0.40	1.11	5.44	1.98	99.14
PC078/1/35	0.35	71.35	0.30	14.05	3.19	0.06	0.20	0.57	5.81	2.51	98.04
PC078/1/35	0.35	71.56	0.36	14.30	3.11	0.14	0.18	0.68	6.03	2.43	98.79
PC078/1/35	0.35	71.63	0.43	14.05	3.34	0.20	0.20	0.62	5.80	2.51	98.78
PC078/1/35	0.35	72.17	0.39	13.96	3.14	0.14	0.22	0.60	5.46	2.38	98.46
PC078/1/112	1.12	53.33	1.79	16.31	8.06	0.14	3.48	7.13	4.35	0.71	95.30
PC078/1/112	1.12	53.97	1.76	15.97	8.01	0.12	3.49	7.11	4.67	0.72	95.82
PC078/1/112	1.12	54.30	2.82	14.54	10.70	0.18	3.08	7.16	4.75	0.79	98.31
PC078/1/112	1.12	54.70	2.02	15.62	9.11	0.17	3.74	7.10	4.59	0.74	97.79
PC078/1/112	1.12	54.70	2.00	15.94	8.48	0.03	3.52	7.00	4.58	0.75	97.00
PC078/1/112	1.12	54.83	1.77	15.73	8.29	0.13	3.61	7.27	4.73	0.66	97.02
PC078/1/112	1.12	54.95	1.91	15.71	8.18	0.09	3.68	7.06	4.63	0.81	97.02
PC078/1/112	1.12	55.00	2.10	13.69	9.80	0.19	3.54	6.90	4.43	1.23	96.88
PC078/1/112	1.12	55.48	1.81	15.31	8.84	0.13	3.58	7.31	4.96	0.81	98.23
PC078/1/112	1.12	57.02	1.99	15.18	8.11	0.16	2.63	5.27	4.75	0.93	96.04
PC078/1/112	1.12	58.11	2.00	15.70	7.78	0.14	2.57	5.38	5.34	1.00	98.02
PC078/1/112	1.12	60.31	0.47	14.60	8.06	0.36	0.04	1.03	7.75	4.49	97.11
PC078/1/112	1.12	60.47	0.41	14.31	7.72	0.42	0.08	1.00	7.63	4.65	96.69
PC078/1/112	1.12	60.87	0.42	14.95	8.49	0.29	0.07	1.02	7.79	4.52	98.42
PC078/2/142	2.66	49.26	1.78	15.14	10.40	0.14	5.82	8.89	4.37	1.03	96.85
PC078/2/142	2.66	50.53	1.87	15.28	9.81	0.16	5.84	9.82	4.16	0.41	97.88
PC078/2/142	2.66	56.33	1.87	14.94	8.11	0.21	3.21	6.08	5.01	0.91	96.67
PC078/2/142	2.66	70.85	0.44	15.21	3.36	0.05	0.47	1.26	5.46	1.95	99.05
PC078/3/0	2.73	50.41	0.60	23.90	3.62	0.04	2.25	11.80	4.00	0.20	96.81
PC078/3/0	2.73	50.75	1.47	15.89	7.87	0.20	5.48	9.42	4.09	0.58	95.75
PC078/3/0	2.73	50.83	1.92	15.09	10.00	0.22	5.19	8.56	4.48	0.58	96.91
PC078/3/0	2.73	51.26	0.65	24.84	3.64	0.07	1.90	11.90	4.08	0.22	98.56
PC078/3/0	2.73	51.40	1.43	15.83	8.37	0.17	5.52	9.05	3.97	0.46	96.20
PC078/3/0	2.73	51.49	1.54	15.32	8.59	0.16	5.29	9.11	4.13	0.54	96.17
PC078/3/0	2.73	51.50	1.82	15.49	9.70	0.25	5.42	9.49	4.30	0.37	98.34
PC078/3/0	2.73	51.51	1.63	15.62	8.40	0.22	5.11	9.38	4.19	0.44	96.50
PC078/3/0	2.73	51.64	1.65	15.13	8.83	0.13	5.81	9.39	4.17	0.55	97.30
PC078/3/0	2.73	51.69	1.65	15.35	8.66	0.16	5.30	9.19	4.26	0.55	96.81
PC078/3/0	2.73	51.83	1.81	15.72	9.03	0.23	5.69	9.03	4.17	0.61	98.12
PC078/3/0	2.73	52.09	1.62	16.08	7.93	0.20	5.12	9.04	4.09	0.49	96.66
PC078/3/0	2.73	52.10	1.59	16.02	8.01	0.19	5.01	9.96	4.49	0.49	97.86
PC078/3/0	2.73	52.34	1.60	16.46	8.08	0.20	5.29	9.82	4.23	0.41	98.43
PC078/3/0	2.73	52.34	1.34	16.12	8.00	0.21	5.26	9.36	4.08	0.44	97.15
PC078/3/0	2.73	52.48	1.00	21.47	5.02	0.06	2.73	10.60	4.71	0.31	98.36
PC078/3/0	2.73	52.70	1.51	16.20	8.06	0.14	5.31	9.12	4.25	0.58	97.87
PC078/3/120	3.93	50.03	1.80	16.08	8.91	0.19	5.36	9.33	3.90	0.42	96.02
PC078/3/120	3.93	50.29	1.69	15.33	8.73	0.16	5.25	9.40	4.21	0.44	95.50
PC078/3/120	3.93	50.83	1.75	14.12	9.61	0.23	5.56	9.83	3.74	0.69	96.36
PC078/3/120	3.93	51.14	1.74	14.27	9.26	0.13	5.29	9.59	3.89	0.38	95.69
PC078/3/120	3.93	51.34	2.42	13.82	10.80	0.18	4.99	8.14	4.22	0.63	96.52
PC078/3/120	3.93	51.36	1.61	15.02	9.20	0.14	4.88	9.31	4.10	0.39	96.01
PC078/3/120	3.93	51.60	1.60	14.46	9.74	0.13	5.17	9.34	4.02	0.42	96.48
PC078/3/120	3.93	51.83	1.70	14.82	9.75	0.21	5.40	9.16	4.15	0.46	97.48
PC078/3/120	3.93	53.01	2.41	14.21	10.90	0.21	3.92	7.48	4.55	0.72	97.44

Core section	depth (mbsf)	SiO$_2$	TiO$_2$	Al$_2$O$_3$	FeO$_T$	MnO	MgO	CaO	Na$_2$O	K$_2$O	Total
PC078/3/120	3.93	56.00	1.93	14.45	9.93	0.17	3.03	6.19	4.46	0.60	96.76
PC078/3/120	3.93	57.13	1.77	14.44	9.98	0.13	3.07	5.88	4.53	0.71	97.64
PC078/3/120	3.93	60.91	0.54	14.89	8.21	0.32	0.16	1.38	7.07	4.59	98.07
Core section	depth (mbsf)	SiO$_2$	TiO$_2$	Al$_2$O$_3$	FeO$_T$	MnO	MgO	CaO	Na$_2$O	K$_2$O	Total
PC079/1/4	0.04	46.60	2.42	15.78	9.92	0.20	5.12	9.78	4.32	1.61	95.75
PC079/1/4	0.04	49.51	2.20	14.25	9.98	0.19	5.31	9.25	4.49	0.41	95.59
PC079/1/4	0.04	49.87	2.44	15.66	10.11	0.26	4.50	8.82	4.70	0.47	96.83
PC079/1/4	0.04	50.41	3.00	14.47	11.40	0.16	4.39	7.91	4.49	0.50	96.73
PC079/1/4	0.04	50.95	2.46	15.35	10.67	0.20	4.35	8.40	4.47	0.47	97.32
PC079/1/4	0.04	50.99	2.46	14.42	11.04	0.25	5.15	7.82	4.13	0.61	96.87
PC079/1/4	0.04	58.04	1.60	15.70	8.09	0.23	2.71	5.17	5.03	0.91	97.48
PC079/1/4	0.04	70.38	0.44	13.88	3.08	0.14	0.19	0.77	5.46	2.52	96.86
PC079/2/24	0.54	50.08	2.40	15.50	10.29	0.20	4.25	8.14	4.73	0.49	96.08
PC079/2/24	0.54	50.19	2.13	15.55	9.99	0.24	4.20	8.32	4.33	0.47	95.42
PC079/2/24	0.54	50.37	2.49	15.64	9.77	0.21	4.19	7.84	4.39	0.49	95.39
PC079/2/24	0.54	52.71	2.15	16.24	8.97	0.19	3.71	7.66	4.72	0.58	96.93
PC079/2/24	0.54	71.70	0.37	13.78	3.31	0.19	0.24	0.55	4.84	2.41	97.39
PC079/2/80	1.10	50.42	2.38	15.71	9.69	0.23	4.40	8.26	4.92	0.50	96.51
PC079/2/80	1.10	50.88	2.08	15.81	9.05	0.22	5.14	9.20	4.44	0.52	97.34
PC079/2/80	1.10	51.00	2.25	15.47	10.06	0.20	4.23	7.87	4.31	0.51	95.90
PC079/2/80	1.10	51.21	2.78	15.03	11.25	0.26	4.26	7.93	4.61	0.49	97.82
PC079/2/80	1.10	51.48	2.37	15.39	10.13	0.21	4.28	8.26	4.48	0.46	97.06
PC079/2/80	1.10	52.83	2.04	17.96	7.68	0.19	3.67	9.73	4.70	0.31	99.11
PC079/2/80	1.10	60.92	1.26	15.37	5.50	0.14	1.48	3.13	5.15	1.40	94.35
PC079/2/132	1.62	49.49	1.82	15.50	8.85	0.23	5.92	10.09	3.97	0.35	96.22
PC079/2/132	1.62	49.59	2.10	15.77	9.52	0.22	4.96	9.18	4.40	0.45	96.19
PC079/2/132	1.62	49.61	2.36	15.27	10.26	0.25	4.17	8.16	4.41	0.52	95.01
PC079/2/132	1.62	49.87	1.72	15.46	8.62	0.20	5.68	9.64	4.21	0.40	95.80
PC079/2/132	1.62	50.10	2.19	16.09	10.16	0.23	4.43	8.53	4.50	0.45	96.68
PC079/2/132	1.62	50.18	2.55	15.17	10.40	0.19	4.30	7.89	4.67	0.60	95.95
PC079/2/132	1.62	50.34	2.26	15.56	10.31	0.21	4.35	8.16	3.89	0.49	95.57
PC079/2/132	1.62	50.36	2.29	15.61	9.91	0.21	4.06	8.05	4.60	0.46	95.55
PC079/2/132	1.62	50.39	1.98	15.86	9.02	0.24	5.33	9.41	4.24	0.36	96.83
PC079/2/132	1.62	50.63	2.54	15.46	10.88	0.18	4.19	7.62	4.32	0.57	96.39
PC079/2/132	1.62	50.81	2.56	15.51	9.36	0.25	4.29	8.70	4.50	0.39	96.37
PC079/2/132	1.62	50.94	2.42	15.58	9.96	0.17	4.02	8.36	4.74	0.48	96.67
PC079/2/132	1.62	51.07	2.43	15.54	10.42	0.23	4.28	7.98	4.61	0.56	97.12
PC079/2/132	1.62	51.14	2.05	16.17	9.14	0.20	5.04	9.14	4.34	0.45	97.67
PC079/2/132	1.62	51.26	2.50	15.86	10.05	0.25	4.22	8.37	4.55	0.54	97.60
PC079/2/132	1.62	51.52	2.29	16.11	10.44	0.22	4.23	8.33	4.49	0.52	98.15
PC079/2/132	1.62	51.64	2.35	15.75	10.47	0.20	4.10	8.27	4.88	0.50	98.16
PC079/2/132	1.62	51.80	2.43	15.76	10.34	0.23	4.05	7.85	4.65	0.52	97.63
PC079/2/132	1.62	54.08	2.04	15.74	8.71	0.23	3.08	6.60	5.03	0.73	96.24
PC079/2/132	1.62	66.12	0.66	14.97	3.56	0.18	0.61	1.48	5.65	1.80	95.03
PC079/2/132	1.62	70.12	0.38	13.62	3.05	0.15	0.24	0.67	5.37	2.23	95.83
PC079/2/132	1.62	71.21	0.28	14.39	3.34	0.13	0.17	0.61	5.24	2.56	97.93
PC079/2/132	1.62	71.54	0.38	13.96	3.26	0.17	0.22	0.80	5.13	2.35	97.81
PC079/2/149	1.80	50.42	2.28	15.42	9.98	0.14	4.02	8.06	4.75	0.48	95.55
PC079/2/149	1.80	50.76	2.36	15.56	10.10	0.11	4.14	8.18	4.70	0.47	96.39
PC079/2/149	1.80	51.13	2.38	15.64	10.60	0.17	4.23	8.48	4.48	0.42	97.52

PC079/2/149	1.80	51.14	2.42	15.49	10.30	0.13	4.17	7.47	4.61	0.39	96.14
PC079/2/149	1.80	51.21	2.38	16.11	10.30	0.18	4.00	7.95	4.78	0.54	97.41
PC079/2/149	1.80	51.23	3	14.47	14.4	0.23	4.16	8.75	4.05	0.51	100.8
PC079/2/149	1.80	51.23	2.46	15.67	10.80	0.15	4.32	8.45	4.39	0.45	97.89
PC079/2/149	1.80	51.37	2.31	15.76	9.88	0.14	4.25	7.96	4.62	0.51	96.80
PC079/2/149	1.80	51.41	2.47	16.00	10.30	0.12	4.17	8.58	3.90	0.52	97.47
PC079/2/149	1.80	51.42	2.52	15.80	10.40	0.12	3.97	8.59	4.10	0.50	97.44
PC079/2/149	1.80	51.66	2.32	15.89	10.60	0.13	4.22	8.57	4.91	0.52	98.78
PC079/2/149	1.80	51.66	2.39	15.69	10.60	0.13	4.40	8.74	4.35	0.48	98.41
PC079/2/149	1.80	51.67	2.35	16.00	9.86	0.15	4.10	8.04	4.26	0.63	97.06
PC079/2/149	1.80	51.69	2.33	15.67	10.30	0.10	4.32	8.68	4.60	0.51	98.21
PC079/2/149	1.80	51.73	2.49	15.80	10.30	0.15	4.30	7.94	4.94	0.49	98.12
PC079/2/149	1.80	51.76	2.39	15.63	9.85	0.12	4.23	7.98	4.80	0.61	97.37
PC079/2/149	1.80	51.99	2.32	15.50	10.70	0.20	4.07	7.87	4.11	0.50	97.22
PC079/2/149	1.80	52.01	2.16	17.65	9.38	0.13	2.40	8.03	4.58	0.66	97.00
PC079/2/149	1.80	52.14	2.44	16.04	10.10	0.16	4.14	8.09	4.83	0.42	98.34
PC079/2/149	1.80	52.17	2.29	17.14	10.60	0.20	4.68	8.45	4.85	0.44	100.80
PC079/2/149	1.80	52.39	1.81	17.44	9.37	0.21	4.41	10.10	3.97	0.52	100.20
PC079/2/149	1.80	52.41	2.42	16.23	10.40	0.18	4.30	8.40	5.59	0.63	100.60
PC079/2/149	1.80	52.48	1.63	19.80	9.29	0.15	2.24	9.07	4.94	0.37	99.97
PC079/2/149	1.80	52.58	2.29	15.63	10.00	0.15	4.47	8.50	4.45	0.44	98.55
PC079/2/149	1.80	52.76	2.68	16.05	10.10	0.21	4.78	8.72	4.79	0.50	100.60
PC079/2/149	1.80	52.87	2.33	16.64	9.26	0.20	3.91	8.60	3.98	0.55	98.34
PC079/2/149	1.80	52.88	2.34	16.37	9.99	0.18	4.36	9.86	3.72	0.60	100.30
PC079/2/149	1.80	54.01	2.38	18.05	10.60	0.22	2.26	7.75	5.77	0.55	101.60
PC079/2/149	1.80	56.07	3.23	13.62	12.90	0.22	2.02	4.45	5.72	0.81	99.07
PC079/2/149	1.80	70.80	0.37	14.05	2.98	0.18	0.18	0.82	5.31	2.46	97.15
PC079/2/149	1.80	70.86	0.37	14.20	3.33	0.19	0.21	0.76	5.12	2.62	97.66
PC079/2/149	1.80	70.93	0.47	13.93	3.19	0.16	0.23	0.72	6.22	2.34	98.19
PC079/2/149	1.80	71.47	0.37	14.36	3.20	0.21	0.20	0.67	5.04	2.53	98.05
PC079/2/149	1.80	71.89	0.28	14.40	3.34	0.25	0.25	0.62	5.98	2.58	99.59
PC079/2/149	1.80	72.42	0.36	14.24	3.49	0.14	0.20	0.72	5.48	2.42	99.47
PC079/2/149	1.80	72.44	0.41	14.13	3.27	0.15	0.26	0.72	4.81	2.68	98.87
PC079/2/149	1.80	72.49	0.33	14.06	3.19	0.13	0.20	0.59	5.35	2.33	98.67
PC079/2/149	1.80	72.97	0.41	14.14	3.37	0.16	0.18	0.77	4.64	2.47	99.11
PC079/2a/5	1.85	49.75	2.41	15.54	10.11	0.21	4.22	8.19	4.97	0.45	95.85
PC079/2a/5	1.85	49.90	2.46	15.32	10.10	0.25	4.22	8.45	4.42	0.53	95.65
PC079/2a/5	1.85	49.90	2.22	15.27	10.20	0.25	4.52	8.93	4.48	0.45	96.22
PC079/2a/5	1.85	49.91	2.30	15.20	9.49	0.16	4.60	8.71	4.41	0.45	95.23
PC079/2a/5	1.85	50.02	2.57	15.09	10.37	0.22	4.39	8.10	4.87	0.57	96.20
PC079/2a/5	1.85	50.25	2.27	15.31	9.86	0.22	4.11	8.30	4.58	0.54	95.44
PC079/2a/5	1.85	50.32	2.34	15.32	10.03	0.30	4.01	7.94	4.49	0.65	95.40
PC079/2a/5	1.85	50.48	2.47	15.47	10.39	0.22	4.11	8.03	4.61	0.53	96.31
PC079/2a/5	1.85	51.05	2.38	16.18	9.93	0.25	3.90	8.08	4.38	0.54	96.69
PC079/2a/5	1.85	51.70	2.01	15.23	8.61	0.18	4.21	7.85	4.78	0.71	95.28
PC079/2a/5	1.85	52.93	2.26	15.53	9.17	0.23	3.31	6.77	4.76	0.72	95.68
PC079/2a/5	1.85	68.03	0.44	13.67	3.13	0.14	0.23	0.71	5.08	2.44	93.87
PC079/2a/5	1.85	69.64	0.34	13.66	3.14	0.17	0.25	0.52	5.43	2.48	95.63
PC079/2a/5	1.85	70.36	0.36	14.17	3.14	0.18	0.27	0.74	4.98	2.68	96.88
PC079/2a/5	1.85	70.99	0.32	13.99	3.14	0.16	0.21	0.57	5.21	2.73	97.32
PC079/3/62	2.57	50.47	2.30	14.33	10.70	0.15	5.07	8.34	4.09	0.60	96.03
PC079/3/62	2.57	51.06	1.76	15.69	8.07	0.10	6.05	9.91	3.77	0.51	96.92
PC079/3/62	2.57	52.42	1.77	19.08	7.02	0.12	2.33	9.73	4.42	0.47	97.36
PC079/3/62	2.57	53.10	1.38	19.55	7.49	0.18	3.76	10.22	4.42	0.29	100.39

PC079/3/62	2.57	53.11	2.23	14.57	10.20	0.20	3.40	6.91	4.17	0.63	95.45
PC079/3/62	2.57	53.94	1.84	16.00	8.22	0.16	3.49	7.11	4.49	0.77	96.02
PC079/3/62	2.57	54.26	2.24	14.87	9.96	0.12	3.38	6.88	4.07	0.63	96.41
PC079/3/62	2.57	54.46	2.00	16.14	8.32	0.15	3.71	7.39	4.54	0.78	97.49
PC079/3/62	2.57	60.04	0.41	14.90	8.11	0.22	0.09	1.12	8.17	4.66	97.72
PC079/3/96	2.91	51.74	2.07	10.86	10.24	0.29	8.83	12.19	3.47	0.35	100.04
PC079/3/96	2.91	52.03	1.90	15.83	9.39	0.16	4.53	8.78	4.54	0.48	97.64
PC079/3/96	2.91	52.04	1.87	16.18	9.26	0.09	4.70	8.79	4.32	0.44	97.69
PC079/3/96	2.91	52.15	1.85	15.98	9.19	0.09	4.43	8.57	4.30	0.48	97.04
PC079/3/96	2.91	52.18	2.06	15.32	9.41	0.18	4.73	8.46	4.57	0.55	97.46
PC079/3/96	2.91	52.19	1.93	15.36	9.27	0.24	4.49	8.35	4.32	0.52	96.67
PC079/3/96	2.91	52.19	2.01	15.82	9.31	0.16	4.65	8.91	4.66	0.54	98.25
PC079/3/96	2.91	52.23	1.78	15.91	9.33	0.17	4.68	8.54	4.60	0.47	97.71
PC079/3/96	2.91	52.30	1.95	15.73	9.41	0.21	4.56	8.73	4.38	0.49	97.76
PC079/3/96	2.91	52.37	1.99	15.51	9.36	0.12	4.64	8.60	4.50	0.46	97.55
PC079/3/96	2.91	52.43	1.90	15.83	9.74	0.13	4.55	8.68	4.38	0.44	98.08
PC079/3/96	2.91	52.49	1.86	15.40	9.42	0.20	4.55	8.41	4.27	0.49	97.09
PC079/3/96	2.91	52.50	1.91	16.03	9.59	0.19	4.73	8.82	4.40	0.47	98.64
PC079/3/96	2.91	52.60	1.89	15.76	9.27	0.20	4.62	8.91	4.49	0.46	98.20
PC079/3/96	2.91	52.60	1.99	15.59	9.39	0.16	4.65	8.53	4.70	0.09	97.70
PC079/3/96	2.91	52.72	1.89	15.92	9.02	0.12	4.59	8.51	4.41	0.47	97.65
PC079/3/96	2.91	52.75	1.69	17.46	7.97	0.14	4.01	8.83	4.73	0.48	98.06
PC079/3/96	2.91	52.78	1.98	17.52	9.27	0.15	4.60	8.66	4.55	0.52	100.00
PC079/3/96	2.91	52.97	1.81	15.68	9.38	0.18	4.56	8.77	4.55	0.42	98.32
PC079/3/96	2.91	53.02	1.90	15.66	9.30	0.21	4.40	8.34	4.42	0.41	97.66
PC079/3/96	2.91	53.13	1.73	15.94	9.39	0.13	4.58	8.55	4.47	0.47	98.38
PC079/3/96	2.91	53.68	1.88	14.92	9.85	0.13	4.94	9.07	3.90	0.53	98.90
PC079/3/96	2.91	54.95	1.74	15.75	8.32	0.11	3.91	7.23	4.85	0.82	97.71
PC079/3/96	2.91	55.47	2.03	17.17	7.96	0.22	2.85	7.80	5.26	0.66	99.42
PC079/3/96	2.91	55.70	1.72	15.22	7.31	0.13	3.71	6.91	4.37	0.61	95.68
PC079/3/96	2.91	60.26	1.36	15.34	7.14	0.17	2.25	4.58	4.87	1.98	97.95
PC079/3/147	3.42	51.22	2.37	16.13	10.50	0.16	4.34	8.45	3.99	0.49	97.62
PC079/3/147	3.42	51.43	2.39	15.98	10.30	0.15	4.34	8.27	4.12	0.49	97.47
PC079/3/147	3.42	51.64	2.45	16.33	10.90	0.20	4.31	8.75	6.05	0.51	101.20
PC079/3/147	3.42	52.10	2.54	15.76	10.60	0.13	4.22	7.87	3.93	0.62	97.80
PC079/3/147	3.42	62.98	1.28	15.75	4.97	0.17	1.40	3.12	2.39	2.69	94.75
PC079/3/147	3.42	62.99	1.19	15.93	5.40	0.23	1.78	3.69	4.15	2.87	98.23
PC079/3/147	3.42	63.46	1.19	16.24	5.07	0.19	1.68	3.53	4.51	2.95	98.82
PC079/3/147	3.42	65.45	1.15	16.12	4.60	0.12	1.17	2.57	4.08	3.22	98.48
PC079/3/147	3.42	65.83	1.28	16.16	4.04	0.19	1.16	2.04	4.87	1.35	96.92
PC079/3/147	3.42	71.37	0.35	14.36	3.39	0.09	0.17	0.68	4.02	2.54	96.97
PC079/4/44	3.89	50.35	2.02	15.00	9.82	0.19	4.92	8.96	4.42	0.40	96.08
PC079/4/44	3.89	50.57	1.50	15.46	8.70	0.20	5.78	9.43	4.05	0.55	96.24
PC079/4/44	3.89	50.92	1.78	15.55	8.82	0.21	5.56	9.78	4.19	0.54	97.35
PC079/4/44	3.89	50.93	1.66	15.63	8.64	0.14	5.34	9.59	4.01	0.52	96.46
PC079/4/44	3.89	51.00	1.90	14.16	9.49	0.23	5.61	9.33	4.26	0.63	96.61
PC079/4/44	3.89	51.20	1.48	15.74	7.77	0.16	5.44	9.77	3.83	0.45	95.84
PC079/4/44	3.89	51.29	1.46	16.03	7.86	0.11	5.21	9.79	3.89	0.38	96.02
PC079/4/44	3.89	51.40	1.66	15.93	8.16	0.21	5.03	8.12	4.29	0.64	95.44
PC079/4/44	3.89	51.40	2.88	12.87	12.60	0.25	3.84	7.35	4.24	0.69	96.08
PC079/4/44	3.89	51.44	1.61	15.72	8.30	0.15	5.21	8.71	4.03	0.58	95.75
PC079/4/44	3.89	51.54	1.59	16.29	8.77	0.14	4.62	8.73	4.42	0.48	96.58
PC079/4/44	3.89	51.61	1.63	15.05	8.45	0.19	5.38	9.33	4.09	0.49	96.22

PC079/4/44	3.89	51.65	1.42	16.54	8.19	0.13	5.21	10.10	3.92	0.49	97.65
PC079/4/44	3.89	51.67	1.70	16.09	7.67	0.23	5.08	9.71	3.70	0.52	96.37
PC079/4/44	3.89	51.87	1.62	15.23	8.91	0.19	5.29	8.85	4.40	0.67	97.03
PC079/4/44	3.89	52.09	1.47	16.15	7.70	0.15	5.06	9.67	3.96	0.45	96.70
PC079/4/44	3.89	52.14	1.56	15.63	8.35	0.17	5.38	9.42	4.20	0.46	97.31
PC079/4/44	3.89	52.31	1.37	15.99	7.83	0.19	5.01	9.30	4.11	0.60	96.71
PC079/4/44	3.89	52.86	2.39	13.91	10.00	0.22	3.78	7.09	4.64	0.76	95.66
PC079/4/44	3.89	55.37	1.67	15.79	7.98	0.17	3.08	6.47	4.86	1.09	96.48
PC079/4/44	3.89	61.47	0.67	14.78	7.32	0.29	0.30	1.30	6.35	4.72	97.20
PC079/4/56	4.01	52.01	1.50	16.21	8.67	0.22	5.68	10.50	3.63	0.34	98.72
PC079/4/56	4.01	53.38	2.01	14.43	9.21	0.21	4.65	7.70	4.42	0.73	96.74
PC079/4/56	4.01	53.54	2.15	13.96	10.30	0.26	3.99	6.85	4.50	0.69	96.25
PC079/4/56	4.01	53.75	2.14	14.59	10.30	0.22	4.38	7.62	4.38	0.67	98.04
PC079/4/56	4.01	54.02	1.86	14.80	8.80	0.22	4.35	7.66	4.51	0.54	96.76
PC079/4/56	4.01	54.20	1.84	15.48	9.51	0.24	3.43	6.99	4.57	0.77	97.03
PC079/4/56	4.01	54.69	2.41	13.86	10.40	0.20	3.48	6.58	4.42	0.78	96.80
PC079/4/96	4.41	50.79	2.11	14.20	10.70	0.21	5.10	9.28	4.46	0.33	97.15
PC079/4/96	4.41	52.47	1.99	16.45	8.88	0.16	4.80	8.95	4.55	0.48	98.73
PC079/4/96	4.41	53.65	2.42	14.41	10.60	0.31	3.71	6.93	4.70	0.57	97.30
PC079/4/96	4.41	55.93	2.30	15.75	8.84	0.21	3.00	6.17	4.79	0.90	97.89
PC079/4/96	4.41	56.10	2.19	15.63	8.70	0.19	2.94	5.94	4.90	0.89	97.48
PC079/4/96	4.41	56.19	2.03	15.31	9.56	0.23	4.00	6.78	4.76	0.82	99.68
PC079/4/96	4.41	56.77	2.20	16.00	8.66	0.14	2.93	5.92	5.42	0.90	98.94
PC079/4/96	4.41	57.88	1.36	15.91	6.18	0.23	2.49	4.78	4.79	2.08	95.70
PC079/4/96	4.41	58.37	2.35	13.99	9.68	0.23	2.27	4.67	5.05	1.20	97.81
PC079/4/96	4.41	62.23	0.30	15.09	5.35	0.17	0.06	0.87	7.84	5.15	97.06
PC079/4/112	4.57	46.77	2.21	17.52	9.44	0.18	4.79	8.34	4.89	1.73	95.87
PC079/4/112	4.57	46.93	2.25	16.83	9.28	0.16	6.49	9.26	4.33	0.80	96.33
PC079/4/112	4.57	47.43	2.21	17.58	9.20	0.17	6.55	9.32	4.20	0.77	97.43
PC079/4/112	4.57	48.27	3.15	15.13	11.30	0.23	4.12	8.25	4.96	1.00	96.41
PC079/4/112	4.57	50.73	2.37	13.66	11.50	0.22	4.69	8.66	4.31	0.48	96.58
PC079/4/112	4.57	51.32	1.84	15.66	8.23	0.11	5.97	8.95	3.89	0.79	96.76
PC079/4/112	4.57	51.44	1.72	13.99	9.32	0.15	6.14	8.54	3.80	0.67	95.77
PC079/4/112	4.57	51.58	1.91	15.16	8.60	0.15	5.50	9.09	3.91	0.84	96.74
PC079/4/112	4.57	52.04	1.78	15.01	10.50	0.17	3.75	7.73	3.67	1.29	95.93
PC079/4/112	4.57	52.20	1.81	15.23	10.60	0.22	3.65	7.65	4.02	1.23	96.61
PC079/4/112	4.57	53.59	2.30	14.67	10.80	0.22	3.67	7.18	4.38	0.73	97.53
PC079/4/112	4.57	54.13	2.89	13.67	10.20	0.26	3.57	7.05	4.63	0.81	97.24
PC079/4/112	4.57	59.88	1.30	14.63	7.62	0.14	2.77	5.59	4.16	1.67	97.76
PC079/4/140	4.85	50.64	3.08	13.55	11.70	0.23	4.32	7.18	4.54	0.71	95.97
PC079/4/140	4.85	50.84	3.13	13.40	11.60	0.25	4.54	7.18	4.41	0.74	96.09
PC079/4/140	4.85	50.88	2.43	14.66	10.70	0.16	4.28	8.09	4.77	0.46	96.43
PC079/4/140	4.85	50.92	3.10	13.29	11.40	0.27	4.41	7.32	4.36	0.76	95.83
PC079/4/140	4.85	50.98	3.09	12.96	11.70	0.25	4.37	7.49	4.31	0.67	95.83
PC079/4/140	4.85	51.01	3.14	13.68	12.30	0.24	4.37	6.91	4.48	0.75	96.85
PC079/4/140	4.85	51.03	3.19	13.35	11.70	0.20	4.36	7.24	4.80	0.72	96.61
PC079/4/140	4.85	51.12	2.97	13.41	11.90	0.27	4.57	7.16	4.43	0.63	96.45
PC079/4/140	4.85	51.15	2.99	13.52	12.00	0.31	4.43	7.21	4.46	0.58	96.68
PC079/4/140	4.85	51.19	2.99	13.82	11.40	0.22	4.37	7.45	4.41	0.62	96.49
PC079/4/140	4.85	51.27	3.01	13.30	11.40	0.25	4.31	6.98	4.38	0.65	95.54
PC079/4/140	4.85	51.33	3.08	12.87	11.80	0.26	4.50	6.92	4.35	0.81	95.88
PC079/4/140	4.85	51.34	2.74	14.94	10.20	0.20	3.92	7.56	4.63	0.62	96.14

Core section	depth (mbsf)	SiO$_2$	TiO$_2$	Al$_2$O$_3$	FeO$_T$	MnO	MgO	CaO	Na$_2$O	K$_2$O	Total
PC079/4/140	4.85	51.38	2.97	13.05	11.40	0.24	4.41	7.19	4.53	0.69	95.86
PC079/4/140	4.85	51.48	2.99	13.68	11.50	0.22	4.40	7.13	4.48	0.57	96.47
PC079/4/140	4.85	51.49	3.08	13.44	11.60	0.23	4.41	7.23	4.49	0.64	96.61
PC079/4/140	4.85	51.55	3.01	13.78	11.60	0.26	4.44	7.37	4.43	0.62	97.02
PC079/4/140	4.85	51.59	2.64	14.25	10.90	0.23	4.01	8.12	4.53	0.58	96.87
PC079/4/140	4.85	51.63	3.11	13.59	11.40	0.24	4.42	7.56	4.56	0.71	97.19
PC079/4/140	4.85	51.73	3.22	12.99	12.90	0.26	3.49	7.37	4.65	0.76	97.34
PC079/4/140	4.85	51.79	3.03	13.46	11.60	0.19	4.34	7.27	4.45	0.70	96.84
PC079/4/140	4.85	51.82	2.93	14.86	10.70	0.22	3.64	7.91	4.67	0.61	97.36
PC079/4/140	4.85	51.86	3.02	14.01	11.50	0.24	4.19	7.40	4.16	0.58	96.92
PC079/4/140	4.85	52.15	3.10	14.11	11.80	0.22	4.32	7.17	4.53	0.61	97.98
PC079/4/140	4.85	52.48	1.99	17.83	7.70	0.17	2.76	8.04	5.06	0.45	96.48
PC079/4/140	4.85	53.85	1.95	14.30	9.44	0.22	4.50	7.50	4.40	0.68	96.84
PC079/4/140	4.85	54.12	0.64	24.03	2.55	0.10	0.82	8.86	6.03	0.23	97.38
PC079/4/140	4.85	54.27	0.52	24.49	2.65	0.00	0.81	9.20	5.83	0.19	97.96
PC079/4/140	4.85	55.08	2.36	14.21	10.40	0.21	2.93	6.03	4.25	0.97	96.40
PC079/4/140	4.85	55.28	2.41	14.24	10.50	0.18	2.88	5.97	4.22	0.97	96.67
PC079/5/52	5.47	50.21	1.84	14.41	9.21	0.21	5.05	9.44	4.50	0.35	95.22
PC079/5/52	5.47	50.24	1.49	15.30	8.80	0.22	5.79	10.36	4.07	0.38	96.65
PC079/5/52	5.47	50.47	1.70	15.32	8.85	0.23	5.37	9.82	4.23	0.41	96.40
PC079/5/52	5.47	50.55	1.69	15.27	9.02	0.22	5.65	10.05	3.99	0.37	96.81
PC079/5/52	5.47	50.59	2.07	14.93	10.55	0.23	4.40	8.49	4.61	0.46	96.33
PC079/5/52	5.47	50.84	2.12	14.91	10.46	0.27	4.45	8.43	4.64	0.40	96.52
PC079/5/52	5.47	51.24	1.89	14.76	10.31	0.20	4.75	8.57	4.48	0.42	96.62
PC079/5/52	5.47	51.25	1.82	14.36	9.48	0.16	5.40	9.08	4.30	0.47	96.32
PC079/5/52	5.47	51.43	1.65	14.54	9.63	0.20	5.20	9.31	4.13	0.43	96.52
PC079/5/52	5.47	51.52	1.75	15.07	8.97	0.20	5.44	9.77	4.24	0.35	97.31
PC079/5/52	5.47	51.74	1.90	14.67	10.11	0.27	4.59	8.43	4.38	0.40	96.49
PC079/5/52	5.47	59.83	0.60	15.14	6.51	0.24	0.34	1.28	6.92	5.22	96.08
PC079/5/84	5.79	50.91	1.60	15.12	8.96	0.23	5.87	10.00	3.85	0.31	96.85
PC079/5/84	5.79	52.30	1.94	15.16	8.98	0.23	4.70	8.58	4.33	0.57	96.79
PC079/5/84	5.79	56.59	1.72	15.24	8.42	0.15	3.11	5.94	5.35	1.06	97.58
PC079/5/108	6.03	52.03	1.75	16.27	8.82	0.19	4.80	9.06	4.22	0.52	97.66
PC079/6/12	6.57	46.97	2.93	16.20	10.20	0.26	3.71	8.41	5.06	2.37	96.11
PC079/6/12	6.57	50.50	1.79	15.53	8.81	0.21	4.52	9.26	4.42	0.44	95.48
PC079/6/12	6.57	50.68	1.83	16.01	8.66	0.20	4.82	9.12	4.33	0.39	96.04
PC079/6/12	6.57	60.16	0.57	14.58	6.85	0.32	0.10	1.15	8.40	4.04	96.17
PC079/6/12	6.57	63.11	0.38	14.23	7.44	0.30	0.00	0.93	6.85	4.80	98.04
PC079/6/36	6.81	50.05	1.94	15.73	8.92	0.19	4.68	9.09	4.34	0.43	95.37
PC079/6/36	6.81	50.33	1.85	15.77	8.99	0.23	4.85	8.48	4.34	0.52	95.36
PC079/6/36	6.81	51.32	1.85	16.11	8.69	0.27	4.59	9.01	4.57	0.49	96.90
PC079/6/36	6.81	60.31	0.69	14.53	7.34	0.29	0.28	1.18	6.21	4.78	95.61
PC079//6/128	7.73	49.78	2.46	15.23	10.93	0.27	3.35	7.49	5.39	1.74	96.64
PC079//6/128	7.73	51.58	1.74	16.17	8.17	0.14	5.03	9.05	4.39	0.48	96.75
Core section	depth (mbsf)	SiO$_2$	TiO$_2$	Al$_2$O$_3$	FeO$_T$	MnO	MgO	CaO	Na$_2$O	K$_2$O	Total
KC081/1/4	0.21	49.70	2.55	14.97	10.60	0.19	4.17	8.31	4.48	0.52	95.49
KC081/1/4	0.21	49.75	2.31	15.05	9.77	0.21	4.74	8.97	4.71	0.49	96.00
KC081/1/4	0.21	49.82	2.36	15.59	9.85	0.17	4.56	8.68	4.48	0.48	95.99

KC081/1/4	0.21	49.84	2.24	15.41	10.12	0.16	4.58	8.73	4.54	0.56	96.18
KC081/1/4	0.21	49.94	1.90	15.74	8.96	0.18	5.60	9.97	3.97	0.39	96.65
KC081/1/4	0.21	50.05	2.59	14.60	11.33	0.21	4.46	8.08	4.63	0.65	96.60
KC081/1/4	0.21	50.08	2.55	15.61	10.26	0.28	4.30	7.79	4.62	0.57	96.06
KC081/1/4	0.21	50.12	2.49	15.51	10.34	0.27	5.00	9.02	4.08	0.51	97.34
KC081/1/4	0.21	50.15	2.33	15.61	10.21	0.25	4.09	8.12	4.41	0.58	95.75
KC081/1/4	0.21	50.41	2.24	15.55	10.08	0.16	4.76	8.56	4.54	0.52	96.82
KC081/1/4	0.21	50.43	2.25	15.63	9.23	0.20	5.11	9.12	4.16	0.48	96.61
KC081/1/4	0.21	50.45	2.56	15.67	11.28	0.20	4.17	8.53	4.75	0.52	98.13
KC081/1/4	0.21	50.46	2.29	15.19	9.67	0.24	4.34	8.47	4.57	0.54	95.77
KC081/1/4	0.21	50.47	2.36	15.16	10.19	0.18	4.14	7.76	4.85	0.58	95.69
KC081/1/4	0.21	50.49	2.47	15.82	9.83	0.16	4.39	8.18	4.50	0.39	96.23
KC081/1/4	0.21	50.61	2.63	15.63	10.23	0.22	4.19	8.09	4.58	0.56	96.74
KC081/1/4	0.21	50.62	2.58	15.16	10.56	0.21	4.43	8.26	4.40	0.56	96.78
KC081/1/4	0.21	50.66	2.68	16.07	10.42	0.21	4.17	8.50	4.82	0.51	98.04
KC081/1/4	0.21	50.83	2.52	15.40	10.35	0.20	4.13	7.73	4.70	0.51	96.37
KC081/1/4	0.21	50.93	2.50	15.64	9.99	0.21	4.04	8.05	4.66	0.53	96.55
KC081/1/4	0.21	51.00	2.49	15.17	10.75	0.22	4.22	8.30	4.71	0.55	97.41
KC081/1/4	0.21	51.03	2.49	15.61	10.35	0.27	4.12	8.12	4.59	0.61	97.19
KC081/1/4	0.21	51.45	2.72	15.98	11.03	0.23	4.37	8.49	4.26	0.55	99.08
KC081/1/4	0.21	51.57	2.34	16.15	10.18	0.20	4.28	9.05	4.88	0.50	99.15
KC081/1/4	0.21	51.79	2.56	15.14	10.26	0.20	4.21	8.03	4.84	0.52	97.55
KC081/1/4	0.21	66.92	0.64	14.49	3.27	0.19	0.58	1.13	5.89	2.00	95.11
KC081/1/4	0.21	68.27	0.70	14.92	3.71	0.20	0.58	1.27	6.04	2.03	97.72
KC081/1/4	0.21	70.09	0.45	13.97	3.18	0.12	0.22	0.63	5.73	2.52	96.91
KC081/1/4	0.21	70.82	0.30	13.97	3.46	0.14	0.20	0.69	5.69	2.62	97.89
KC081/1/4	0.21	70.95	0.38	13.95	3.39	0.11	0.20	0.59	5.62	2.63	97.82
KC081/1/4	0.21	71.19	0.43	14.01	3.27	0.13	0.19	0.57	5.84	2.62	98.25
KC081/1/4	0.21	71.54	0.30	13.92	3.38	0.11	0.18	0.73	5.73	2.32	98.21
KC081/1/4	0.21	71.60	0.37	13.95	3.34	0.15	0.21	0.67	4.65	2.63	97.57
KC81/1/74	0.91	48.83	1.96	15.69	10.69	0.12	5.32	9.08	4.34	0.89	96.92
KC81/1/74	0.91	49.04	2.06	15.69	10.00	0.11	6.26	10.58	4.23	0.34	98.31
KC81/1/74	0.91	49.14	2.02	15.26	10.10	0.22	6.15	10.34	4.11	0.39	97.73
KC81/1/74	0.91	49.29	1.95	15.14	9.80	0.12	5.96	10.54	3.98	0.39	97.17
KC81/1/74	0.91	49.37	1.91	15.78	10.56	0.11	5.31	9.24	4.38	0.99	97.65
KC81/1/74	0.91	49.69	2.79	14.38	12.19	0.19	4.21	7.98	4.28	0.56	96.27
KC81/1/74	0.91	49.78	1.98	15.96	10.77	0.05	5.14	9.06	4.27	0.93	97.94
KC81/1/74	0.91	49.80	2.05	15.65	10.64	0.09	5.39	9.24	4.36	1.09	98.31
KC81/1/74	0.91	68.67	0.66	15.42	4.07	0.12	0.82	2.19	3.67	1.58	97.20
KC081/1/102	1.19	47.91	2.29	16.50	8.68	0.20	5.18	9.75	4.86	1.67	97.04
KC081/1/102	1.19	48.36	1.69	16.12	9.21	0.17	5.94	9.50	4.08	1.26	96.33
KC081/1/102	1.19	48.50	2.73	13.34	12.66	0.25	4.95	9.61	3.93	1.04	97.01
KC081/1/102	1.19	49.70	1.61	15.97	7.98	0.20	6.07	9.91	3.74	0.49	95.67
KC081/1/102	1.19	51.25	1.99	14.81	9.04	0.19	4.35	8.33	4.22	0.48	94.66
KC081/1/102	1.19	51.73	2.02	15.53	9.20	0.15	4.62	8.61	4.50	0.37	96.73
KC081/1/102	1.19	52.38	1.92	14.62	8.89	0.09	5.28	8.83	3.78	0.60	96.39
KC081/1/102	1.19	52.60	1.60	15.08	10.28	0.23	3.80	8.04	3.56	1.10	96.29
KC081/1/102	1.19	53.03	1.52	15.33	8.12	0.12	5.70	9.25	3.85	0.60	97.52
KC081/1/102	1.19	53.71	2.51	13.26	11.42	0.21	3.87	6.98	4.26	0.75	96.97
KC081/1/102	1.19	54.28	1.97	15.61	8.59	0.12	3.63	7.14	4.35	0.75	96.44
KC081/1/102	1.19	54.63	1.29	13.93	9.25	0.19	4.74	8.64	3.22	0.94	96.83
KC081/1/102	1.19	55.30	1.23	14.69	9.58	0.16	3.16	6.16	3.37	3.23	96.88
KC081/1/102	1.19	55.64	1.47	15.04	9.21	0.22	3.15	6.53	3.94	1.67	96.87
KC081/1/102	1.19	55.82	1.53	14.41	9.24	0.23	3.21	6.44	4.03	1.72	96.63

Core section	depth (mbsf)	SiO₂	TiO₂	Al₂O₃	FeOₜ	MnO	MgO	CaO	Na₂O	K₂O	Total
KC081/1/102	1.19	60.10	1.52	14.37	7.99	0.19	1.77	4.35	4.32	1.73	96.34
KC081/1/142	1.59	50.99	0.89	15.37	8.10	0.19	6.72	11.19	3.12	0.65	97.22
KC081/1/142	1.59	51.07	2.11	15.82	9.25	0.18	4.35	8.62	4.52	0.50	96.42
KC081/1/142	1.59	51.11	2.06	15.55	9.40	0.22	4.57	8.48	4.52	0.44	96.35
KC081/1/142	1.59	51.27	2.19	15.96	8.94	0.21	4.47	8.50	4.38	0.46	96.38
KC081/1/142	1.59	51.39	2.06	15.84	9.46	0.19	4.38	8.50	4.62	0.50	96.94
KC081/1/142	1.59	51.82	1.96	16.05	9.62	0.23	4.59	8.56	4.59	0.43	97.85
KC081/1/142	1.59	51.93	1.95	15.62	9.42	0.19	4.45	8.65	4.56	0.41	97.18
KC081/1/142	1.59	52.06	2.00	15.82	9.43	0.14	4.73	8.37	4.68	0.38	97.61
KC081/1/142	1.59	52.08	2.09	15.64	9.29	0.17	4.59	8.69	4.70	0.50	97.75
KC081/1/142	1.59	52.15	2.16	16.01	10.62	0.17	4.26	8.78	4.59	0.49	99.23
KC081/1/142	1.59	52.23	2.12	15.99	9.71	0.24	4.53	8.34	4.45	0.47	98.08
KC081/1/142	1.59	52.33	2.16	15.71	9.54	0.21	4.56	8.37	4.30	0.48	97.66
KC081/1/142	1.59	52.56	2.28	16.03	10.70	0.18	5.01	9.07	4.46	0.53	100.82
KC081/1/142	1.59	53.45	1.84	17.90	7.78	0.13	3.59	9.13	4.69	0.35	98.86
KC081/1/142	1.59	56.21	1.92	14.05	9.95	0.25	3.21	6.25	4.62	1.22	97.71
KC081/2/32	1.99	45.15	3.31	16.43	10.45	0.14	4.59	9.97	4.82	1.83	96.69
KC081/2/32	1.99	45.86	3.40	16.14	10.73	0.20	4.74	10.04	5.12	1.79	98.02
KC081/2/32	1.99	47.50	1.87	16.74	11.02	0.13	5.73	9.32	4.18	0.89	97.38
KC081/2/32	1.99	50.21	1.72	16.37	9.08	0.11	5.36	9.45	3.93	0.30	96.53
KC081/2/32	1.99	51.49	2.12	14.84	10.28	0.13	4.58	8.58	4.16	0.56	96.74
KC081/2/32	1.99	51.56	1.99	14.98	10.06	0.15	4.66	8.56	3.99	0.54	96.49
KC081/2/32	1.99	57.44	1.91	14.86	10.12	0.15	3.05	5.72	4.52	1.02	98.79
KC081/2/96	2.63	50.95	1.43	16.78	7.73	0.14	4.89	10.14	3.82	0.36	96.24
KC081/2/96	2.63	51.76	1.61	16.10	8.24	0.21	5.09	9.52	4.17	0.55	97.25
KC081/2/96	2.63	51.94	1.72	16.11	8.54	0.14	4.99	9.30	4.19	0.48	97.41
KC081/2/96	2.63	52.50	1.66	16.60	8.41	0.19	5.33	9.67	4.16	0.50	99.02
KC081/2/96	2.63	52.62	1.86	15.24	9.81	0.19	5.60	9.04	4.25	0.57	99.18
KC081/2/96	2.63	52.90	1.67	16.59	8.82	0.21	4.52	9.24	4.28	0.61	98.84
KC081/2/96	2.63	52.98	1.79	15.96	8.46	0.17	5.38	8.86	4.40	0.67	98.67
KC081/2/96	2.63	53.67	1.82	15.41	8.41	0.13	4.95	8.17	4.74	0.69	97.99
KC081/2/96	2.63	54.32	2.00	14.77	9.74	0.20	4.10	7.09	4.51	0.76	97.49
Core section	depth (mbsf)	SiO₂	TiO₂	Al₂O₃	FeOₜ	MnO	MgO	CaO	Na₂O	K₂O	Total
GC114/3/98	2.98	48.55	1.75	16.06	8.12	0.21	6.29	10.56	4.06	0.31	95.91
GC114/3/98	2.98	49.59	2.06	14.27	9.73	0.19	8.42	10.21	3.32	0.55	98.34
GC114/3/98	2.98	49.85	2.58	14.77	10.15	0.24	4.65	8.50	4.65	0.57	95.96
GC114/3/98	2.98	50.21	2.98	14.26	11.33	0.29	4.08	7.56	4.77	0.63	96.11
GC114/3/98	2.98	51.67	2.62	14.32	10.80	0.20	4.26	7.56	4.61	0.64	96.68
GC114/3/98	2.98	51.68	1.95	14.68	9.36	0.20	5.32	9.31	4.11	0.56	97.17
GC114/3/98	2.98	51.78	1.91	14.61	9.26	0.22	5.36	9.47	4.08	0.49	97.18
GC114/3/98	2.98	51.78	2.49	13.68	10.10	0.26	4.39	8.24	4.36	0.59	95.89
GC114/3/98	2.98	52.14	2.60	14.47	10.04	0.19	4.39	7.66	4.82	0.77	97.08
GC114/3/98	2.98	52.30	1.53	15.83	7.67	0.18	4.20	8.15	4.90	0.75	95.51
GC114/3/98	2.98	52.37	1.50	16.41	8.02	0.20	4.32	8.29	4.72	0.62	96.45
GC114/3/98	2.98	52.53	1.53	16.25	7.72	0.13	4.21	8.07	4.49	0.59	95.52
GC114/3/98	2.98	52.72	1.58	16.18	7.94	0.21	4.02	7.89	4.77	0.76	96.07
GC114/3/98	2.98	52.75	1.76	15.12	8.54	0.24	4.24	7.68	4.42	0.70	95.45
GC114/3/98	2.98	52.76	1.80	18.49	8.97	0.16	3.93	9.85	4.82	0.32	101.10
GC114/3/98	2.98	52.94	1.70	15.35	8.50	0.21	4.49	7.89	4.55	0.76	96.39
GC114/3/98	2.98	52.95	1.73	15.72	8.30	0.21	4.72	7.76	4.42	0.61	96.42
GC114/3/98	2.98	53.02	1.64	15.97	7.59	0.21	4.06	7.70	4.71	0.79	95.69

GC114/3/98	2.98	53.06	1.41	16.31	7.44	0.20	3.91	7.66	4.66	0.67	95.32
GC114/3/98	2.98	53.06	1.67	15.62	8.21	0.20	4.42	8.07	4.59	0.70	96.54
GC114/3/98	2.98	53.16	2.60	14.10	9.97	0.23	3.18	7.14	4.51	0.73	95.62
GC114/3/98	2.98	53.16	1.63	16.12	8.41	0.20	4.40	7.88	4.71	0.64	97.15
GC114/3/98	2.98	53.21	1.72	15.63	8.00	0.15	3.95	7.45	4.63	0.71	95.45
GC114/3/98	2.98	53.28	1.61	15.65	7.95	0.19	4.43	7.99	4.53	0.72	96.35
GC114/3/98	2.98	53.33	2.00	17.54	6.74	0.15	2.17	7.65	5.60	0.51	95.69
GC114/3/98	2.98	53.35	1.77	14.94	8.96	0.22	4.32	7.75	4.54	0.70	96.55
GC114/3/98	2.98	53.37	1.87	15.46	8.50	0.18	4.66	7.66	4.70	0.65	97.05
GC114/3/98	2.98	53.61	1.54	16.55	7.39	0.16	3.99	7.63	4.51	0.67	96.05
GC114/3/98	2.98	53.68	1.54	16.07	7.61	0.13	4.26	7.81	4.56	0.67	96.33
GC114/3/98	2.98	53.71	1.55	15.74	7.57	0.18	3.90	7.76	4.54	0.63	95.58
GC114/3/98	2.98	53.73	1.57	16.19	8.08	0.19	4.16	7.77	4.74	0.57	97.00
GC114/3/98	2.98	53.80	1.53	16.11	7.18	0.16	3.75	7.27	4.69	0.84	95.33
GC114/3/98	2.98	53.81	1.67	16.43	7.60	0.18	4.03	7.78	4.62	0.72	96.84
GC114/3/98	2.98	53.85	1.49	16.24	7.78	0.20	4.06	7.57	4.72	0.68	96.59
GC114/3/98	2.98	53.92	2.16	14.59	9.16	0.16	3.68	6.57	4.64	0.88	95.76
GC114/3/98	2.98	54.02	1.59	15.71	7.92	0.20	4.14	7.43	4.43	0.69	96.13
GC114/3/98	2.98	54.08	1.41	16.28	7.09	0.19	3.89	7.58	4.79	0.68	95.99
GC114/3/98	2.98	54.26	1.53	16.15	7.92	0.13	3.94	7.34	4.60	0.68	96.55
GC114/3/98	2.98	54.43	1.55	16.28	7.79	0.18	3.79	7.50	4.79	0.71	97.02
GC114/3/98	2.98	54.65	1.58	16.47	7.45	0.15	3.90	7.49	4.56	0.72	96.97
GC114/3/98	2.98	54.74	1.44	16.49	6.84	0.14	3.60	7.04	4.97	0.77	96.03
GC114/3/98	2.98	54.83	2.39	14.06	9.56	0.19	3.08	6.00	4.78	1.20	96.09
GC114/3/98	2.98	55.30	1.59	16.54	7.12	0.13	3.64	7.26	4.69	0.77	97.04
GC114/3/98	2.98	57.10	2.49	13.62	9.99	0.25	2.44	5.27	4.66	1.22	97.04
GC114/3/98	2.98	57.38	2.46	13.77	9.58	0.20	2.37	5.15	4.54	1.26	96.71
GC114/3/98	2.98	69.44	0.37	13.68	3.09	0.14	0.18	0.54	5.30	2.60	95.34
GC114/3/112	3.12	50.83	2.09	14.38	10.10	0.19	5.99	9.60	3.75	0.71	97.68
GC114/3/112	3.12	51.97	2.93	13.21	12.30	0.23	3.57	7.47	4.44	0.62	96.77
GC114/3/112	3.12	52.21	1.78	15.34	8.44	0.16	4.80	7.80	4.56	0.60	95.69
GC114/3/112	3.12	52.47	2.61	14.31	10.50	0.21	3.67	7.21	4.54	0.81	96.31
GC114/3/112	3.12	52.65	1.61	15.57	7.70	0.20	4.21	7.83	4.61	0.62	95.00
GC114/3/112	3.12	52.80	2.45	15.19	10.20	0.15	4.00	7.42	4.68	0.57	97.49
GC114/3/112	3.12	52.84	3.04	13.52	11.50	0.26	3.37	6.88	4.79	0.84	97.08
GC114/3/112	3.12	52.84	3.17	13.38	11.30	0.25	3.43	7.07	4.51	0.81	96.71
GC114/3/112	3.12	53.17	2.11	15.07	9.58	0.21	4.54	8.63	4.34	0.59	98.24
GC114/3/112	3.12	53.30	1.54	16.19	8.06	0.20	4.21	8.03	4.62	0.65	96.80
GC114/3/112	3.12	53.41	1.53	16.15	7.86	0.15	4.11	7.95	4.44	0.67	96.27
GC114/3/112	3.12	53.45	1.73	15.78	8.05	0.17	4.39	7.65	4.43	0.68	96.33
GC114/3/112	3.12	53.53	1.18	19.23	5.58	0.13	3.02	8.62	4.86	0.38	96.53
GC114/3/112	3.12	53.58	2.92	13.06	11.40	0.22	3.33	6.59	4.34	0.78	96.25
GC114/3/112	3.12	53.67	1.53	16.16	7.84	0.17	4.27	8.08	4.48	0.62	96.82
GC114/3/112	3.12	53.84	1.54	16.18	7.90	0.20	4.23	7.56	4.60	0.70	96.75
GC114/3/112	3.12	53.95	1.63	16.35	7.67	0.14	4.01	7.55	4.67	0.82	96.79
GC114/3/112	3.12	54.73	1.58	15.88	7.65	0.14	3.80	6.85	4.76	0.79	96.18
GC114/3/112	3.12	55.11	1.48	15.93	6.85	0.15	3.81	7.19	4.69	0.83	96.04
GC114/3/112	3.12	55.46	1.64	16.34	7.24	0.12	3.72	7.06	4.69	0.77	97.04
GC114/3/112	3.12	55.87	1.36	18.17	5.92	0.15	2.68	7.90	5.50	0.62	98.17
GC114/3/112	3.12	55.95	2.53	13.59	10.20	0.21	2.82	5.75	4.39	0.97	96.38

II. Appendix II – Trace element compositions

Core and sample depth (mbsf)	Ni	Rb	Sr	Y	Zr	Nb	Ba	Ce
PC108	63	121	9	60	963	170	38	231
PC108	60	121	9	60	959	169	37	229
PC108	71	118	9	60	949	165	38	230
PC108	95	143	10	63	977	173	42	242
PC108	66	118	10	61	958	167	40	233
PC108	64	116	9	60	937	162	38	225
PC108	68	116	9	59	932	161	38	222
PC108	65	116	9	59	915	158	37	219
PC108	67	115	9	60	945	162	38	228
PC108	64	117	9	61	949	162	37	225
PC108	76	119	14	60	951	165	41	228
PC108	97	117	10	60	930	162	39	227
PC108	67	116	10	59	926	160	39	224
PC108	64	116	10	60	947	164	39	226
PC108	63	116	10	60	960	165	62	222
PC108	74	123	10	61	974	171	39	228
PC108	61	115	9	61	959	167	39	236
PC111	61	113	9	61	940	163	38	229
PC111	77	125	9	60	951	167	37	233
PC111	64	114	9	59	920	158	37	223
PC111	64	112	9	60	945	162	37	228
PC111	137	119	11	60	945	165	42	227
PC111	77	122	9	57	899	161	38	222
PC111	71	121	9	61	954	167	39	233
PC111	71	114	9	59	920	158	37	221
PC111	307	111	16	61	944	160	47	231
PC111	70	113	9	59	920	157	37	219
PC029-3.42	489	2	389	21	134	5	67	22
PC029-3.42	430	4	316	22	150	5	68	23
PC029-3.42	455	3	347	21	134	5	65	22
PC029-3.42	450	3	323	24	155	5	66	24
PC029-3.42*	501	6	565	23	170	6	122	55
PC029-3.42*	480	5	589	21	153	5	116	51
PC029-3.42	366	14	193	17	94	2	146	21
PC029-3.42**	347	17	208	16	98	2	177	22
PC029-3.42**	357	16	204	17	100	2	162	23
PC029-3.42	424	3	330	22	142	5	62	22
PC029-3.64***	415	7	347	21	160	5	97	26
PC029-3.64***	426	3	392	16	128	4	60	19
PC029-3.64****	392	4	319	21	154	5	74	24
PC029-3.64****	361	2	465	12	104	3	59	16
PC029-3.64****	356	2	537	7	59	2	54	10
PC029-3.64	410	2	453	12	88	3	50	14
PC029-3.64	394	4	342	20	153	5	76	24
PC029-3.64	372	4	356	20	146	4	79	24

PC029-3.64	410	3	340	19	133	4	66	22
PC079-1.80b	389	4	312	28	186	6	65	28
PC079-1.80b	375	4	308	28	185	6	64	27
PC079-1.80b	364	4	313	30	200	6	79	29
PC079-1.80b	268	4	480	11	82	3	67	13
PC079-1.80b*	432	4	325	30	203	7	76	30
PC079-1.80b*	377	3	307	29	187	6	67	28
PC079-1.80b	268	4	480	11	82	3	67	13
PC079-1.80b	356	4	312	30	193	6	70	30
PC079-1.80b	374	4	313	30	195	6	68	30
PC079-1.80b	361	4	296	34	227	7	73	33
PC079-1.80b	354	4	318	29	190	7	70	28
PC079-1.80b	388	4	326	29	196	6	73	31
PC079-1.80b	408	5	357	32	214	7	84	33
PC079-1.80b	370	4	312	30	197	6	70	30
PC079-1.80b	388	4	312	30	195	6	75	28
PC079-1.80b	414	4	356	18	133	4	90	18
PC079-1.80b	380	6	275	32	215	7	77	32
PC079-1.80b	426	3	327	24	166	5	54	23
PC079-1.80b	383	4	354	29	192	6	70	28
PC079-1.80r	42	28	15	64	849	24	194	73
PC079-1.80r	42	27	15	64	850	24	191	73
PC079-1.80r	65	44	43	72	883	27	263	95
PC079-1.80r	89	48	25	68	980	29	247	91
PC079-3.42	325	18	215	19	149	4	155	28
PC079-3.42	369	12	339	11	90	3	124	19
KC081-0.21b	453	3	286	23	149	4	47	21
KC081-0.21b	338	4	284	31	202	7	67	29
KC081-0.21b	329	4	295	27	181	6	66	27
KC081-0.21b	321	4	294	27	184	6	66	27
KC081-0.21b	345	5	293	29	195	6	72	28
KC081-0.21b	340	3	357	25	167	5	62	25
KC081-0.21b	340	3	357	25	167	5	62	25
KC081-0.21b	332	6	279	33	225	8	77	34
KC081-0.21b	350	5	297	30	197	7	76	31
KC081-0.21b	361	5	263	34	223	7	74	32
KC081-0.21b*	340	4	313	29	191	6	69	28
KC081-0.21b*	351	4	311	29	188	6	67	28
KC081-0.21b*	353	4	310	29	188	6	67	28
KC081-0.21b	340	3	295	28	184	6	62	27
KC081-0.21r	47	32	34	57	803	25	285	73
KC081-0.21r	71	32	126	54	758	23	194	70
KC081-0.21r	36	31	17	65	904	27	201	81
KC081-2.46	393	5	302	24	200	6	83	29
KC081-2.46	374	3	457	14	119	4	61	18
KC081-2.46	384	4	342	21	154	5	73	24
KC081-2.46	384	4	338	20	153	5	72	24
KC081-2.46	449	2	250	23	131	3	37	16
KC081-2.46	404	6	337	20	148	5	85	24

III. Appendix III– Long axis measurements of sediment drift glass shards (µm)

SED06 Lower	SED06 Upper	SED07	E5-24	PC103	GC105	PC106	PC108	PC110	PC111	PC113
45	55	45	50	55	50	35	50	45	45	35
50	55	50	50	60	55	50	50	50	50	35
50	55	55	50	70	60	50	50	50	55	45
50	60	60	55	70	60	50	50	55	55	45
55	60	60	60	75	60	55	55	55	60	45
65	60	60	60	75	70	55	55	55	60	50
65	60	70	60	80	70	55	55	60	60	50
65	60	70	60	80	70	55	60	60	60	50
65	60	70	60	80	70	60	60	60	60	50
65	65	70	60	80	75	60	60	65	60	50
70	65	75	60	80	80	60	60	65	60	50
70	65	75	60	80	80	60	65	65	65	50
70	70	75	60	80	80	60	65	65	70	50
70	70	80	65	80	85	65	65	70	70	55
70	70	80	65	80	90	65	65	70	70	55
70	70	80	65	85	90	65	65	70	70	55
70	70	80	70	85	90	70	70	70	70	55
70	70	80	70	85	90	70	70	70	70	60
70	70	80	70	85	90	70	70	70	70	60
70	70	80	70	85	90	70	70	70	70	60
75	70	80	70	90	95	70	70	70	75	60
75	70	80	75	90	100	70	70	70	75	60
75	70	80	75	90	100	70	70	75	80	60
75	70	80	75	90	100	70	70	75	80	65
80	70	80	75	90	100	75	70	75	80	65
80	80	85	75	90	100	75	75	75	80	65
80	80	85	75	90	100	75	75	75	80	65
80	80	85	75	90	100	75	80	75	80	70
80	80	85	75	95	100	80	80	75	80	70
80	80	85	75	95	100	80	80	80	80	70
85	80	85	80	95	100	80	80	80	85	70
90	80	85	80	95	100	80	80	80	85	70
90	80	85	80	100	100	80	80	80	85	70
90	80	90	80	100	105	90	80	80	85	70
95	80	90	80	100	105	90	85	80	85	75
95	85	90	80	100	105	90	85	80	90	75
95	85	90	80	100	110	90	85	80	90	75
95	85	90	80	100	110	90	90	80	90	75
95	85	95	80	100	110	90	90	85	90	75
100	85	100	80	100	110	95	90	85	90	75
100	85	100	80	110	110	95	90	85	90	80
100	90	100	80	110	110	100	95	85	90	80
100	90	100	80	110	110	100	95	85	90	80
100	90	100	80	110	115	100	100	85	95	80
100	90	100	80	110	120	100	100	90	95	80
100	95	100	85	110	120	100	100	90	95	80
100	100	105	85	115	120	100	100	90	95	80
105	100	105	85	115	120	100	100	90	95	80
105	100	105	85	115	120	105	100	90	100	80

105	100	105	90	120	120	105	105	95	100	80
110	105	110	90	120	125	105	110	95	100	85
110	105	110	90	120	125	110	110	95	105	85
110	105	110	90	120	125	115	110	100	110	85
110	110	110	90	120	130	115	115	100	110	85
110	110	110	95	120	130	120	115	100	110	85
115	110	110	95	120	130	120	115	100	110	85
115	110	110	95	120	130	120	115	100	110	90
115	110	110	95	120	130	120	120	100	110	90
120	110	115	95	120	130	120	120	100	110	90
120	110	115	100	120	135	120	120	100	115	90
120	110	115	100	120	140	120	120	100	115	90
120	110	115	100	120	140	120	120	100	120	90
120	110	115	100	125	140	125	120	105	120	95
120	115	120	100	130	140	125	120	110	120	100
120	115	120	100	130	150	125	125	110	120	100
120	120	120	100	130	150	125	125	110	125	100
120	120	120	100	130	150	130	125	110	125	100
120	125	120	105	130	150	130	125	110	125	105
120	130	120	110	130	150	130	130	115	130	105
125	130	125	110	130	150	135	130	120	130	110
130	130	125	110	130	150	135	130	120	130	110
130	130	130	110	130	155	135	130	120	130	110
130	130	130	115	130	155	140	135	125	130	110
130	130	130	115	135	155	140	140	125	130	110
130	130	130	120	135	160	140	140	125	130	110
130	135	130	120	135	160	140	140	130	130	110
130	140	135	120	140	160	140	140	130	130	115
130	140	135	120	140	160	150	140	130	135	115
130	140	140	130	140	160	155	145	130	135	115
140	145	140	130	140	160	155	150	140	140	120
140	145	140	130	145	160	155	150	140	150	120
150	150	140	130	150	160	160	150	140	150	120
150	150	145	130	150	160	160	155	140	150	120
160	150	150	135	160	170	160	155	145	160	120
170	150	150	135	170	170	170	160	155	160	125
170	160	150	135	170	180	170	160	155	160	130
170	160	150	140	175	180	170	165	160	160	130
180	165	160	140	175	190	175	165	160	165	130
180	170	160	140	180	190	175	170	170	170	145
185	170	170	140	185	190	175	180	170	170	150
185	180	170	140	185	200	180	180	180	175	150
195	185	175	145	185	200	180	190	185	180	150
195	190	180	150	190	200	190	190	190	185	150
200	190	180	150	190	210	200	195	190	190	155
205	190	185	150	195	210	210	200	195	190	160
210	205	190	175	200	210	220	200	200	190	160
275	220	230	180	210	230	260	200	200	200	165
280	220	235	185	210	230	275	230	230	220	175
290	230	250	195	210	250	285	265	240	220	180
620	250	270	200	245	280	380	280	355	340	185